2012

Design and Synthesis of New Hydrogen Storage Materials Functioning by Weak Chemisorption

Tuan Khoa Anh Hoang
University of Windsor

Design and Synthesis of New Hydrogen Storage Materials Functioning by Weak Chemisorption

By

Tuan Khoa Anh Hoang

A Dissertation Submitted to the Faculty of Graduate Studies through Chemistry and Biochemistry in Partial Fulfillment of the Requirements for the Degree of Doctor of Philosophy at the University of Windsor

Windsor, Ontario, Canada

2012

Design and Synthesis of New Hydrogen Storage Materials Functioning by Weak Chemisorption

by

Tuan Khoa Anh Hoang

APPROVED BY:

_____

A. Matzger, External Examiner
University of Michigan

_____

D. Northwood
Mechanical, Automotive & Materials Engineering

_____

S. Johnson
Department of Chemistry and Biochemistry

_____

H. Eichhorn
Department of Chemistry and Biochemistry

_____

D. Antonelli, Advisor
Department of Chemistry and Biochemistry

_____

Dr. E. Maticka-Tyndale, Chair of Defense
Faculty of Graduate Studies and Research

January 16th, 2012

Declaration of Co-Authorship / Previous Publication

1. Co-authorship Declaration

I hereby declare that this thesis incorporates materials that is result of joint research, as follows:

This research incorporates the work undertaken in collaboration with Dr. Michel L. Trudeau at Hydro-Quebec Research Institute related to X-ray Photoelectron Spectroscopy. The collaboration with Ahmad Hamaed in Chapter 2; with Michael I. Webb, Ahmad Hamaed, Hung V. Mai, Dr. Charles J. Waslby in Chapter 3; with Ahmad Hamaed, Dr. Golam Moula, Dr. Ricardo Aroca in Chapter 4; with Dr. Jeremy Rawson in Chapter 5; with Leah Morris in Chapter 5, 6, and 7 under the supervision of Dr. Antonelli. In all cases, the key ideas, primary contributions, experimental designs, data analysis and interpretation, were performed by the first author.

I am aware of the University of Windsor Senate Policy on Authorship and I certify that I have properly acknowledged the contribution of other researchers to my thesis, and have obtained written permission from each of the co-authors to include the above materials in my thesis.

I certify that, with the above qualification, this thesis, and the research to which it refers, is the product of my own work.

2. Declaration of Previous Publication

This thesis includes seven original papers that have been previously published or submitted for publication in peer reviewed journals, as follows:

Thesis Chapter	Publication title/full citation	Publication Status
Chapter 1 Introduction	Hoang, T. K. A.; Antonelli, D. M. * "Exploiting the Kubas Interaction in the Design of Hydrogen Storage Materials". *Adv. Mater*. **2009**, 21, 1787 – 1800.	Published

Chapter 2	Hoang, T. K. A.; Hamaed, A..; Trudeau, M.; Antonelli, D. M.* "Bis(benzene) and Bis(cyclopentadienyl) V and Cr Doped Mesoporous Silica with High Enthalpies of Hydrogen Adsorption". *J. Phys. Chem. C* **2009**, 113 (39), 17240–17246.	Published
Chapter 3	Hoang, T. K. A.; Webbs, M. I.; Mai, H. V.; Hamaed, A.; Walsby, C. J.; Trudeau, M.; Antonelli, D. M.* "Design and synthesis of vanadium hydrazide gels for Kubas-type hydrogen adsorption: a new class of hydrogen storage materials". *J. Am. Chem. Soc*. **2010**, 132, 11792 – 11798.	Published
Chapter 4	Hoang, T. K. A.; Morris, L.; Rawson, J. M.; Trudeau, M. L.; Antonelli, D. M.* "Multivalent Manganese Hydrazide Gels for Kubas-type Hydrogen Storage". Manuscript submitted to *Chem. Mater*. **2012**.	Submitted
Chapter 5	Hoang, T. K. A.; Morris, L.; Trudeau, M. L.; Antonelli, D. M.* "Titanium Hydrazide Gels for Kubas-type Hydrogen Storage". Manuscript submitted to *J. Am. Chem. Soc*. **2012**.	Submitted
Chapter 6	Hoang, T. K. A.; Hamaed, A.; Moula, G.; Aroca, R.; Trudeau, M.; Antonelli, D. M.* "Kubas-type Hydrogen Storage in V(III) Polymers Using Tri- and Tetradentate Bridging Ligands". *J. Am. Chem. Soc*. **2011**, 133, 4955 – 4964.	Published
Chapter 7	Hoang, T. K. A.; Morris, L.; Trudeau, M. L.; Antonelli, D. M.* "The role of TiH_5 and TiH_7 in Ti(III) hydride gels for Kubas-type hydrogen storage". Manuscript submitted to *Nature* **2012**.	Submitted

I certify that I have obtained a written permission from the copyright owner(s) to include the above published material(s) in my thesis. I certify that the above material describes work completed during my registration as graduate students at the University of Windsor.

I declare that, to the best of my knowledge, my thesis does not infringe upon anyone's copyright nor violate any proprietary rights and that any ideas, techniques, quotations, or any other material from the work of other people included in my thesis, published or otherwise, are fully acknowledged in accordance with the standard referencing practices. Furthermore, to the extent that I have included copyrighted material that surpassed the bounds of fair dealing within the meaning of the Canada Copyright Act, I certify that I have obtained a written permission from the copyright owner(s) to include such material(s) in my thesis.

I declare that this is a true copy of my thesis, including any final revisions, as approved by my thesis committee and the Graduate Studies office, and that this thesis has not been submitted for a higher degree to any other University or Institution.

Abstract

In the first project, hexagonal packed mesoporous silica (HMS) was synthesized, using dodecyl amine as neutral templating agent. Bis(benzene) and bis(cylopentadienyl) V and Cr were treated with HMS arriving in doping level of 5 wt % for Kubas-type hydrogen adsorption. All doped materials had higher hydrogen adsorption capacities than that of pristine silica. Each Cr center could accommodate 2.2 H_2 molecules at 77 K and 60 bar while each V center adsorbs 1.73 H_2 at the same condition. The Cr doped silica preserved a substantial degree of its adsorption at room temperature and after three months storage in an inert atmosphere.

The second project involved in the synthesis and hydrogen storage performance of vanadium hydrazide gels. The third project focused on the manganese hydrazide for hydrogen storage. The fourth project concentrated on the preparation of titanium hydrazide gels for hydrogen storage. These materials used low-coordinate metal centers as the principal Kubas H_2 binding sites with only negligible contribution of physisorption. Hydrazide samples were characterized by Powder X-ray diffraction (PXRD), X-ray photoelectron spectroscopy (XPS), Infrared Spectroscopy (IR), Elemental Analysis (EA), Electron Paramagnetic Resonance (EPR), Raman Spectroscopy, nitrogen adsorption (BET), and hydrogen adsorption. The vanadium hydrazide gels possess an excess reversible storage of 4.04 wt% at 77 K and 85 bar, corresponding to a true volumetric adsorption of 80 kg/m^3 and an excess volumetric adsorption of 60.01 kg/m^3. These values are in the range of the ultimate DOE goal for volumetric density (70 kg/m^3) while the manganese hydrazide gels possess 24.2 kg/m^3 volumetric at 298K and 85bar.

The fifth project employed commercially available organic compounds to react with $V(Mes)_3 \cdot THF$ to create vanadium-containing polymers for hydrogen storage. The sixth project involved in the synthesis of a porous titanium(III) hydride for hydrogen storage. Ti(III) hydride gels are a promising new hydrogen storage medium, which exploit the first example of solid-state hypervalent hydrides. The material with the highest capacity has an excess reversible storage of 3.49 wt % at 140 bar and 298 K, which corresponds to 44.3 kg/m^3 of volumetric density, surpassing the DOE 2017 volumetric goal of 40 kg/m^3

H_2 without saturation. At adsorption level of 3.49 wt%, TiH_3 is be converted to hypervalent TiH_5 and TiH_7, which contain 3.93 wt% and 7.86 wt% H_2, respectively.

There are high expectations that hydrogen storage performance of hydrazide and hydride materials might provide even higher storage capacities at higher hydrogen pressure in this thesis so that a system contains these materials might surpass the US Department of Energy ultimate system targets (7.5 wt% and 70 kg/m^3).

To my family with love …

Acknowledgements

First of all, I would like to express my highest gratitude to Professor David M. Antonelli for granting me the opportunity to work in his lab, which possesses an excellent working environment. I sincerely appreciate his guidance, help, support, patience, and friendship through my graduate study years. Without his talent in chemistry research and his open-mind in exploring new research areas, our works about hydrogen storage materials would never come to light and would be one of the leaders in hydrogen storage technologies. He has been patiently teaching me how to do research, how to write, submit, correct, and revise the manuscripts, from one to another.

I am indebted of Dr. Michel L. Trudeau for his continuous help in Xray photoelectron spectroscopy measurements and data deconvolution.

A special thank goes to Dr. Ricarod Aroca and Dr. Golam Moula for their help in acquiring Raman spectroscopy. The help of Dr. Jeremy Rawson in training and acquiring EPR results is highly appreciated.

I am grateful to my committee members Professor Holger Eichhorn, Professor Samuel Johnson, and Professor Derek Northwood, who gave me continuous support and help, especially when my PhD supervisor is not physically available. Professor Eichhorn is highly appreciated for his training and help with XRD, TGA, and DSC instrumentation. I am indebted of Professor Johnson for the discussion, suggestion, and explaination about organometallic chemistry, and his help in elemental analysis instrumentation.

I would like to thank the University of Windsor Office of Research Services, Department of Chemistry & Biochemistry, Dr. Philip Dutton, Ms. Elizabeth Kickham, Ms. Marlene Bezaire, and Mr. Horst Schmidt for the help in administration, funding, and managing our group account in the last two years and one semester of this work.

The present and former members of Dr. Antonelli group Dr. Ahmad Hamaed, Dr. Sun Jing, Dr. Junjie Kang, Dr. Yuxiang Rao, Van Hung Mai, and Leah Morris are thanked for their help and making graduate studies a memorable times.

Save the best for last, I would like to express greatest gratitude to my parents, my family, and my wife for their continuous supports, their care, their love, and their encouragement, and provide me the meaning to life.

Table of Contents

List of Tables

List of Figures

List of Schemes

List of Appendices

List of Abbreviations, Symbols, Nomenclature

atm	atmosphere
BET	Brunauer – Emmett – Teller
BDT	1,4-benzeneditetrazolate
BTT	1,3,5-benzenetritetrazolate
^{o}C	Degree Celsius
DOE	United State Department of Energy
DSC	Differential Scanning Calorimetry
EA	Elemental Analysis
EPR	Electron Paramagnetic Resonance
h	hour
HMS	hexagonally packed mesoporous silica
INS	Inelastic Neutron Scattering
IR	Infrared Spectroscopy
Me	Methyl group
Mes	Mesityl group
MOF	Metal Organic Framework
NMR	Nuclear Magnetic Resonance
R	Gas Constant
T	Temperature
TGA	Thermogravimetric Analysis (or Thermal Gravimetric Analysis)
TPD	Temperature Programmed Desorption
THF	Tetrahydrofuran
wt%	weight percent
XPS	Xray Photoelectron Spectroscopy
XRD	Xray Diffraction

Chapter 1 – Introduction

1.1 Introduction

The increase in crude oil consumption and the rapid exhaustion of petroleum reservoirs has led to a boom in research in the area of alternative fuel.[1] New sources of energy should be clean, efficient, low cost, and easy to transport. Some candidates are wind, solar, geothermal, biomass, nuclear energy, and hydrogen.[2] Hydrogen is an attractive energy source for mobile applications such as vehicles because it has the highest energy density of any substance and produces only water as a waste product when used in a fuel cell.[3] Unfortunately hydrogen is difficult to store and transport. Therefore, to commercialize hydrogen technology, the bottleneck represented by the storage and delivery steps must be overcome.

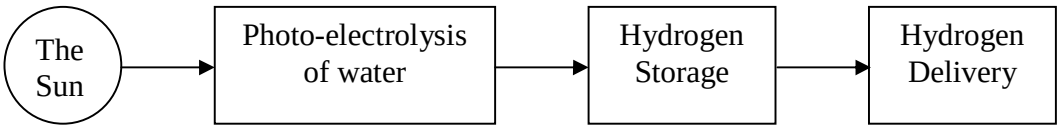

Significant advances have been made in the search for suitable materials for hydrogen storage. While compressed gas is still being explored as an option, materials that absorb hydrogen as carriers are also being investigated. The two major technologies for chemical storage are metal hydrides, which store hydrogen as a discrete M-H bond, and high surface materials for cryogenic hydrogen physisorption.[4] However, no material explored to date meets the US Department of Energy (DOE) 2017 system target of 5.5 wt % weight adsorption or 40 kg/m^3.[5] These system targets were established by the DOE and its partners (FreedomCAR and United States Council for Automotive Research). A hydrogen storage system might exhibit a much lower volumetric performance than that of the adsorbing materials. Partial consumption of system volume for cylinder shells and cylinder's accessories lead to a small storage volume to hold the functioning materials, especially in the storage system operating at high pressures or low temperatures. Therefore, only materials with volumetric adsorption higher than the DOE standards are

promising. Nevertheless, the use of DOE gravimetric and volumetric system targets is still necessary in evaluating the adsorption performance of materials with the idea in mind that it is not the final net performance of the hydrogen storage system employing these materials.

New materials and concepts are currently being explored and new storage strategies are being developed.[6] One of the most overlooked features of a hydrogen storage material is the enthalpy of adsorption. If this value is too high, as in metal hydrides which generally have enthalpies in the 80 kJ/mol range, energy is required to drive off hydrogen for use and enormous amounts of heat are released on recharging. If this value is too low, as in the case of physisorption materials, expensive and cumbersome cryogenic cooling is required to keep the hydrogen on the material. In spite of this, physisorption of hydrogen on solid-state materials shows promising properties such as high gravimetric storage, fast adsorption and desorption kinetics. Numerous high surface area microporous and mesoporous materials have been studied in this application. The adsorption mechanism is dominated by weak Van der Waals forces which have adsorption enthalpy between 4 – 10 kJ/mol. Typical materials, such as carbon nanotubes, fullerenes, and metal-organic frameworks (MOFs) possess very high surface areas and high hydrogen physisorption at cryogenic temperature, but their adsorption capacities at room temperature are limited due to the limited adsorption enthalpy. For example, Zuettel et al investigated the hydrogen storage capacities of 60 carbon samples under ambient conditions, resulting in reversible storage capacities in the 0.04 – 0.46 wt% range.[7] This is because the 4 – 10 kJ/mol binding enthalpies are too weak to hold the hydrogen to the surface under these conditions. Calculations have demonstrated that the ideal enthalpy for room temperature operation of a hydrogen storage system is 20 – 30 kJ/mol. Other research has indicated that 15-20 kJ/mol is a minimum requirement for room temperature hydrogen storage. For this reason many researchers are pursuing strategies to strengthen the interaction between the substrate and hydrogen. Many of these new approaches involve the use of σ-π H_2 complexes (i.e. the Kubas interaction) to bind the hydrogen to the active metal sites on the surface.[8] Hydrogen spillover using Pd is also thought to increase enthalpy of binding and this has been reviewed elsewhere.[9] The Kubas interaction stands midway between hydrides and physisorption in binding strength, and for this reason, may be ideal in

hydrogen storage systems designed for room temperature applications. The initial discovery of Kubas and many of the subsequent works in this area focus on stable dihydrogen organometallic complexes at ambient pressure and temperature, in which vacuum must be applied to remove the dihydrogen species. For mobile vehicle applications, hydrogen is preferred to be stored at moderate pressures of 50-100 bar. This allows for hydrogen to be released simply by opening a valve and reducing the pressure, rather than applying heat or vacuum. Thus compounds which possess stable dihydrogen ligands at room temperature and pressure may not be suitable for hydrogen storage, because these would require heat or vacuum to liberate the H_2. Unsaturated coordination metal species which exhibit Kubas interactions with multiple hydrogen molecules at ambient temperature and higher pressures are thus preferred.

In this report, we present recent developments in hydrogen adsorption and storage. Our focus is on new materials that exhibit higher adsorption enthalpies as well as some theoretical research on titanium decorated bulkyballs, nanotubes, and polymers. New MOFs containing unsaturated coordination metal sites and small pores, titanium materials and surface titanium species that exhibit high heat of adsorption exploiting the Kubas binding strategy will also be discussed, however a recent review focussing exclusively on MOFs has just appeared while this report was in progress.[10]

1.2 Carbon nanotube and fullerene modified materials

Carbon materials have been modified with many different species to improve the hydrogen uptake capacities. The strategy here is to decorate the surface with metal species that either add more binding sites, improve the adsorption capacity of the surface through electronic interactions, or both. Computational studies suggest that transition metal atoms, especially early metals in low oxidation states, can bind to fullerene C_{60} or $C_{48}B_{12}$ via the Kubas interaction to form stable media for hydrogen storage.[11] Y. Zhao et al[11a] proposed the formation of stable organo-scandium bulkyballs using Sc(0) as shown in Figure 1.1 (note: Sc(0) here becomes Sc(II) after oxidative addition of one dihydrogen to form a dihydride). In this hypothetical molecule each scandium species can bind up to 11 hydrogen atoms, ten of which are in the form of dihydrogen and can be adsorbed and desorbed reversibly. Species such as $C_{60}[ScH_2]_{12}$ and $C_{48}B_{12}[ScH]_{12}$ are stable and can

reversibly adsorb additional hydrogen, resulting in the uptake of 7.0 and 8.77 wt % hydrogen, respectively. The binding energies of hydrogen molecules to these adsorbates range within 0.3 – 0.4 eV (29 – 39 kJ/mol) which are suitable for ambient temperature applications. (Note: 1 eV/molecule is equivalent to 96.5 kJ/mol)

Scandium species are stable on the fullerene surface due to the binding energy of 2.8 eV. $C_{60}[ScH_2]_{12}$ can reversibly bind four dihydrogen molecules to one scandium atom (Figure 1.1) to form $C_{60}[ScH_2(H_2)_4]_{12}$, corresponding to 7.0 wt % hydrogen uptake capacity. The authors propose that modification of the carbon framework of the fullerene may lead to further storage benefits. Laser vaporization of graphite pellets containing boron nitride powder produces fullerenes in which one or more atoms in the hollow carbon cage are replaced by a boron atom.[12] This substitution doping leads to a decrease in material weight and enhancement of the stability. Boron atoms in the fullerene structure should also draw more charge from the scandium, or any other transition metal, resulting in an increase in binding energy between the Sc atom and the bulkyballs. In the case of $C_{48}B_{12}[ScH]_{12}$, the binding energy of Sc to the bulkyballs is 3.6 eV and each Sc can reversibly bind up to 5 hydrogen molecules to form $C_{48}B_{12}[ScH(H_2)_5]_{12}$, resulting in a reversible hydrogen uptake capacity of 8.77 wt%. This satisfies the ultimate DOE goal.

Table 1.1: Calculated consecutive binding energies of H_2 molecules (in eV/H_2). In the case of bulkyballs, twelve H_2 were added per calculation. (Reprinted with permission from [11a]. Copyright 2005, American Physical Society).

	1^{st} H_2	2^{nd} H_2	3^{rd} H_2	4^{th} H_2	5^{th} H_2
$Cp[ScH_2]$	0.29	0.28	0.46	0.23	
$C_{60}[ScH_2]_{12}$	0.30	0.35	0.42	0.26	
$C_{48}B_{12}[ScH_2]_{12}$	0.31	0.35	0.30	0.33	0.24

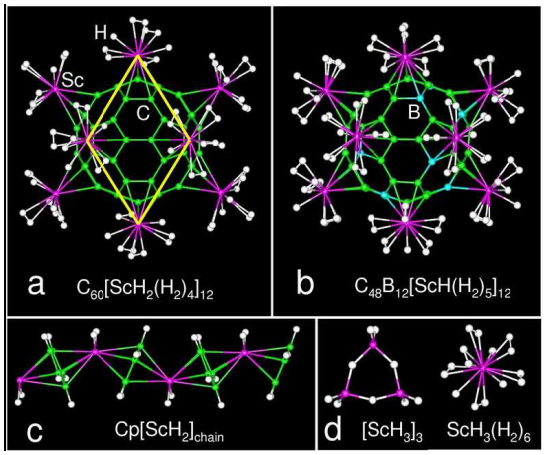

Figure 1.1: Optimized atomic structures of (a) $C_{60}[ScH_2(H_2)_4]_{12}$, (b)$C_{48}B_{12}[ScH(H_2)_5]_{12}$, (c) $Cp[ScH_2]$ chain, and (d) $[ScH_3]_3$ (left) and $ScH_3(H_2)_6$ (right). For clarity, only part of each buckyball is shown. A close-packed vdW solid formed from $C_{48}B_{12}[ScH(H_2)_5]_{12}$ would have a volumetric storage density of 43 kgH_2 m^{-3} even without consideration of the possibility of interlocking using the large open spaces indicated by the rhombus in (a). (Reprinted with permission from [11a]. Copyright 2005, American Physical Society).

While organo-scandium bulkyballs have yet to be synthesized, fullerenes doped with titanium, vanadium, niobium and tantalum have been synthesized via laser assisted vaporization of metals. Titanium and vanadium are able to bind directly to the fullerene structure via carbide bonding.[13] Fullerenes doped with titanium or vanadium seem to be stable whereas niobium and tantalum severely destabilize the fullerene structure. Mass spectroscopy studies on the $C_{60}V_x$ species synthesized at low laser intensities show that the cluster of $C_{60}V_{62}$, $C_{60}V_{73}$, and $C_{60}V_{86}$ are particularly stable. Similar species of $C_{60}Ti_x$ and $C_{70}Ti_x$ have been observed using titanium instead of vanadium. These materials are considered as possible candidates for hydrogen storage; however no data is yet available.

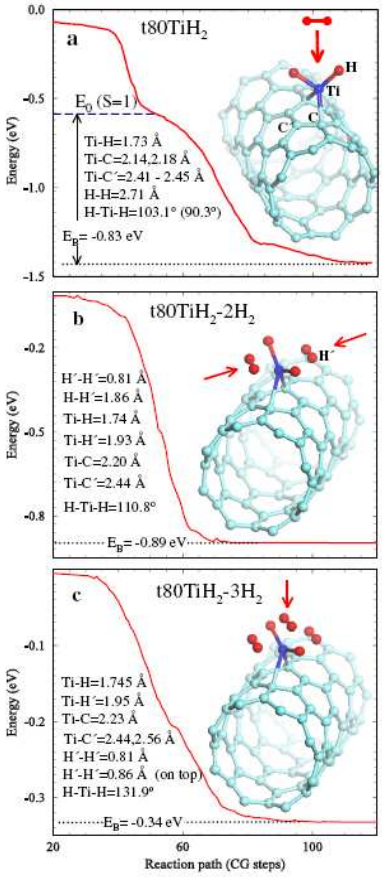

Figure 1.2: Energy vs reaction paths for successive dissociative and molecular adsorption of H_2 over a single Ti coated (8,0) nanotube. (a) H_2 + t80Ti $\rightarrow$ t80TiH_2. (b) $2H_2$ + t80TiH_2 $\rightarrow$ t80TiH_2 -$2H_2$. (c) H_2 + t80TiH_2-$2H_2$ $\rightarrow$ t80TiH_2-$3H_2$. The zero of energy is taken as the sum of the energies of the two reactants. The relevant bond distances and binding energies (E_B) are also given. (Reprinted with permission from [14]. Copyright 2005, American Physical Society).

Hydrogen adsorption on carbon nanotubes decorated with titanium atoms was studied computationally by Yildirim et at.[14] In this approach the nanotubes act as a scaffolding to support the Ti centers for Kubas binding of hydrogen. Calculations show a zero-energy barrier for adsorption. The first hydrogen molecule is dissociated to two hydrides by oxidative addition to the titanium. During this process, the H-H distance increases from 0.75Å to 2.71Å and the binding energy of hydrogen atom to titanium atom is 0.83 eV.

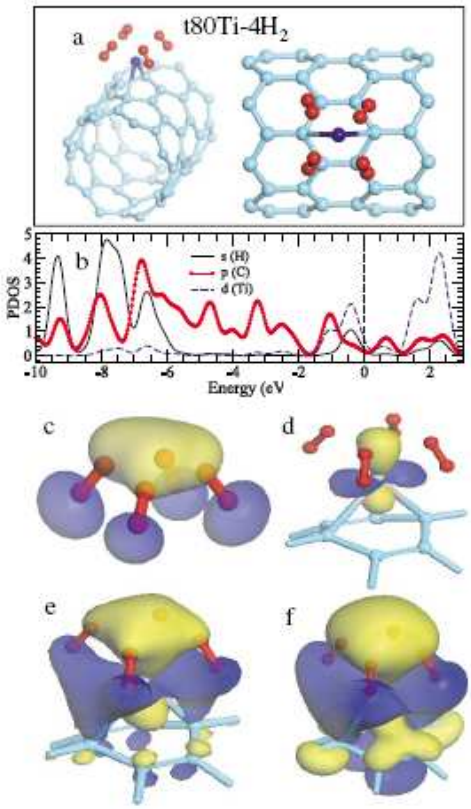

Figure 1.3: (a) Two different views of the optimized structure of t80Ti-4H_2. The relevant structural parameters are H-H = 0.84 Å, Ti-H = 1.9 Å, Ti-C = 2.17Å, Ti-C = 2.40 Å. (b) The PDOS at the Γ point contributed from Ti, four H_2 molecules, and the six carbons of the hexagon on which Ti and H_2 molecules are bonded. (c) The σ* antibonding orbital of the tetra H_2 complex; (d)–(f) isosurface of the state just below E_F at three different values: at ψ = 0.08 it is mainly Ti-*d* orbital; at ψ = 0.04 there is hybridization between the *d* orbital, two carbon π orbitals, and the 4H_2 σ* antibonding orbitals. At ψ = 0.02 it is clear that the other four carbon atoms are also involved in the bonding. (Reprinted with permission from [14]. Copyright 2005, American Physical Society).

The second, third, and fourth hydrogen molecules bind to titanium atom without dissociation in a Kubas type fashion. Calculations demonstrate that the system is stable until four hydrogen molecules are adsorbed. The H-H bonds elongate to 0.81 Å in the case of 2 adsorbed hydrogen molecules with adsorption energies of 0.45 eV/H_2, and to 0.86 Å in the case of 4 adsorbed molecules with adsorption energies of 0.34 eV/H_2. This strategy is thus similar to that above described for Sc coated fullerenes in that it uses a carbon support as a grafting site for Kubas binding of hydrogen.

Experimental preparations of transition metal decorated nanotubes have been carried out by vapor deposition, but it is not clear whether these would be ideal substrates for hydrogen storage. Using this technique, nanowires of Ti, Ni, and Pd were fabricated with widths of <10 nm and continuous length of up to tens of microns.[15] Metals were introduced into the nanotubes to increase the conduction properties or coated onto the nanotubes to create a thin metallic layer. Due to the weak interactions between the metal atoms and nanotube surface, the chemical vapour deposition technique tends to create discrete metallic nanoclusters rather than surface atomic species. For hydrogen storage applications, the metal centers should ideally exist on the nanotube surface in the atomic form and not as clusters in order to maximize the available binding sites for hydrogen adsorption.

1.3 Bis(titanium)ethylene complex

The binding abilities of metals to ethylene through σ donation have been widely studied.[16] Since ethylene is much lighter as a substrate than fullerenes or carbon nanotubes, it may represent an ideal support for metal binding for hydrogen storage systems exploiting the Kubas interaction. Main group metals and especially transition metals can bind to ethylene in several different ways. For example, calculations show that ethylene can complex with two lithium atoms to form a stable compound with a binding energy of 0.70 eV/Li. This complex exhibits a predicted hydrogen adsorption capacity of 16 wt % when each lithium atom adsorbs 2 hydrogen molecules. Durgun et al. performed calculations to show that a single ethylene molecule can form a stable complex with 2 titanium atoms.[17] This new molecule Ti_2-ethylene can adsorb up to ten hydrogen molecules according to calculation, reaching a gravimetric storage of 14 wt %. These high predicted capacities demonstrate that ethylene may indeed be a better support than C_{60} or nanotubes for this application.

The first hydrogen molecule is adsorbed dissociatively by each titanium atom to form the complex $C_2H_4(TiH_2)_2$ with a binding energy of 1.18 eV/H_2. Consecutive hydrogen molecules are adsorbed non-dissociatively around each titanium atom. When each titanium ligates two hydrogen molecules $C_2H_4(TiH_2\text{-}2H_2)_2$ forms with a binding energy of

0.38 eV/H_2 and an H-H bond length of 0.81 Å. A third hydrogen molecule is energetically favored to bind at the top side of the TiH_2 group with a binding energy of 0.40 eV and a 0.82 Å H-H bond lengths.

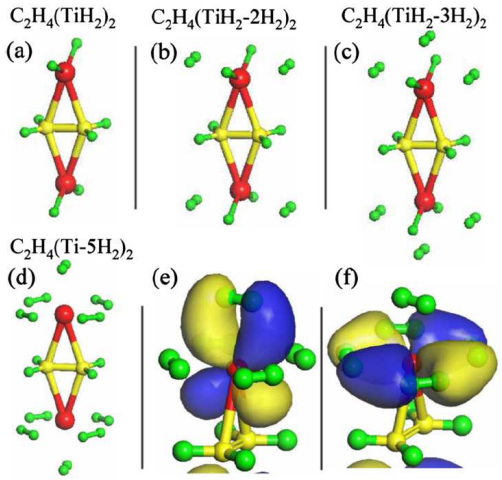

Figure 1.4: Atomic configurations of an ethylene molecule functionalized by two Ti atoms, holding (a) two dissociated H_2 molecules, (b) six H_2 molecules, and (c) eight H_2 molecules. Panel (d) shows a configuration where ten H2 molecules are bonded all as discrete ligands. Spin-polarized calculations gave energies (in eV) by 1.5, 0.37, 0.16, and 0.06 for the configurations shown in (a)–(d), respectively, suggesting a magnetic ground state in all cases with a moment of $\mu \approx 2\mu_B$. Panels (e) and (f) show the bonding orbital for the top (e) and side-on hydrogen ligands, respectively. Note that the hydrogen σ^*-antibonding orbitals are hybridized with Ti-*d* orbitals, suggesting Kubas interaction for the H_2-Ti bonding. (Reprinted with permission from [17]. Copyright 2006, American Physical Society).

Figure 1.4(d) proposes the adsorption of 5 hydrogen molecules per titanium atom, resulting in a hydrogen uptake capacity of 14 wt %. In all cases, the H-H bond of the adsorbed H_2 is elongated, consistent with the Kubas interaction scheme, and suggests the reversible adsorption of hydrogen on the adsorbent. While these molecules are encouraging from the standpoint of theory, the synthesis of such systems has remained elusive. These studies do, however, point in the direction of using anchored alkenes as binding sites on surfaces for low-coordinate metal species for hydrogen storage.

The binding of Ti to many other support materials other than ethylene and carbon nanotubes has also been studied by theory. Lee et al. proposed complexes of titanium with six different types of functional groups by first principle density functional electric

structure calculations (Table 1.2). The functional groups used were 2-mercaptoethyl sulfide, ethane-1,2-diol, acetylene, poly ether ether ketone (PEEK), benzo-nitril, and methyl-isocyanate. The results showed that each complex can reversibly bind up to 6 hydrogen molecules per titanium atom (figure 1.5).

Table 1.2: The calculated usable number of H_2 molecules of titanium decorated functional groups. (Reprinted with permission from [18]. Copyright 2006, Elservier).

Materials	Functional Moieties	N_{ads}	N_{des}	N_{use}/N_{max}
2-mercaptoethyl sulfide	Thiol	3.10	1.10	2.00/6
Ethane-1,2-diol	Hydroxyl	3.55	1.02	2.53/6
Acetylene	Alkynyl	4.00	3.95	0.05/5
Poly ether ether ketone	Carbonyl	4.99	4.17	0.82/6
Benzo-nitril	Nitril	4.10	3.95	0.15/6
Methyl-isocyanate	Isocyanate	5.00	3.73	1.27/6

N_{ads} and N_{des} are the numbers of adsorbed H_2 molecules per Ti under the conditions of adsorption (30 atm and 25 ^oC) and desorption (3 atm and 100 ^oC), respectively. N_{use} is the thermodynamical usable number of H_2 molecules obtained from $N_{ads} - N_{des}$. N_{max} is the maximum number of attachable H_2 ligands.

Titanium atoms were shown to bind in a stable manner with binding energies of the Ti atom to thiol, hydroxyl, alkynyl, carbonyl, nitrile, and isocyanate of 2.5, 3.0, 2.8, 2.1, 2.3, and 2.4 eV, respectively. In every case, each Ti adsorbed 5 – 6 hydrogen molecules non-dissociately with binding energies falling in the desirable range of 0.25 – 0.35 eV. This leads to a maximum gravimetric density of 13 wt % in the case of ethane 1,2 diol, with a reversible uptake of 5.5 wt % under ambient conditions. The non-dissociative hydrogen molecules are elongated in H-H length from 0.75 Å to ≈ 0.83 Å consistent with a Kubas-bonding mode. While many of these compounds may be very difficult to synthesize alone or as encapsulated species in zeolite cavities, this work does show that Kubas type complexes in stable ligand environments may be useful in on-board hydrogen storage applications at room temperature.

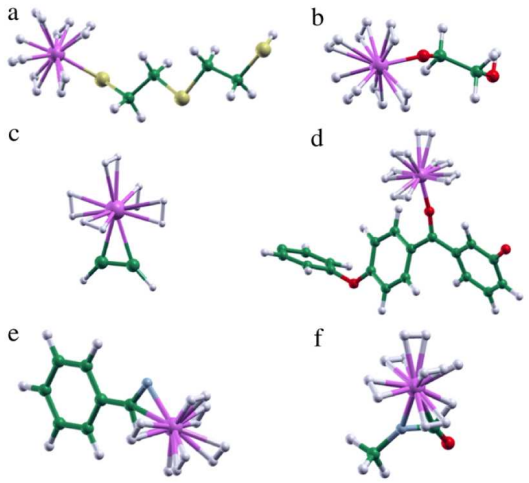

Figure 1.5: Atomic structures of Ti-functional group complexes with the maximum number of H_2 molecules attached. White, green, grey, red, yellow, and pink dots indicate the hydrogen, carbon, nitrogen, oxygen, sulfur, and titanium atoms, respectively. (a)–(f) Ti-functional group complexes with maximally adsorbed H_2 molecules in 2-mercaptoethyl sulfide, ethane-1,2-diol, acetylene, PEEK, benzo-nitrile, and methyl-isocyanate, respectively. (Reprinted with permission from [18]. Copyright 2006, Elsevier).

1.4 Titanium decorated polymers

Polymers are also possible substrates for hydrogen storage. For example, a microporous polymer based on the triptycene monomer can hold up to 2.7 % H_2 by mass at 10 bar and 77 K.[19] Polymers can also serve as excellent backbone materials to support active metal sites due to their rich and diverse functional moieties and relatively light constitution. Among the polymers considered in this application to date are trans- and cis-polyacetylene, polyaniline, polyphenol, poly para phenylene, and poly ether ether ketone, polypyrrole, polythiophene, polyvinyl alcohol, and carbon hydrate. Theoretical studies by Jisoon Ihm and co-workers show that simple polymers decorated with light transition metal atoms may be useful for hydrogen storage.[20] Cis-polyacetylene decorated with titanium atoms can adsorb up to 12 wt % of hydrogen. The formula for this material is $(C_4H_4{\cdot}2Ti{\cdot}10H_2)_n$. In this complex, hydrogen molecules bind to titanium atoms in a Kubas fashion with binding energies ranging from 0.42 – 0.58 eV, slightly higher than the binding energies of hydrogen molecules bound to titanium and scandium decorated nanotubes and bulkyballs.[11a, 14] Of the five adsorbed hydrogen per Ti, 3.16 hydrogen

molecules could be desorbed reversibly, resulting in 7.6 wt % practical storage capacity equivalent to 63 kg m^{-3} volumetric density. These figures are very promising and the synthesis of this material may be more practical than some of the molecular bound Ti systems proposed above.

1.5 Metal organic frameworks (MOFs)

Since MOF type materials were discovered, significant advances have been made in synthesis and design to optimize them for applications in adsorption and catalysis.[21] A few hundred MOF type materials have already been prepared with different morphologies, structures and compositions. Due to their high specific surface area, MOF materials have been studied for use in hydrogen storage.[4, 22] Promising hydrogen adsorption capacities of 6.5 % - 7.5 % have been achieved at cryogenic temperatures.[23] For example IRMOF-8 was thought to possess an adsorption capacity of 2 wt % at room temperature and 10 bar pressure [22] but later adsorption results from this research group at 77 K and 1 bar on IRMOF-8 possessing a BET of 1466 m^2 g^{-1} only demonstrated an adsorption capacity of 0.74 wt %.[24] Most MOF materials have adsorption capacities in the range of 0 – 1.0 wt % at room temperature, which are too low for practical interest.[25]

Because of this, researchers have attempted to enhance the hydrogen adsorption capacities of MOFs by different methods including impregnation, doping, ion exchange, increasing hydrogen uptake by spillover, narrowing pore size, and the fabrication of new MOF materials with unsaturated coordination metal centers.[26-32] Two main ways to significantly enhance the adsorption capacities have been pursued. The first is narrowing the materials' pore size to allow hydrogen molecules to interact with more than one wall of the material and hence improves its binding. For example, the microporous coordination solid $Mg_3(O_2C\text{-}C_{10}H_6\text{-}CO_2)_3$ possesses hydrogen binding energy up to 9.5 kJ/mol.[29] The second method is the synthesis of MOF materials with different coordinative unsaturated metals incorporated in the structure for use as binding centers via metal – H_2 interactions.[30 - 32] An extensive review focus on hydrogen storage on MOFs with exposed metal centers has just been published.[10] According to the adsorption analysis from Bhatia and Myers, for ambient temperature storage and delivery of hydrogen at a pressure between 30 and 1.5 bar, the optimal adsorption enthalpy should be

close to 15.1 kJ/mol.[33] This is somewhat different from the calculation results from Zhao et al regarding the ideal adsorption enthalpy range of 20 – 30 kJ/mol.[11] MOFs with Ni and Mn in the framework have been developed for hydrogen storage because these metals exhibit superior binding with hydrogen. The heat of adsorption increased from typically 4 – 7 kJ/mol in a standard MOF up to around 10 kJ/mol on inclusion of these metals. Although these values still fall short of the target enthalpies for room temperature application, these results demonstrate that modification of the MOF structure can lead to enhanced hydrogen uptake capacities through what appears to be the Kubas interaction. This result is also important because it shows that surface area is not the only important factor in hydrogen binding to porous materials.

1.5.1 Hydrogen storage on novel MOF-74

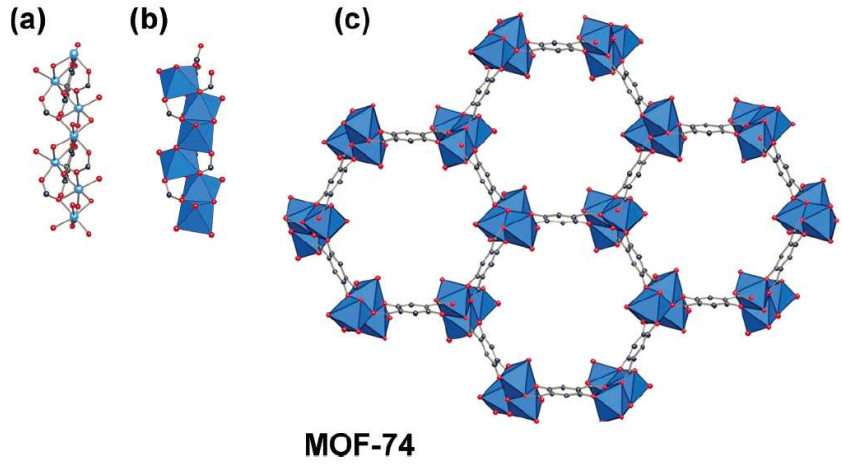

Figure 1.6: MOF-74: ball-and-stick representation of SBU (a); SBU with Zn shown as polyhedra (b); and view of crystalline framework with inorganic SBUs linked together via the benzene ring of 2,5-dihydroxybenzene-1,4-dicarboxylate (c) (DMF and H_2O guest molecules have been omitted for clarity). (Reprinted with permission from [34]. Copyright 2005, American Chemical Society).

MOF-74 is included in this review because of its structure, which features open Zn^{2+} sites (figure 1.6a) which enhance the hydrogen adsorbed by the framework.[34]

Figure 1.7 shows the hydrogen adsorption on MOF-74 and the isoteric heat of hydrogen adsorption.[28] At low surface coverage, MOF-74 exhibits an adsorption enthalpy of ≈8.8 kJ/mol, the highest value amongst MOF materials containing Zn. Inelastic neutron

scattering studies at 4 K and 60 K suggest strong bonding between hydrogen molecules toward the Zn^{2+} centers without dissociation.[35] Similar inelastic neutron scattering evidence was observed on the Cu^{2+} center in HKUST-1 materials,[36a] and the Cu^{+} center of Cu-exchanged ZSM-5, which shows a maximum adsorption capacity of 0.57 H_2/Cu at 298 K and 14 bar.[36b-d]

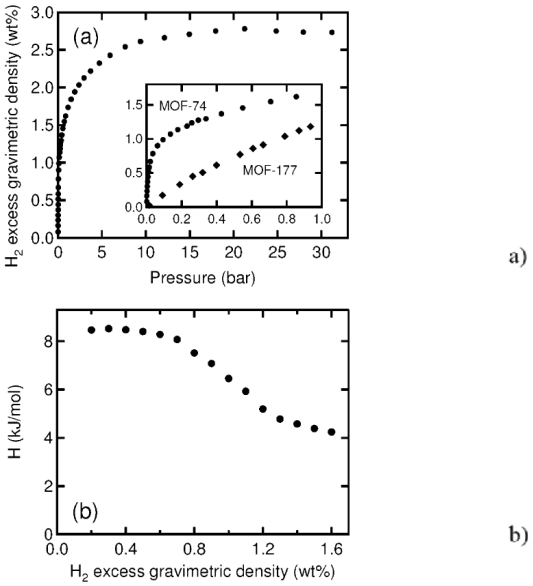

Figure 1.7: H_2 Isotherm measurements on MOF-74. (a) The H_2 adsorption/desorption isotherms at 77 K. The inset compares the H_2 adsorption isotherms for MOF-74 and MOF-177. (b) The H_2 adsorption enthalpy of MOF-74 is shown with an initial H_2 adsorption enthalpy of ≈ 8.8 kJ/mol. (Reprinted with permission from [28]. Copyright 2008, American Chemical Society).

1. 5. 2 Hydrogen storage on microporous metal – organic frameworks incorporating 1,4-benzeneditetrazolate (BDT^{2-})

MOF materials which employ microporous frameworks along with unsaturated metal centers for Kubas binding have also been developed.[30-32, 37] Materials obtained from this synthetic strategy enhance the hydrogen uptake capacity at room temperature not only by increasing the interactions between hydrogen molecules and the material walls, but also by the higher adsorption enthalpy of hydrogen on the unsaturated metal sites. Reaction between H_2BDT with hydrated salts of Mn^{2+}, Zn^{2+} in the mixture of N,N – diethylformamide (DEF) and methanol produces the porous, three-dimensional framework solids $Zn_3(BDT)_3(DMF)_4(H_2O)_2 \cdot 3.5CH_3\text{-}OH$ (3),

$Mn_3(BDT)_3(DMF)_4(H_2O)_2{\cdot}3CH_3OH{\cdot}2H_2O{\cdot}DMF$ (4), $Mn_2(BDT)Cl_2(DMF)_2{\cdot}1.5CH_3OH{\cdot}H_2O$ (5). When solvent is removed under mild conditions, these materials exhibit permanent porosity, with BET surface areas between 200 – 640 $m^2\ g^{-1}$ and show 0.82 – 1.46 wt % of hydrogen adsorption at 77 K and 1 atm with an H_2 binding enthalpy of 6.0 – 8.8 kJ mol^{-1}.

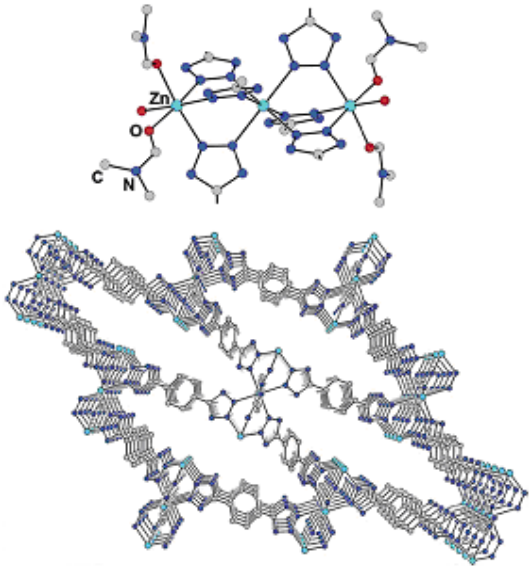

Figure 1.8: Portions of the crystal structure of 3, showing the trinuclear Zn_3 building units (upper) and, upon removing the DMF and water ligands, the arrangement of channels along the [001] direction. Hydrogen atoms and solvate guest molecules are omitted for clarity. Selected mean interatomic distances (Å) and angles (deg) from the isotypic structures of 3 (M) Zn) and 4 (M) Mn), respectively: M-O, 2.08(4), 2.15(4); M-N, 2.15(3), 2.25(2); M···M, 3.763, 3.951; N-M-N, 90(3), 89(3); O-M-O, 90(2), 90-(2); M-N-N, 125(3), 125(2). (Reprinted with permission from [30]. Copyright 2006, American Chemical Society).

These materials possess three dimensional structures containing metal units linked via BDT^{2-} bridges to form neutral materials. Compounds (3) and (4) are isomorphous and the metals adopt a linear bonding mode with the BDT^{2-} bridges, while in material (5), Mn^{2+} possesses an octahedral geometry and the structure features a 19.6 Å wide one dimensional channel along [100] direction.

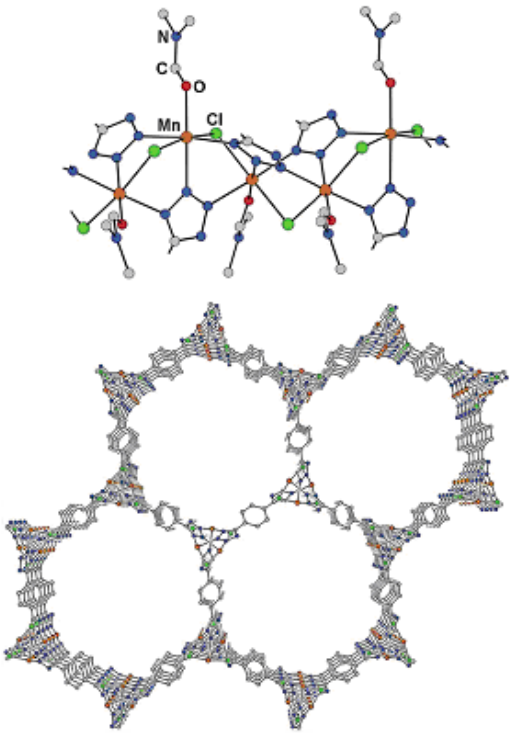

Figure 1.9: Portions of the crystal structure of 5, showing part of the infinite helical chains composed of Mn^{2+} and Cl^- ions (upper) and, upon removing the DMF molecules, the one-dimensional channels formed along the [001] direction (lower). Hydrogen atoms and guest solvent molecules are also omitted for clarity. Selected mean interatomic distances (Å) and angles (deg): Mn-Cl, 2.51(1); Mn-O, 2.139(1); Mn-N, 2.29(2); Mn···Mn, 3.759-(1); Cl-Mn-N, 88(3); Mn-N-N, 117(19); Mn-Cl-Mn, 93(4). (Reprinted with permission from [30]. Copyright 2006, American Chemical Society).

At 77 K and 880 torr, the adsorption capacites are 1.46 wt % for (3) – $Zn_3(BDT)_3$; 0.97 wt % for (4) – $Mn_3(BDT)_3$; and 0.82 wt % for (5) – $Mn_2(BDT)Cl_2$. The three adsorption curves are steep at low pressure; reflecting the strong binding of hydrogen toward the coordinatively unsaturated metal centers. The heats of adsorption range from 6.8 – 8.7 kJ mol^{-1} for $Zn_3(BDT)_3$; 6.3 – 8.4 kJ mol^{-1} for $Mn_3(BDT)_3$; and 6.8 – 8.8 kJ mol^{-1} for $Mn_2(BDT)Cl_2$. These values are comparable with the heat of adsorption on MOF-74 and are much higher than those for MOF-5 and carbon.[38, 39]

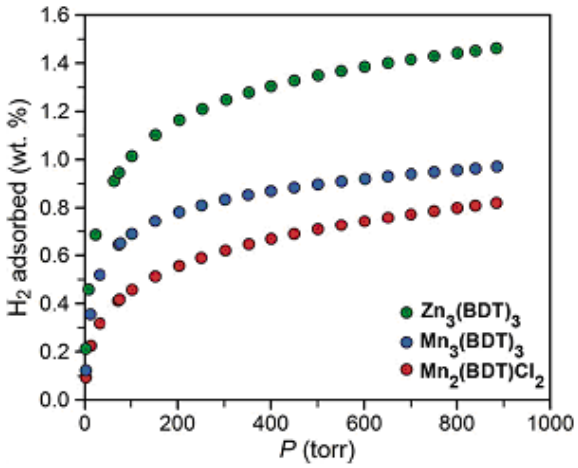

Figure 1.10: Adsorption isotherms for the H_2 uptake in desolvated samples of 3 (dark green circles), 4 (blue circles), and 5 (red circles) at 77 K. (Reprinted with permission from [30]. Copyright 2006, American Chemical Society).

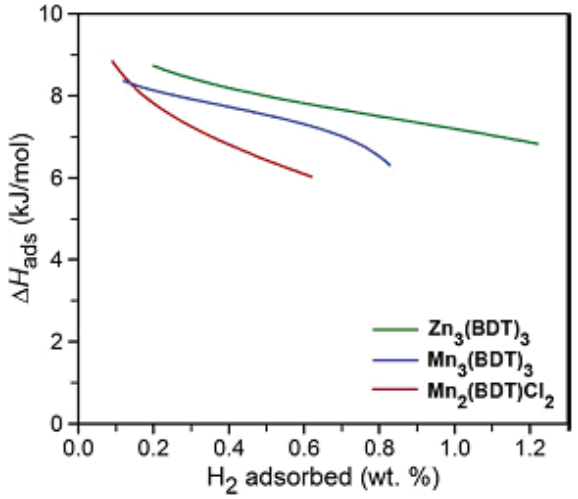

Figure 1.11: Enthalpy of adsorption plots as a function of the uptake of H_2 in desolvated samples of 3 (dark green), 4 (blue), and 5 (red). (Reprinted with permission from [30]. Copyright 2006, American Chemical Society).

1. 5. 3 Hydrogen storage on microporous metal – organic frameworks incorporating 1,3,5-benzenetritetrazolate (BTT^{3-})

By using different bridging ligands, new MOF materials $[Mn(DMF)_6]_3[(Mn_4Cl)_3(BTT)_8(H_2O)_{12}]_2 \cdot 42DMF \cdot 11H_2O \cdot 20CH_3OH$ (1), and $[Mn(CH_3OH)_6]_3[(Mn_4Cl)_3(BTT)_8(CH_3OH)_{12}]_2 \cdot 42CH_3OH$ (1m), based on Mn^{2+} and BTT^{3-} as linkers were prepared.[31] After (1) and (1m) were desolvated material (1') and (1m')

were obtained with the formulas of $[Mn(DMF)_6]_3[(Mn_4Cl)_3(BTT)_8(DMF)_{12}]_2$ and $Mn_3[(Mn_4Cl)_3(BTT)_8(CH_3OH)_{10}]_2$ and specific surface areas of 1100 and 2100 m^2/g, respectively.

XRD studies elucidated the structure of (1) as shown below.

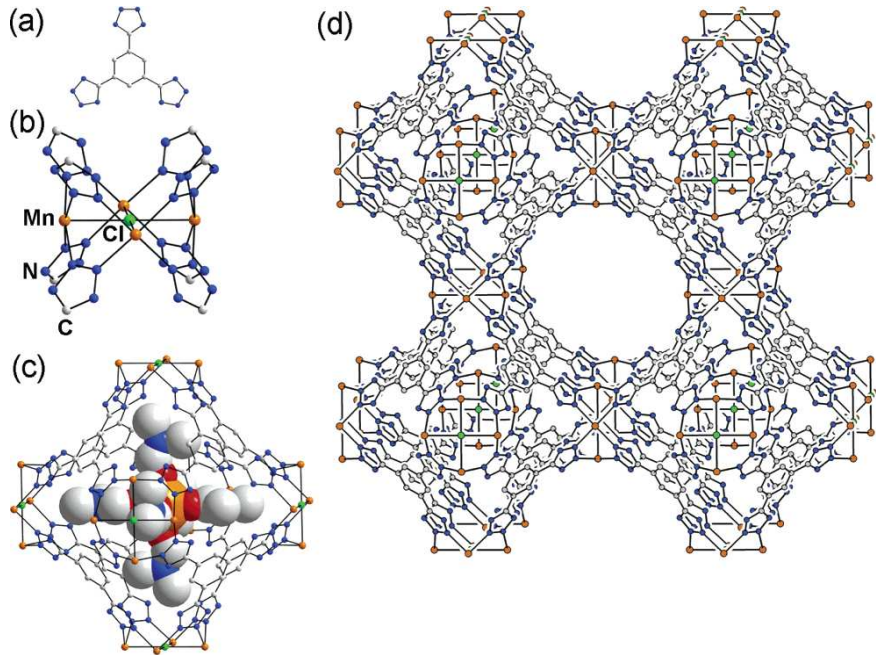

Figure 1.12: Crystal Structure of (1). (a) molecular structure of the tritopic ligand H3BTT, (b) a square-planar Mn_4Cl cluster surrounded by eight tetrazolate rings, (c) a sodalite cage-like unit encasing a $[Mn(DMF)_6]^{2+}$ complex, and (d) a cube of eight such units sharing square Mn_4Cl faces. Hydrogen atoms and solvent molecules are omitted for clarity. Selected interatomic distances (Å) and angles (°): Mn-Cl 2.736(1), Mn-N 2.227(3), Mn···Mn 3.869-(2), Mn-Cl-Mn 90.0, N-Mn-N 87.6(1), 91.4(1), Mn-N-N 125.3(2). (Reprinted with permission from [31]. Copyright 2006, American Chemical Society).

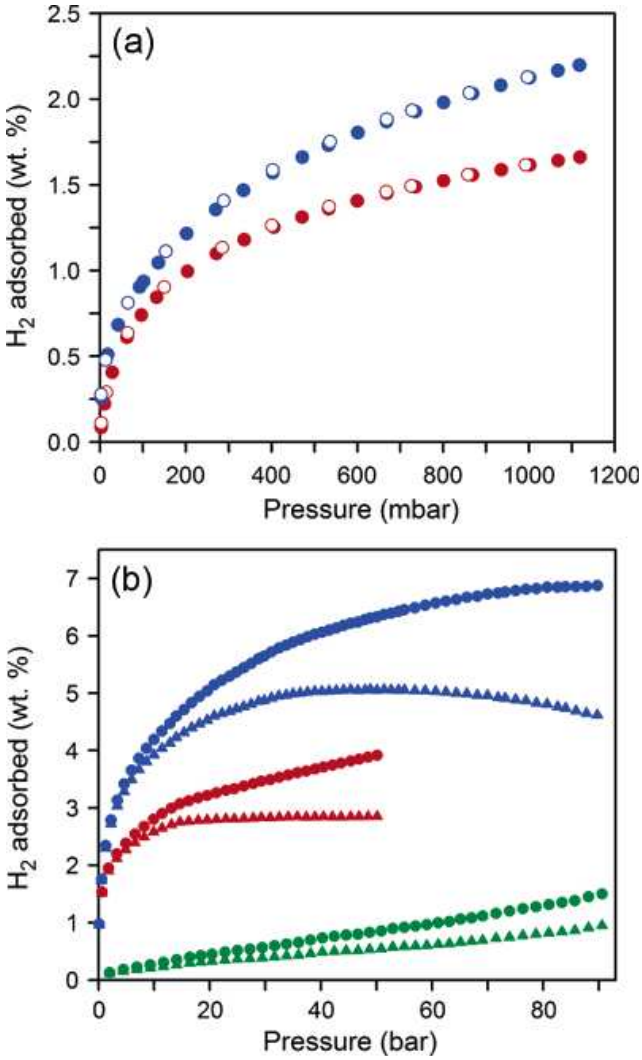

Figure 1.13: H_2 adsorption isotherms (a) below 1.2 bar and (b) up to 90 bar within 1' (red) and 1m' (blue) at 77 K, and within 1m' at 298 K (green). Triangles and circles represent excess and total H_2 adsorption, respectively, while filled and open symbols represent adsorption and desorption data, respectively. (Reprinted with permission from [31]. Copyright 2006, American Chemical Society).

At 77 K, material (1') exhibitted 3.9 wt % hydrogen uptake capacity at 50 bar and 6.9 wt % for material (1') at 90 bar, resulting in a volumetric excess adsorption of 43 kg m^{-3} and total volumetric uptake of 60 kg m^{-3}, the highest value for any physisorption material ever reported. Unlike other MOFs,[40] this material shows no hysteresis in the adsorption-desorption cycle. At 298 K, material (1m') adsorbs up to 0.95 wt % at 90 bar.

Due to the strong interaction of unsaturated coordination Mn^{2+} sites with hydrogen, the heat of adsorption of (1m') reaches 10.1 kJ mol^{-1}, suggesting some contribution from

Kubas bonding of hydrogen molecules to the adsorption sites. Neutron powder diffraction revealed that hydrogen molecules interact directly in a stable fashion with Mn centers in the framework. Similar evidence has been observed on the Cu^{2+} active sites in the related material HKUST-1[36b] as well as cation-exchanged Mn^{2+} MOFs that will be discussed below.

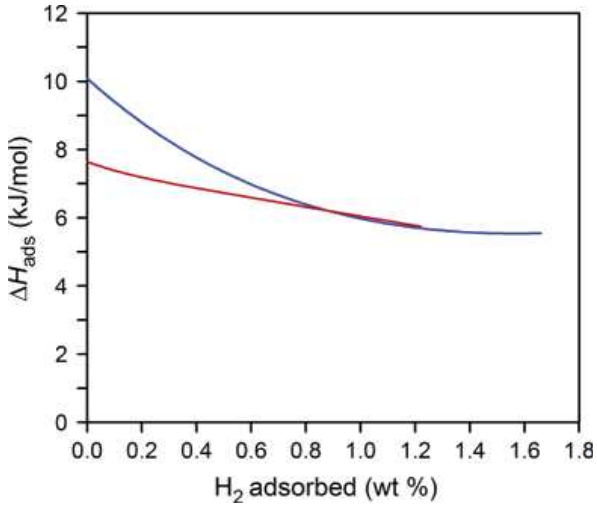

Figure 1.14: Isosteric heat of adsorption curves for H_2 uptake in 1' (red) and 1m' (blue). (Reprinted with permission from [31]. Copyright 2006, American Chemical Society).

The guest Mn^{2+} in $Mn_3[(Mn_4Cl)_3(BTT)_8(CH_3OH)_{10}]_2$ can be exchanged by different cations as described in table 1.3 below. Different adsorption capacities of the cation exchanged materials reflect the role of these unsaturated metal centers in the framework. The Co^{2+} exchanged material has an adsorption enthalpy up to 10.5 kJ mol^{-1} while materials exchanged with later transition metals such as Ni^{2+}, Cu^{2+}, Zn^{2+} have lower adsorption enthalpies as well as lower adsorption capacities. Late transition metals have weaker interaction with hydrogen molecules due to the increase in effective nuclear charge shrinking the d-orbitals and thus disrupting the back-bonding interaction toward hydrogen and causing the (η^2-H_2)-metal interaction to become less favourable. This trend very clearly illustrates the role of Kubas binding in increasing the overall binding enthalpies as well as the adsorption capacities of these materials. New framework solids are being synthesized every year that exploit this interaction. For example, in 2008 an MOF possessing a binding enthalpy of 13.5 kJ/mol was synthesized.[41] This is the highest binding enthalpy recorded to date for an MOF material. The structure features exposed

Ni^{2+} as binding sites and can adsorb significant amount of hydrogen at 180 K. This demonstrates that the higher enthalpies do indeed lead to adsorption at higher temperatures. In situ IR revealed the formation of $Ni^{2+}\cdots H_2$ complex with high intensities.

Table 1.3: Composition and gas sorption properties of cation-exchanged compounds 1-M. (Reprinted with permission from [32]. Copyright 2007, American Chemical Society).

Comp	Formula	M/Mn ratio (expt/found)	$N_{2\ ads}$ (cm_3/g)[c]	SA_{BET} (m^2/g)	SA_{Lang} (m^2/g)	H_2 ads (wt%)[d]	ΔH_{ads} (kJ/mol)[e]	Color before/after desolvation.
1-Mn^{2+}	$Mn_3[(Mn_4Cl)_3(BTT)_8]_2$	N/A	547	2057	2230	2.23	5.5-10.1	Colorless/colorless
1-Fe^{2+}	$Fe_3[(Mn_4Cl)_3(BTT)_8]_2\cdot FeCl_2$	0.169/0.170	542	2033	2201	2.21	5.5-10.2	Lt.green/brown
1-Co^{2+}	$Co_3[(Mn_4Cl)_3(BTT)_8]_2\cdot 1.7CoCl_2$	0.210/0.210	563	2096	2268	2.12	5.6-10.5	Pink/dk.blue
1-Ni^{2+}	$Ni_{2.75}Mn_{0.25}[(Mn_4Cl)_3(BTT)_8]_2$	0.121/0.121	554	2110	2282	2.29	5.2-9.1	Lt.blue/brown
1-Cu^{2+}	$Cu_3[(Cu_{2.9}Mn_{1.1}Cl)_3(BTT)_8]_2\cdot 2CuCl_2$	3.925/3.999	500	1695	1778	2.02	6.0-8.5	Dk.green/black
1-Zn^{2+}	$Zn_3[(Zn_{0.7}Mn_{3.3}Cl)_3(BTT)_8]_2\cdot 2ZnCl_2$	0.553/0.546	508	1927	2079	2.10	5.5-9.6	Colorless/colorless
1-Li^{+}	$Li_{3.2}Mn_{1.4}[(Mn_4Cl)_3(BTT)_8]_2\cdot 0.4LiCl$	0.017/0.017	530	1904	2057	2.06	5.4-8.9	Colorless/colorless
1-Cu^{+}	$Mn_3[(Mn_4Cl)_3(BTT)_8]_2\cdot 0.75CuPF_6$	N/A	518	1911	2072	2.00	5.6-9.9	Colorless/colorless

a Based on the relative ration of M^{n+}/Mn^{2+} as determined using ICP-AA and on C, H, and N analysis. b For simplicity, guest solvents are obmitted from these formulas. c Obtained at 77K and 760 torr. d Obtained at 77K and 760 torr. e Determined using a virial fit to the 77 and 87K H_2 adsorption isotherms.

1.6 Pure and modified mesoporous titanium oxide

Titanium materials have also been considered as hydrogen storage materials due to the the potential for a strong interaction between hydrogen and titanium. Titanium oxide which contains as high as 59.93 wt % of Ti can be synthesized with different structures, morphologies, pore sizes and large surface areas. Moreover, the Ti centers on the surface can be reduced by different chemical agents to populate d-orbitals on these centers and thus enhance binding to hydrogen.

The hydrogen adsorption performance of titanate nanotubes were studied.[42] These materials exhibit an adsorption capacity of up to 3.8 wt % at 77 K and 6 bar. However, large hysteresis was observed due to clatharate formation in the titanate material. The adsorbed hydrogen is only completely released at 200 ^oC and it takes several hours for the materials to reach adsorption equilibration.

In another study, microporous and mesoporous titanium oxide with pore sizes ranging from 12 – 26 Å were synthesized by neutral amine templating agents.[43] These materials were then studied for hydrogen adsorption.[44] This material is special in that it can be readily reduced by alkali metals or bis(toluene)titanium to leave low valent metal centers on the vast internal surface area of up to 1200 m^2/g. In the pristine micro- or mesoporous titanium oxide, the titanium atoms have empty t_{2g} orbitals thus they are not expected to form a stable interaction with hydrogen. But when these centers are reduced, a Kubas type interaction becomes possible. Thus, reduction of the 12-electron MX_4L_2 Ti octahedra leads to population of the t_{2g} set and more effective π back bonding to the H_2 molecules. The different binding modes for hydrogen are shown in Figure 1.15.

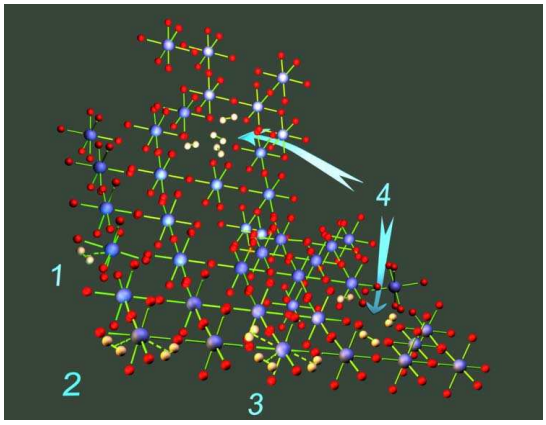

Figure 1.15: Schematic representation of H_2 binding sites in the monolayer wall of micro-and mesoporous titanium materials, where 1, 2, and 3 refer to mono, bis, and tris dihydrogen complexes, respectively, and 4 represents the compressed gas phase in the porous voids in the solid. (Reprinted with permission from [44]. Copyright 2006, American Chemical Society).

Pristine microporous titanium oxide was reduced by the following reducing agents in the liquid phase: Li-naphthalene, Na-naphthalene, and bis(toluene) titanium. XPS studies on these reduced samples exhibit a trend in decreasing binding energies of the Ti 3p 1/2 emmission from 37.9 eV in the case of pristine material to 36.8; 36.4; and 15.1 eV, respectively.[43] The volumetric hydrogen uptake capacities increased with decreasing surface titanium oxidation state from 29.37 kg/m^3 at 77 K and 100 atm to 31.10 kg/m^3, 31.58 kg/m^3, and 40.46 kg/m^3, respectively.

While these numbers are not staggering, the dramatic increase of the volumetric capacity on reduction with bis(toluene) Ti demonstrates that surface reduction leads to an increase in hydrogen adsorption capacity (Figure 1.16). The material reduced with bis(toluene)-titanium has the lowest surface area, but the highest capacities, demonstrating once again that surface area is not the only important factor in cryogenic hydrogen storage.

The most interesting find in this study was the trend in enthalpies with reduction and surface coverage (Figure 1.17). While pristine titanium exhibits pure physisorption toward hydrogen with a heat of adsorption ranging from 3.0 – 4.2 kJ/mol decreasing as surface coverage increases, consistent with physisorption, the heat of adsorption measured for all reduced samples actually *increases* with surface coverage. This is highly unusual behavior and suggests a contribution from some other binding mechanism than physisorption, possibly Kubas binding. Also, as the oxidation state of the surface titanium decreases, the heat of adsorption increases. In the case of the bis(toluene)-titanium reduced sample, the adsorption enthalpies rise to 8.02 kJ/mol.

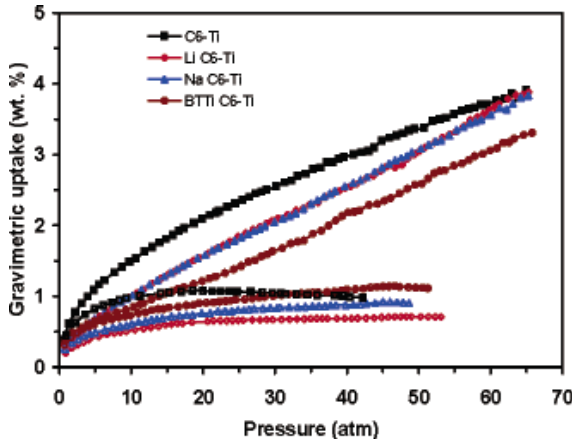

Figure 1.16: High-pressure H_2 isotherms for pristine and reduced microporous titanium oxides synthesized using hexylamine as the template at 77 K in gravimetric uptake. Filled markers represent storage capacity and open markers denote adsorption capacity. (Reprinted with permission from [44]. Copyright 2006, American Chemical Society).

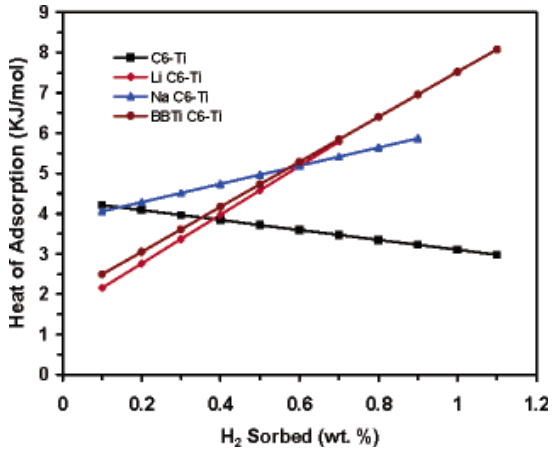

Figure 1.17: Enthalpy of H_2 adsorption for pristine and reduced microporous titanium oxides synthesized using hexylamine as the template. (Reprinted with permission from [44]. Copyright 2006, American Chemical Society).

Similar unusual rising enthalpy trends (Figue 1.18) are observed when microporous titanium oxide is treated with early transition metal organometallic sandwich compounds.[45] Thus, when microporous titanium oxide synthesized using a hexylamine template was reduced with excess bis(benzene)chromium, bis(benzene)vanadium, bis(cyclopentadienyl)chromium, or bis(cyclopentadienyl)vanadium, the resulting materials exhibit better storage capacities than the pristine material, from 29.37 kg/m^3 to 31.61 kg/m^3, 33.42 kg/m^3, 30.49 kg/m^3, and 30.30 kg/m^3 at 77 K and 100 atm, respectively for these reagents.

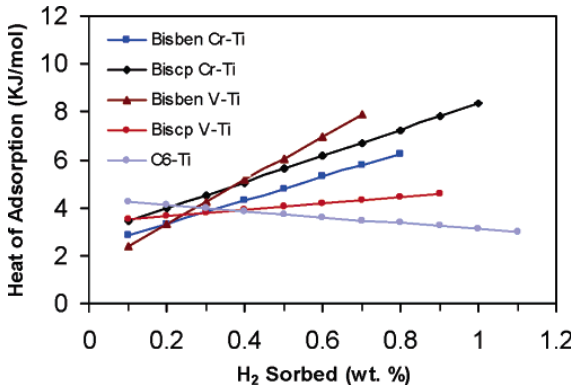

Figure 1.18: Enthalpy of H_2 adsorption for pristine and reduced microporous titanium oxides. (Reprinted with permission from [45]. Copyright 2007, American Chemical Society).

The binding sites in these materials are likely a mixture of the deposited metal fragments and the reduced Ti centers (a mixture of Ti (III) and Ti(IV) by XPS) on the wall.[46] Mesoporous Ti oxide was also treated with Li and Na fullerides in order to reduce the surface of the Ti oxide and allow for Kubas binding, while also eliminating much of the void space in the pores and replacing it with fullerene binding sites.[47] There is also the potential for hydrogen interacting with the Ti oxide walls and the fulleride in a similar fashion as proposed for microporous MOFs discussed earlier. These materials showed a disappointing drop in storage capacity of 27.35 kg/m^3 from 29.37 kg/m^3 at 77 K and 100 atm, however the same trend of rising enthalpies with all materials containing low valent Ti was observed. The Na-Na_3C_{60}Ti sample, formed by further reducing the mesoporous titanium oxide intercalated with Na_3C_{60} in the void space with excess Na-napthalene, achieved the highest heat of adsorption of 6.55 kJ/mol[1].

These studies demonstrate that surface area is not the only important factor in cryogenic hydrogen storage and that binding of hydrogen increases with oxidation state of Ti, as long as this factor is not offset by other parameters. It also demonstrates that a rise in enthalpy on surface coverage occurs whenever there is a transition metal with d-electrons on the surface. The reason for this rise is not yet understood, but calculations by Yildirim discussed earlier predict an increase in binding enthalpy with increasing hydrogen ligation in Kubas compounds with multiple H_2 ligands. Whether this is the reason for the rising enthalpy or not will require more research.

1.7 Surface titanium materials in hydrogen adsorption and storage

While the above system served as a model to confirm the relation between surface reduction of Ti and hydrogen binding capacity, XPS studies showed that the majority of Ti atoms are still in the (IV) oxidation state and therefore unable to bind hydrogen directly.[44] It is also likely that these centers are beneath the surface of the walls and would be inaccessible even if they were reduced to lower oxidation states. For these reasons, a new titanium supported system was developed, based on mesoporous silica.[48] Silica represents a more effective support because it is inexpensive, lower weight than titania, and has a higher surface area than porous titanium oxides. Moreover, the number

of hydroxyl groups on the surface can be controlled [49] and these can act as anchoring sites for organometallic Ti centers with tunable oxidation states and coordination geometries.

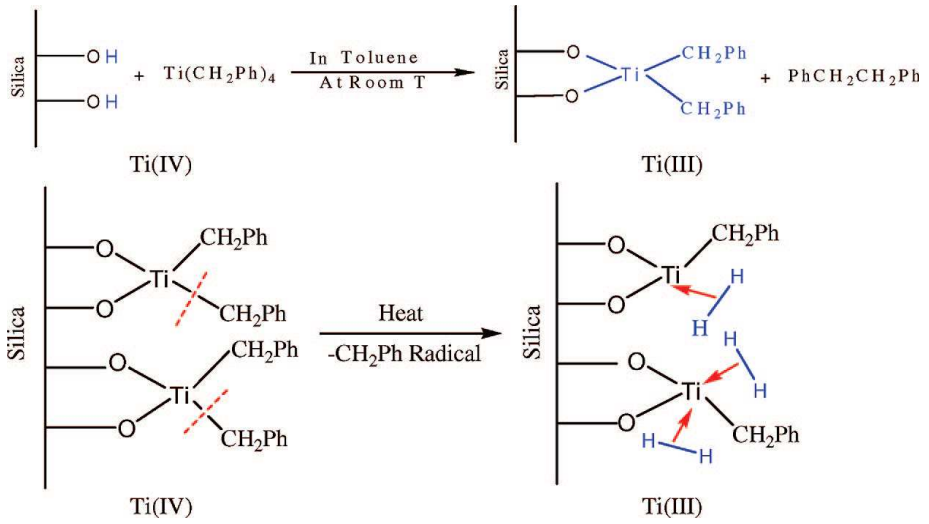

Scheme 1.1: Schematic representation of the grafting of benzyl Ti species onto the surface of mesoporous silica and the subsequent formation of tunable low-coordinate H_2 binding sites with enthalpies of 23 kJ/mol. (Reprinted with permission from [48]. Copyright 2008, American Chemical Society).

Tetrabenzyltitanium was anchored on the surface of mesoporous silica (Scheme 1.1), resulting in the formation of four coordinate Ti(IV) species on the surface which were determined to be a mixture between tribenzyl siloxy and dibenzyl disiloxy complexes.[48, 50] Heating the materials at 180 ^{o}C results in the reductive cleavage of the Ti benzyl bond and expulsion of benzyl radicals which then couple and are subsequently removed in vacuo. This leaves Ti(III) benzyl species behind on the surface which can now exhibit stable Kubas interaction with hydrogen because of the Ti d electron.

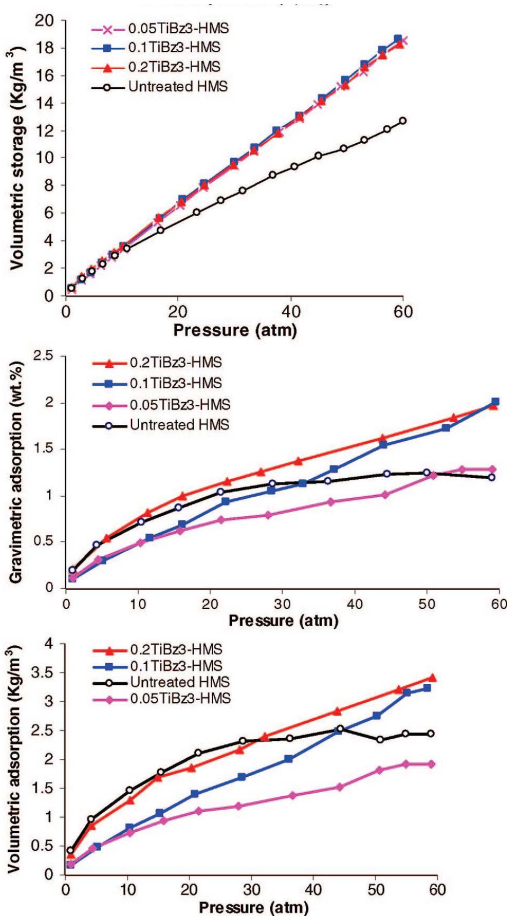

Figure 1.19: Hydrogen adsorption and storage isotherms at 77 K for mesoporous silica treated with various molar equivalents of tribenzyl titanium. Note that for the adsorption isotherms the untreated silica sample reaches saturation but all treated samples do not. (Reprinted with permission from [48]. Copyright 2008, American Chemical Society).

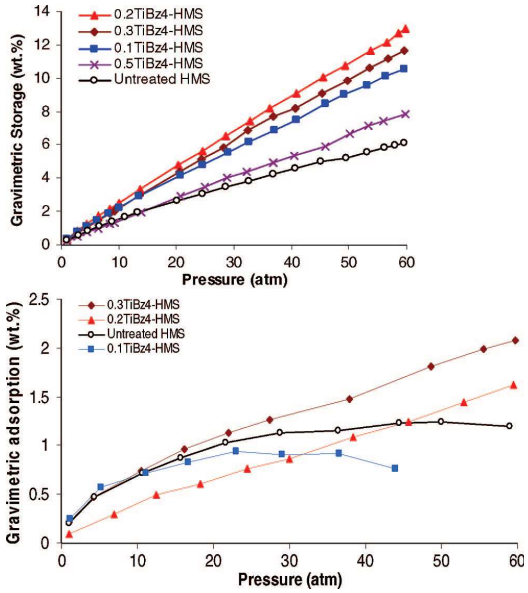

Figure 1.20: Hydrogen storage isotherms at 77 K for mesoporous silica treated with various molar equivalents of tetrabenzyl titanium: (a) gravimetric storage density; (b) gravimetric adsorption (excess storage) density. Slight fluctuations at higher pressure in some adsorption isotherms were not related to temperature fluctuations, as this parameter was strictly controlled. (Reprinted with permission from [48]. Copyright 2008, American Chemical Society).

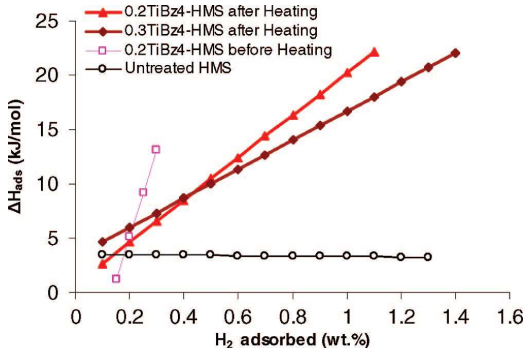

Figure 1.21: Hydrogen binding enthalpies. Pristine silica (black), the 0.2 molar equiv tetrabenzyltitanium material after heating at 180 °C (red), the 0.3 molar equiv tetrabenzyltitanium material after heating at 180 °C (brown), and the 0.2 molar equiv tetrabenzyltitanium material before heating (pink). (Reprinted with permission from [48]. Copyright 2008, American Chemical Society).

According to the 18 electron rule, each Ti(III) species can adsorb up to 5 hydrogen molecules. A series of Ti (III) grafted samples with various Ti/Si molar ratio of 0.05; 0.10; and 0.20 (ca. 5 wt % Ti) were prepared and exhibited adsorption capacities of 1.38 wt %, 1.99 wt % and 2.02 wt % at 77 K and 60 atm in comparison with silica precursor at 1.21 wt %. The volumetric storage capacity at 77 K and 100 atm on these treated samples increases to 30.67 kg/m^3; 31.14 kg/m^3 and 30.27 kg/m^3, respectively, from just 20.34 kg/m^3 storage capacity of silica. At 60 atm and 77 K, there are 2.7 H_2 molecules per Ti atom, short of the maximum 5 H_2 molecules that can be reached according to the 18 electron rule. This non-integer number suggests an equilibrium between several different species with different numbers of dihydrogen ligands. The adsorption isotherms of these treated samples do not saturate at 60 atm and continue increasing, reflecting that more hydrogen molecules can be adsorbed at higher pressures. This is also consistent with a pressure dependent equilibrium between mono, di, tri, and higher ligations of hydrogen to Ti.

Table 1.4: Sumary of gravimetric adsorption capacities (wt%) on the 0.20 molar equivalent tetrabenzyl titanium material after heating at 180 ^oC. (0.20 Ti/HMS). Calculated on the basis of ICP analysis result in 4.08 wt % of titanium in the material.

Sample	-196 ^oC	-78 ^oC	25 ^oC
Silica	1.21	0.58	0.44
0.20Ti/HMS	1.66	0.99	0.69
Number of H_2/Ti	2.7	2.4	1.1

Hydrogen binding enthalpies versus hydrogen surface coverage of the Ti(III) samples show the same rising trend observed for reduced mesoporous Ti oxide materials. Silica exhibits a heat of adsorption of 3.5 kJ/mol which gradually decreases as the surface coverage increases. When Ti(III) species are introduced into the system, the binding enthalpies increase to 22.15 kJ/mol and 22.04 kJ/mol with 0.20 and 0.30 Ti/Si ratios, respectively. This is the highest adsorption enthalpy achieved by experiment for a porous material and falls in the ideal enthalpy range of 20 – 30 kJ/mol predicted by Zhao et al. [11a] and allows the sample to exhibit high adsorption rates at higher temperature.

At -196 ^{o}C and -78 ^{o}C, a single Ti center can bind up to 2.7 and 2.4 H_2/Ti, respectively. There is thus very little loss of H_2 binding capacity at each Ti at -78 ^{o}C. At room temperature each Ti can bind 1.2 hydrogen molecules, corresponding to 59 % loss of activity at room temperature (0.7 wt %). This result is encouraging because it is a much greater ratio of retained activity at room temperature than offered by physisorption. Although this result is low compared to the DOE goals, it is essentially double that of compressed hydrogen under these same conditions. Furthermore, when extrapolated to a commercially available pressure of 350 atm, this material can store up to 60.75 kg/m^3 in pellet form at room temperature, much closer to the ultimate DOE goal of 70 kg m^{-3}.

1.8 Characterization techniques in solid state hydrogen storage materials

This section focuses on a brief introduction to methods to quantify directly the adsorption quantity of hydrogen on solid state materials as well as the concomitant desorption process. Methods to probe the interaction of hydrogen and metal hosts are also discussed.

1.8.1 Hydrogen adsorption measurements:

There are two main types of characterization of hydrogen storage performance.[51] They are kinetics measurements and pressure-composition-temperature (PCT) measurements. Kinetics measurements probe the rate of change of hydrogen concentration in a sample after the sample has been perturbed from quasi-equilibrium. This experiment is meaningful in studying hydrogen storage on hydrides, which possess slow and variable speeds of hydrogen adsorption and desorption versus temperature. Pressure-composition-temperature measurements are the most widely used in academic research. When temperature is set constant, the pressure – composition isotherms (PCIs) will be collected and plotted on two-dimensional (2D) graphs. The effect of temperature can be gauged by running a PCI at various temperatures. The PCT method records data when samples are at equilibrium, so it can be used to determine thermodynamic properties, such as heat of adsorption. From chapter 2 to chapter 7, readers can explore the hydrogen adsorption data presented on 2D plots as well as the heat of adsorption derived from adsorption data at 77 K and 87 K by mean of Clausius – Clapeyron I equation.

To obtain kinetic data or PCT data, the common techniques used in the laboratory can be classified into three categories: gravimetric, volumetric, and temperature – programmed desorption (TPD). Thermo-gravimetric analysis, and differential scanning calorimetry, and other spectroscopy methods, such as inelastic neutron scattering, infrared spectroscopy, raman spectroscopy, are normally considered as complementary characterization techniques to probe bonding and structure rather than adsorption quantity.

1.8.1.1 Gravimetric technique: this technique records the change of sample mass by employing a sensitive analytical balance. With the aid of a pressure gauge, dosing or removing hydrogen gas on to the sample results in changes of mass observed by the balance. Temperature is recorded by using a thermocouple, and thus PCT data can be derived.

1.8.1.2 Volumetric technique: also known as the manometric or Sieverts method, in honor of the German chemist who used temperature – pressure – volume correlations to identify hydrogen storage behaviour of materials.

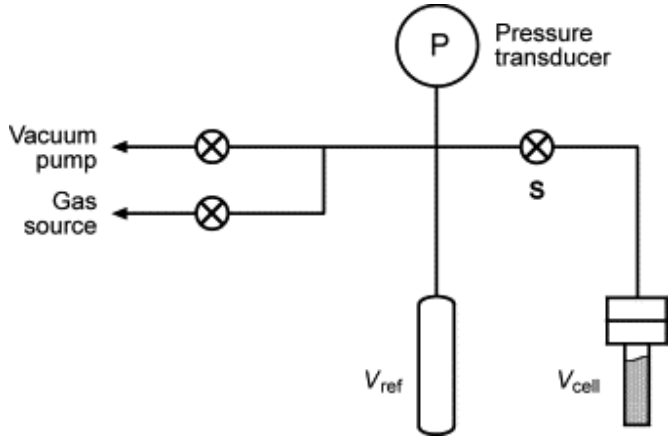

Figure 1.22: Minimal Sieverts apparatus for determining the uptake of gas atoms or molecules by the sample contained in a cell with empty volume Vcell, based on the initial pressure of gas in Vref and a further measurement of pressure after the valve S has been opened. (Reprinted with permission from [52]. Copyright 2007, Elsevier).

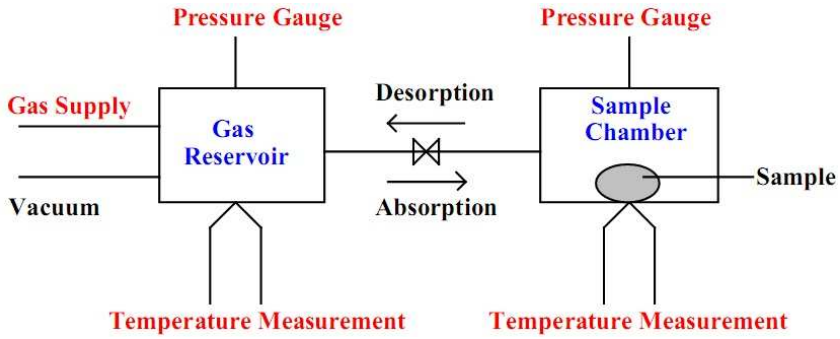

Figure 1.23: Schematic drawing of a Gas Reaction Controller (GRC) system supplied by Advanced Materials Corporation.

A simple Sieverts apparatus is sketched in figure 1.22,[52] and a schematic drawing of the GRC system by Advanced Materials Corporation is sketched in figure 1.23. The apparatus consists of a gas supply connected to a sample chamber. Because the volumetric technique measures hydrogen concentration indirectly through temperature – pressure – volume correlations, the volume and temperature of the sample chamber and gas reservoirs must be known prior to running the experiment. The system volumes are carefully calibrated, the temperature of gas reservoirs and sample chamber are kept constant by mean of external temperature controller, i. e. liquid nitrogen bath or electric oven. At constant volume and fixed temperature, pressures can be accurately measured by using pressure transducers and thus pressure – concentration isotherms can be generated. On a commercially available Sieverts instrument, the sample amounts should be more than 100 mg to ensure high accurate pressure readings because higher amount of sample will produce larger pressure changes due to adsorption or desorption. In some instruments, such as the PCI from Advanced Materials, the skeletal densities of samples are important parameters, which must be accurately determined because this value is used by the instrument to calculate the gas volume displaced by the sample and thus, free volume in the sample holder is precisely determined. In other instruments, such as the PCT by Setaram, the volume of the sample chamber with the sample in it is measured directly by the instrument.

1.8.1.3 Temperature – Programmed Desorption Technique:

The TPD method is normally applied to probe hydrogen adsorption and desorption versus temperature. In a typical experiment, temperature change is programmed and hydrogen desorbed from a sample can be probed by means of a TCD detector or, better, by a mass spectrometer. Temperature – Programmed Reaction Spectroscopy (TPRS) is a newly developed method based on TPD and can be used for both reversible and irreversible hydrogen adsorption/desorption process.[53]

1.8.2 Complementary Characterization Techniques

1.8.2.1 Thermal Gravimetric Analysis Technique:

While gravimetric techniques operate at constant temperature with a control over pressure of hydrogen gas, thermal gravimetric analysis (TGA) often operates under vacuum or in a flow of inert gas, such as helium, to probe hydrogen desorption. Hydrogen adsorption can be achieved by operation of a TGA under the flow of hydrogen gas. In this experiment, temperature can be kept constant or ramping can be preset using a programme. Changes in sample mass versus time and temperature can be recorded and plotted.

1.8.2.2 Differential Scanning Calorimetry Technique:

Differential Scanning Calorimetry (DSC) measures the heat flow as a function of temperature. It can be used in the investigation of thermodynamic properties of materials by measuring the energy needed to maintain a sample and an inert reference material over a desired temperature range. The relative heat flow to the sample versus temperature can be controlled to accurately determine heat of adsorption or related thermodynamic properties, such as phase change.

While TGA and DSC techniques quantify the composition of sorbed hydrogen, the interaction modes between sorbed hydrogen molecules and adsorption centers can be investigated by inelastic neutron scattering, vibrational spectroscopy, and nuclear magnetic resonance. The employment of electron paramagnetic resonance (EPR) is limited since this technique can only prove the ($\eta^2 - H_2$) – metal interaction indirectly by observation of different signals due to different electronic structures or different numbers

of unpaired electrons on the metal centers before and after H_2 addition. Moreover, the EPR spectra of systems with more than one unpaired electron are difficult to interpret.

1.8.3 Inelastic neutron scattering

Inelastic neutron scattering (INS) involves in the determination of energy transfer between bombarded neutrons and the scattering sample.[54] This technique can be used to probe the local environment of atomic hydrogen in a material or to determine the quantized excitation energies of adsorbed molecular hydrogen. The scattering can be coherent or incoherent, but in hydrogen storage we are primarily concerned with incoherent INS. The strong scattering exhibited by hydrogen relative to other heavier elements is an indispensable advantage of INS. While IR and Raman spectroscopy are restricted by symmetry requirements which lead to selection rules, INS is not affected by this rule at all and all vibrational modes are neutron active and can be identified. INS is also sensitive to modes at all wavevectors across the Brillouin zone and can be applied to amorphous or crystalline materials.

Information regarding diffusion rate of hydrogen gas can be probed by Quasi-Elastic Neutron Scattering (QENS), in which the broadening of the elastic scattering peak is measured. Employing both INS and QENS to study hydrogen storage materials has been implemented elsewhere.

INS can be applied to elucidate rotational transitions of sorbed hydrogen molecules in microporous materials. By this, five different adsorption sites have been determined in MOF-5[55] and three main adsorption sites were discovered on HKUST-1.[56] When employing INS to study the interaction between H_2 and Cu-exchanged ZMS-5 zeolite, at least two types of Cu adsorption sites were observed and the formation of a Kubas-type ($\eta^2 - H_2$) – Cu complex was confirmed (Figure 1.24).[36b]

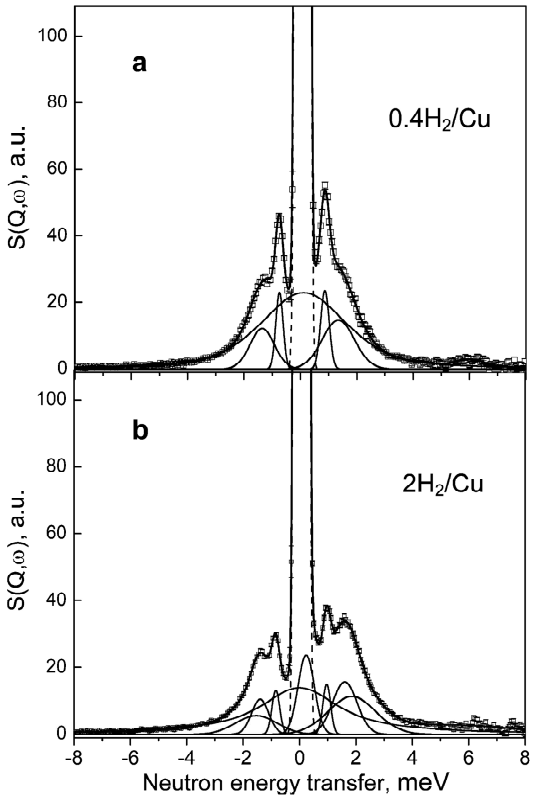

Figure 1.24: INS spectra of 0.4 and 2H2/Cu measured at 4 K are shown in panels a and b, respectively. Neutron energy loss processes are shown on the positive side of the elastic line. (Reprinted with permission from [36b]. Copyright 2007, American Chemical Society)

1.8.4 Vibrational Spectroscopy

Vibrational spectroscopy is indispensable in the charaterization of dihydrogen complexes. The IR spectra of $W(CO)_3\{P(iPr)_3\}_2(H_2)$ (compound 1 on figure 1.25) exhibited bands at 1575, 953, 462, cm^{-1}.[57] The bands 1575 cm^{-1} and 953 cm^{-1} were attributed to $\nu_{as}(M\text{-}H_2)$. Consistent with considerable weakening of the H – H interaction upon binding, there is a bathochromic shift of ν(H-H) of 4300 cm^{-1} in free H_2 to ca. 2700 cm^{-1} in the bound dihydrogen complex. The band assigned for $\nu_s(M\text{-}H_2)$ at 2690 cm^{-1} was obscured by a broad band from CO, which is not an uncommon situation in metal carbonyl complexes. It should be noticed that these IR bands are different from metal hydride vibration bands ν(M-H) at 1700 – 2300 cm^{-1} and δ(M-H) at 700 – 900 cm^{-1}. When H_2 was replaced by D_2, the $W(CO)_3\{P(iPr)_3\}_2(D_2)$, these bands above disappeared and new bands at 1144,

703, 442, and 319 cm^{-1} appeared and the band representing CO at 2360 cm^{-1} decreased in intensities (Compound 1-d_2 on Figure 1.25).

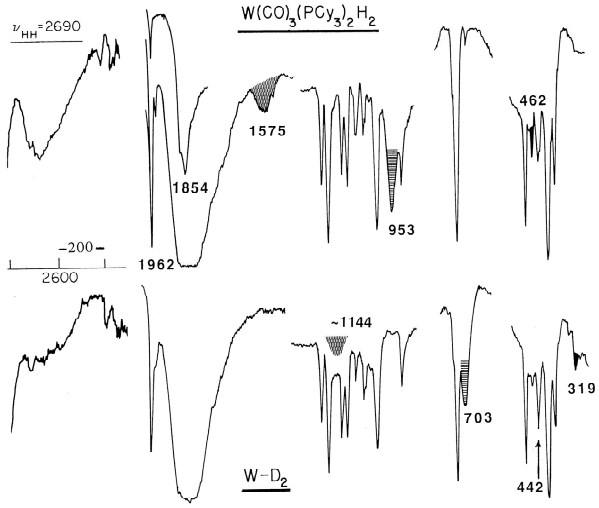

Figure 1.25: Infrared spectra of Nujol mulls of 1 (upper) and 1-d_2 (lower). The ν(HH) region was recorded for the perdeuteriophosphine species. (Reprinted with permission from [57]. Copyright 2007, American Chemical Society)

$W(CO)_3\{P(iPr)_3\}_2$ reacts cleanly with H_2 to create $W(CO)_3\{P(iPr)_3\}_2(H_2)$ at 1 atm of H_2 and the sorbed H_2 can be removed only when applying partial vacuum or an argon stream. The Cr analog exhibits a band at 1838 cm^{-1} due to $Cr(CO)_3(PCy)_2(D_2)$ and at 1822 cm^{-1} due to $Cr(CO)_3(PCy)_2$ at a D_2 pressure of 6.1 atm. This fact prompted the application of Cr materials toward hydrogen storage using pressure as a toggle, i.e. the materials adsorb H_2 in pressurized atmosphere of H_2 and may desorb H_2 when pressure is released.[57] Research by George and co-workers suggest that low valent V, Nb, Ta complexes may serve as hosts for hydrogen binding.[58]

Recently, variable-temperature infrared (VTIR) spectroscopy was implemented to characterize hydrogen adsorption materials. Spectral acquisition can be conducted under isobaric conditions or under variable hydrogen pressure. Vittilo and co-workers determined the adsorption enthalpies of hydrogen on MOF-5, HKUST-1, and CPO-27-Ni using this VTIR technique.[41] The heat of adsorption on HKUST-1 or CPO-27-Ni was determined to be 10.1 kJ/mol or 13.5 kJ/mol, respectively. Heat of hydrogen adsorption

on MOF-5 was identified at 3.5 or 7.4 kJ/mol, depending on which IR band was used in the calculation.

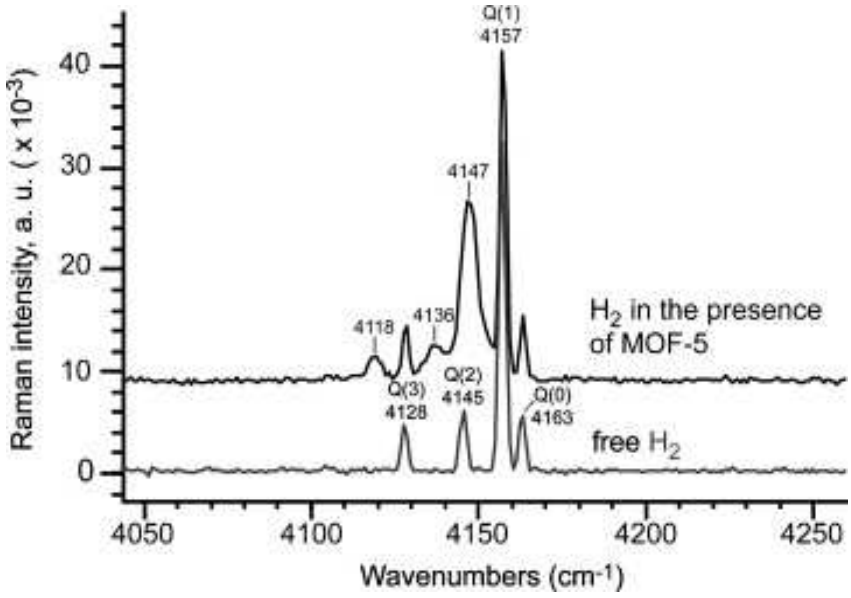

Figure 1.26: Raman spectra of hydrogen as a free gas and in the presence of MOF-5 at room temperature and 30.3 bar (baseline correction was applied to remove the fluorescence background). (Reprinted with permission from [59]. Copyright 2005, Elsevier).

The H_2 molecule is IR inactive. However, the CO ligand in organometallic compounds is capable of inducing an H – H dipole moment if H_2 is bound on the metal center and thus IR can be used to probe the vibration. Interactions between H_2 and materials which do not contain CO ligands can be characterized by Raman spectroscopy. Kubas materials generally possess heats of hydrogen adsorption that may be characterized under 1 atm of H_2 gas.[57] However, physisorbents may require hydrogen pressure up to 30 – 40 bar or cryogenic temperature to observe the signals of sorbed H_2 because the cross section of H_2 is very small. A study by Centrone and co-workers employed Raman spectroscopy to observe the change of MOF-5 in an H_2 or D_2 atmosphere.[59] New peaks at 4118, 4136 cm^{-1} and the enhancement of peak 4147 cm^{-1} were observed when MOF-5 was placed under 30.3 bar pressure of H_2. Raman spectroscopy was also used to elucidate the interaction of H_2 with crystalline silicon,[60] and amino borane at high pressure.[61]

1.8.5 Nuclear Magnetic Resonance

Nuclear magnetic resonance (NMR) spectroscopy can be used with any isotope possessing a nuclear magnetic moment, for example hydrogen, deuterium, or tritium.[62,63] Spectral acquisition can be conducted with a solution sample or solid-state materials. Since it is difficult to locate a hydrogen atom by X-ray crystallography, an important NMR method for H_2 versus hydride coordination is the J_{HD} for the isotopomer of a dihydrogen complex. HD gas possesses a J_{HD} of 43 Hz, corresponding to a d_{HD} = 0.74 Å. J_{HD} (in Hertz) is identified from solution NMR by the empirical relationship of d_{HH} (in Å) in the solid state using two similar equations independently developed from different groups:

$$d_{HH} = 1.42 - 0.0167J_{HD} \quad \text{(by Morris)}^{62}$$

or $$d_{HH} = 1.44 - 0.0168J_{HD} \text{ (by Heinekey)}^{63}$$

Apart from these equations, d_{HH} can be obtained by neutron diffraction or solid-state NMR spectroscopy, or, even better, by inelastic neutron scattering. The identification of d_{HH} in dihydrogen complexes is important because this d_{HH} is longer than the H-H distance of a free hydrogen molecule (0.74 Å), but smaller than the distance between the hydrogen atom in metal dihydrides (> 1.65 Å).

Other methods used in the characterization of hydrogen storage materials are nitrogen adsorption to determine specific surface areas, pore size distribution and void space determination. The void space or skeletal density of materials can be obtained via helium pycnometry. Powder X-ray diffraction can be applied to study the structure of materials. X-ray photo-electron spectroscopy can be employed to elucidate different oxidation states of surface species. Theoretical chemistry and computational modelling can be employed to predict or design future materials as well as confirm or rationalize experimental results.

1.9 Concluding remarks

Significant strides have been made in the search for suitable materials for hydrogen storage. But in order to reach the 2015 DOE goal it is necessary to develop materials

which have high storage capacity, appropriate thermodynamic and kinetic properties, durability, low cost and high mechanical strength. To increase the hydrogen adsorption capacities of promising materials such as amorphous carbons, MOFs, porous materials it is crucial to increase the heat of adsorption. Recent advances have shown that this can be achieved by focussing on materials which exhibit strong (η^2-H_2)-metal interaction and have as many active metal sites as possible. While no system in this review is close to practical application, it is not inconceivable that by designing a system with the maximum number of metal atoms in the lowest coordination number possible and appropriate oxidation state and ionization potential, commercially viable materials can be developed. Future research needs to focus on determining the optimal metal coordination environment and oxidation state in these myriad systems while also decreasing the amount of void space in the solids, which reduce the relative improvement of the systems with respect to compressed gas. Physical studies of these systems and Kubas type compounds under high pressure should also be conducted because most of the organometallic literature focuses on pressures suitable for standard NMR applications which are too low for on-board applications where pressure release and not increase of temperature represents the best toggle for hydrogen feed to the engine. While many studies use IR or Raman as a means of spectroscopically characterizing these compounds, developing techniques to conduct NMR and ESR at high pressures near 100 bar would be useful. Further studies on temperature programmed desorption and inelastic neutron scattering are also required to gain more information about binding enthalpies and the location of individual hydrogens than can be gained by standard X-ray techniqures, gas adsorption, and use of the Clausius Clapeyron equation. This promising field thus appears to be in its infancy with many new challenges in the synthetic, computational, and physical arenas.

1.10 References

(1) Seayad, A. M.; Antonelli, D. M. *Adv. Mater*. **2004**, 16, 765.

(2) Fuel Cell Technologies Program Multi-Year Research, Development and Demonstration Plan.

http://www1.eere.energy.gov/hydrogenandfuelcells/mypp/ Retrieved January 19th, 2012.

(3) Schlapbach, L.; Zuettel, A. *Nature* **2001**, 414, 353.

(4) a) Orimo, S.; Nakamori, Y.; Eliseo, J. R.; Zuettel, A.; Jensen, C. M. *Chem. Rev*. **2007**, 107, 4111; b) Sandrock, G. *J. Alloys Comp*. **1999**, 877, 293; c) Yaghi, O. M.; O'Keeffe, M.; Ockwig, N. W.; Chae, H. K.; Eddaoudi, M.; Kim, J. *Nature* **2003**, 423, 705; d) van den Berg, A. W. C.; Arean, C. O. *Chem. Commun*. **2008**, 668.

(5) 2006 Annual Merit Review Proceedings Plenary. http://www.hydrogen.energy.gov/annual_review06_plenary.html Retrieved January 19th, 2012.

(6) a) Felderhoff, M.; Weidenthaler, C; von Helmolt, R.; Eberle, U. *Phys. Chem. Chem. Phys.* **2007**, 9, 2643; b) Zuettel, A. *Material Today* **2003**, Sept, 24; c) Fichtner, M. *Advanced Engineering Materials* **2005**, 7, 443.

(7) Zuettel, A.; Sudan, P.; Mauron, P.; Kiyobayashi, T.; Emmenegger, C.; Schlapbach, L. *Int. J. Hydrogen Energy*, **2002**, 27, 203.

(8) a) Kubas, G. J.; Ryan, R. R.; Swanson, B. I.; Vergamini, P. J.; Wasserman, H. J. *J. Am. Chem. Soc*. **1984**, 106, 451; b) Kubas, G. J. *Acc. Chem. Res*. **1988**, 21, 120; c) Kubas, G. J. *J. Organometal. Chem*. **2001**, 635, 37; d) Kubas, G. J. *J. Chem. Soc., Chem. Commun*. **1980**, 61; d) Crabtree, R. H. *Acc. Chem. Res*. **1990**, 23, 95; e) Kubas, G. J. *Metal Dihydrogen and s–Bond Complexes*; Kluwer Academic/Plenum Publishers: New York, **2001**; f) Kubas, G. J. *Chem. Rev*. **2007**, 107, 4152; g) Heinekey, D. M.; Lledós, A.; Lluch, J. M. *Chem. Soc. Rev*. **2004**, 33, 175; Heinekey, D. M.; Oldham, Jr., W. J. *Chem. Rev*. **1993**, 93, 913.

(9) Wang, L.; Yang, R. T. *Energy Environ. Sci.* **2008**, 1, 268.

(10) Dincă, M.; Long, J. R. *Angew. Chem. Int. Ed*. **2008**, 47, 6766.

(11) a) Zhao, Y.; Kim, Y.; Dillon, A. C.; Heben, M. J.; Zhang, S. B. *Phys. Rev. Lett*. **2005**, 94, 155504; b) Sun, Q.; Wang, Q.; Jena, P.; Kawazoe, Y. *J. Am. Chem. Soc***. 2005**, 127, 14582.

(12) Guo, T.; Jin, C.; Smalley, R. E. *J. Phys. Chem*. **1991**, 95, 4948.

(13) Tast, F.; Malinowski, N.; Frank, S.; Heinebrodt, M.; Billas, I. M. L.; Martin, T. P. *Phys. Rev. Lett*. **1996**, 77, 3529.

(14) Yildirim, T.; Ciraci, S. *Phys. Rev. Lett*. **2005**, 94, 175501.

(15) Zhang, Y.; Dai, H. *App. Phys. Lett.* **2000**, 77, 3014; (b) Zhang, Y.; Franklin, N. W.; Chen, R. J.; Dai, H. *Chem. Phys. Lett*. **2000**, 331, 35.

(16) Zhou, W.; Yildirim, T.; Durgun, E.; Ciraci, S. *Phys. Rev. B* **2007**,76, 085434.

(17) Durgun, E.; Ciraci, S.; Zhou, W.; Yildirim, T. *Phys. Rev. Lett*. **2006**, 97, 226102.

(18) a) Lee, H.; Nguyen, M. C.; Ihm, J. *Solid State Commun*. **2008**, 146, 431; b) Nguyen, M. C.; Lee, H.; Ihm, J. *Solid State Commun*. **2008**, 147, 419.

(19) McKeown, N. B.; Budd, P. M. *Chem. Soc. Rev*. **2006**, 35, 675.

(20) a) Lee, H.; Choi, W. I.; Ihm, J. *Phys. Rev. Lett.* **2006**, 97, 056104; b) Lee, H.; Choi, W. I.; Nguyen, M. C.; Cha, M. H.; Moon, E.; Ihm, J. *Phys. Rev B* **2007**, 76, 195110.

(21) a) Hoskins, B. F.; Robson, R. J. *J. Am. Chem. Soc*. **1989**, 111, 5962; b) Seo, J. S.; Whang, D.; Lee, H.; Jun, S. I.; Oh, J.; Jeon, Y. J.; Kim, K. *Nature* **2000**, 404, 982.

(22) a) Rossi, N. L.; Eckert, J.; Addaoudi, M.; Vodak, D. T.; Kim, J.; O'Keeffe, M.; Yaghi, O. M. *Science* **2003**, 300, 1127; b) Rowsell, J. L. C.; Yaghi, O. M. *Angew. Chem. Int. Ed*. **2005**, 44, 4670.

(23) Wong-Foy, A. G.; Matzger, A. J.; Yaghi. O. M. *J. Am. Chem. Soc*. **2006**, 128, 3494.

(24) Rowsell, J. L.; Millward, A. R.; Park, K. S.; Yaghi. O. M. *J. Am. Chem. Soc*. **2004**, 126, 5666.

(25) a) Poirier, E.; Chahine, R.; Benard, P.; Dorval-Douville, G.; Lafi, L.; Chandonia, P. A. *Langmuir* **2006**, 22, 8784; b) Hirscher, M.; Panella, B. *Scr. Mater.* **2007**, 56, 809; c) Bénard, P.; Chahine, R. *Scr. Mater.* **2007**, 56, 803.

(26) Han, S. S.; Goddard III, W. A. *J. Am. Chem. Soc*. **2007**, 129, 8422.

(27) a) Li, Y.; Yang, R. T. *J. Am. Chem. Soc*. **2006**, 128, 726; b) Li, Y.; Yang, R. T. *J. Am. Chem. Soc*. **2006**, 128, 8136.

(28) Liu, Y.; Kabbour, H.; Brown, C. M.; Neumann, D. A.; Ahn, C. C. *Langmuir* **2008**, 24, 4772.

(29) Dincă, M.; Long, J. R. *J. Am. Chem. Soc*. **2005**, 127, 9376.

(30) Dincă, M.; Yu, A. F.; Long, J. R. *J. Am. Chem. Soc*. **2006**, 128, 8904.

(31) Dincă, M.; Dailly, A.; Liu, Y.; Brown, C. M.; Neumann, D. A.; Long, J. R. *J. Am. Chem. Soc*. **2006**, 128, 16876.

(32) Dincă, M.; Long, J. R. *J. Am. Chem. Soc*. **2007**, 129, 11172.

(33) Bhatia, S. K.; Myers, A. L. *Langmuir* **2006**, 22, 1688.

(34) a) Rosi, N. L.; Kim, J.; Eddaoudi, M.; Chen, B.; O'Keeffe, M.; Yaghi, O. M. *J. Am. Chem. Soc*. **2005**, 127, 1504; b) Rowsell, J. L. C.; Yaghi, O. M. *J. Am. Chem. Soc*. **2006**, 128, 1304.

(35) Liu, Y.; Brown, C. M.; Neumann, D. A.; Kabbour, H.; Ahn, C. C. *Mater. Res. Soc. Symp. Proc*. Vol. 1041, **2008**, 75.

(36) a) Liu, Y.; Brown, C. M.; Neumann, D. A.; Peterson, V. K.; Kepert, C. J. *J. of Alloys and Compounds* **2007**, 446–447, 385; b) Georgiev, P. A.; Albinati, A.; Mojet, B. L.; Ollivier, J.; Eckert, J. *J. Am. Chem. Soc.* **2007**, 129, 8086; c) Serykh, A. I.; Kazansky, V. B. *Phys. Chem. Chem.Phys.* **2004**, 6, 5250; d) Georgiev, P. A.; Albinati, A.; Eckert, J. *Chem.Phys. Lett*. **2007**, 449, 182.

(37) Dincă, M.; Han, W. S.; Liu, Y.; Dailly, A.; Brown, C. M.; Long, J. R. *Angew. Chem. Int. Ed*. **2007**, 46, 1419.

(38) a) Dailly, A.; Vajo J. J.; Ahn, C. C. *J. Phys. Chem. B* **2006**, 110, 1099; b) Panella, B.; Hirscher, M.; Pütter H.; Müller, U. *Adv. Funct. Mat.* **2006**, 16, 520; c) Langmi, H.W.; Book, D.; Walton, A.; Johnson, S. R.; Al-Mamouri, M. M.; Speight, J. D.; Edwards, P. P. Harris I. R.; Anderson, P. A. *J. Alloy. Compd*. **2005**, 404–406, 637; d) Kaye S. S.; Long, J. R. *J. Am. Chem. Soc*. **2005**, 127, 6506.

(39) Strobel, R.; Garche, J.; Moseley, P. T.; Jorissen, L.; Wolf, G. *J. Power Sources* **2006**, 159, 781.

(40) a) Choi, H. J.; Dincă, M.; Long, J. R. *J. Am. Chem. Soc*. **2008**, 130, 7848; b) Zhao, X.; Xia, B.; Fletcher, A. J.; Thomas, K. M.; Bradshaw, D.; Rosseinsky, M. J. *Science* **2004**, 306, 1012.

(41) Vitillo, J. G.; Regli, L.; Chavan, S.; Ricchiardi, G.; Spoto, G.; Dietzel, P. D. C.; Bordiga, S.; Zecchina, A. *J. Am. Chem. Soc*. **2008**, 130, 8386.

(42) a) Bavykin, D. V.; Lapkin, A. A.; Plucinski, P. K.; Friedrich, J. M.; Walsh, F. C. *J. Phys. Chem. B* **2005**, 109, 19422; b) Bavykin, D. V.; Friedrich, J. M.; Walsh, F. C. *Adv. Mater*. **2006**, 18, 2807; c) Lim, S. H.; Luo, J.; Zhong, Z.; Ji, W.; Lin, J. *Inorg. Chem*. **2005**, 44, 4124.

(43) Antonelli. D. M. *Microporous and Mesoporous Materials* **1999**, 30, 315.

(44) Hu, X.; Skadtchenko, B. O.; Trudeau, M.; Antonelli, D. M. *J. Am. Chem. Soc*. **2006**, 128, 11740.

(45) Hu, X.; Trudeau, M.; Antonelli. D. M. *Chem. Mater*. **2007**, 19, 1388.

(46) He, X.; Antonelli, D. M. *Angew. Chem. Int. Ed.* **2002**, 41, 214.

(47) Hu, X.; Trudeau, M.; Antonelli, D. M. *Inorg. Chem*. **2008**, 47, 2477.

(48) Hamaed, A.; Trudeau, M.; Antonelli, D. M. *J. Am. Chem. Soc*. **2008**, 130, 6992.

(49) Zhuravlev, L. T. *Colloid Surf. A* **2000**, 173, 1.

(50) a) Maksimov, N. G.; Nesterov, G. A.; Zakharov, V. A.; Stchastnev, P. V.; Anufrienko, V. F.; Yermakov, Y. I. *J. Mol. Catal*. **1977**, 4, 167. b) Nesterov, G. A.; Zakharov, V. A.; Paukshitis, E. A.; Yurchenko, E. N.; Ermakov, Y. I. *Kinetika i Kataliz* **1979**, 20, 429.

(51) Broom, D. P. *Hydrogen Storage Materials – The Characterisation of Their Storage Properties*; Springer, **2011**, pp 131 – 154.

(52) Blach, T. P.; Gray, E.MacA. *J. Alloys Compounds* **2007**, 692.

(53) Broom, D. P. *Hydrogen Storage Materials – The Characterisation of Their Storage Properties*; Springer, **2011**, pp 155 – 198.

(54) Walker, G. *Solid-State Hydrogen Storage*; Woodhead Publishing and Maney Publishing, CRC Press, Cambridge, England, **2008**. Chapter 6: *Neutron Scattering Studies for Analyzing Solid-State Hydrogen Storage*. By: Ross, D. K. pp 150 – 189.

(55) Mulder, F. M.; Dingermans, T. J.l Schimmel, H. G.; Ramirez-Cuesta, A. J.; Kearley, G. J. *Chem. Phys*. **2008**, 351, 72.

(56) Brown, C. M.; Liu, Y.; Yildirim, T.; Peterson, V. K.; Kepert, C. J. *Nano Technology* **2009**, 20, 204025.

(57) Bender, B. R.; Kubas, G. J.; Jones, L. H.; Swanson, B. I.; Eckert, J.; Capps, K. B.; Hoff, C. D. *J. Am. Chem. Soc*. **1997**, 119, 9179.

(58) George, M. W.; Haward, M. T.; Hamley, P. A.; Hughes, C.; Johnson, F. P. A.; Popov, K. V.; Poliakoff, M. *J. Am. Chem. Soc*. **1993**, 115, 2286.

(59) Centrone, A.; Siberio-Perez, D. Y.; Millward, A. R.; Yaghi, O. M.; Matzger, A. J.; Zerbi, G. *Chem. Phys. Lett*. **2005**, 411, 516.

(60) Leitch, A. W. R.; Alex, V.; Weber, J. *Phys. Rev. Lett*. **1998**, 81, 421.

(61) a) Trudel, S.; Gilson, D. F. R. *Inorg. Chem*. **2003**, 42, 2814; b) Lin, Y.; Mao, W. L.; Drozd, V.; Chen, J.; Daemen, L. L. *J. Chem. Phys*. **2008**, 129, 234509.

(62) Maltby, P. A.; Schlaf, M.; Steinbeck, M.; Lough, A. J.; Morris, R. H.; Klooster, W. T.; Koetzle, T. F.; Srivastava, R. C. *J. Am. Chem. Soc*. **1996**, 118, 5396.

(63) Luther, T. A.; Heinekey, D. M. *Inorg. Chem*. **1998**, 37, 127.

Chapter 2 - Bis(benzene) and bis(cyclopentadienyl) V and Cr doped mesoporous silica with high enthalpies of hydrogen adsorption

2.1 Introduction

The increasing demand on the world's resources of fossil fuel over the past several years has led to a dramatic increase in alternative energy research.[1-12] While battery technology is improving steadily, the moderate energy capacity and slow recharging rates of Li batteries are still unattractive for commercial vehicles. The use of hydrogen as an alternative fuel is attractive because it possesses the highest energy density of any substance and only generates water as a byproduct. The major drawback of hydrogen as a fuel is that it is very light and difficult to compress. For this reason, substances that store hydrogen have been employed as carriers.[4] These include metal hydrides in which hydrogen is stored in the form of M-H hydride bonds, metal alloys in which hydrogen occupies interstitial spaces in the metal lattice, and physisorption materials, which absorb hydrogen on the surface at cryogenic temperatures.[13, 14] As of today no member of any of these three classes of materials currently meets the ultimate Department of Energy (DOE) system targets of 7.5 wt % and 70 kg/m^3 at ambient temperature.[15] An often overlooked feature of a hydrogen storage material is the binding enthalpy of the hydrogen to the solid. In metal hydrides the binding enthalpy is generally greater than 70 kJ/mol, which means large amounts of heat are released on fuelling and a large amount of heat is needed to drive off the hydrogen required by the engine, resulting in a net loss of energy for the system.[13] In physisorption materials, the problem is that the enthalpies are in most cases less than 10 kJ/mol.[16] For this reason energy-consuming cryogenic refrigeration is required to keep the hydrogen bound to the surface. Calculations have shown that the ideal enthalpy for room temperature applications is in the range of 20-30 kJ/mol.[17] In a recent paper we showed that grafting single site benzyl Ti(III) fragments to the surface of mesoporous silica led to materials with increased hydrogen storage capacity and enthalpies that rise on surface coverage to 22.15 kJ/mol,[18-19] the highest known for any cryogenic hydrogen storage material. This rising trend is opposite that expected for physisorption and has been interpreted as a mixture of physisorption to the silica surface and Kubas type binding of the dihydrogen molecule to the Ti fragments in a σ - π ligand

interaction.[18-21] Kubas binding has been demonstrated in a series of metal-organic frameworks (MOF) and Prussian Blue materials, but none of these materials show enthalpies in the calculated 20-30 kJ/mol range.[22] Recently, a MOF possessing a binding enthalpy of 13.5 kJ/mol was synthesized.[23] The Ti fragments in our silica material retained a promising 41 % of their activity at room temperature, demonstrating that the higher enthalpies indeed lead to better performance at ambient temperature than pure physisorption, which generally shows less than 10 % of it activity under these conditions. One drawback of our system is that, although it shows reversibility over 20 cycles in laboratory conditions, the Ti fragments are thermally unstable and decompose over several weeks under nitrogen leading to lower performance. In this paper we study silica supported bis(benzene) and bis(cyclopentadienyl) vanadium and chromium analogues and show that the bis(cyclopentadienyl)chromium system possesses adsorption enthalpies up to 18.43 kJ/mol, the second highest recorded for a cryogenic material, and also possesses higher thermal stabilities than the Ti (III) system, retaining 100 % performance after three months storage under nitrogen. While these materials still possess adsorption capacities much lower than stipulated by the DOE, the aim of our studies is to establish trends in hydrogen binding at ambient temperatures and high pressures to extremely reactive metal centers grafted on silica surfaces which would otherwise be unstable and difficult to synthesize and study, with the long term goal of developing extended solids using the same underlying principles to meet and surpass these DOE goals.

2.2 Experimental Section

2.2.1 Preparation of hexagonally packed mesoporous silica: Hexagonally packed mesoporous silica (HMS) was prepared by the neutral templating method[24] using dodecylamine, water, ethanol, and tetraethyl orthosilicate. In a typical preparation, 0.27 mol of dodecylamine, 9.09 mol ethanol, and 29.6 mol deionized water were added together. 1.0 mol of tetraethyl orthosilicate was then added to the solution with vigorous stirring. The reaction mixture was then aged at room temperature for 18 h and then filtered to get the solid material, which was then air-dried on a plate. The template was removed by stirring 1 g of the air-dried HMS with 150 ml of hot ethanol for 1 h. The product was then filtered and washed with a second 100 ml portion of ethanol. This

extraction procedure was repeated several times, and the crystalline product was dried at 200 ^{o}C in vacuum overnight.

2.2.2 Preparation of silica treated with sandwich compounds: Three organometallic-grafted samples were prepared from this silica by treating it with bis(cyclopentadienyl)-chromium, bis(cyclopentadienyl)vanadium, or bis(benzene)vanadium in benzene or toluene, under nitrogen at a 5 wt % metal doping level. The treated samples were named 5%Cr(bisCp), 5%V(bisCp), and 5%V(bisben), respectively. These dopants were used previously by our group as reducing agents for mesoporous Ti oxide,[25] but in the present case they are used exclusively to introduce Kubas type binding sites on the redox inactive surface. Bis(cyclopentadienyl)chromium and bis(cyclopentadienyl)vanadium were purchased from Sigma-Aldrich and were used without further treatment. Bis(cyclopentadienyl)chromium and bis(cyclopentadienyl)-vanadium were reacted with silica in dry benzene. Bis(benzene)vanadium was prepared from vanadium tetrachloride according to the literature.[26] In a typical preparation of silica supported bis(cyclopentadienyl)chromium, 0.2766 g of bis(cyclopentadienyl)chromium was added to 100 ml benzene with stirring. 1.5 g silica was then added and the resulting reaction mixture was then stirred vigorously at room temperature under an inert atmosphere for 12 h. The mixture was then filtered to obtain the solid material, which was then heated at 90 ^{o}C in vacuum overnight. The supported bis(benzene)vanadium materials were made by reaction of the organometallic with silica in a toluene solution in a sealed ampoule. In a typical preparation, 0.3 g of bis(benzene)vanadium was dissolved in 100 ml of toluene, 1.5 g silica was then added and the mixture was heated at 140 ^{o}C in a closed ampoule for 24 h. The reaction mixture was then filtered and the remaining solid heated under vacuum at 140 ^{o}C.

Nitrogen adsorption and desorption data were collected on a Micromeritics ASAP 2010. All X-ray Photoelectron Spectroscopy (XPS) peaks were referenced to the carbon C-(C, H) peak at 284.8 eV, and the data were obtained using a Physical Electronics PHI-5500 spectrometer using charge neutralization. Elemental analysis was performed by Galbraith Labs, Knoxville Tennessee.

2.2.3 Hydrogen adsorption and storage measurements: Hydrogen adsorption isotherms were obtained by using a computer controlled commercial Gas Reaction Controller manufactured by Advanced Materials Corporation, Pittsburgh, PA. High purity hydrogen (99.9995% purity) was used as the adsorbent. Before all measurements the silica supported bis(cyclopentadienyl)chromium and the silica supported bis(cyclopentadienyl)vanadium were activated in vacuo at 90 ^{o}C to remove any physisorbed water or volatile impurities. Silica supported bis(benzene)vanadium was activated in vacuum at 100 – 140 ^{o}C.

Hydrogen storage measurements on a standard AX-21 sample (4.5 wt%) were performed to ensure proper calibration and functioning of the instrumentation. Leak testing was also performed during each measurement by checking for soap bubbles at potential leak points. These measurements are necessary to ensure the veracity of the isotherms. In the H_2 adsorption-desorption experiments complete reversibility was observed for all samples across the whole range of pressures. Samples were run at liquid nitrogen temperature (77 K), liquid argon temperature (87 K), and room temperature (298 K) to 60 bar. The skeletal density was measured using a Quantachrome Ultrapycnometer. When the skeletal density was used for the hydrogen uptake measurement, the compressed hydrogen within the pores is treated as part of the sample chamber volume. Therefore only the hydrogen physisorbed to the walls of the structure will be recorded by the PCI instrument as the adsorption capacity of the material. When the apparent density (measured on a bench-top density scale) is input for the PCI measurement instead of the skeletal density, the compressed gas in the void is not subtracted out and the resulting value for hydrogen storage represents the total hydrogen confined within the physical boundaries of the macroscopic sample and contains both hydrogen physisorbed to the walls and the compressed gas in the pores.

Enthalpies of adsorption were calculated using a variant of the Clapeyron – Clausius I equation taking both 77 K and 87 K hydrogen adsorption data.

$$\ln\left(\frac{P_2}{P_1}\right) = \Delta H_{ads}.\frac{T_2 - T_1}{R.T_2.T_1} \qquad (1)$$

Where P_n = pressure for isotherm n, T_n = temperature for isotherm n, R: gas constant.

Pressure as a function of the amount adsorbed was determined by using exponential fit for each isotherm; the first 10 – 11 points of the isotherms were selected and fit to the exponential equation. This exponential equation gives an accurate fit over the pressure up to 10 bar with a goodness of fit (R^2) above 0.99. The corresponding P_1 and P_2 values at a certain amount of H_2 adsorbed at both temperatures can be obtained by the simulated exponential equation. Inputting these numbers into equation 1, we then calculate the enthalpies of the adsorption.

2.3 Results and Discussions

Table 2.1: Nitrogen adsorption data of silica and silica treated with Cr and V sandwich compounds

Sample Name	Surface Area (m^2/g)	BJH Pore Size (Å)
Silica	1413	23.64
5%Cr(bisCp)/HMS	1438	23.92
5%V(bisCp)/HMS	1422	23.40
5%V(bisben)/HMS	1458	23.68

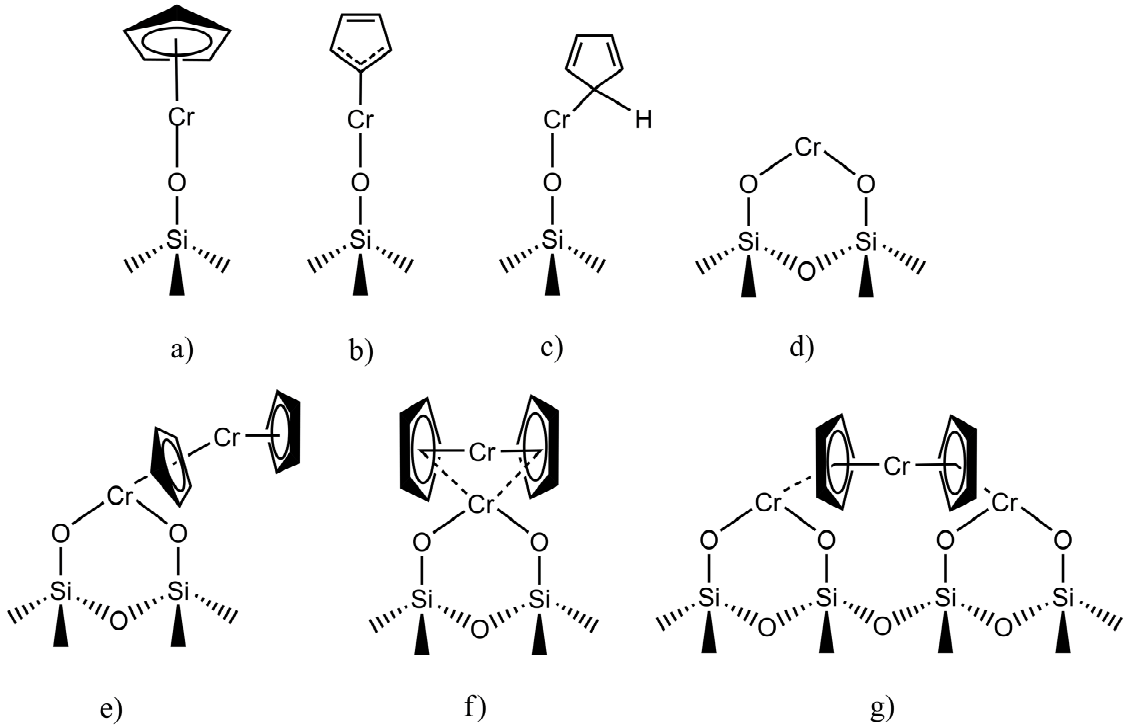

Figure 2.1: Possible surface species proposed previously for bis(cyclopentadienyl) chromium on silica dehydrated at 200 ^{o}C.[27, 28]

All samples retained the original reflection at d = 32 Å in the XRD after treatment with the organometallic. The nitrogen adsorption data for these samples is shown in Table 2.1. The specific surface areas of the treated samples are slightly higher than that of pristine silica. This may be because the anchoring of organometallic species on the silica surface creates internal surface features which effectively increase the surface area for physisorption of dinitrogen.

Analogous silica supported organometallic chromium and vanadium species have been widely studied as Ziegler Natta catalysts and the possible structures of the surface species have already been elucidated by XPS and other methods resulting in the proposed structures shown in Figure 2.1 and 2.2.[27-29]

In order to compare our results to those previously reported for other analogous silica supported systems using bis(cyclopentadienyl) and bis(benzene)vanadium and chromium species, X-ray photoelectron spectroscopy studies were conducted. Figure 2.3 shows the

emissions in the Cr 2p 3/2, 1/2 region and the simulated results. The main emissions at 576.3 eV and 585.6 eV can be attributed to Cr^{+2} species, as they closely match the emissions observed at 576.1 eV and 586.5 eV for $Cr(II)Cl_2C_5H_5$.[30] The emissions at 578.7 eV and 587.6 eV can be assigned to Cr^{+3} species by comparison with the spectrum of Cr_2O_3, which displays emissions at 578.4 eV and 587.9 eV.[31] There are also emissions at 581.6 eV and 590.2 eV for more highly oxidized Cr species, which closely match the emissions for Cr^{+6} in $K_2Cr_2O_7$ at 580.8 eV and 589.9 eV.[31, 32] The simulated emissions at 573.3 eV and 583.9 eV may arise from metallic Cr or other Cr(0) species because they are close to emissions observed for Cr metal.[32] The two emissions observed at very low binding energies of 569.2 eV and 571.3 eV do not correspond to any known chromium species and thus can be assigned to plasmons or emissions from other elements. Many structural possibilities have been proposed in the literature for bis(cyclopentadienyl) chromium doped silica.[27,28] Polarographic valence determination by Karol et al[28] on bis(cyclopentadienyl) chromium supported on silica showed that Cr(II), $Cr(C_5H_5)_2$, and Cr(III) were the dominant surface species. Further NMR studies from Blumel et al. suggested that the surface species from fig. 2.1a is one of the principal products with a strong ^1H NMR signal at 282 ppm. This product is dominant at low surface chromium concentration.[27b]

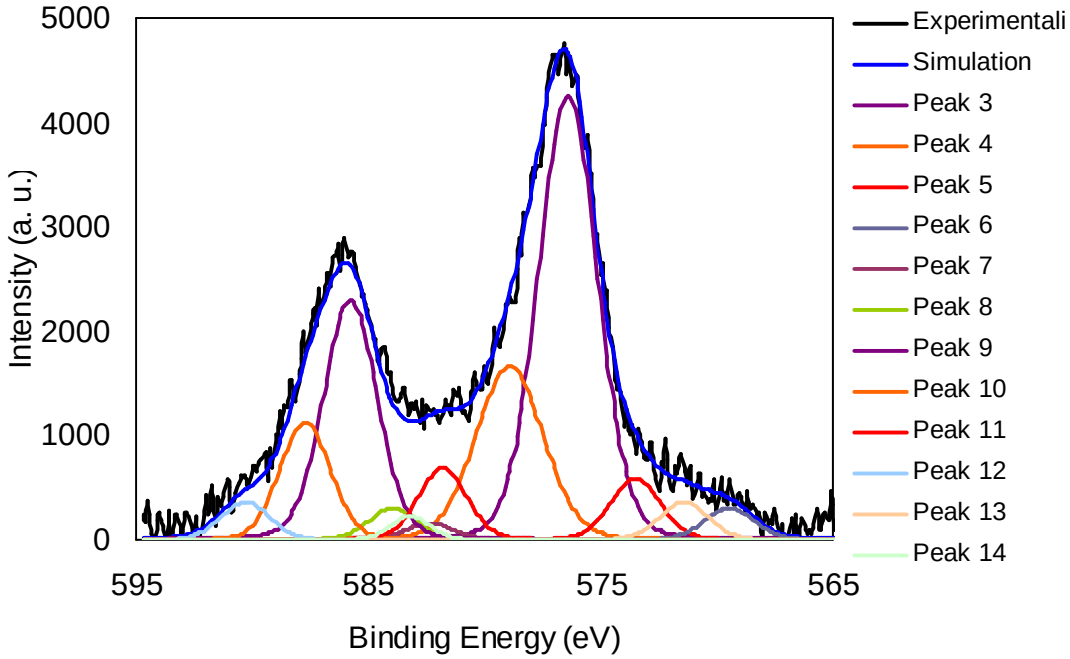

Figure 2.2: XPS Spectrum of the 5%Cr(bisCp) sample, showing the Cr 2p ½ and 3/2 region.

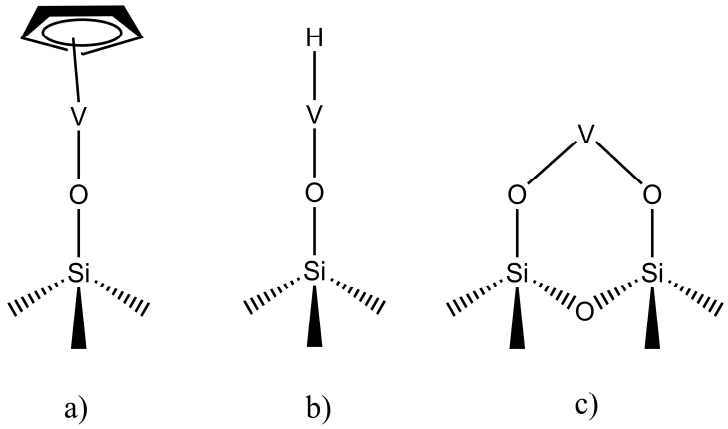

Figure 2.3: Possible surface species proposed previously for bis(cyclopentadienyl) vanadium (a) or bis(benzene) vanadium (b, c) on silica dehydrated at 200 °C.[25, 29]

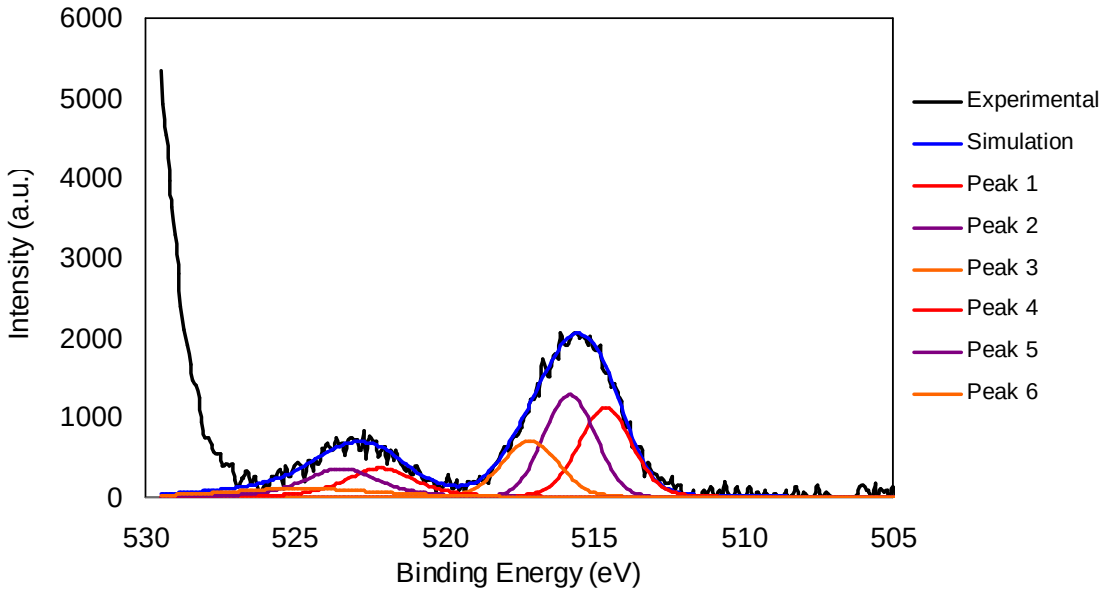

Figure 2.4: XPS Spectrum of 5%V(bisCp) sample, showing the V 2p ½ and 3/2 region.

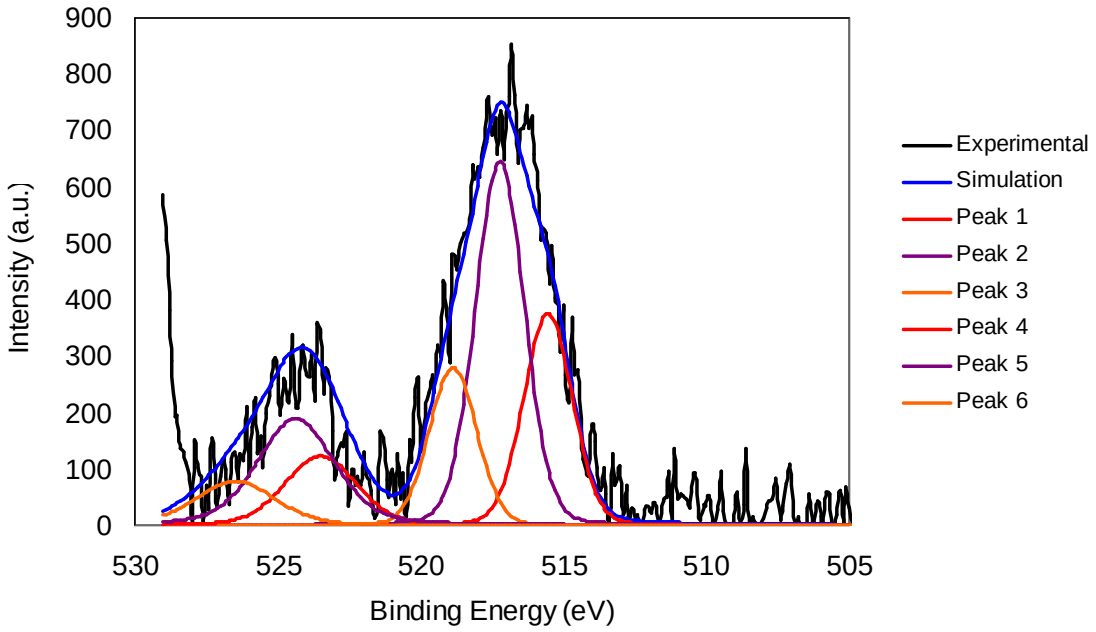

Figure 2.5: XPS Spectrum of the 5%V(bisben) sample, showing the 2p ½ and 3/2 region.

Figure 2.4 shows two broad XPS emissions of the V 2p 3/2, 1/2 region of the silica treated with bis(cyclopentadienyl) vanadium. The emissions at 514.5 eV and 522.1 eV

match other reported V^{+1} species, which display emissions at 514.5 eV and 522.1 eV. The compound $(cyclopentadienyl)_2V^{+1}$ is expected to be formed from the oxidation of the metallocene by protic oxygen species in the porous framework.[34] The emissions at 515.6 eV and 523.4 eV can be attributed to a V^{+2} species by comparison with the XPS spectrum of the V-doped mesoporous titania analogue, which displays emissions at 515.6 eV and 523.2 eV.[33] On the basis of the C,H and V elemental analysis from this previous study we proposed a surface species as shown in figure 2.3a. Finally, the emission at 517.5 eV matches that for VO_2 at 517.4 eV.[35]

Figure 2.5 shows the two XPS emissions in the V 2p 3/2 and 1/2 region of the silica treated with bis(benzene)vanadium. The emission at 515.3 eV and 523.3 eV can be attributed to the previously proposed organometallic V^{2+} species obtained on treatment of amorphous silica with bis(benzene) vanadium shown in figure 3 b and c.[25, 29] This also fits well with the values for analogous V(II) species doped into mesoporous Ti and Nb oxide (515.6 eV and 523.2 eV). The emission at 517.1 eV and 524.2 eV can be assigned to V^{+4} by direct comparison with the VO_2 emission at 517.4 eV. The emission at 518.6 eV and 526.4 eV can be assigned to V^{+5}, matching that for V_2O_5 supported on SiO_2 at 518.7 eV and 526.5 eV. [35]

The gravimetric and volumetric hydrogen adsorption data for the treated samples and pristine silica at 77 K are shown in figure 2.6 and figure 2.7. Pristine silica adsorbs 1.22 wt. % hydrogen at 60 bar while the 5%V(bisben), 5%V(bisCp), and 5%Cr(bisCp) samples adsorb 1.30 wt. %, 1.41 wt. %, and 1.60 wt. % hydrogen under these conditions, respectively. The value for 5%Cr(bisCp) rivals that of silica treated with benzyltitanium under these same conditions, however all samples in this report reach saturation at 30 bar. This is not the case for benzyltitanium treated samples, where saturation isn't reached even at 65 bar (6.5 MPa).[18, 19] This was previously attributed to a pressure dependent equilibrium involving mono, di, tri, tetra, and penta hapto dihydrogen complexes of Ti, where at 60 bar and 77 K, an average of 3.2 H_2 molecules per Ti (out of a possible 5 allowed by the 18 electron rule) were bound to the organometallic fragments. Bis(cyclopentadienyl) chromium on silica generates a surface 12 electron cyclopentadienyl-chromium(II) hydroxyl species proposed previously for

bis(cyclopentadienyl)chromium on silica,[27, 28] that can adsorb up to 3 hydrogen molecules per chromium according to the 18 electron rule. In order to more accurately quantify the amount number of H_2 ligands per Cr center, ICP analysis was conducted on the Cr doped silica material, yielding a more precise value of 4.50 wt% Cr in this sample. The experimental data on hydrogen adsorption at 77 K in addition to the 4.50 wt% Cr present in the sample results in each chromium species adsorbing 2.9 hydrogen molecules, close to the 3 molecules expected from the 18 electron rule. So under these conditions the bis(cyclopentadienyl) chromium doped silica is much closer to saturation than the benzyltitanium doped silica, and this may explain the difference between the two isotherms with respect to saturation behavior. The 4.50 wt % loading level of the bis(cyclopentadienyl) chromium doped silica corresponds to 0.33 Cr per nm^2, less than the 0.43 Ti per nm^2 observed in the tetrabenzyltitanium doped system. Loading levels of 7.5 % and 10 % led to diminished hydrogen storage capacity in all cases, which suggests that interference between neighboring surface species can be a problem at higher loading levels.

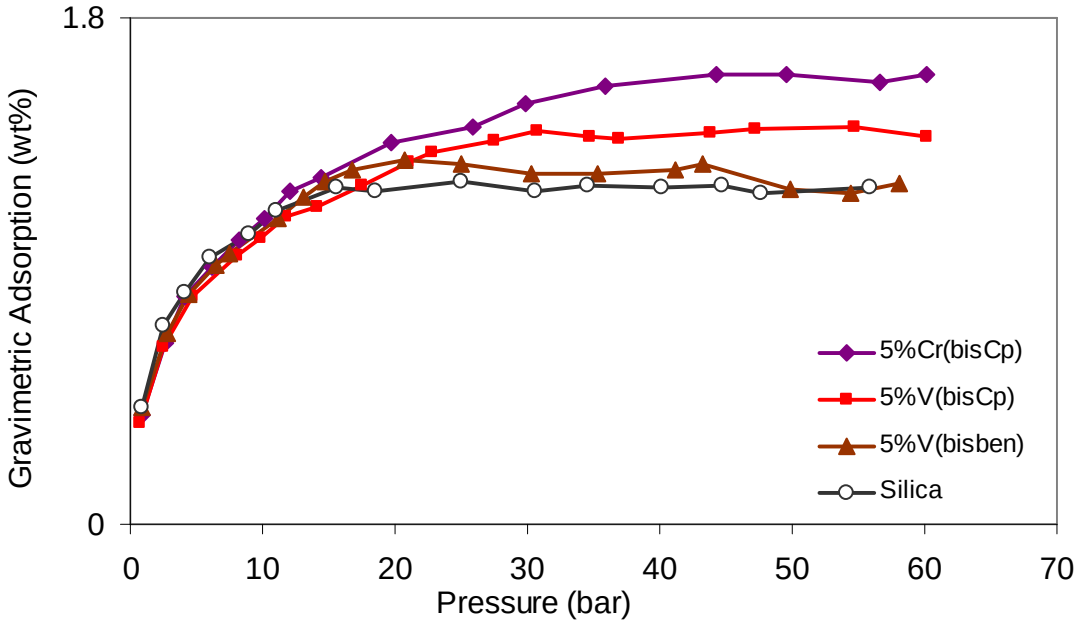

Figure 2.6: Gravimetric hydrogen adsorption on silica and silica treated with Cr and V sandwich compounds at 77 K.

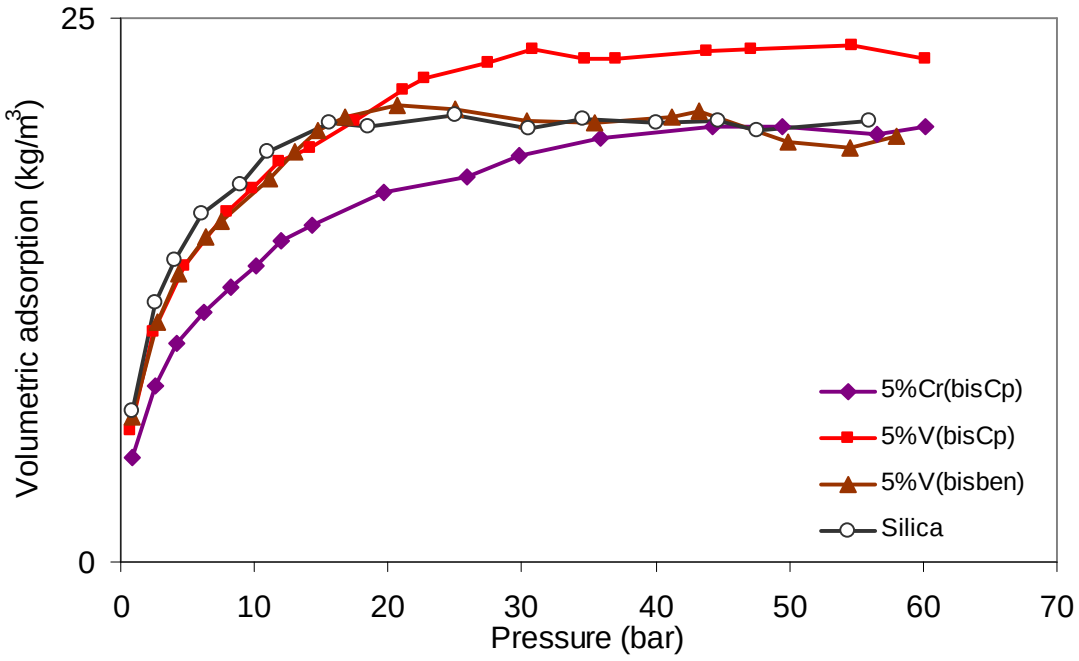

Figure 2.7: Volumetric adsorption isotherms of hydrogen on sandwich organometallic supported silica at 77 K.

Table 2.2: Adsorption and storage data of silica and silica reduced by sandwich compounds.

Sample Name	Skeletal Density (g/cm^3)	Apparent Density (g/cm^3)	Gravimetric Adsorption at 77 K and 60 bar (wt. %)	Gravimetric Storage at 77 K and 60 bar (wt. %)	Volumetric Storage at 77 K and 60 bar (kg/m^3)
Silica	1.6866	0.2286	1.22	8.56	19.20
5%Cr(bisCp)/HMS	1.2500	0.2134	1.60	9.11	19.46
5%V(bisCp)/HMS	1.6833	0.2411	1.41	8.00	19.31
5%V(bisben)/HMS	1.6220	0.2065	1.30	9.31	19.21

Instrument was calibrated with Carbon AX-21 at 4.5 wt. % adsorption at 77 K and 60 bar.

When using bis(cyclopentadienyl)vanadium as dopant, cyclopentadienyl vanadium hydroxyl moieties similar to those of silica supported bis(cyclopentadienyl)chromium are observed.[25] The silica treated with bis(cyclopentadienyl)vanadium sample possesses higher adsorption and storage capacities than that of pristine silica, but lower than that of the chromium analogue. While the surface species should also be able to absorb up to 3

H_2 per metal, the reason for the lower capacity at the same metal loading level may be related to the greater electron richness of the Cr center (d^4) as compared to the V analogue (d^3) leading to more effective back-bonding to H_2 for Cr than V.

When using bis(benzene)vanadium as precursor, the resulting grafted species are different from the Cr and V cyclopentadienyl precursors. Two benzene rings are released and vanadium is deposited on the silica surface as a V(II) hydride. Thus the species b) and c) in figure 2.3 are likely the active species in hydrogen adsorption,[29] and are obviously not as effective at binding H_2 than the cyclopentadienyl analogues for reasons that are not yet clear.

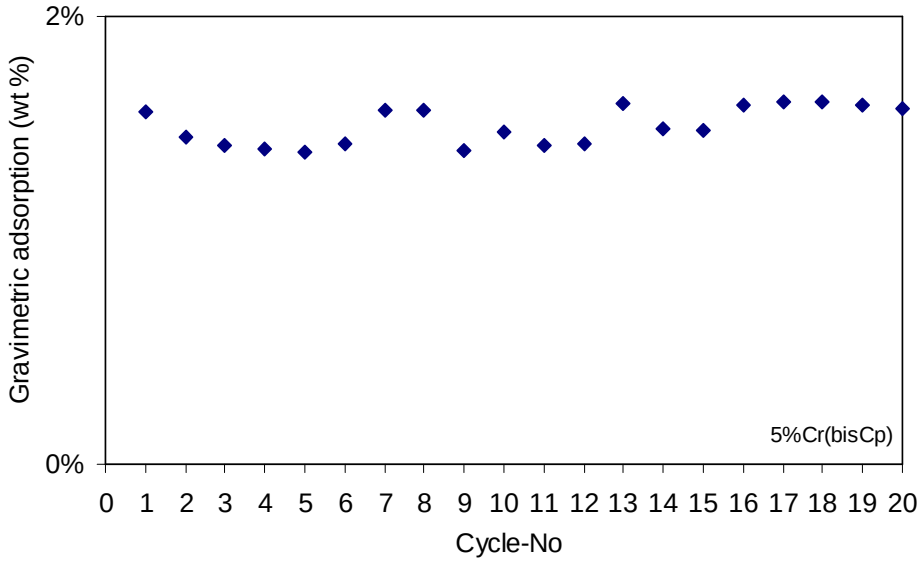

Figure 2.8: Hydrogen adsorption capacity at 77 K in a 20 cycle test of the 5%Cr(bisCp) sample.

While hydrogen adsorption measures the amount of hydrogen adsorbed on the surface of a material, the total storage capacity consists of the adsorbed hydrogen on the surface in addition to the compressed hydrogen gas in the void space within the pore volume of the mesoporous materials. This number is dependent on the apparent density of the sample, which changes with sample compression, but is included because it gives an accurate reading of the amount of hydrogen present within a certain weight or volume of a sample at a certain level of powder compression. This data is shown for all materials in table 2.2.

The 5%Cr(bisCp) sample had the highest volumetric hydrogen storage value of 19.46 kg/m^3 at 77 K and 60 bar, higher than that of pristine silica with 19.20 kg/m^3.

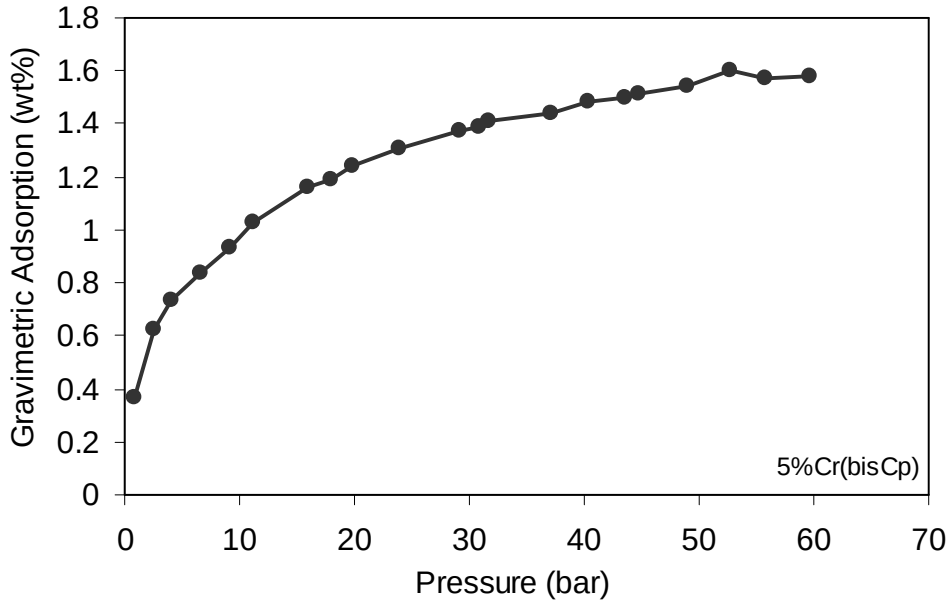

Figure 2.9: Gravimetric hydrogen adsorption isotherm at 77 K of the 5%Cr(bisCp) sample. Preparation date: July 08th, 2008. Test date: October 02nd, 2008.

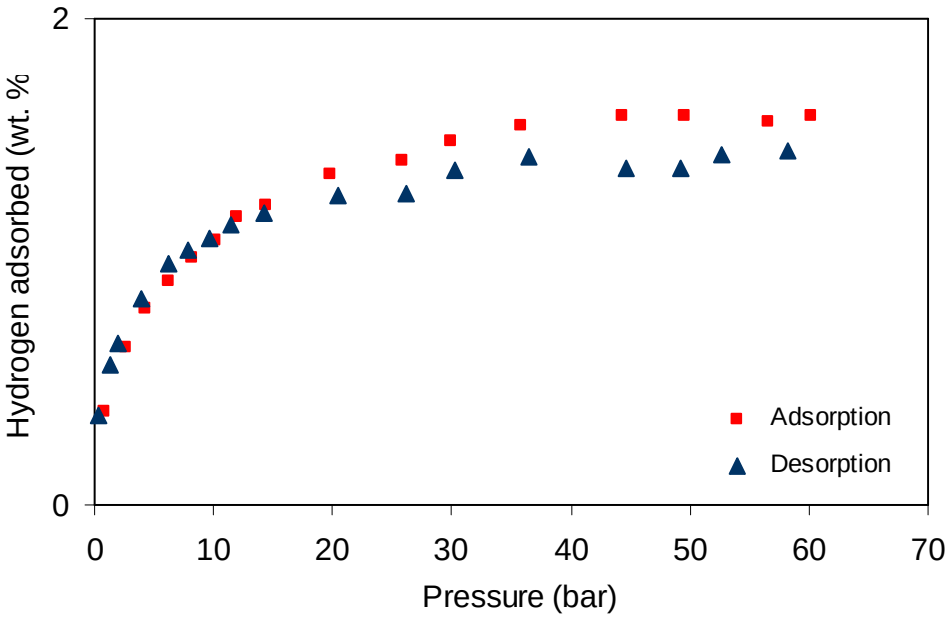

Figure 2.10: Hydrogen adsorption and desorption at 77 K of the 5%Cr(bisCp) sample.

The reversibility and long-term performance over several cycles is also of crucial importance. 20 adsorption cycles of the 5%Cr(bisCp) sample were performed during a week period and show stable performance of this material under these conditions (fig. 2.8). The adsorption capacity was completely retained during this time. Furthermore, it was found that the hydrogen adsorption capacity of this sample was fully retained three months after the preparation date when stored under inert atmosphere (figure 2.9). The adsorption – desorption isotherms at 77 K of this sample shown in figure 2.10 demonstrate fully reversible adsorption – desorption with a slight hysteresis at high pressure. This differs from the tetrabenzyltitanium system which shows a 53 % reduction in adsorption capacity after three weeks under nitrogen at room temperature, suggesting that the Cr system may lead to the development of downstream materials with a much greater chance of commercial application.

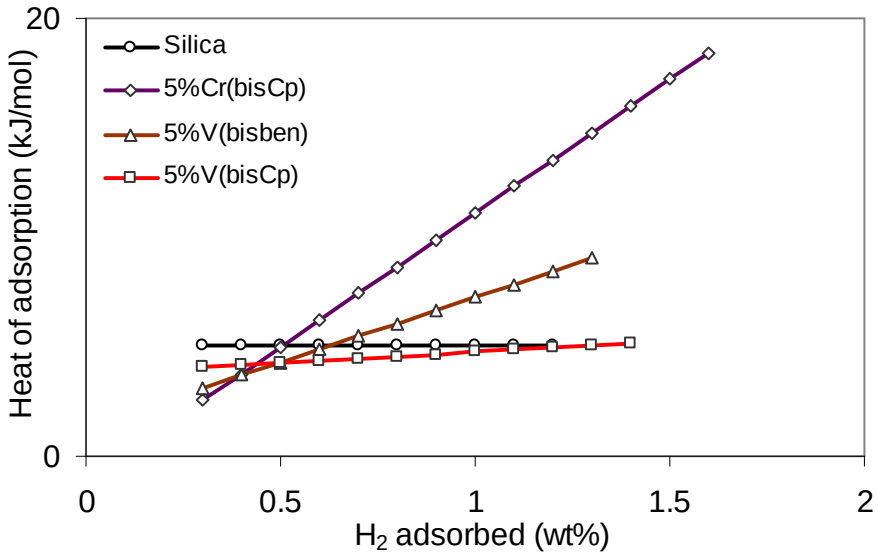

Figure 2.11: Adsorption enthalpies of pristine silica and pristine silica treated with sandwich compounds.

Two sets of adsorption data at 77 K and 87 K were used to calculate the adsorption enthalpies using a variant of the Clapeyron – Clausius I equation. The results obtained showed the same unusual trend of rising adsorption enthalpies with surface coverage observed for all materials studied in our group involving reduced transition metal centers as binding sites.[18, 19, 25, 36] The heat of adsorption on bis(cyclopentadienyl) chromium

supported silica sample rises to 18.43 kJ mol H_2^{-1} at a maximum surface coverage of 1.60 wt. % of hydrogen (Figure 2.11). This is the second highest value recorded under cryogenic conditions, directly behind our tetrabenzyltitanium system at 22.15 kJ/mol.[18] The bis(cyclopentadienyl) vanadium and bis(benzene) vanadium supported silica samples also show this rising trend, however, the heats of adsorption rise only to 9.02 kJ/mol and 5.04 kJ/mol, respectively. These lower enthalpies correspond with the lower hydrogen uptake of these samples at 77 K. The hydrogen adsorption of bis(cyclopentadienyl) chromium supported on silica is higher and stronger than that of bis(cyclopentadienyl) chromium supported on mesoporous titanium oxide previously studied by our group, which absorbs up to 1.01 wt % with an adsorption enthalpy of 8.353 kJ/mol. This may be due to the higher concentration of low-valent chromium species in the silica supported sample than the titania supported sample, as confirmed by XPS studies, under the assumption that electron rich metals bind H_2 more effectively. Hence, with similar doping amounts (5 wt % on silica and 5.4 wt % on titania), higher XPS intensities are observed on the doped-silica material. Although the value of 18.43 kJ/mol still falls short of the ideal enthalpies calculated by Zhao et al,[16] adsorption analysis from Bhatia and Meyers[37] suggests that a heat of adsorption of 15.1 kJ/mol is optimal for reversible adsorption at 253 K.

As expected for a material with a higher binding enthalpy, a substantial amount of the capacity is retained at higher temperatures. At -78 ^{o}C and 60 bar, 0.89 wt % adsorption was achieved on the bis(cyclopentadienyl) chromium doped sample in comparison with 0.63 wt % on the pristine silica (Table 2.3). This corresponds to only a 44 % loss in total excess adsorption capacity when comparing to adsorption capacity at 77 K and 60 bar at 1.60 wt%. Since this total adsorption contains a component of physisorption to the silica surface and a component of binding to the transition metal fragments, it is important to also calculate the amount of hydrogen retained on the Cr center only. Calculations based on 5 wt% Cr and the hydrogen adsorption of pristine silica under these conditions thus demonstrate that each Cr center retains 71 % of its capacity with each chromium species holding 1.51 H_2 molecules, as compared to 2.2 at 77 K. At room temperature, only 18 % adsorption capacity of each chromium species is retained, which is lower than the 41 % retention exhibited by the tetrabenzyltitanium material. This may be expected due to the

higher adsorption enthalpy of 22.15 kJ/mol in this material related to the 18.43 kJ/mol in the Cr doped material.

To reduce the void space within the pore areas of the materials and increase the volumetric number of active species, pellets were made by compressing the materials at 4000 psi. The compressed material was found to have higher volumetric storage capacity than the powder sample, up to 22.81 kg/m^3 at 77 K and 60 bar.

Table 2.3: Hydrogen storage capacities of pristine and Cr-grafted mesoporous silica at different temperature.

Sample Name	Skeletal Density (g/cm^3)	Apparent Density (g/cm^3)	Gravimetric Adsorption at 77 K and 60 bar (wt. %)	Gravimetric Storage at 77 K and 60 bar (wt. %)	Volumetric Storage at 77 K and 60 bar (kg/m^3)
Silica at -196 ^{o}C	1.6866	0.2286	1.22	8.56	19.20
Silica at -78 ^{o}C	1.6866	0.2286	0.63	3.22	7.38
Silica at 25 ^{o}C	1.6866	0.2286	0.44	2.43	5.55
5%Cr(bisCp)/HMS at -196 ^{o}C	1.2500	0.2134	1.60	9.11	19.46
5%Cr(bisCp)/HMS at -78 ^{o}C	1.2500	0.2134	0.89	4.06	8.73
5%Cr(bisCp)/HMS at 25 ^{o}C	1.2500	0.2134	0.51	2.43	5.17
5%Cr(bisCp)/HMS Pellet at -196 ^{o}C	1.7559	0.7564	1.23	3.11	22.81
5%Cr(bisCp)/HMS Pellet at -78 ^{o}C	1.7559	0.7564	0.37	0.91	10.99
5%Cr(bisCp)/HMS Pellet at 25 ^{o}C	1.7559	0.7564	0.25	0.66	5.25

Instrument was calibrated with AX-21 at 4.5 wt. % adsorption at 77 K and 6.0 MPa.

2.4 Conclusions

In summary, a series of mesoporous silicas grafted with V or Cr sandwich compounds were prepared and investigated as substrates for hydrogen storage exploiting the Kubas interaction. In all cases, the metal fragment grafted to the surface improved the adsorption of hydrogen with respect to pristine silica, The bis(cyclopentadienyl) chromium doped sample showed the highest performance, with adsorption values of 1.6 wt % at 77 K and an enthalpy of 18.43 kJ/mol, the second highest recorded for a cryogenic material. This material also proved thermally stable for several months under nitrogen, making it superior in many ways to previously studied tetrabenzyltitanium

doped silica, which was stable for only a few weeks under these conditions. As expected for high enthalpy materials, a substantial degree of the performance of the metal centers was retained at –78 °C and room temperature.

2.5 References

(1) Seayad, A. M; Antonelli, D.M. *Adv. Mater*. **2004**, 16, 765.

(2) Hoang, T. K. A.; Antonelli, D. M. *Adv. Mater.* **2009**, 21, 1787.

(3) Fuel Cell Technologies Program Multi-Year Research, Development and Demonstration Plan. http://www1.eere.energy.gov/hydrogenandfuelcells/mypp/ Retrieved August 06th, 2009.

(4) Schlapbach, L.; Zuettel, A. *Nature* **2001**, 414, 353.

(5) Yaghi, O. M.; O'Keeffe, M.; Ockwig, N. W.; Chae, H. K.; Eddaoudi, M.; Kim, J. *Nature* **2003**, 423, 705.

(6) Felderhoff, M.; Weidenthaler, C.; von Helmolt, R.; Eberle, U. *Phys. Chem. Chem. Phys*. **2007**, 9, 2643.

(7) Zuettel, A. *Material Today* **2003**, 6, 9, 24.

(8) Fichtner, M *Advanced Engineering Materials* **2005**, 7, 443.

(9) Zuettel, A.; Sudan, P.; Mauron, P.; Kiyobayashi, T.; Emmenegger, C.; Schlapbach, L. *Int. J. Hydrogen Energy*, **2002**, 27, 203.

(10) Dincă, M.; Long, J. R. *Angew. Chem. Int. Ed*. **2008**, 47, 6766.

(11) Mark Thomas, K. *Dalton Trans*., **2009**, 1487-1505.

(12) van den Berg, A. W. C.; Arean, C. O. *Chem. Commun*. **2008**, 6, 668.

(13) Orimo, S.; Nakamori, Y.; Eliseo, J. R.; Zuettel, A.; Jensen, C. M. *Chem. Rev*. **2007**, 107, 4111.

(14) Sandrock, G.; *J. Alloys Comp*. **1999**, 293, 877.

(15) 2011 Interim Update – Technical Plan – Storage. http://www1.eere.energy.gov/hydrogenandfuelcells/mypp/pdfs/storage.pdf Retrieved in August 06th, 2009.

(16) a) Dailly, A.; Vajo, J. J.; Ahn, C.C. *J. Chem. Phys. B* **2006**, 110, 1099; b) Panella, B.; Hirscher, M.; Pütter, H.; Müller, U. *Adv. Funct. Mat*. **2006**, 16, 520; c) Langmi, H. W.; Book, D.; Walton, A.; Johnson, S. R.; Al-Mamouri, M. M.; Speight, J. D.; Edwards, P. P.; Harris, I. R.; Anderson, P. A. *J. Alloy. Compd*. **2005**, 404–406, 637; d) Kaye, S. S.; Long, J. R. *J. Am. Chem. Soc*. **2005**, 127, 6506; e) Strobel, R.; Garche, J.; Moseley, P. T.; Jorissen, L.; Wolf, G. *J. Power Sources* **2006**, 159, 781; f) Hirscher, M.; Panella, B. *Scripta Materialia* **2007**, 56, 809; g) Hirscher, M.; Panella, B. *Scripta Materialia* **2007**, 56, 803.

(17) Zhao, Y.; Kim, Y.; Dillon, A. C.; Heben, M. J.; Zhang, S. B. *Phys. Rev. Lett*. **2005**, 94, 155504.

(18) Hamaed, A.; Trudeau, M.; Antonelli, D. M. *J. Am. Chem. Soc*. **2008**, 130, 6992.

(19) Hamaed, A.; Hoang, T. K. A.; Trudeau, M.; Antonelli, D. M. *J. Organomet. Chem*. **2009**, 694, 2793.

(20) a) Kubas, G. J.; Ryan, R. R.; Swanson, B. I.; Vergamini, P. J.; Wasserman, H. J. *J. Am. Chem. Soc*. **1984**, 106, 451; b) G. J. Kubas, *Chem. Rev*. **2007**, 107, 4152.

(21) a) Heinekey, D. M.; Lledós, A.; Lluch, J. M. *Chem. Soc. Rev*. **2004**, 33, 175; b) Heinekey, D. M.; Oldham, Jr., W. J. *Chem. Rev*. **1993**, 93, 913.

(22) a) Kaye, S. S.; Long, J. R. *J. Am. Chem. Soc*. **2005**, 127, 6506; b) Dinca, M.; Long, J. R. *J. Am. Chem. Soc*. **2005**, 127, 9376; c) Dinca, M.; Yu, A. F.; Long, J. R. *J. Am. Chem. Soc*. **2006**, 128, 8904; d) Dinca, M.; Dailly, A.; Liu, Y.; Brown, C. M.; Neumann, D. A.; Long, J. R. *J. Am. Chem. Soc*. **2006**, 128, 16876; e) Dinca, M.; Long, J. R. *J. Am. Chem. Soc*. **2007**, 129, 11172.

(23) Vitillo, J. G.; Regli, L.; Chavan, S.; Ricchiardi, G.; Spoto, G.; Dietzel, P. D. C.; Bordiga, S.; Zecchina, A. *J. Am. Chem. Soc.* **2008**, 130, 8386.

(24) Tanev, P. T.; Pinnavaia, T. N. *Science* **1995**, 267, 865.

(25) Hu, X.; Trudeau, M.; Antonelli. D. M. *Chem. Mater*. **2007**, 19, 1388.

(26) Fischer, E. O.; Reckziegel, A. *Chem. Ber.* **1961**, 94, 2204.

(27) a) Fu, S. L.; Lunsford, J. H. *Langmuir* **1990**, 6, 1774; b) Schnellbach, M.; Kohler, F. H.; Blumel, J. *J. Organometal. Chem*. **1996**, 520, 227.

(28) a) Karol, F. J.; Karapinka, G. L.; Wu, C. -S.; Dow, A. W.; Johnson, R. N.; Carrick, W. L. *J. Polym. Sci. A-1*, **1972**, 10, 2621; b) F. R. Karol, C. –S. Wu, W. T. Reichle, N. J. Maraschin, *J. Catal*. **1979**, 60, 68.

(29) Zakharkin, A. A.; Bagdasar'yan, A. K.; Makovetskii, K. L.; Dolgoplosk, B. A. *Izvestiya Akademii Nauk SSSR, Seriya Khimicheskaya* **1986**, 12, 2817.

(30) Handbook of X-ray Photoelectron Spectroscopy: Physical Electronics Division, Perkin-Elmer Corp.: Eden Prairie, MN.

(31) Desimoni, E.; Malitesta, C; Zambonin, P.G.; Riviere, J. C. *Surf. Interface Anal*. **1988**, 13, 173.

(32) NIST X-ray Photoelectron Spectroscopy Database. http://srdata.nist.gov/xps/Default.aspx Retrieved on August 06th, 2009.

(33) a) He, X.; Trudeau, M.; Antonelli, D. M. *Inorg. Chem*. **2001**, 40, 6463; b) He, X.; Trudeau, M.; Antonelli, D. M. *Adv. Mater*. **2000**, 12, 1036.

(34) Ozin, G. A.; Gil, C. *Chem. Rev*. **1989**, 89, 1749.

(35) Nag, N. K.; Massoth, F. E. *J. Cata*. **1990**, 124, 127.

(36) a) Hu, X.; Skadtchenko, B. O.; Trudeau, M.; Antonelli, D. M. *J. Am. Chem. Soc*. **2006**, 128, 11740. b) Hu, X.; Trudeau, M.; Antonelli, D. M. *Inorg. Chem*. **2008**, 47, 2477.

(37) Bhatia, S. K.; Myers, A. L. *Langmuir* **2006**, 22, 1688.

Supplemental Information for Chapter 2 – Bis(benzene) and bis(cyclopentadienyl) V and Cr doped mesoporous silica with high enthalpies of hydrogen adsorption

Example of adsorption enthalpy calculation using hydrogen adsorption data at 77 K and 87 K.

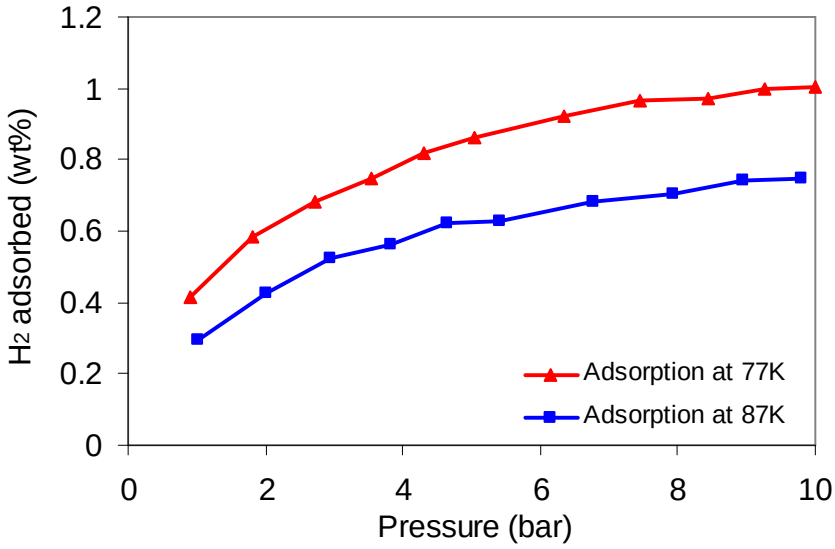

Figure S1.1: Hydrogen adsorption from 0 to 10 atm at 77 K and 87 K of 5%Cr(bisCp) materials.

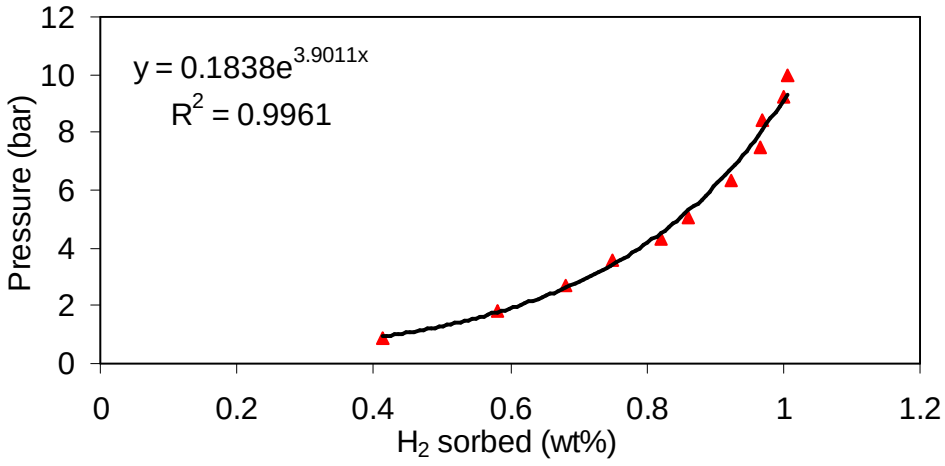

Figure S1.2: Exponential fitting of adsorption data at 77 K.

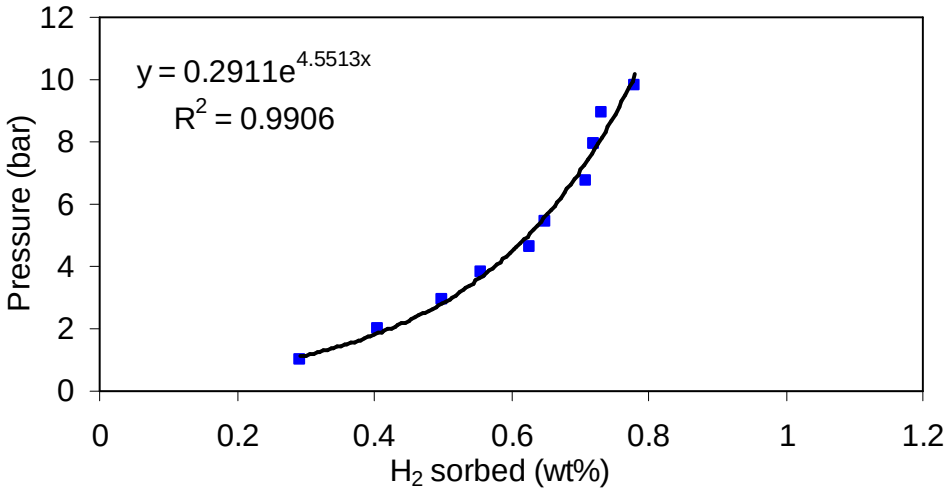

Figure S1.3: Exponential fitting of adsorption data at 87 K.

Heat of adsorption is calculated as the table below:

H_2 sorbed (wt%)	Pressure P_1 at T_1 = 77 K	Pressure P_2 at T_2 = 87 K	Calculated adsorption enthalpy (kJ/mol)
0.3	0.634525	1.000543	2.54
0.4	0.824706	1.619589	3.76
0.5	1.071888	2.621647	4.98
0.6	1.393156	4.243688	6.20
0.7	1.810714	6.869303	7.43
0.8	2.353424	11.11942	8.65
0.9	3.058796	17.99912	9.87
1.0	3.975583	29.13536	11.09
1.1	5.167151	47.16173	12.31
1.2	6.715857	76.34120	13.54
1.3	8.728743	123.5743	14.76
1.4	11.34494	200.0311	15.98
1.5	14.74526	323.7924	17.20
1.6	19.16473	524.1263	18.43

Chapter 3 - Design and synthesis of vanadium hydrazide gels for Kubas-type hydrogen adsorption: a new class of hydrogen storage materials

3.1 Introduction

Hydrogen is an ideal fuel because it is clean and renewable and possesses the highest amount of energy per gram of any chemical substance. However, the storage of hydrogen still remains elusive.[1] Some metal hydrides[2] contain enough hydrogen to satisfy the 2017 gravimetric (5.5 wt%) and volumetric (40 kg/m^3) targets established by the US Department of Energy (DOE), however sluggish kinetics and problems due to high enthalpies of adsorption (70 kJ/mol) necessitate exotic engineering solutions that substantially lower these values in any practical system. In contrast, physisorption materials[3] adsorb up to 7.5 wt.% of hydrogen at 77 K with heats of adsorption in the range of 4 – 13 kJ/mol H_2,[4] but cooling to cryogenic temperatures dramatically cuts into the efficiency of this technology. Because of the limitations of these technologies researchers have begun to explore the potential of the Kubas interaction, a non-dissociative weak form of hydrogen chemisorption that relies on strong back-donation of electron density into the H-H antibonding orbital.[5-9] Calculations by Zhao et al[7] and Yildirim et al[10] demonstrated that this approach is viable using systems containing a high concentration of low-coordinate early transition metal species in low oxidation states with ideal heats of adsorption within the range of 20 – 30 kJ/mol. In this regard, many high surface area materials, including manganese-containing metal-organic framework materials,[11] in which one Mn can bind up to 1 H_2, have been studied. Silica-supported organotitanium(III),[12] and organochromium[13] species which adsorb up to an average of 3.8, and 2.2 H_2 per metal atom at 77 K and 60 bar, respectively, with enthalpies in the 18 – 23 kJ/mol range have also been studied. Because of these higher enthalpies, up to 41% of the adsorption at the Ti center is retained at 298 K, corresponding to 1.8 H_2/Ti. However the active metal in these systems corresponds to at most 5% of the total weight, making the contribution from the Kubas interaction negligible. For this reason we chose to fabricate new extended solids using a small and light linker group to bridge coordinatively unsaturated metal centers capable of binding H_2. Hydrazine is the ideal linker because it is large enough to keep the metal centers apart and prevent clustering,

yet also small enough to minimize void space, which decreases volumetric performance. The hypothetical microporous solid MN_2H_x (M = Cr, V, Ti) should hold roughly 5% H_2 at room temperature based on 1.8 H_2 per metal, on the basis of the molecular weight, and the best results observed in the silica-supported systems. These microporous solids have a high density of transition metal centers which are capable of forming Kubas interactions with appropriate energy. Thus, by analogy to the protolysis reaction of trimethylaluminium with hydrazine to yield an amorphous aluminium hydrazide gel,[14] we hypothesized that the reaction of a low-valent, low-coordinate early transition metal alkyl complex possessing bulky ligands to stabilize the low coordination number, with just enough hydrazine to eliminate the alkyl groups and bridge the transition metals should create a microporous network in which the metal centers are kinetically "frozen" into an unusually low coordination state capable of binding H_2. Using this method a cyclopentadienyl chromium hydrazide gel was recently synthesized in our group that possesses a low specific surface area of 32 m^2/g, but adsorbs up to 1.75 wt% of hydrogen at 77 K and 80 bar.[15] The most exciting feature of this material is that 49% of the 77 K adsorption capacity is retained at room temperature as compared to less than 15% for physisorption materials. This is because of the high adsorption enthalpies, which rise from 10 to 45 kJ/mol with adsorption. While these materials were a step forward in many ways, the Cr centers still retained one cyclopentadienyl group, essentially limiting the activity by shutting down 3 coordination sites per metal that could be used as binding sites for dihydrogen. In this work, trimesitylvanadium(III)·(THF) was chosen as a precursor because of its ease of synthesis, low coordination number, and the ability of V(III) to back-bond to the H-H antibonding orbital. Previous results from our group also showed that vanadium(III) organometallic fragments grafted on silica coordinate 2.68 and 0.37 H_2/V at 80 bar and 77 K or 298 K, respectively.[16] Mesitylene ligands are also more readily eliminated by protolysis reactions than cyclopentadienyl groups and should thus allow for a greater concentration of Kubas binding sites per unit volume than the Cr hydrazide materials mentioned above.

3.2 Experimental Section

Chemicals were purchased from Aldrich and used as is.

3.2.1 Preparation of $V(Mes)_3 \cdot THF$: To 50ml of mesitylmagnesiumbromide 1 M (MesMgBr) in tetrahydrofuran (THF) was added 33.33 ml of THF. 6.22 g of $VCl_3 \cdot 3THF$ 97% was then added portion by portion. The obtained solution was stirred vigorously at room temperature for 2 hours after which a clear blue solution was obtained. 21.66 ml of dioxane was then added to the solution with stirring. After 2 more hours, stirring was ceased and the solution was left to settle before filtering. The filtrate was collected and concentrated in vacuum until crystals formed. 16.67 ml of diethyl ether was then added and the remaining product precipitated. The solid product was then collected by filtration and washed several times with a solution of THF and ether (THF: ether = 1:3 by volume) before drying in vacuum.[17]

3.2.2 Preparation of anhydrous hydrazine: Pure hydrazine was prepared from hydrazine monohydrate by azeotropic distillation with toluene to remove water and avoid possible explosion. 100ml of hydrazine monohydrate and 250ml of toluene were added to a 500 ml one neck round bottom flask, equipped with a thermometer to measure the gas temperature. A water condenser was connected and followed by 2 flasks to collect the waste liquid and dry hydrazine. The first step of distillation was carried out under argon and atmospheric pressure with water and toluene as products, which were collected at the first flask and removed at the end of this step. In the second step, 35 g of NaOH was added to the hydrazine-toluene flask and the system was distilled under vacuum. Pure hydrazine was collected in the second flask.[14b]

3.2.3 Preparation of A100 and A150 vanadium hydrazide samples: The A100 sample was synthesized as follows: $V(Mes)_3 \cdot THF$ (3.0 g, 6.24 mmol) was dissolved in 75ml of dry toluene at room temperature in an Erlenmeyer flask. 0.15 ml of hydrazine (0.15 ml, 4.68 mmol) was then added by syringe with vigorous stirring. The solution was stoppered and stirring was continued for 12 hours. The solution was then heated to 100 ^oC for 3 hours with stirring. After this, the system was filtered and a black solid was obtained. This solid was transferred to an air-free tube and was put under vacuum at room temperature for 12 h, followed by heating at 60 ^oC in vacuum for a period of 6 hours followed by another 6 hours in vacuum at 100 ^oC. The A150 sample was obtained by continuing heating the A100 at 150 ^oC for 6 hours in vacuum.

Preparation of B100 and B150 sample: the same procedure was followed as with the A100, and A150 samples, but with 0.20 ml of hydrazine.

Preparation of C100 and C150 sample: the same procedure was followed as with the A100, and A150 samples, but with 0.30 ml of hydrazine.

Preparation of D100 and D150 sample: the same procedure was followed as with the A100, and A150 samples, but with 0.40 ml of hydrazine.

3.2.4 Characterization. Powder X-ray diffraction (XRD) was performed on Siemens diffractometer D-500 with Cu Kα radiation (40KV, 40mA) source. The step size was 0.02° and the counting time was 0.3 s for each step. Diffraction patterns were recorded in the 2θ range 2.3 - 52°. Samples for XRD analysis were put in a sealed capillary glass tube to protect sample from air and moisture during experiment.

Nitrogen adsorption and desorption data were collected on a Micromeritics ASAP 2010. All X-ray Photoelectron Spectroscopy (XPS) measurements were collected on samples prepared and loaded in a glove box, using a Physical Electronics PHI-5500 spectrometer. Obtained data were referenced to the carbon C-(C, H) peak at 284.8 eV. Elemental analysis was performed by Galbraith Labs, Knoxville Tennessee.

Infrared spectroscopy was conducted a Bruker Vector 22 instrument. In a typical experiment, 2 mg of sample was mixed with 500 mg of dry KBr and the pellet is made in inert atmosphere. The pellets were then transferred outside and the measurements were conducted immediately.

3.2.5 Hydrogen adsorption measurements. Hydrogen adsorption isotherms were obtained by using a computer controlled commercial Gas Reaction Controller manufactured by Advanced Materials Corporation, Pittsburgh, PA. High purity hydrogen (99.9995% purity) was used as the adsorbent. Hydrogen storage measurements on a standard AX-21 sample (4.5 wt. %) were performed to ensure proper calibration and functioning of the instrumentation. Leak testing was also performed during each measurement by checking for soap bubbles at potential leak points. These measurements are necessary to ensure the veracity of the isotherms. In the H_2 adsorption-desorption

experiments complete reversibility was observed for all samples across the entire range of pressures. Samples were run at liquid nitrogen temperature (77 K), liquid argon temperature (87 K), and room temperature (298 K) to 85 bar. Isotherms were always measured first at room temperature and then at 77 K or 87 K and the temperature is kept constant by keeping the sample chamber in liquid N_2, liquid Ar, or water. The skeletal density was measured using a Quantachrome Ultrapycnometer. The bulk density was recorded on a bench top density apparatus on finely ground powder samples of the materials. When the skeletal density is used for the gravimetric hydrogen uptake measurement, the compressed hydrogen within the pores is treated as part of the sample chamber volume. Therefore only the hydrogen contained on or beneath the walls of the structure will be recorded by the PCI instrument. This gravimetric value is termed the adsorption or excess storage. When the bulk density is used for this measurement the hydrogen in the pores of the sample is automatically included in the calculation without any further correction and the final value is termed the total storage[18] or absolute storage,[19] which represents all hydrogen contained in the sample including the compressed gas in the voids and the hydrogen adsorbed on or beneath the walls of the structure. Gravimetric densities are recorded as read directly from the isotherms while volumetric densities are calculated from the adsorption data and the skeletal or bulk density, depending on the desired value. The excess volumetric storage is typically calculated from the excess storage and the bulk density and gives a measure of the gas adsorbed on or in the solid phase of the material scaled across the entire volume occupied by the sample including the void space. In materials such as MOF's that posses a well-defined and constant ratio between mass and void space this value is often quoted. For compressible materials that may have variable ratios of solid mass and void space it can often help to scale the volumetric density to the solid phase alone as the void space will vary on sample preparation. For this purpose, we define the true volumetric adsorption as the amount of hydrogen adsorbed on or in the solid portion of the sample. This is calculated from the excess storage data and the skeletal density. This value neglects the void space and is useful in comparing volumetric densities ball-milled powders and gels to pure solid phase materials such as metal hydrides. Since the materials in this study are between hydrides and physisorption materials in their mechanism of storage, this value is

important. It also allows us to compare volumetric adsorption values of the solid phase alone from one sample to another without having to subtract out the void space. The absolute volumetric adsorption has also been defined[19] and is a representation of the sum of the excess volumetric storage plus the compressed gas in the void space. This can be calculated from the volumetric storage as measured from the instrument and the bulk density, or by taking the volumetric adsorption and adding on the amount in the void space calculated from the pore volume and the ideal gas law.[19] The first method is only possible when using the Advanced Materials instrument. In this paper we have chosen not to calculate this value (or the total gravimetric storage) because the differences between the skeletal densities and bulk densities are much smaller than in MOFs and hence the void space contribution is negligible.

Enthalpies of adsorption were calculated using a variant of the Clapeyron – Clausius I equation taking both 77 K and 87 K hydrogen excess storage data.

$$\ln\left(\frac{P_2}{P_1}\right) = -\Delta H_{adsorption}\,\frac{T_2 - T_1}{R.T_2.T_1} \qquad (1)$$

Where P_n = pressure for isotherm n, T_n = temperature for isotherm n, R: gas constant.

Pressure as a function of the amount adsorbed was determined by using exponential fit for each isotherm; the first 10 – 11 points of the isotherms were picked up and fit to the exponential equation. This exponential equation gives an accurate fit over the pressure up to 1 MPa with the goodness of fit (R^2) above 0.99. The corresponding P_1 and P_2 values at a certain amount of H_2 adsorbed at both temperatures can be obtained by the simulated exponential equation. Inputting these numbers into equation 1, we then calculate the adsorption enthalpies.

3.2.6 EPR experimental details: EPR spectra were collected at room temperature using a Bruker EMXplus X-band (~9.4 GHz) spectrometer. Samples were placed in 4 mm outer-diameter quartz tubes sealed with 'O' ring needle valves. Sample volumes were ~300 μL. To produce hydrogen loaded samples, hydrogen gas (grade 6) was applied directly, at a

pressure of 1 atmosphere, to the sample within the EPR tube using an air-tight purge valve to ensure an inert environment.

3.3 Results and Discussions

Trimesitylvanadium(III)·THF was reacted with varying ratios of anhydrous hydrazine in dry toluene. After 12 hours stirring, the reaction mixture was heated to 100 ^{o}C for 3 hours followed by filtration to obtain a black solid. This air and moisture sensitive material was heated in vacuum at 100 ^{o}C or 150 ^{o}C and the resulting materials named A100 and A150, respectively, for a $V(Mes)_3$·THF/N_2H_4 ratio of 4/3. Three other $V(Mes)_3$·THF/N_2H_4 ratios of 1/1, 2/3, and 1/2 were also employed and the samples named B100, B150, C100, C150, and D100, D150, respectively. A possible mechanism for this reaction is shown in scheme 3.1.

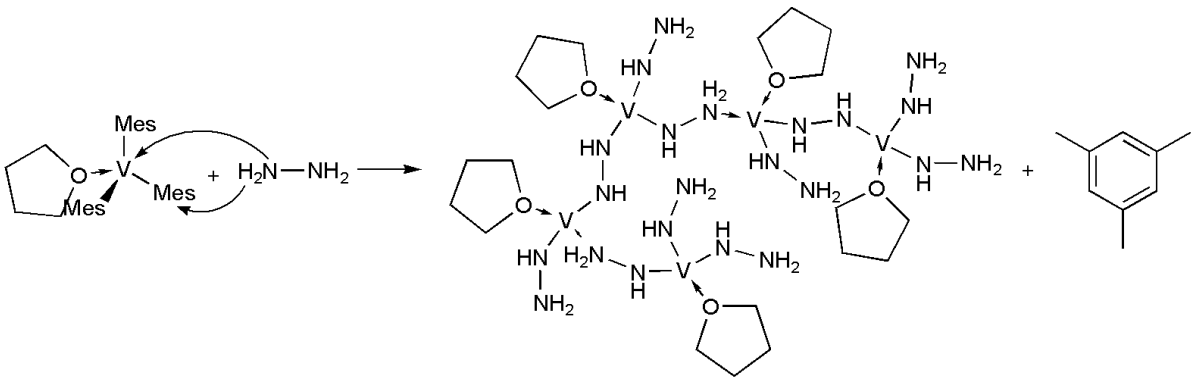

Scheme 3.1: Possible mechanism for the reaction between $V(Mes)_3$·THF and N_2H_4.

The powder x-ray diffraction (XRD) patterns for the vanadium hydrazide materials heated at 150 ^{o}C in vacuum are shown in figure S3.1. All patterns were similar and exhibit a single broad reflection corresponding to a $d_{spacing}$ of 1.96 nm. The position of this reflection suggests nanoscopic periodicity while the broadness reflection represents a lack of long-range order. Nitrogen adsorption isotherms recorded at 77 K are shown in figure S2. These isotherms show a small amount of microporosity comprising ca. 20% the total volume adsorbed, with additional mesoporosity and textural porosity accounting for the remaining adsorption in roughly equal proportions as evidenced by the slow rise between 0.2 and 0.8 P/P_0 and the sharp incline above 0.8 P/P_0, respectively. The specific

surface areas of all materials decrease with increasing the drying temperature from 100 to 150 ^{o}C. For example, C100 possesses a Brunauer – Emmett – Teller (BET) surface area of 524 m^2/g, but after heating in vacuum to 150 ^{o}C, the surface area decreases to 348 m^2/g.

Table 3.1: C, H, N and V concentration of vanadium hydrazide materials.

Sample	$V(Mes)_3 \cdot THF/N_2H_4$ ratio	Vanadium (%)	Carbon (%)	Hydrogen (%)	Nitrogen (%)
A150	4/3	37.00	13.58	2.46	10.54
B150	1/1	33.70	4.60	2.53	12.39
C150	2/3	52.25	4.01	1.87	16.60
D150	1/2	44.85	3.94	1.71	12.89

The C, H, N, and V elemental analysis data of vanadium hydrazide materials are shown in table 3.1 and reflect the decreasing trend in carbon concentration with increasing hydrazine at 150 °C, from 13.58 wt% to 3.94 wt%, consistent with a greater degree of elimination of arene with increased concentration of hydrazine. However, these carbon values are low due to carbide and nitride formation on combustion in the elemental analysis experiment, leading to less than 100% for all elements present. Drying at 150 ^{o}C leads to progressive arene elimination as monitored by IR spectroscopy (C-H stretch at 2850-2950 cm^{-1}) presumably by the thermally driven protolysis reaction between coordinated hydrazine and mesitylene groups. Aromatic C-C stretches are detected at 1589.62 cm^{-1} and 1405.12 cm^{-1} in the spectrum of the C150 sample as well as C – O stretches for THF (962.15 cm^{-1}), confirming the presence of residual THF and mesitylene in this material (fig. S3.13b).

X-ray Photoelectron Spectroscopy (XPS) studies of the vanadium hydrazides were conducted and the results are shown in figure S3.3 – S3.8. No charge neutralization was required and emissions are observed at the Fermi level, suggesting that these materials are metallic. Multiple oxidation states of vanadium are detected in the vanadium 2p 1/2,3/2 region (fig. S3.4 – S3.5). By comparison with literature values, the emissions at 512.8 eV and 520.0 eV correspond to V(0),[20] the emission at 513.8 eV and 520.9 eV can be assigned to a V(I) species,[21] and the emissions at 515.0 eV and 522.3 eV represents

V(III),[22] while the emissions at 516.4 eV and 523.8 eV correspond to V(IV).[23] The appearance of multiple oxidation states both lower and higher than the V(III) starting material is consistent with disproportionation, common with V. The XPS spectra of all materials in the N 1s region exhibit a broad emission centered at 396 eV with a shoulder at 398.5 eV which can be simulated as 3 major peaks (fig. S3.6 – S3.7). The first simulated emission located at 395.6 eV likely corresponds to an NH nitrogen bound directly to V.[24] The second emission located at 396.4 – 396.6 eV likely represents unbound terminal -NH_2 species,[25] while the third emission at 398 eV can be assigned to a quaternary hydrazinium species bound to V.[26] The A150 sample has a low intensity simulated peak at 398.8 eV, corresponding to a fourth nitrogen environment, possibly arising from a quaternary hydrazide nitrogen bound to V in a higher oxidation state than that from the emission at 398 eV.[27] There is also evidence for bound THF in the XPS from the oxygen region (fig. S3.8), as indicated by the high intensity emissions centered at 530.4 eV.[28] The difficulty removing THF is not surprising due to the well-documented high oxophilicity of early transition metals.

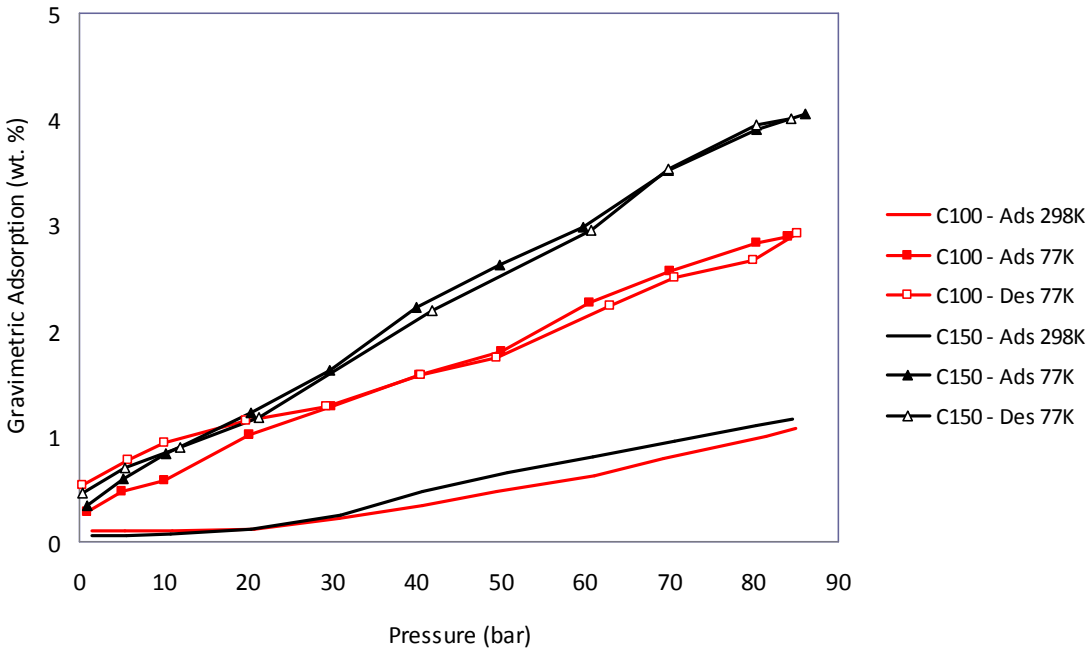

Figure 3.2: Hydrogen adsorption – desorption excess storage isotherms of C-series vanadium hydrazide materials synthesized with a V:hydrazine ratio of 1:1.5.

Table 3.2: Summary of excess storage results on vanadium hydrazide materials and carbon AX-21. Data recorded at 85 bar.

Material	BET Surface Area (m^2/g)	Skeletal Density (g/cm^3)	Gravimetric Adsorption (wt. %)	True Volumetric Adsorption (kg/m^3)	Retention (%)
A100	268	1.9174	2.08 (at 77 K) 0.84 (at 298 K)	40 (at 77 K) 16.1 (at 298 K)	40
A150	242	2.3795	1.66 (at 77 K) 0.68 (at 298 K)	39.5 (at 77 K) 18.2 (at 298 K)	41
B100	378	2.1640	2.22 (at 77 K) 0.70 (at 298 K)	48 (at 77 K) 15.2 (at 298 K)	32
B150	329	2.2000	1.50 (at 77 K) 0.43 (at 298 K)	33 (at 77 K) 9.5 (at 298 K)	29
C100	524	2.1557	2.88 (at 77 K) 1.07 (at 298 K)	62 (at 77 K) 23.1 (at 298 K)	37
C150	348	1.9792	4.04 (at 77 K) 1.17 (at 298K)	80 (at 77 K) 23.2 (at 298 K)	29
D100	307	2.0413	3.87 (at 77 K) 0.84 (at 298 K)	79 (at 77 K) 17.2 (at 298 K)	22
D150	256	2.4125	2.48 (at 77 K) 0.70 (at 298 K)	60 (at 77 K) 16.9 (at 298 K)	28
AX-21	3225	2.103	4.2 (at 77 K, 65 bar) 0.55 (at 298 K)	14 (at 77 K, 65 bar) -	13
MOF-5	3534		5.10 (at 77 K) 0.28 (at 298 K)		5.5

The excess storage isotherms of C100 and C150 samples are shown in figure 3.2. At 77 K these isotherms show an initial rise at low pressure consistent with a small amount of physisorption expected from the surface areas in the 242-524 m^2/g range, followed by a

linear region which only begins to reach saturation in the D series of these samples (table 3.2). At room temperature there is very little adsorption until 30 bar, after which a linear region emerges. Linear behavior without saturation is not typical of physisorption and suggests a different mechanism of hydrogen storage is operative in these materials. The gravimetric adsorption of the C150 sample is 1.17 wt. % at 85 bar and 298 K while the true volumetric adsorption of this sample is 23.2 kg H_2/m^3 (see experimental for full explanation of volumetric capacities). This represents the amount of hydrogen contained in and on the surface of the solid portion of the sample without the compressed gas in the void space. For comparison these values are over three times greater than those of compressed gas under the same conditions. At 77 K, this sample adsorbs 4.04 wt. %, corresponding to a true volumetric adsorption of 80 kg H_2/m^3. Using the bulk density measured for this sample of 1.49 g/cm^3 excess volumetric storage capacities of 60.01 kg H_2/m^3 and 17.43 kg H_2/m^3 can be determined. These volumetric capacities at 77 K are in the range of the ultimate DOE goal of 70 kg/m^3, while the capacities measured at ambient temperature are close to the DOE 2010 goal of 28 kg/m^3. The volumetric performance of 60.01 kg H_2/m^3 is greater than that of MOF-177, which possesses a excess volumetric storage of 32.0 kg H_2/m^3 at 77 K and an absolute volumetric adsorption at 77 K of 49.0 kg H_2/m^3.[19] By comparing the gravimetric adsorption at 298 K and 77 K, the retentions of excess adsorption capacities can be calculated, and range from 41% to 22%. This is much higher than that of MOF-5 and carbons AX-21, which retain 5.5% and 13%, respectively, and once again suggests a different mechanism than simple physisorption. These results establish that a molar ratio of 1:1.5 and heating temperature of 150 ^oC is the optimal synthesis condition for hydrogen adsorption performance.

Further discussion on the relationship between the synthesis conditions and physical properties of these materials is useful. The elemental analysis results demonstrate that hydrazine ratios of 1:1 and 4:3 are not sufficient to remove enough alkyl groups to ensure high activity by reducing the steric profile around the metal center and lowering the system weight through substitution of mesitylene for hydrazine, but the highest ratio of 2:1 leads to a material in which saturation is reached at 80 bar. This is consistent with excess hydrazine blocking coordination sites that would otherwise be available for H_2. Heating these materials to 150 ^oC causes an increase in skeletal densities and decreases of

gravimetric adsorption capacities of all samples except for the C100 sample. The increase in density is likely due to the elimination of alkyl groups, a process that was monitored by observation of the C-H stretch in the IR. Heating at 150 °C also eliminates the adsorption – desorption hysteresis at 0 – 20 bar pressure observed in the samples heated only to 100 ^{o}C. This hysteretic effect also diminishes with decreasing $V(Mes)_3.THF/N_2H_4$ reaction ratio.

Calculations on the basis of gravimetric adsorption and the vanadium content in each sample result in an average number of hydrogen molecules per vanadium atom (table 3.3) ranging from 1.13 – 1.96 H_2/V at 77K and 0.32 – 0.57 H_2/V at 298K. The reason for the lower than expected number of active binding sites is possibly due to inhomogeneity in the hydrazide gel which results in V(IV) and V(V) centers that do not bind H_2 and other V centers that may not be sterically accessible.

Table 3.3: Average number of hydrogen molecule adsorbed on each vanadium site at 85 bar.

Sample	Number of H_2/V at 77 K	Number of H_2/V at 298 K
A150	1.14	0.47
B150	1.13	0.32
C150	1.96	0.57
D150	1.41	0.40

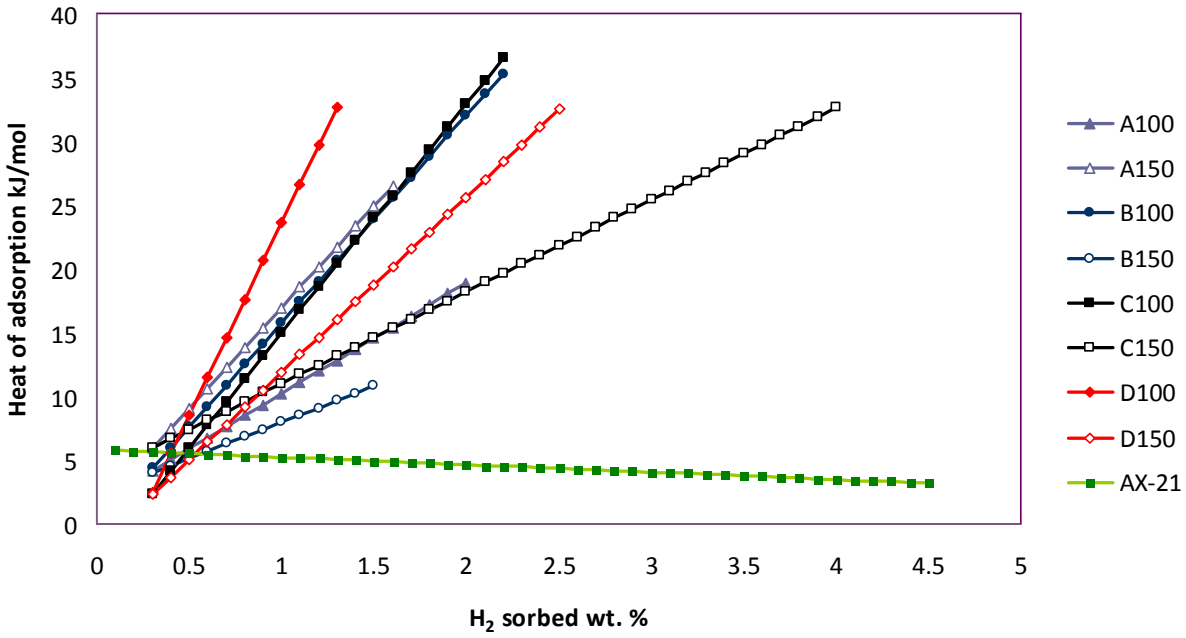

Figure 3.3: Heat of hydrogen adsorption on vanadium hydrazide materials and carbon AX-21.

A 20 cycle run at 298 K with pressures up to 85 bar was carried out on C150 sample. The results show no significant loss of excess adsorption capacity through cycling (Figure S3.12). By fitting the adsorption isotherms at 77 K and 87 K into the Clausius – Clapeyron equation, the isosteric heats of hydrogen adsorption can be calculated. The data for materials heated at 100 ^{o}C and 150 ^{o}C, as well as that of carbon AX-21 as a standard were measured under the same conditions (Figure 3.3). This isosteric heat of adsorption of all vanadium hydrazide materials rises from roughly 3-5 kJ/mol H_2 up to 36.5 kJ/mol H_2, contrasting strongly to the behavior of AX-21, which has enthalpies which decrease from 6 kJ/mol H_2 down to 3.3 kJ/mol H_2, typical of physisorption. The average value of the vanadium hydrazides falls in the range of 20 – 30 kJ/mol H_2, believed to be the ideal heat of hydrogen adsorption of suitable room temperature hydrogen storage materials.[7] The rising enthalpies with surface coverage, observed in all previous publications from our group concerning hydrogen storage on supported low-coordinate low-valent organometallic fragments, suggest a different adsorption mechanism, likely involving the Kubas interaction.[5, 12, 13] Rising enthalpies for Kubas-type hydrogen storage have been predicted in computations on hypothetical scandium

decorated bulkyballs, which show increasing binding energies for subsequent coordination of H_2 ligands from 0.30 eV for the first, to 0.35 eV for the second, and 0.42 eV for the third.[7]

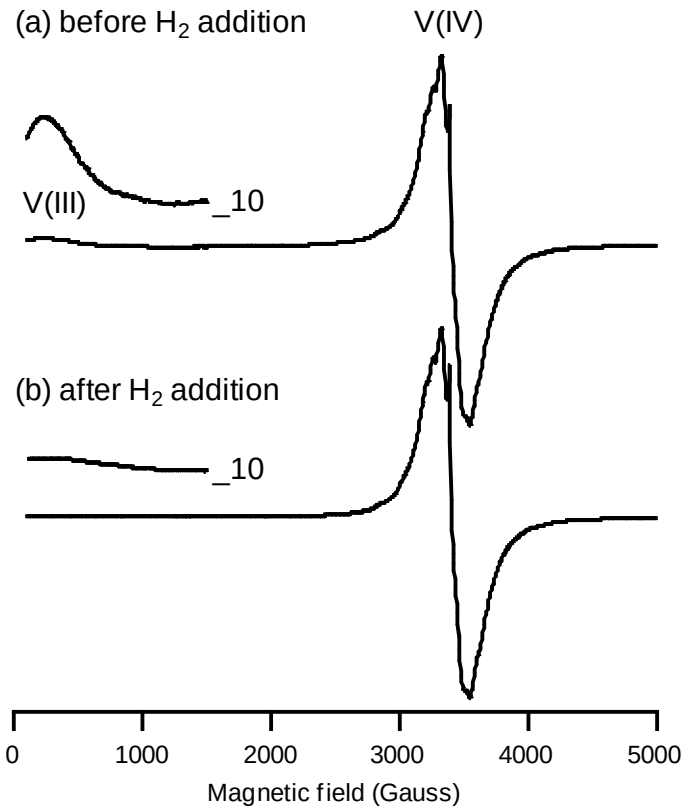

Figure 3.4: Room-temperature EPR spectra of vanadium hydrazide gel C150, (a) prior to exposure to hydrogen gas, and (b) after exposure to hydrogen gas. Insets: low-field region magnified by a factor of ten. *Experimental conditions*: frequency = 9.382 GHz, microwave power = 20 mW, time constant = 20.48 ms, modulation amplitude = 10 G, average of three 45 s scans.

In order to further confirm Kubas binding in this system, electron paramagnetic resonance (EPR) spectroscopic measurements were conducted on the C150 sample before and after hydrogen loading.[29] Prior to hydrogen addition, the X-band (9.4 GHz) EPR spectrum at room temperature shows a strong signal centered at 3411 G (g = 1.96), diagnostic of a V(IV) centre ($3d^1$, S = ½), with characteristic partially resolved hyperfine splittings (51V, I = 7/2, isotopic abundance = 99.75 %) (Figure 3.4 (a)).[29] A second paramagnetic species

was also observed, exhibiting a broad low-field peak (270 G), corresponding to a V(III) center ($3d^2$, S = 1).[30] EPR measurements of such species have been reported relatively infrequently, due to difficulties in measuring spectra from V(III) "non-Kramers" integer spin systems. Commonly, the zero-field splitting (zfs) of V(III) complexes is much larger than the microwave quantum used in EPR experiments (~0.3 cm^{-1} for X-band EPR) so that normally allowed transitions (DMS = ±1) are no longer within the field/frequency range of conventional spectrometers.[31,32] However, in high symmetry systems the zfs is relatively small, permitting normally allowed transitions to be observed, as in the experiments described here.[31] Due to the amorphous nature of this material only a small fraction of the V (III) centers are of high enough symmetry to be observed, leading to a lower intensity than expected for this signal.[33] This explains why the XPS shows a much higher relative proportion of V(III) to V(IV) than the EPR. After hydrogen gas was added to the sample, the EPR signal from the V(III) species was reduced in intensity by ~90% (Figure 4(b)). This observation is consistent with the lowering of symmetry at the V(III) center caused by hydrogen binding (Scheme 1), which increases the zfs, resulting in a new "EPR silent" species. Since very little hydrogen is adsorbed at ambient pressure, an on-off equilibrium favoring the gas phase under these conditions is clearly enough to perturb this signal on the EPR time scale. By contrast, the signal from the V(IV) center was unchanged both in shape and intensity, indicating that hydrogen binding occurs preferentially with the vanadium ions in the 3+ oxidation state in C150. Removing the hydrogen leads to a restoration in the intensity of the signal for V(III). At 77 K this signal is still unresolved, but this is expected due to the greater quantity of H_2 bound to the V (III) under these conditions leading to an even further loss of symmetry on the EPR time scale. These observations are consistent with weak and reversible chemisorption to the V(III) centers through the Kubas interaction.

3.4 Conclusions

Vanadium hydrazides constitute a new class of hydrogen storage materials distinct from hydrides or physisorption materials, that can function at room temperature and use pressure as a toggle switch to load or release hydrogen with a minimal kinetic barrier. By extending this class of materials to other transition metals systems with even better

propensity for Kubas binding and a greater concentration of open coordination sites, it is likely that even higher storage capacities will be realized. The moderate enthalpies involved are just enough to allow room temperature binding while not so strong as to create heat management issues in the system. Furthermore, the pressures used in this study fall short of the 200 bar norm used in the hydrogen transport industry. Since saturation was not reached in many of the isotherms at 85 bar it is likely that isotherms recorded at 200 bar will show even higher capacities. These materials can potentially be used under the same conditions as compressed gas, which is already the main method of hydrogen storage in prototypes, but with higher volumetric capacities. Since hydrogen storage has been identified as the key problem in realizing the widespread use of hydrogen as a fuel, this new class of materials may show applications in the implementation into actual vehicles and power systems.

Supporting Information Available: X-ray powder diffraction, Brunauer-Emmett-Teller surface areas for all samples which were dried at 150 ^{o}C, and X-ray photoelectron spectroscopy measurements for vanadium, oxygen, and nitrogen, hydrogen adsorption isotherms at 77 K and 298 K for A, B, and D sample series. Infrared red spectroscopy of C150 sample and the $V(Mes)_3$·THF precursor, and the cycling result of C150.

3.5 References

(1) a) Schlapbach, L.; Zuettel, A. *Nature*, **2001**, 414, 353; b) Seayad, A. M; Antonelli, D.M. *Adv. Mater.* **2004**, 16, 765; c) Yaghi, O. M.; O'Keeffe, M.; Ockwig, N. W.; Chae, H. K.; Eddaoudi, M.; Kim, J. *Nature* **2003**, 423, 705; d) Mark Thomas, K. *Dalton Trans*. **2009**, 1487-1505; e) Yang R. T.; Wang, Y. *J. Am. Chem. Soc*. **2009**, 131, 4224; f) Lochan, R. C.; Head-Gordon, M.; *Phys. Chem. Chem. Phys*. **2006**, 8, 1357; g) Eberle, U.; Felderhoff, M.; Schueth, F. *Angew. Chem., Int. Ed*. **2009**, 48, 2.

(2) a) Orimo, S.; Nakamori, Y.; Eliseo, J. R.; Zuettel, A.; Jensen, C. M. *Chem. Rev*. **2007**, 107, 4111 – 4132; b) Sandrock, G. *J. Alloys Comp*. **1999**, 293, 877.

(3) a) Wong-Foy, A. G.; Matzger, A. J.; Yaghi, O. M. *J. Am. Chem. Soc.*, **2006**, 128, 3494; b) Dailly, A.; Vajo, J. J.; Ahn, C. C. *J. Chem. Phys. B* **2006**, 110, 1099; c) Panella,

B.; Hirscher, M.; Pütter, H.; Müller, U. *Adv. Funct. Mat.* **2006**, 16, 520; d) Langmi, H. W.; Book, D.; Walton, A.; Johnson, S. R.; Al-Mamouri, M. M.; Speight, J. D.; Edwards, P. P.; Harris, I. R.; Anderson, P. A. *J. Alloy. Compd*. **2005**, 404–406, 637; e) Kaye, S. S.; Long, J. R. *J. Am. Chem. Soc*. **2005**, 127, 6506; f) Strobel, R.; Garche, J.; Moseley, P. T.; Jorissen, L.; Wolf, G. *J. Power Sources* **2006**, 159, 781; g) Hirscher, M.; Panella, B. *Scr. Mater.* **2007**, 56, 809; h) Bénard, P.; Chahine, R. *Scr. Mater.* **2007**, 56, 803; i) Yan, Y.; Lin, X.; Yang, S.; Blake, A. J.; Dailly, A.; Champness, N. R.; Hubberstey, P.; Schroeder, M. *Chem. Commun*. **2009**, 1025.

(4) Vitillo, J. G.; Regli, L.; Chavan, S.; Ricchiardi, G.; Spoto, G.; Dietzel, P. D. C.; Bordiga, S.; Zecchina, A. *J. Am. Chem. Soc.* **2008**, 130, 8386.

(5) a) Kubas, G. J.; Ryan, R. R.; Swanson, B. I.; Vergamini, P. J.; Wasserman, H. J. *J. Am. Chem. Soc*. **1984**, 106, 451; b) G. J. Kubas, *Chem. Rev*. **2007**, 107, 4152.

(6) Heinekey, D. M.; Lledós, A.; Lluch, J. M. *Chem. Soc. Rev*. **2004**, 33, 175.

(7) Zhao, Y.; Kim, Y.; Dillon, A. C.; Heben, M. J.; Zhang, S. B. *Phys. Rev. Lett*. **2005**, 94, 155504.

(8) Hoang, T. K. A.; Antonelli, D. M. *Adv. Mater*. **2009**, 21, 1787.

(9) Heinekey, D. M.; Oldham Jr, W. J. *Chem. Rev*. **1993**, 93, 913.

(10) Yildirim, T.; Ciraci, S. *Phys. Rev. Lett*. **2005**, 94, 175501.

(11) Dinca, M.; Dailly, A.; Liu, Y.; Brown, C. M.; Neumann, D. A.; Long, J. R. *J. Am. Chem. Soc*. **2006**, 128, 16876.

(12) a) Hamaed, A.; Trudeau, M.; Antonelli, D. M. *J. Am. Chem. Soc*. **2008**, 130, 6992; b) Hamaed, A.; Hoang, T. K. A.; Trudeau, M.; Antonelli, D. M. *J. Organomet. Chem*. **2009**, 694, 2793.

(13) Hoang, T. K. A.; Hamaed, A.; Trudeau, M.; Antonelli, D. M. *J. Phys. Chem. C* **2009**, 113, 17240.

(14) a) Fetter, N. R.; Bartocha, B. K. W. U. S. Navy, U. S. Pat. 3321503 (3 April **1962**/23 May 1967); CA 67, 55828; b) Schmidt, E. W. "*Hydrazine and its Derivatives. Preparation, Properties, Application*". John Wiley & Sons, Inc., **2001**, page 99 – 105.

(15) Mai, H. V.; Hoang, T. K. A.; Hamaed, A.; Trudeau, M.; Antonelli, D. M. *Chem. Commun*., **2010**, 46, 3206.

(16) Hamaed, A.; Mai, H, V.; Hoang, T. K. A.; Trudeau, M.; Antonelli, D. M. *J. Phys. Chem. C* **2010**, 114, 8651.

(17) Seidel, V. W.; Kreisel, G. *Z. Anorg. Allg. Chem*. **1977**, 435, 146.

(18) Hu, X.; Skadtchenko, B. O.; Trudeau, M.; Antonelli, D. M. *J. Am. Chem. Soc*., **2006**, 128, 11740.

(19) Furukawa, H.; Miller, M. A.; Yaghi, O. *J. Mater. Chem*. **2007**. 17, 3197.

(20) Franzen, H.F.; Sawatzky, G. *J. Solid State Chem*. **1975**, 15, 229.

(21) Groenenboom, C. J.; Sawatzky, G.; Meijer, H. J. D.; Jellinek, F. *J. Organometal. Chem*. **1974**, 76, C4 – C6.

(22) Horvath, B.; Strutz, J.; Geyer-Lippmann, J.; Horvath, E. G. *Z. Anorg. Allg. Chem*. **1981**, 483, 181.

(23) Kasperkiewicz, J.; Kovacich, J. A.; Lichtman, D. *J. Electron Spectrosc. Relat. Phenom*. **1983**, 32, 123.

(24) Grunert, W.; Feldhaus, R.; Anders, K.; Shpiro, E. S.; Antoshin, G. V.; Minachev, Kh.M. *J. Electron Spectrosc. Relat. Phemon*. **1986**, 40, 187.

(25) Kafizas, A.; Hyett, G.; Parkin, I. P. *J. Mater. Chem*. **2009**, 19, 1399.

(26) Lindberg, B.; Maripuu, R.; Siegbahn, K.; Larsson, R.; Golander, C.-G.; Erikkson, J. C. *J. Colloid Interface Sci*. **1983**, 95, 308.

(27) Larkins, F. P.; Lubenfeld, A. *J. Electron Spectrosc. Relat. Phenom*. **1979**, 15, 137.

(28) Yatsimirskii, K. B.; Nemoshalenko, V. V.; Aleshin, V. G.; Bratushko, Y. I.; Moiseenko, E. P. *Chem. Phys. Lett*. **1977**, 52, 481.

(29) Weil, J.A.; Bolton, J.R. **2007** *Electron Paramagnetic Resonance: Elementary Theory and Practical Applications. (Second Edition)*. Hoboken, New Jersey: John Wiley & Sons Inc.

(30) Abragam, A.; Bleaney, B. **1970** *Electron Paramagnetic Resonance of Transition Ions*. Ely House, London: Oxford University Press.

(31) Krzystek, J.; Fiedler, A.T.; Sokol, J. J.; Ozarowski, A.; Zvyagin, S. A.; Brunold, T. C.; Long, J. R.; Brunel, L. -C.; Telser, J. *Inorg. Chem.* **2004**, 43, 5645.

(32) Telser, J.; Wu, C. -C.; Chen, K.-Y.; Hsu, H.-F.; Smirnov, D.; Ozarowski, A.; Krzystek, J. *J. Inorg. Biochem.* **2009**, 103, 487.

(33) Alonso, P. J.; Forniés, J.; García-Monforte, A.; Martín, A.; Menjón, B. *Chem. Comm.* **2001**, 2138.

Supplemental Information for Chapter 3 - Design and synthesis of vanadium hydrazide gels for Kubas-type hydrogen adsorption: a new class of hydrogen storage materials

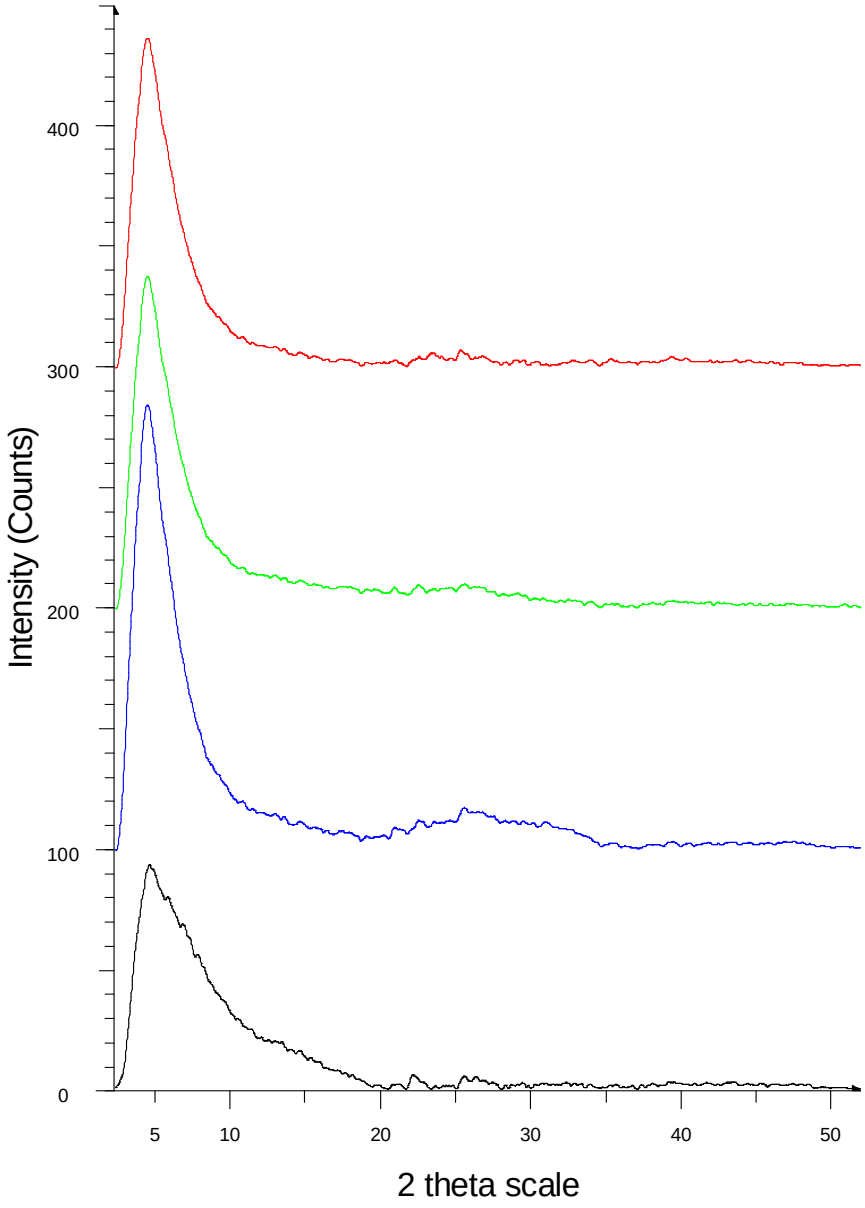

Figure S3.1: Powder X-ray diffraction of vanadium hydrazide materials. From top to bottom: A150, B150, C150, and D150 samples.

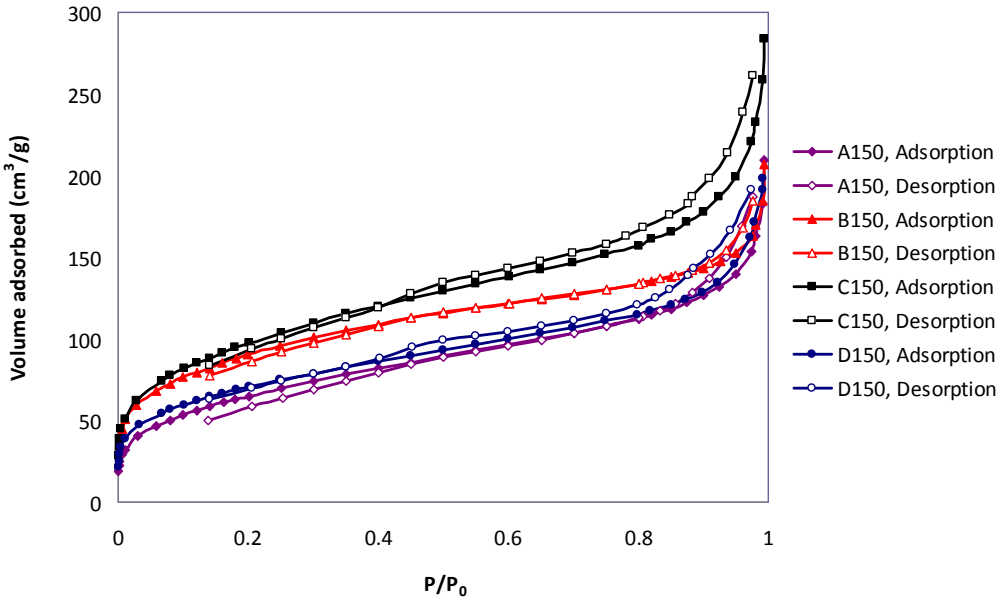

Figure S3.2: Nitrogen adsorption – desorption isotherms. Samples were measured on an ASAP-2010 instrument at 77K.

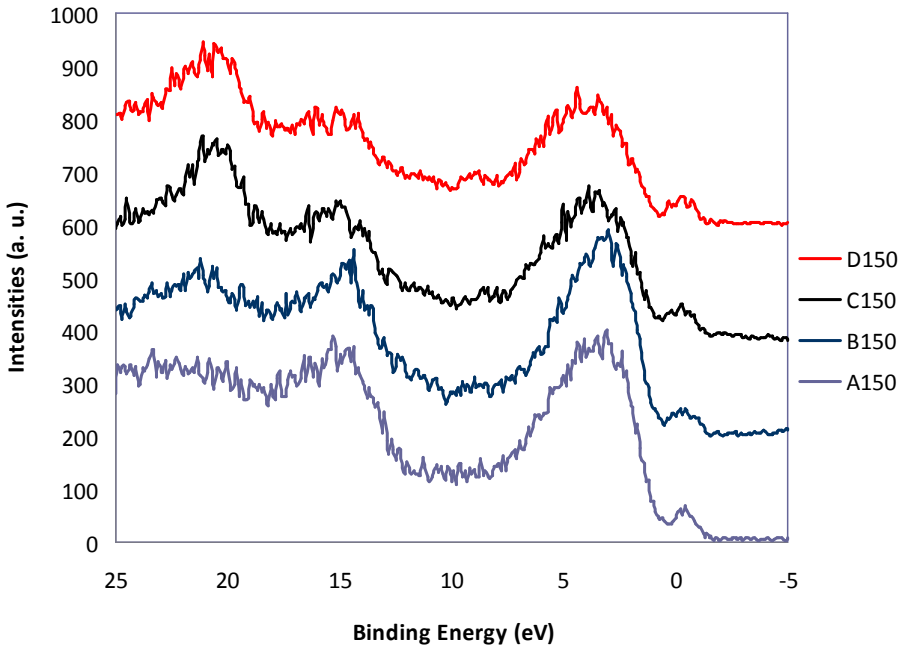

Figure S3.3: Valence region of XPS spectrum of vanadium hydrazide materials heated to 150 °C with different ratios of hydrazine.

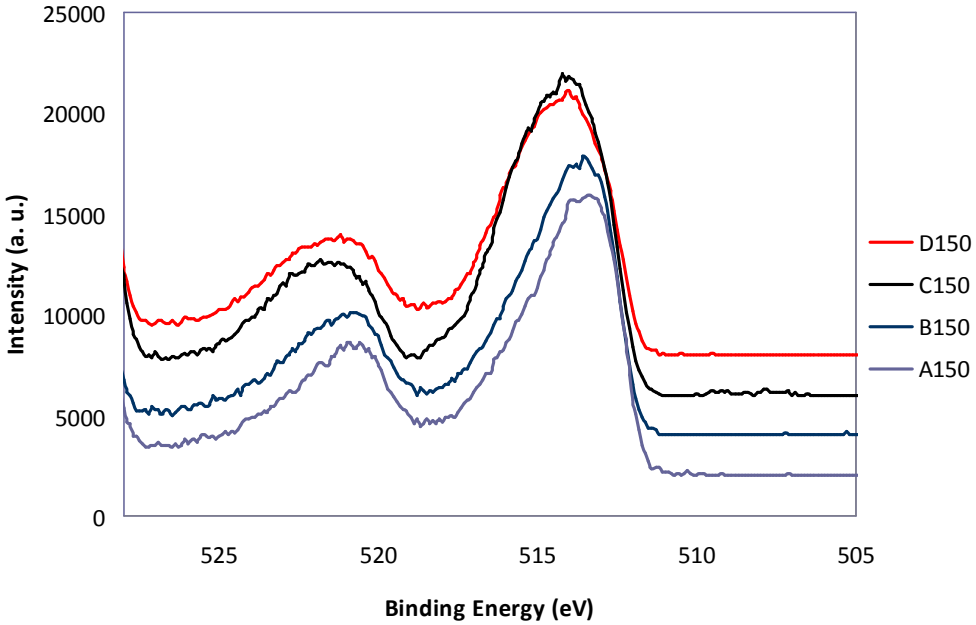

Figure S3.4: Vanadium 2p1/2 and 2p3/2 region of XPS spectrum of vanadium hydrazide materials heated to 150 °C with different ratios of hydrazine.

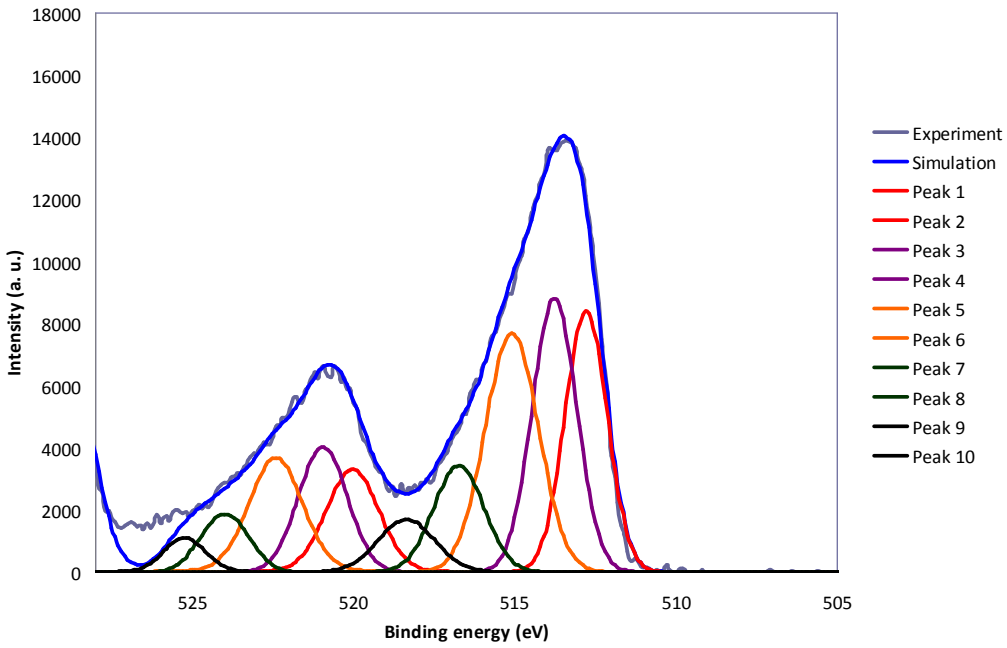

Figure S3.5a: Peak fitting of vanadium 2p1/2 and 2p3/2 emissions in the XPS spectrum of A150 sample.

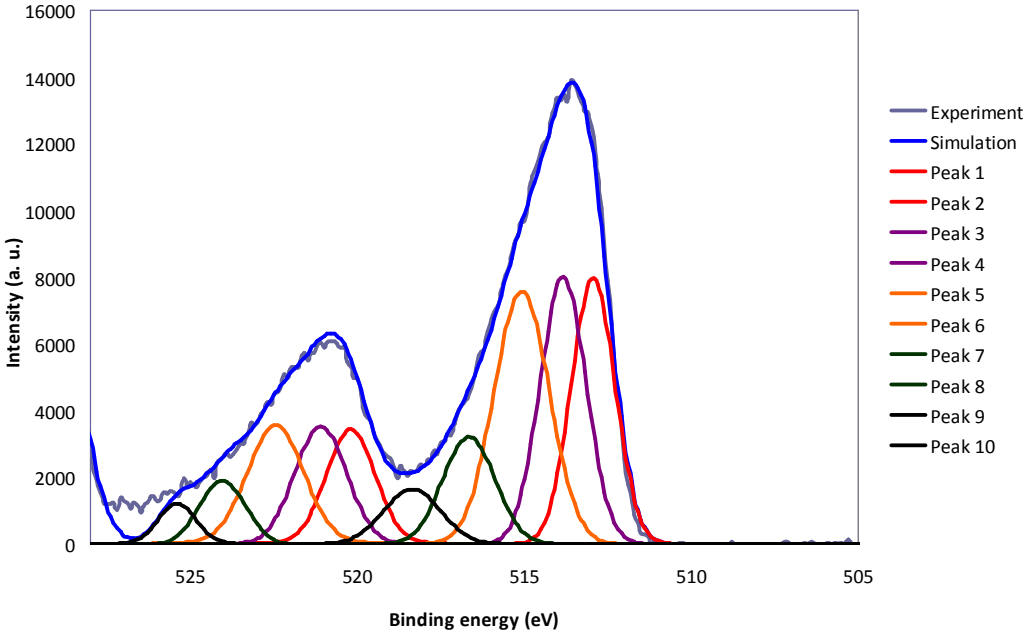

Figure S3.5b: Peak fitting of vanadium 2p1/2 and 2p3/2 emissions in the XPS spectrum of B150 sample.

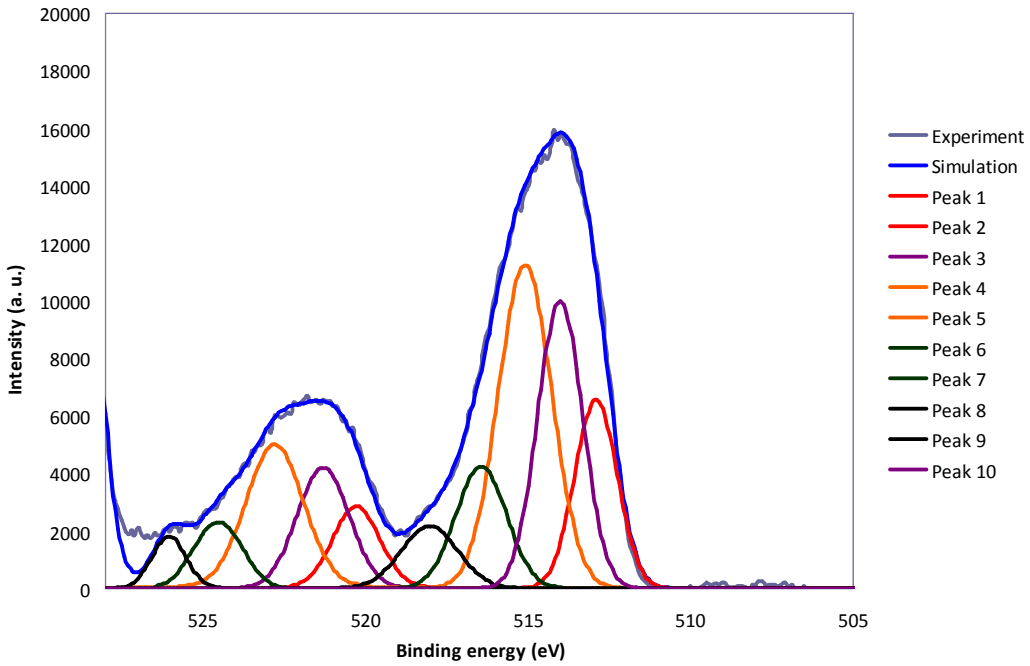

Figure S3.5c: Peak fitting of vanadium 2p1/2 and 2p3/2 emissions in the XPS spectrum of C150 sample.

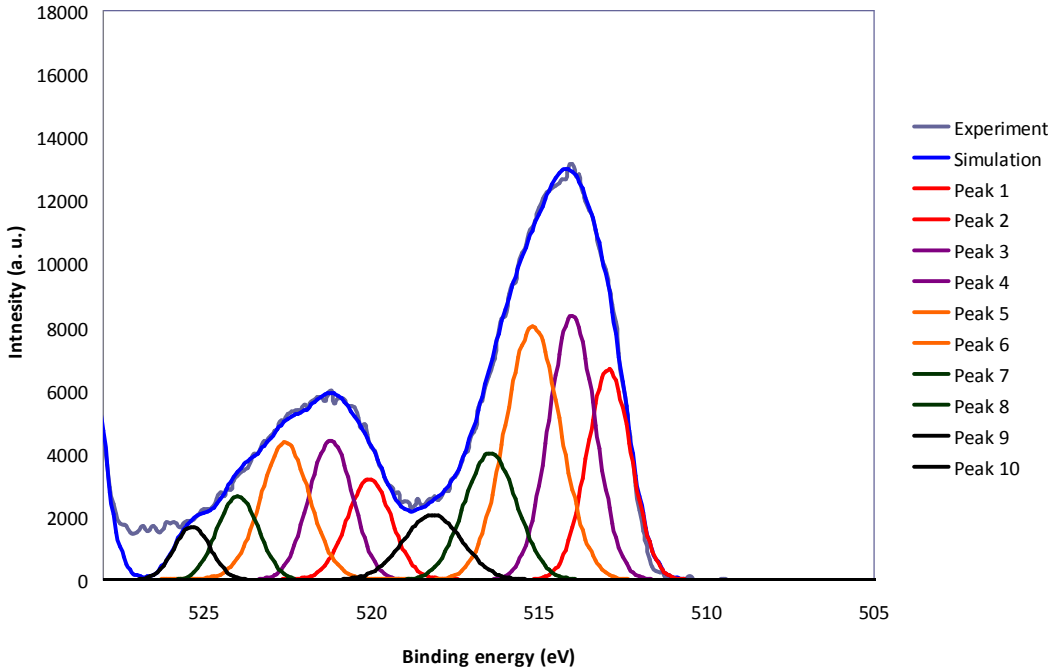

Figure S3.5d: Peak fitting of vanadium 2p1/2 and 2p3/2 emissions in the XPS spectrum of D150 sample.

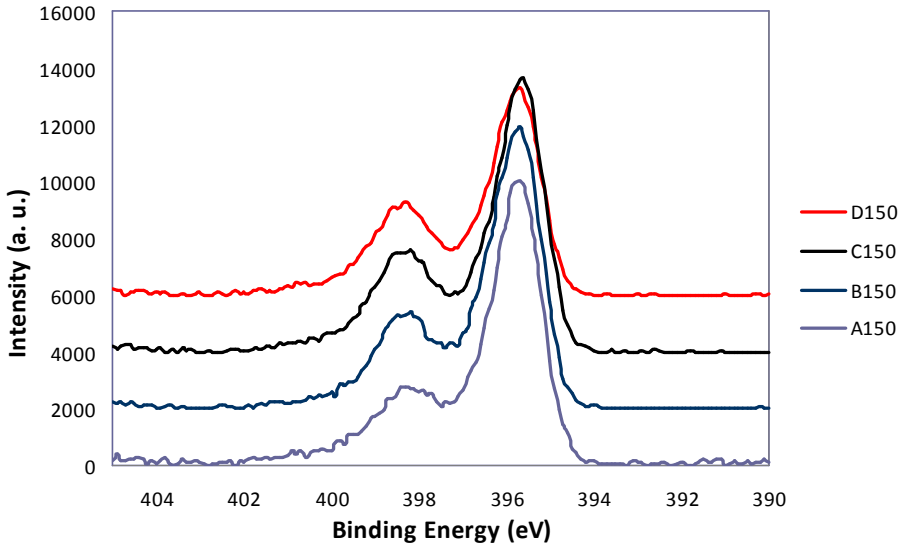

Figure S3.6: N 1S region of XPS Spectrum of vanadium hydrazide materials heated to 150 °C with different ratios of hydrazine.

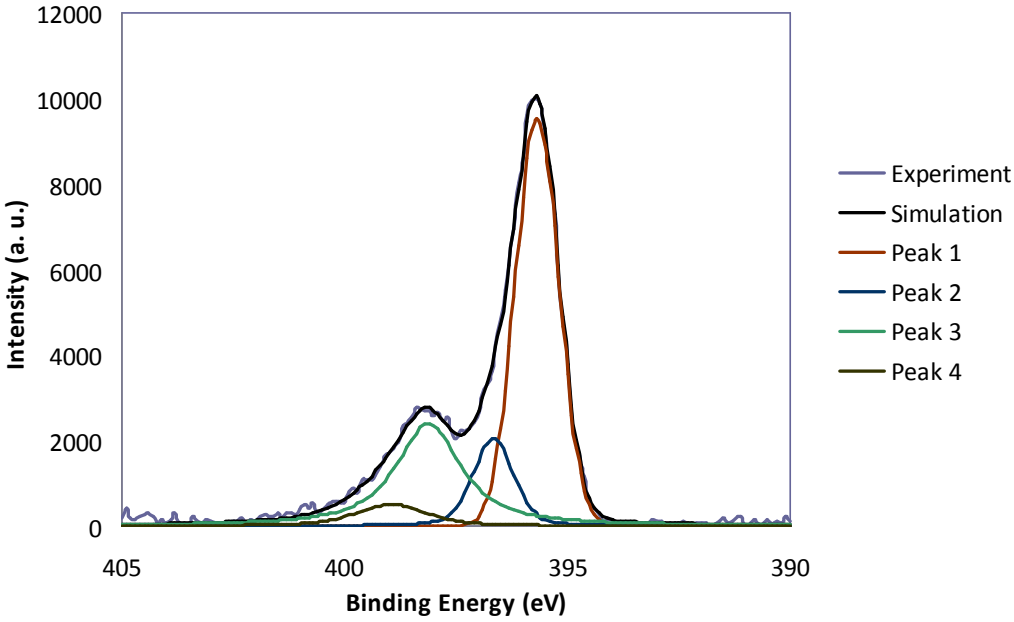

Figure S3.7a: Peak fitting of N 1S region of XPS Spectrum of A150 sample.

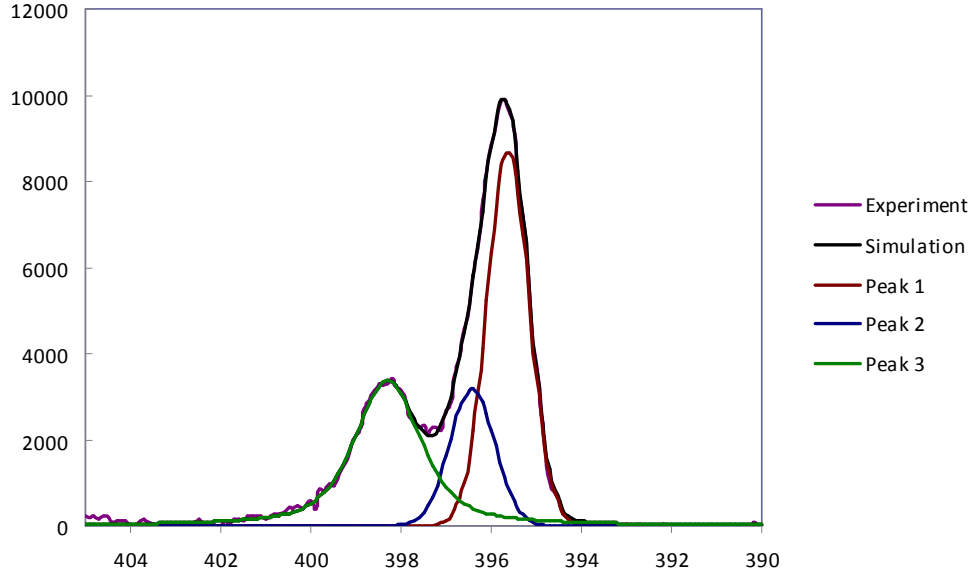

Figure S3.7b: Peak fitting of N 1S region of XPS Spectrum of B150 sample.

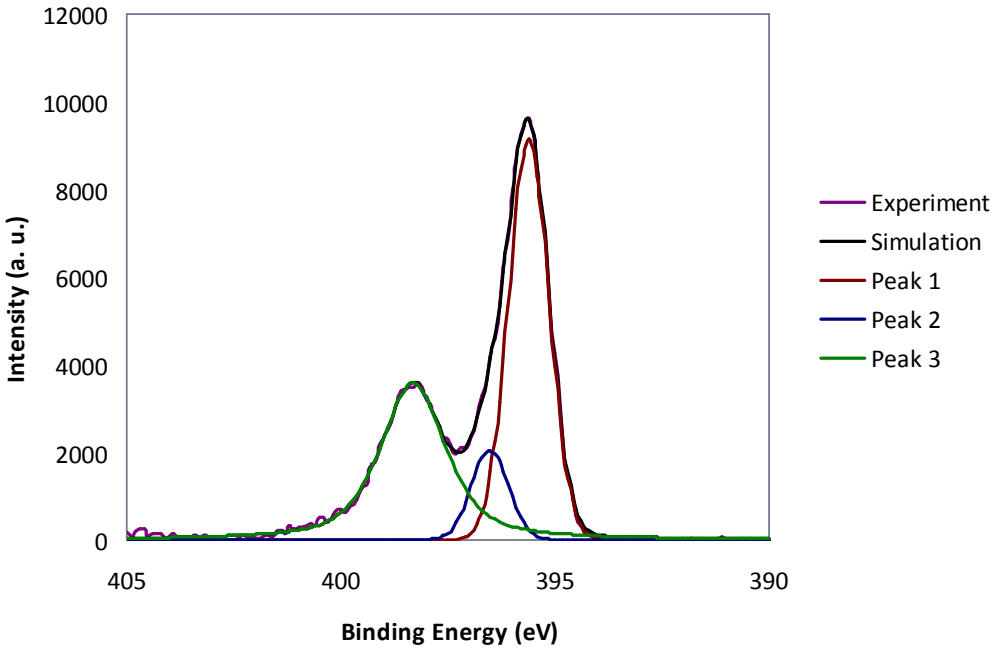

Figure S3.7c: Peak fitting of N 1S region of XPS Spectrum of C150 sample.

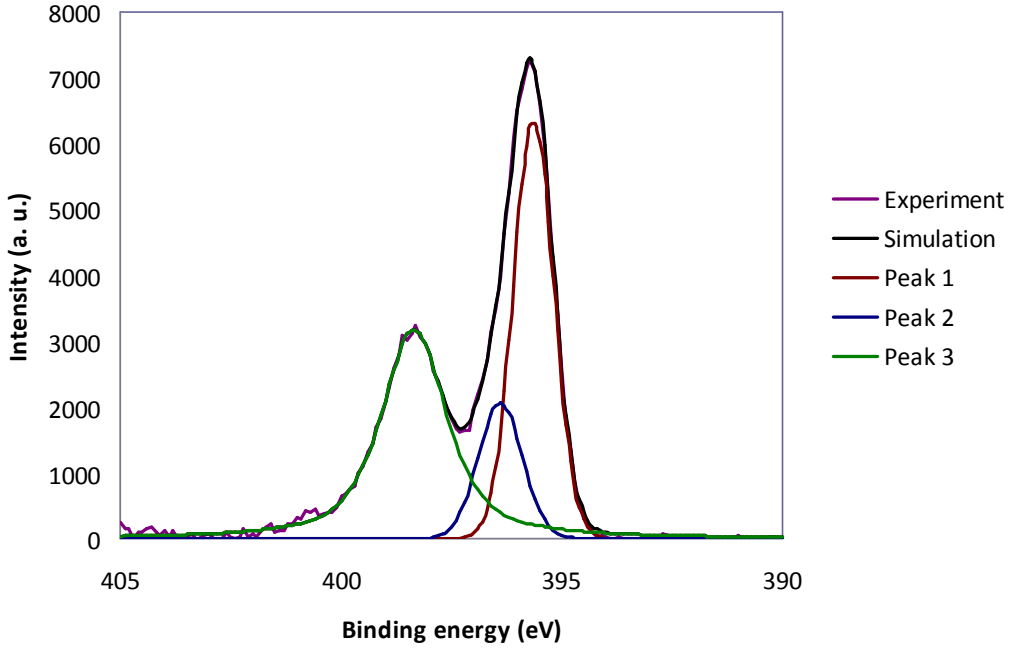

Figure S3.7d: Peak fitting of N 1S region of XPS Spectrum of D150 sample.

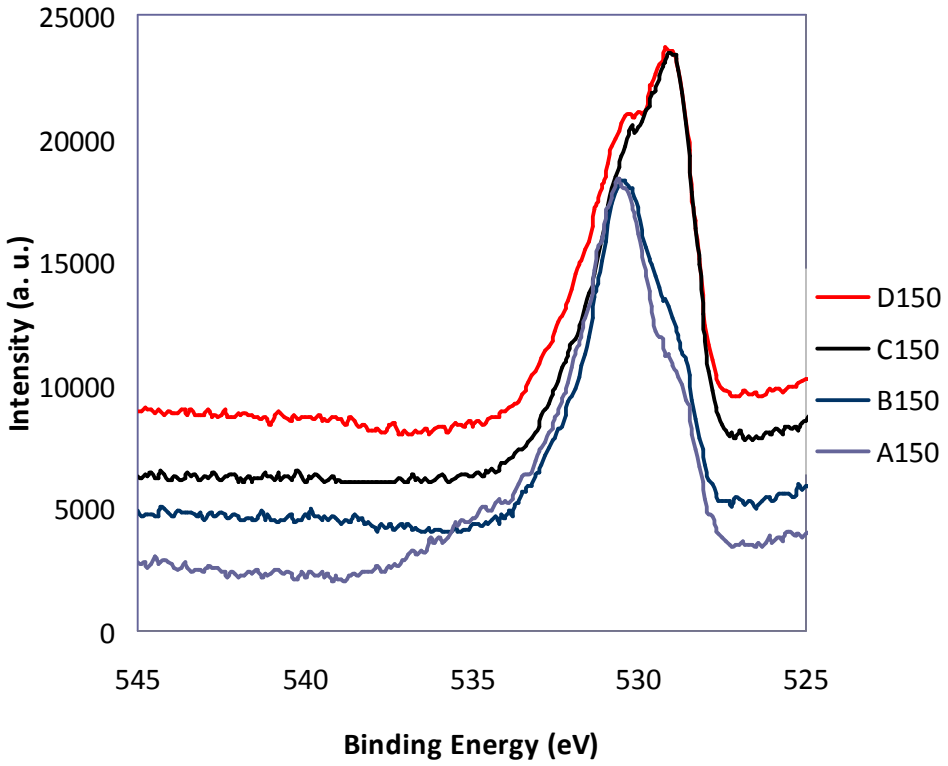

Figure S3.8: Oxygen 1S region of XPS Spectrum of vanadium hydrazide materials heated to 150 °C with different ratios of hydrazine.

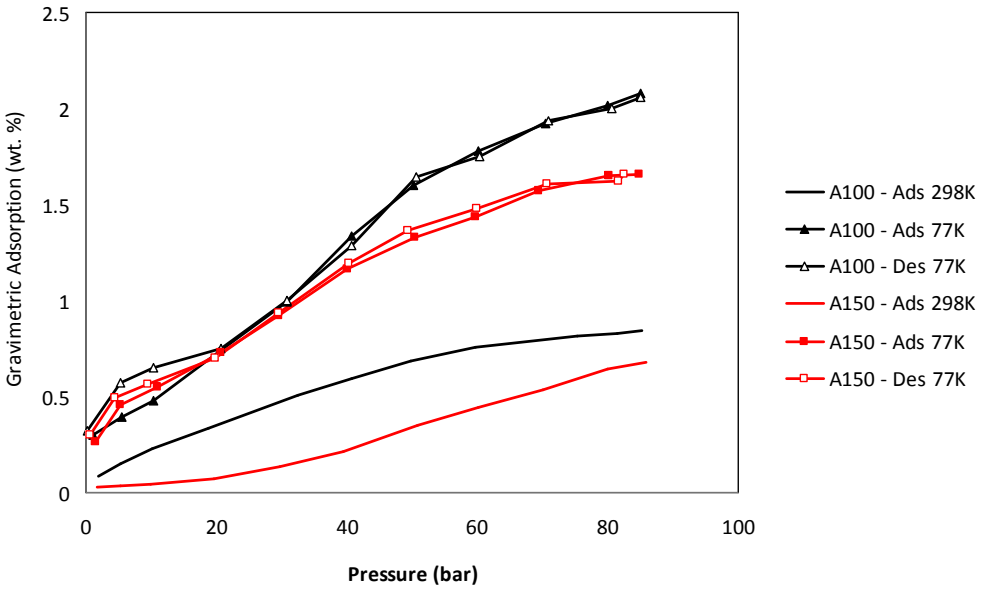

Figure S3.9: Hydrogen adsorption – desorption excess storage isotherms of A-series vanadium hydrazide materials synthesized with a V:hydrazine ratio of 4:3. Desorption isotherms recorded at 298 K omitted for clarity.

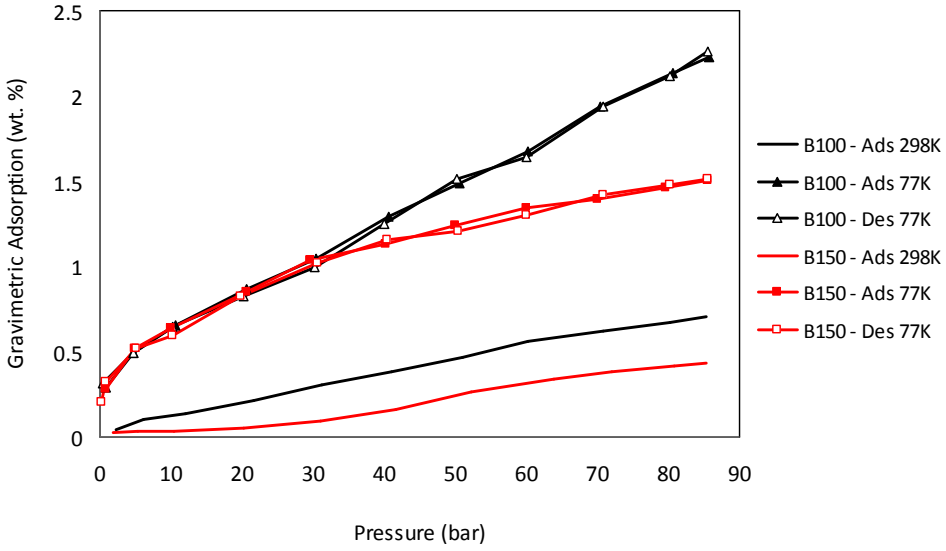

Figure S3.10: Hydrogen adsorption – desorption excess storage isotherms of B-series vanadium hydrazide materials synthesized with a V:hydrazine ratio of 1:1. Desorption isotherms recorded at 298 K omitted for clarity.

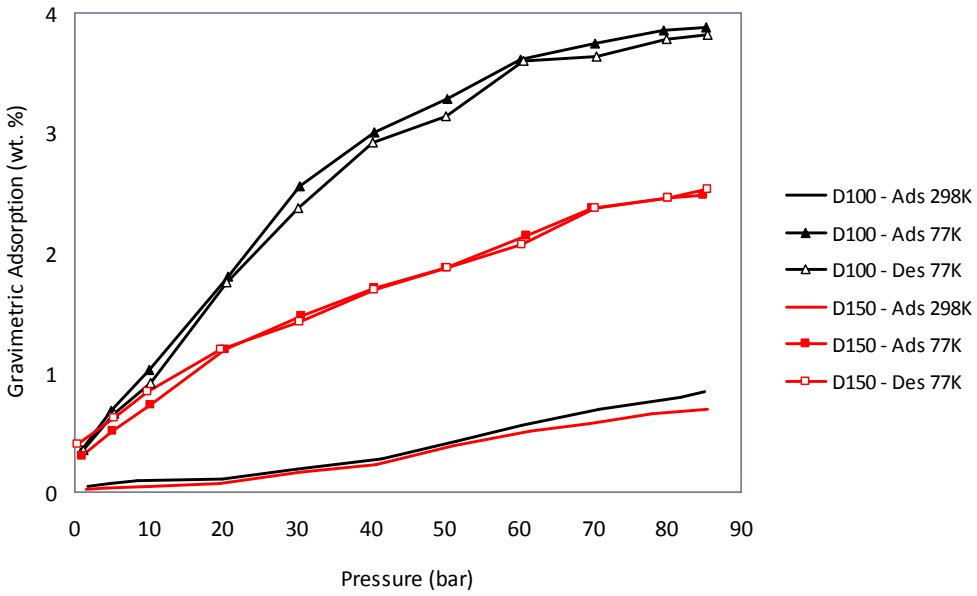

Figure S3.11: Hydrogen adsorption – desorption excess storage irotherms of D-series vanadium hydrazide materials synthesized with a V:hydrazine ratio of 1:2. Desorption isotherms recorded at 298 K omitted for clarity.

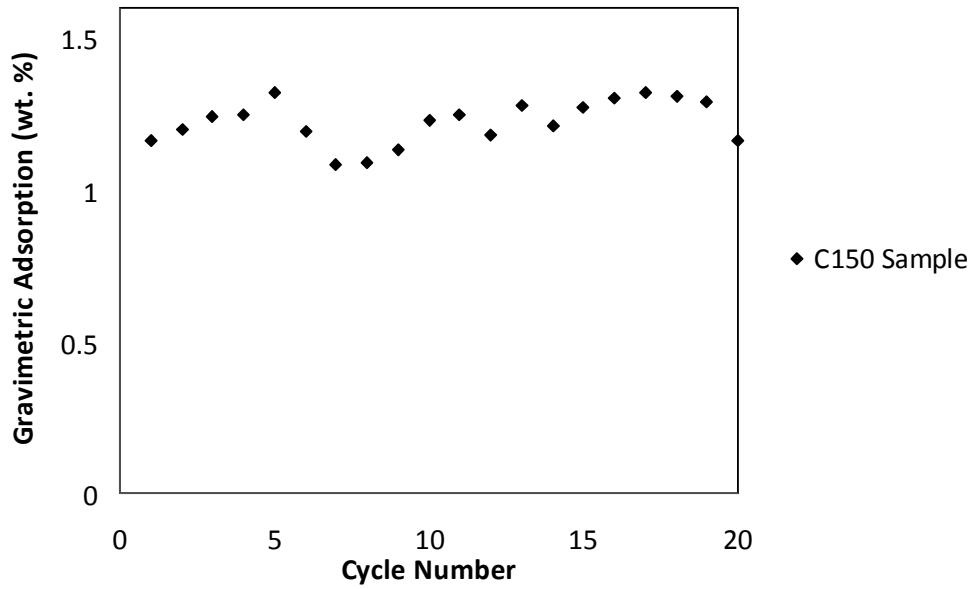

Figure S3.12: Hydrogen adsorption capacity at 298K in a 20 cycle test of the C150 sample.

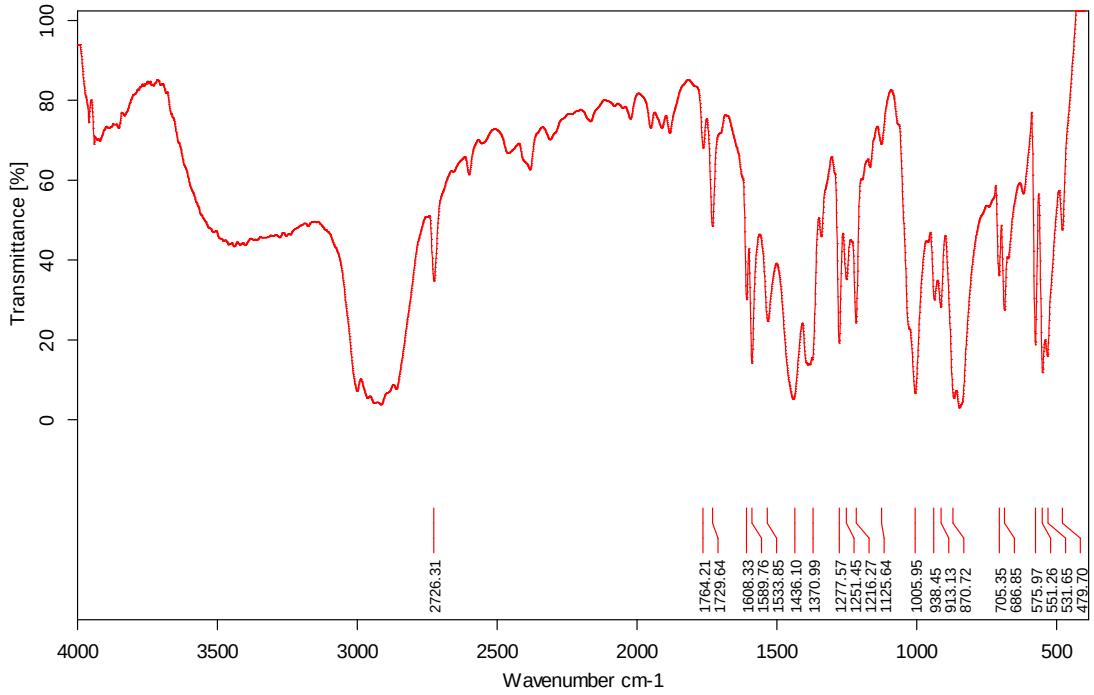

Figure S3.13a: IR spectrum of $V(Mes)_3$.THF

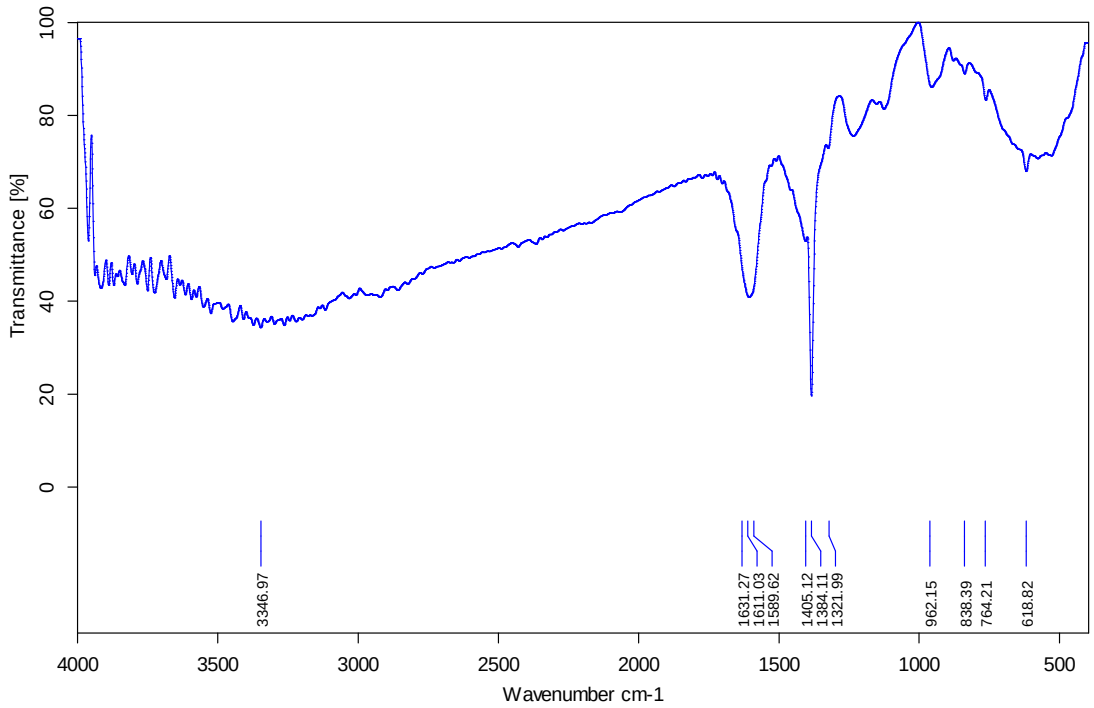

Figure S3.13b: IR Spectrum of C150 sample.

Chapter 4 – Multivalent Manganese Hydrazide Gels for Kubas-type Hydrogen Storage

4.1 Introduction

Hydrogen represents the most attractive alternative energy resource because it possesses the highest energy density of any chemical substance (120 MJ/kg compared to 44.4 MJ/kg for gasoline) and produces only water as a by-product when used in a fuel cell. However, the low density of hydrogen (0.089 g/L at STP) leads to a volumetric energy density significantly lower than any conventional fuel.[1] Because of this hydrogen must be liquefied at 20 K or compressed to dangerously high pressures (> 500 bar) to achieve commercially viable vehicle ranges.[2] Thus, effective methods for chemical hydrogen storage are of great technological and environmental significance in terms of realizing a low carbon economy.[3] Chemical hydrides and physisorbents have been studied extensively for hydrogen storage.[4] Hydrides typically posses a high volumetric density of hydrogen, such as $Mg(BH_4)_2$ with 146.5 kg H_2/m^3, more than double that of liquid hydrogen (70.8 kg/m^3). But because of high heats of adsorption (≥ 70 kJ/mol) and slow kinetics of desorption at ambient temperature, practical use of chemical hydrides has been limited.[5] On the other hand, high surface area physisorbents absorb significant quantities of hydrogen at 77 K (9.05 wt% for NU-100)[6] without any of the kinetic problems of hydrides. However, because of low heat of adsorption (≤ 10 kJ/mol), hydrogen molecules do not adhere strongly enough to the surface and thus lose up to 90% of their activity at 298 K.[7] In order to achieve effective storage under ambient conditions approaching the United States Department of Energy (DOE) ultimate system targets (7.5 wt% and 70 kg/m^3)[8], the ideal H_2 binding energy is predicted to be in the range of 20 – 30 kJ/mol.[9] Because of this, many theoretical and experimental studies have been conducted on the design and synthesis of adsorbents with improved binding enthalpies.[10] The majority of these studies have concentrated on the exploitation of the Kubas interaction in hydrogen storage.[11] In Kubas type hydrogen binding, H_2 donates electron density from the H-H σ-bonding orbital to the metal center, while the metal center in turn donates d-electron density into the H-H anti-bonding orbitals of the ligated H_2.[12] This results in a lengthening of the H-H bond without rupture to a dihydride. The stability of the Kubas

interaction depends largely on strong back-donation of electron density, which is closely related to the oxidation state of the metal center and its ligand environment.[12] In 2008 our group reported a model system for Kubas-type hydrogen storage in which silica supported benzyl Ti(III) fragments were used as binding sites for H_2.[13] While this system still contained a significant component of physisorption, the 5 wt% Ti fragments could bind up to 4 H_2 at 77 K and 1.8 H_2 at 298 K.[14] Similar chemically reduced mesoporous Ti oxide previously studied by our group,[15] the enthalpies in this silica-supported system displayed an unusual rising trend with surface coverage, reaching values as high as 22 kJ/mol. In like fashion low valent organometallic V(III), Cr(II), and Cr(III) fragments supported on silica enhanced the hydrogen adsorption over pristine silica through what was thought to be the Kubas interaction, although spectroscopic evidence was still lacking at this stage.[16] To create a new class of materials maximizing the number of transition metal coordination sites per unit weight and volume in an effort to use Kubas binding in a practical system, hydrazine was employed as a lightweight bridging agent to connect low coordinate, low valent transition metal species in a microporous supramolecular array.[17] These materials were thus synthesized readily by treatment of a sterically hindered low valent, low coordinate transition metal alkyl with a minimum amount of hydrazine. This strategy has so far yielded cyclopentadienyl chromium (II) hydrazide,[17] vanadium(III) hydrazide,[18] and chromium (II) hydrazide gels[19] for use in Kubas type hydrogen storage. These materials possess predominantly linear isotherms, enthalpies that rise with surface coverage from 20-40 kJ/mol, and retentions of activity at 298 K relative to 77 K ranging from 25-90% depending on the material. The chromium (II) hydrazide gels have so far reached the highest activities (40.8 kg/m^3 at 170 bar and 298 K without achieving saturation with no recognizable kinetic hindrance, well in range of the DOE 2017 system target of 40 kg/m^3 for volumetric storage. The role of the Kubas interaction in the storage mechanism was confirmed by Raman spectroscopy in the Cr hydrazide gels and suggested by ESR in the vanadium hydrazide gels. In this report, new Mn(II) hydrazide gels were synthesized by using the reaction between bis(trimethylsilylmethyl)manganese with anhydrous hydrazine. The rational for extending this new family of materials to Mn is that manganese is a cheaper metal than chromium and Mn (II) is a less air sensitive oxidation state than Cr (II). Assuming a

tetrahedral Mn center similar to that in Al hydrazides[20] MnL_2X_2 (L = datively coordinated hydrazine; X = hydrazide) should be able to bind up to 2 H_2 per Mn according to the 18-electron rule, translating into ca. 5 wt% H_2 storage for the MnN_2H_x hydrazide. The best manganese hydrazide materials in this study possess a volumetric hydrogen density surpassing that of the THF-coordinated vanadium hydrazide materials reported by our group[18] (23.2 kg/m^3 at 85 bar and 298 K).

4.2 Experimental Section

Anhydrous manganese dichloride was purchased from Alfa-Aesar, other chemicals were purchased from Sigma-Aldrich and used without further purification. Diethyl ether and toluene were distilled over sodium/benzophenone to remove oxygen and moisture. Distilled solvents were transferred to a Schlenk flask using a canula. Dry Ar gas was bubbled through the flask for 30 min before transferring into a dry-box. H_2 grade 6.0, N_2, Ar, and He were obtained from Praxair Canada. Manipulations were performed in an Ar glove box and on an Ar Schlenk line as low valence Mn species are sensitive to air and moisture. Anhydrous hydrazine was distilled from hydrazine hydrate using a procedure described elsewhere.[20] Hydrazine is toxic, flammable, explosive and must be handled with extreme care. Me_3SiCH_2MgCl was synthesized from the reaction of Me_3SiCH_2Cl and Mg. $Mg(CH_2SiMe_3)_2$ was prepared from Me_3SiCH_2MgCl by manipulation of the Schlenk equilibrium via dioxane condensation, resulting in a white solid. Sublimation of this white product at 175 ^oC under dynamic vacuum yielded in pure $Mg(CH_2SiMe_3)_2$. *Anal*. Calcld for $Mg(CH_2SiMe_3)_2$: C, 48.34; H, 11.16. Found: C, 48.17; H, 10.99.

4.2.1 Preparation of [{Mn(CH$_2$SiMe$_3$)$_2$}$_\infty$]. [{$Mn(CH_2SiMe_3)_2$}$_\infty$] was prepared following the procedure described elsewhere,[21] 1.95 g of $MnCl_2$ (97%) (1.50 mmol) was added to a 60 mL of ether solution containing 3.00 g (1.50 mol) of $Mg(CH_2SiMe_3)_2$ while stirring. Stirring was maintained for 3 days at room temperature. Ether was removed *in vacuo* resulting in a dull orange solid, which was then dissolved in hot toluene with stirring. White $MgCl_2$ then precipitated and the orange solution was filtered and stored in a freezer (-31 ^oC). [{$Mn(CH_2SiMe_3)_2$}$_\infty$] precipitated as orange needle crystals. *Anal*. Calcld [{$Mn(CH_2SiMe_3)_2$}$_\infty$]: C, 41.89; H. 9.66. Found: C, 38.70; H: 9.57.

4.2.2 Preparation of 1:1 manganese hydrazide gels. 3.00 g (13.1 mmol) of [{$Mn(CH_2SiMe_3)_2$}$_\infty$] was added to 50 mL toluene with stirring. 0.4180 mL (13.1 mmol) of hydrazine was added dropwise into the solution. The resulted solution turned dark within seconds and was stirred at room temperature for 24 h at 25 ^oC, 50 ^oC for 24 h, and 100 ^oC for 24 h. The solution was then filtered and a solid product was obtained, which was then heated in vacuum for 8 h at room temperature and 8 h at 100 ^oC. This sample was named B100. Heating the freshly filtered material at 150 ^oC under vacuum for 8h gives B150.

4.2.3 Preparation of 2:1 manganese hydrazide gels. The same procedure as above was applied, using 0.2090 mL hydrazine. The sample heated at 100 ^oC for 8 h was labelled A100 and the sample heated at 150 ^oC for 8 h was named A150.

4.2.4 Preparation of 1:1.5 and 1:2 manganese hydrazide gels. The same procedure as above was applied. Samples C100 and C150 were obtained using 0.6270 mL hydrazine and the solid products were heated at 100 ^oC, 150 ^oC for 8 h, respectively. Samples D100 and D150 were obtained using 0.8360 mL hydrazine and the solid products were heated at 100 ^oC and 150 ^oC for 8 h, respectively.

4.2.5 Characterization. Powder X-ray diffraction (PXRD) was performed on Siemens D-500 diffractometer with a Cu Kα radiation (40 kV, 40 mA) source. The step size was 0.02° and the counting time was 0.3s for each step. Diffraction patterns were recorded in the 2θ range 1.5 - 52°. Samples for PXRD analysis were put in sealed glass capillary tube to protect sample from air and moisture during the experiment. Nitrogen adsorption and desorption data were collected on a Micromeritics ASAP 2010. All X-ray Photoelectron Spectroscopy (XPS) emissions were referenced to the carbon C-(C, H) emission at 284.8 eV, and the data were obtained using a Physical Electronics PHI-5500 spectrometer. Samples were loaded in an Ar glove box to maintain sample integrity. Elemental analysis (EA) was conducted using a Perkin – Elmer Series II CHNO/S 2400 Analyzer, calibrated with acetanilide standard. Samples for EA are loaded in glove box, using tin capsules. Infrared spectroscopy was conducted on a Bruker Vector 22 instrument; the sample was either covered by Nujol; or mixing with KBr powder (2 mg of sample with 500 mg of

KBr) to prepare a disc. Thermo-gravimetric analysis was conducted on a Mettler Toledo TGA SDTA 851e, using helium (99.99%) as purging gas with the rate of 30 mL/min. Samples were held at 25 ^{o}C for 20 min before heating to 550 ^{o}C at a rate of 5 ^{o}C/min.

4.2.6 Electron Paramagnetic Resonance (EPR) Measurements. In a typical experiment, an EPR quartz tubes fitted with J-Young valves were used and loaded with 50 mg of the manganese hydrazide powder. For the first measurement the tube was held under Ar. Then, Ar gas was replaced by H_2 and further EPR measurements were carried out. Measurements were conducted from 500 to 6000 Gauss, with four accumulations, at 298 K and at 77 K on a Bruker X-band ESP 300E EPR Spectrometer (9.4 GHz).

4.2.7 Hydrogen adsorption measurements. Hydrogen adsorption isotherms were obtained by using a computer controlled commercial Gas Reaction Controller manufactured by Advanced Materials Corporation, Pittsburgh, PA, except in the case of the isotherm recorded at 298 K and 170 bar, which was obtained on a Hy-Energy PCT Pro. High purity hydrogen (99.9995% purity) was used as the adsorbent. All measurements were performed exactly as reported previously by our group to ensure reproducibility.[15] Skeletal densities were collected using a Quantachrome Ultrapycnometer housed in an Ar glove box. This instrument was calibrated bi-monthly as per user manual, using a small sphere with a known volume of 0.0898 cm^3 to monitor the instrument's performance. The volume of an empty cell is collected over several running cycles using He until the values are within ± 2% difference. A pre-weighed portion of sample is loaded into the cell under inert conditions and the volume of the system (sample + cell) is then determined. The skeletal volume of the sample is the difference between volume of sample + cell and the volume of empty cell. Skeletal density is obtained by using the sample mass divided by the sample volume. Excess hydrogen storage measurements on a standard AX-21 sample (4.2 wt. % at 30 bar and 77 K, 0.55 wt. % at 80 bar and 298 K) were performed to ensure proper calibration (Figure S4.1, Supporting Information).[19] Leak testing was also performed during each measurement by checking for soap bubbles at potential leak points. These measurements are all necessary to ensure the veracity of the isotherms. In the H_2 adsorption-desorption experiments a high level of reversibility was observed for all samples across the whole

range of pressures. Samples were run at liquid nitrogen temperature (77 K), liquid argon temperature (87 K), and room temperature (298 K) to 85 bar on the Advanced Materials instrument. Isotherms were always measured first at room temperature and then at 77 K or 87 K and the temperature was kept constant by keeping the sample chamber in liquid N_2, liquid Ar, or water. In the Advanced Materials instrument the sample weight and skeletal density are used to determine the volume of the sample in the sample chamber, which is then subtracted from the sample chamber volume to provide an accurate void space volume. When the skeletal density is used for the gravimetric hydrogen uptake measurement, the compressed hydrogen within the pores is treated as part of the sample chamber volume and hence subtracted. Therefore only the hydrogen contained on or beneath the walls of the structure will be recorded by the PCI instrument. This gravimetric value is termed the adsorption or excess storage. When the bulk density is used the hydrogen in the pores of the sample is automatically included in the calculation without any further correction factors and the final value is termed the total storage or absolute storage,[15,22] which represents all hydrogen contained in the sample including the compressed gas in the voids and the hydrogen adsorbed on or beneath the walls of the structure. Gravimetric densities are recorded as read from the isotherms while volumetric densities are calculated from the adsorption data and the skeletal or bulk density, depending on the desired value. The excess volumetric storage is typically calculated from the excess storage and the bulk density and gives a measure of the gas adsorbed on or in the solid phase of the material scaled across the entire volume occupied by the sample including the void space. In materials such as MOFs that posses a well-defined and constant ratio between mass and void space this value is often quoted. For compressible materials that may have variable ratios of solid mass and void space it can often help to scale the volumetric density to the solid phase alone as the void space will vary on sample preparation. For this purpose, we have defined the true volumetric adsorption[18] as the amount of hydrogen adsorbed on or in a given volume of the solid portion of the sample. This is calculated from the excess storage data and the skeletal density. This value neglects the void space and is useful in comparing volumetric densities of ball-milled powders and gels (materials with textural porosity only and no intrinsic pore structure) to pure solid phase materials such as metal hydrides. Since the

materials in this study stand between hydrides and physisorption materials in their mechanism of storage, this value is important. It also allows us to compare volumetric adsorption values of the solid phase alone from one sample to another without having to correct for the different textural void space in each material. The absolute volumetric adsorption has also been defined[22] and is a representation of the sum of the excess volumetric storage plus the compressed gas in the void space. This can be calculated from the volumetric storage as measured from the instrument and the bulk density, or by taking the volumetric adsorption and adding the amount in the void space calculated from the pore volume and the ideal gas law.[15] The first method is only possible when using the Advanced Materials instrument. In this paper we have chosen not to calculate this value (or the total gravimetric storage) because the differences between the skeletal densities and bulk densities are much smaller than in MOFs and hence the void space compressed gas contribution is negligible and will also vary due to sample preparation.

Enthalpies of adsorption were calculated using a variant of the Clapeyron – Clausius I equation taking both 77 K and 87 K hydrogen excess storage data.[15] Pressure as a function of the amount adsorbed was determined by using exponential fit for each isotherm; the first 10 – 11 points of the isotherms were picked up and fit to the exponential equation. This exponential equation provides an accurate fit over the pressure up to 1 MPa with the goodness of fit (R^2) above 0.97. The corresponding P_1 and P_2 values at a certain amount of H_2 adsorbed at both temperatures can be obtained by the simulated exponential equation. Inputting these numbers into equation 1, we then calculate the adsorption enthalpies. This technique is commonly used to measure enthalpies of amorphous carbons and MOFs. The enthalpy for carbon AX-21 calculated using this method using hydrogen adsorption data measured on The Advanced Materials PCI as described above is shown in Figure S4.2. Since the enthalpy of a reaction does not vary with temperature, unlike Gibbs free energy, this method provides information on hydrogen binding that is meaningful over a wide temperature range.

4.2.8 H_2/Mn Calculations. Calculations on manganese hydrazide samples were based on %Mn values obtained from the thermo-gravimetric analysis data from Table S1. As an example calculation, A100 absorbs 0.74 wt % of hydrogen at 85 bar and 298 K. This

corresponds to 0.0074 g or 0.0037 mol of H_2 for 1 g of sample. Based on the 61.30 wt% Mn in the sample from Table S4.1, this translates into an average of 0.33 molecules of H_2 per metal center.

4.3 Results and Discussions

Bis(trimethylsilylmethyl) manganese was stirred with different ratios of anhydrous hydrazine in dry toluene for 24 h at 25 ^{o}C, 24 h at 50 ^{o}C, and 24 h at 100 ^{o}C. The reaction mixture was filtered to yield a dark air and moisture sensitive solid, which was then heated at 100 ^{o}C and 150 ^{o}C under vacuum. For the $Mn(CH_2SiMe_3)_2$:N_2H_4 ratio of 2:1 the resulting materials were given the annotations A100 and A150, respectively. The three other Mn/N_2H_4 ratios (1:1, 1:1.5, and 1:2) were named B100 and B150, C100 and C150, D100 and D150, respectively. In this reaction we propose that the hydrazine acts as a nucleophile and the manganese alkyl group acts as a base, thereby deprotonating the hydrazine to afford a manganese hydrazide monomer (Scheme 4.1) and that further heating is required to drive this polymerization and condensation reaction to completion.

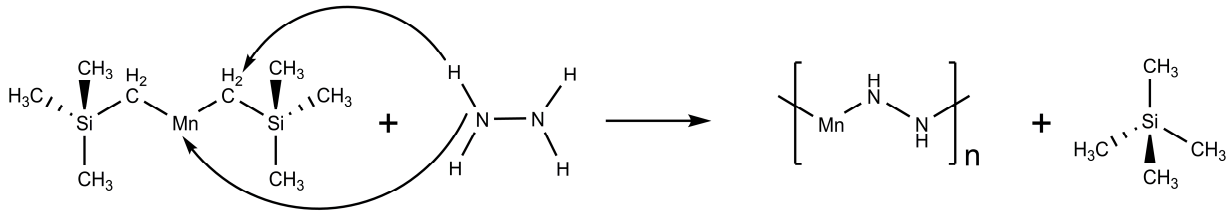

Scheme 4.1: Possible mechanism for the reaction between [{$Mn(CH_2SiMe_3)_2$}$_\infty$] and N_2H_4, reaction ratio 1:1.

The powder x-ray diffraction (PXRD) patterns for the manganese hydrazide materials heated at 100 ^{o}C in vacuum are shown in Fig. 4.1. All patterns were similar and no distinct reflection was detected, indicating a lack of long range order. This result is different from both vanadium hydrazides[18] and vanadium oxamide,[23] which display a single broad reflection at low angle suggesting mesoscopic order, and chromium hydrazides, which show a more complex pattern that gains definition and intensity with longer heating.[19] Nitrogen adsorption isotherms recorded at 77 K are shown in Figure 4.2. These isotherms show a small amount of microporosity comprising ca. 15 – 20 % the total volume adsorbed, with additional mesoporosity and textural porosity accounting for

the remaining adsorption in roughly equal proportions as evidenced by the slow rise between 0.2 and 0.8 P/P_o and the sharp incline above 0.8 P/P_o, respectively. The specific surface areas of all materials decrease with increased drying temperature from 100 to 150 ^oC. For example, B100 possesses a Brunauer – Emmett – Teller (BET) surface area of 279 m^2/g, but after heating in vacuum to 150 ^oC to form B150, the surface area is reduced to 230 m^2/g, suggesting a densification with loss of porosity. Because these materials are pyrophoric in air, transmission electron microscopy (TEM) studies of the structure are precluded. Since Mn (II) is an air-stable oxidation state, the reaction with air likely involves the exothermic oxidation of hydrazide to N_2 catalyzed by the Mn center.

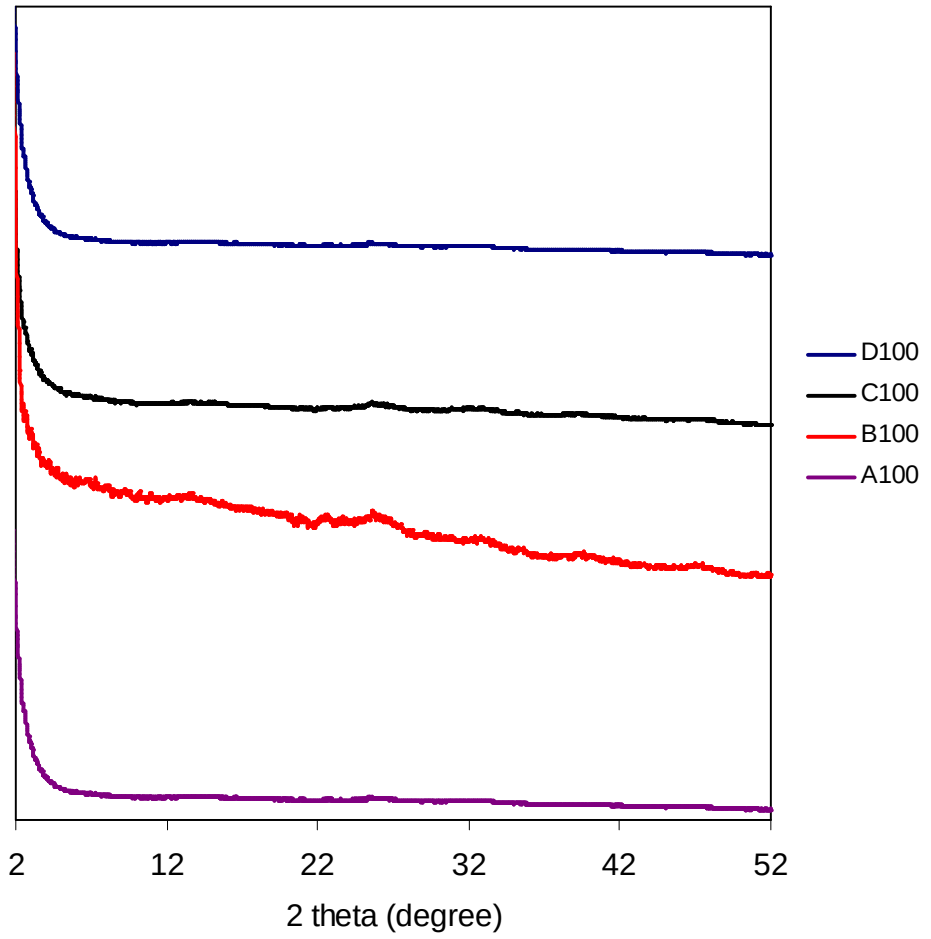

Figure 4.1: Powder X-ray diffraction of manganese hydrazide materials. From top to bottom: D100, C100, B100, then A100.

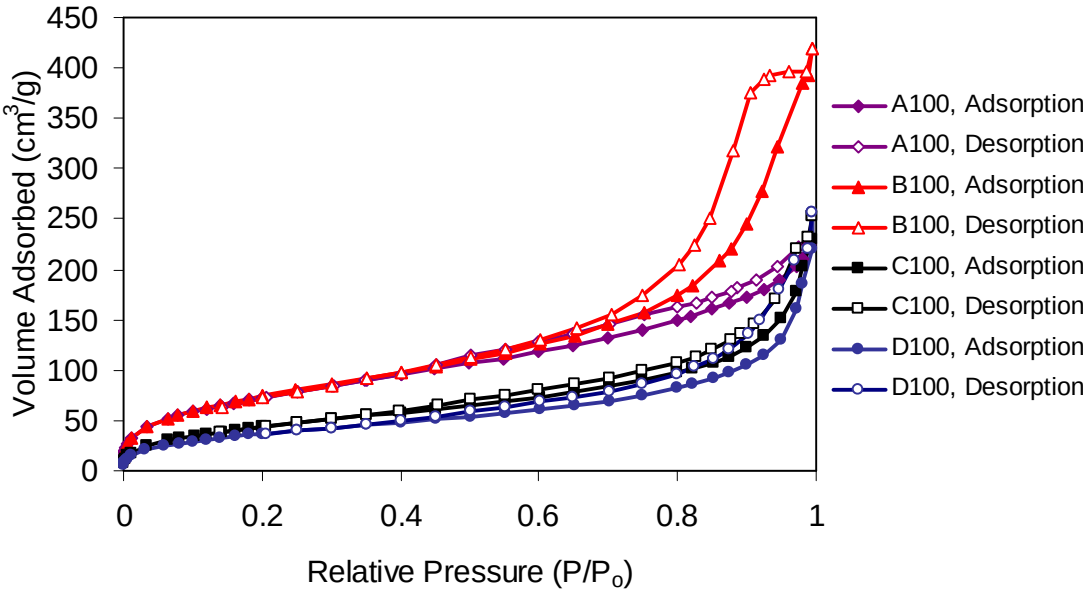

Figure 4.2: Nitrogen adsorption – desorption isotherms of manganese hydrazide materials heated to 100 °C. Samples were measured on an ASAP-2010 instrument at 77 K.

The C, H, N, and Mn elemental analysis data of manganese hydrazide materials are shown in Table S4.1 (Supporting Information) and display an expected decreasing trend in metal concentration from 50.70 wt% to 28.70 wt% with increasing hydrazine for samples heated to 100 °C. These values are generally lower than the values expected (Table S4.2), possibly due to incomplete digestion of the samples during the ICP analysis. The carbon and nitrogen values are also somewhat low due to carbide and nitride formation on combustion in the elemental analysis experiment, leading to less than 100% for all elements present. Low metal, carbon and nitrogen values were observed in analogous CpCr, V, and Cr hydrazide gels synthesized previously by our group.[17-19] Drying at 150 °C leads to progressive hydrocarbon elimination as monitored by IR spectroscopy (C-H stretch at 2850-2950 cm^{-1}) presumably by the thermally driven protolysis reaction between coordinated hydrazine and residual trimethylsilylmethyl groups. Further heating to temperatures of 180 °C was required to eliminate all the hydrocarbon, however, this had the negative effect of decreasing the hydrogen adsorption performance at room temperature (see later), presumably through decomposition of the hydrazide network. This was observed in chromium hydrazide materials,[19] however

further hydrocarbon could be removed by heating under H_2, which removes the excess hydrocarbon by replacement of a Mn alkyl with a Mn hydride, as opposed to simple heating, which relies on protic cleavage of the Mn-R to form a Mn-N bond. This second reaction would require a concomitant densification of the structure through excessive hydrazine crosslinking, which could have the effect of limiting hydrogen diffusion through the network to the active sites.

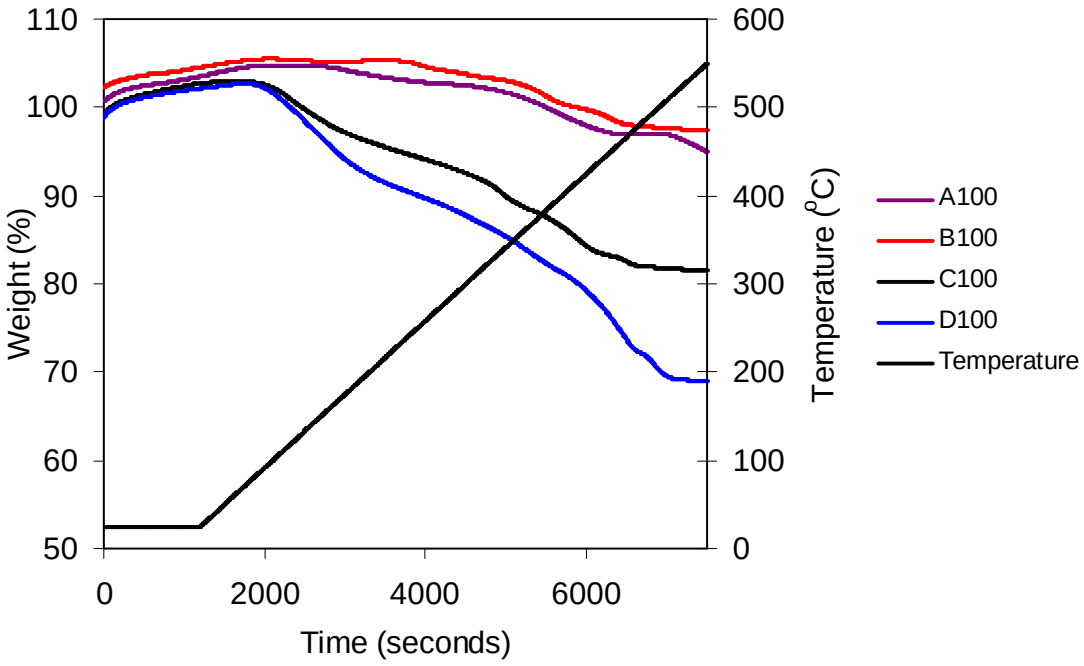

Figure 4.3: Thermo-gravimetric analysis results of manganese hydrazide materials heated to 100 ^{o}C.

Figure 4.3 provides the thermo-gravimetric analysis results of manganese hydrazide materials heated at 100 ^{o}C in vacuum. After 20 minutes under 25 ^{o}C, the materials gained weight slightly because of oxidation, followed by mass decreasing as the temperature approached 400 – 550 ^{o}C. At the heating limit, sample A100 and B100 retained 97 and 97.7 % of their original mass, respectively. Higher levels of weight loss were observed for sample C100 and D100, which retained 81.5 and 68.9 %, respectively. The results for Mn content based on these results are shown in Table S4.1 and are closer than the ICP results to the calculated percentages based on the hypothetical formulas in Table S4.2.

X-ray Photoelectron Spectroscopy (XPS) studies of the manganese hydrazides are shown in Figures 4.4 and 4.5. No charge neutralization was required and emissions are observed close to the Fermi level, suggesting that these materials are narrow bandgap semiconductors or semimetals (Figure S4.3). While metallic behavior was observed for Cr and V hydrazides, this is unexpected in this case because most Mn (II) materials are Mott-Hubbard insulators. This suggests that multiple oxidation states of Mn may be present leading to a polaron conduction mechanism. Increasing hydrazine leads to a decreasing in conductive properties of the materials as observed by increased charging in the XPS spectra.

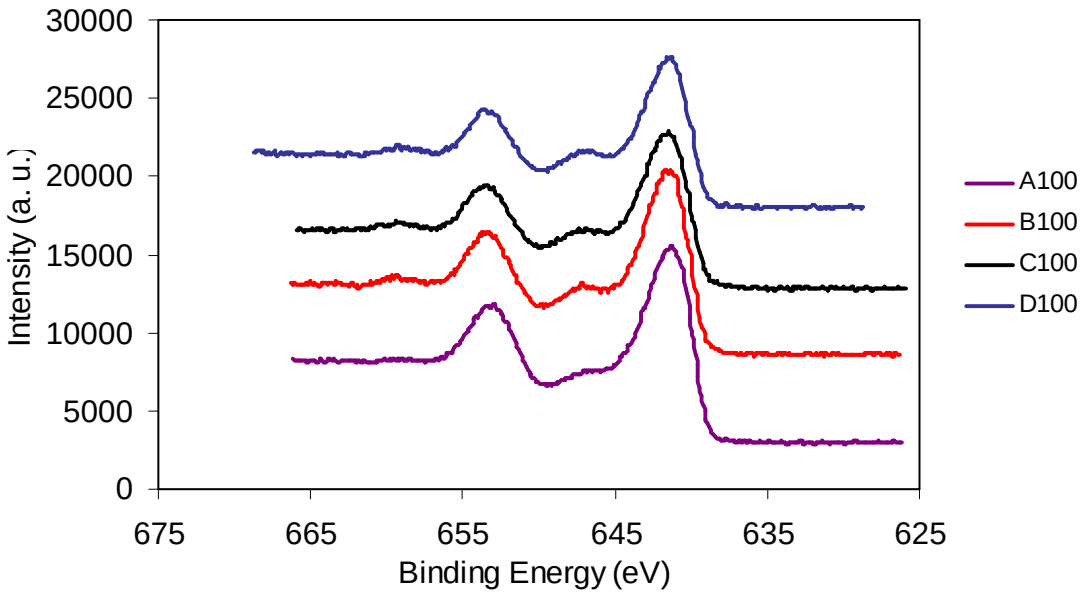

Figure 4.4: Manganese 2p1/2 and 2p3/2 region of XPS spectrum of manganese hydrazide materials heated to 100 °C. From top to bottom: D100, C100, B100, then A100.

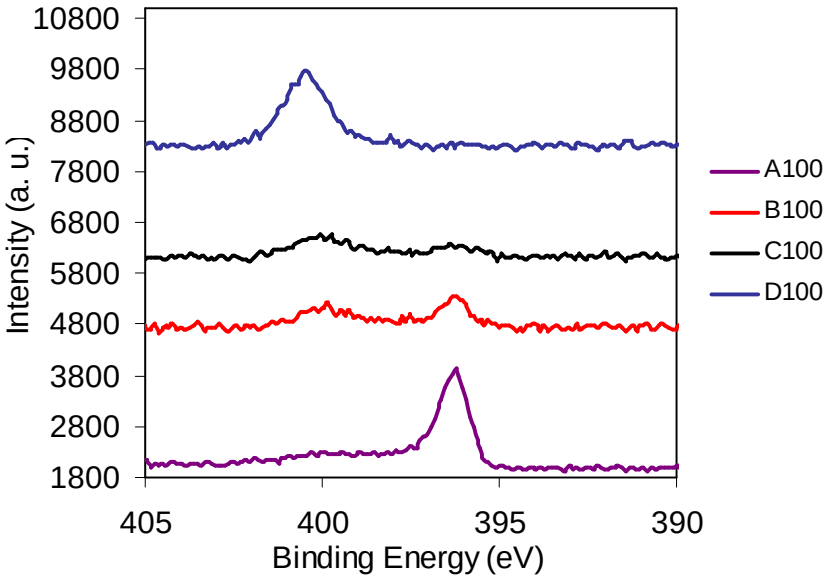

Figure 4.5: N 1s region of XPS Spectrum of manganese hydrazide materials heated to 100 °C. From top to bottom: D100, C100, B100, then A100.

Examination of the XPS data shows that multiple oxidation states of manganese can indeed detected in the manganese 2p 1/2,3/2 region by simulation of the spectra (Figure S4.4a-S4.4d). By comparison with literature values, the emissions at 640.4 eV and 651.6 eV correspond to Mn(0),[24] the main emission at 641.4 eV and 651.3 eV can be assigned to a Mn(II) species,[25] while the emission at 642.6 eV and 654.4 eV represents Mn(IV),[26] and the lowest intensity emission at 646.4 eV and 659.0 eV corresponds to Mn(VII).[27] The appearance of multiple oxidation states both lower and higher than the Mn(II) starting material can be attributed to disproportionation and has been observed in the XPS spectra of CpCr, Cr, and V hydrazides studied previously by our group.[16-19] The intensities of emissions representative of Mn(VII) species increase with the increasing the hydrazine ratio at the expense of lower valence Mn species, suggest that excess hydrazine may be acting as an oxidant of the Mn (II) centers either through the reduction of the acidic protons or the reductive cleavage of the N-N bond to form nitride. Figure 5 shows the XPS spectra of all materials in the N 1s region. A major emission at 396 eV is observed in the A100 material with a minor second emission at 399.4 eV the sum of which can be deconvoluted into 3 major peaks (fig. S5a to S5d). Because metal nitrides typically come at 396.4 eV[28] and protic nitrogen species such as ammonia come at 398.8

eV,[29] the first simulated emission located at 396.2 eV likely corresponds to an N bound directly to two Mn centers. The second emission located at ~ 396.6 eV likely represents a H-N-Mn species, while the third emission at 398 eV can be assigned to a terminal -NH_2 species. This could be confirmed by the IR band of -NH_2 observed in 3400 – 3500 cm^{-1} region (Figure S11). The D100 sample has a major peak at 399.8 eV, corresponding to a fourth nitrogen environment, possibly arising from a quaternary hydrazide nitrogen bound to Mn in a higher oxidation state and consistent with the higher intensities of the XPS emissions of Mn(VII) species in the Mn 2p region. These assignments are consistent with the change in hydrazine concentration in the samples, as those with lower hydrazine concentrations have a predominance of the emissions centered at 396 eV, suggesting a greater degree of metal hydrazine bridging required by the fewer hydrazine N centers available for ligation, and those samples with higher concentrations of hydrazine show a greater ratio of the emissions centered at 399 eV for terminal unbound hydrazine NH_2 centers.

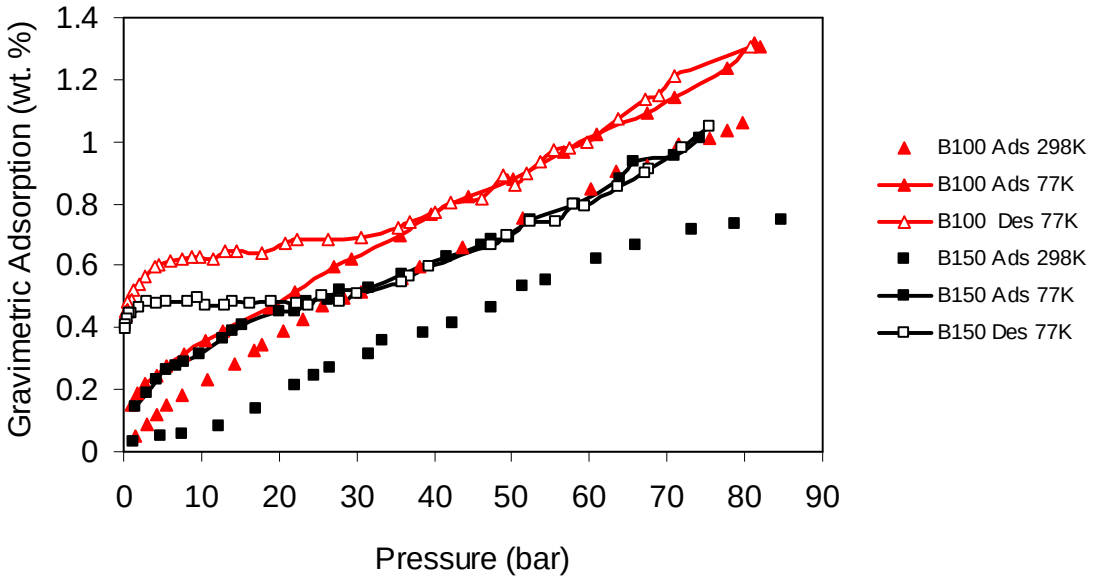

Figure 4.6: Gravimetric hydrogen adsorption – desorption isotherms of B-series manganese hydrazide materials synthesized with a Mn : N_2H_4 ratio of 1:1.

Table 4.1: Summary of excess storage results on manganese hydrazide materials and carbon AX-21, MOF-5. Data recorded at 85 bar.

Material	BET Surface Area (m^2/g)	Skeletal Density (g/cm^3)	Gravimetric Adsorption (wt%)	True Volumetric Adsorption (kg/m^3)	Retention (%)
A100	273	2.2107	1.33 (at 77 K) 0.74 (at 298 K)	29 (at 77 K) 16.3 (at 298 K)	56
A150	142	2.9373	1.09 (at 77 K) 0.38 (at 298 K)	32 (at 77 K) 11.2 (at 298 K)	35
B100	279	2.2875	1.31 (at 77 K) 1.06 (at 298 K)	30 (at 77 K) 24.2 (at 298 K)	81
B150	230	3.1640	1.01 (at 77 K) 0.75 (at 298 K)	32 (at 77 K) 23.7 (at 298 K)	74
C100	169	2.1104	0.95 (at 77 K) 0.86 (at 298 K)	20 (at 77 K) 18.1 (at 298 K)	90
C150	123	2.9716	0.63 (at 77 K) 0.54 (at 298 K)	19 (at 77 K) 16.0 (at 298 K)	86
D100	116	2.5780	0.54 (at 77 K) 0.37 (at 298 K)	14 (at 77 K) 9.5 (at 298 K)	69
D150	97	2.9318	0.48 (at 77 K) 0.32 (at 298 K)	14 (at 77 K) 9.4 (at 298 K)	67
AX-21	3225	2.1030	4.2 (at 77 K, 65 bar) 0.55 (at 298 K)	14 (at 77 K, 65 bar) -	13
MOF-5	3534		5.10 (at 77 K) 0.28 (at 298 K)		5.5

The excess storage isotherms of B100 and B150 samples are shown in figure 4.6. At 77 K these isotherms show an initial rise at low pressure consistent with a small amount of physisorption expected from the surface areas in the 230-279 m^2/g range, followed by a linear region up to 85 bar without saturation to 1.3 wt%. This initial rise is similar, but

less intense than those exhibited by both vanadium and chromium hydrazide gels.[18,19] Isotherms for A, C, and D materials are shown in Figures S4.6-S4.8 and show similar behavior, with slightly lower adsorption values at 77 K. The desorption isotherms are also shown in Figure 4.6 and show a small amount of irreversibility equivalent to approximately 30% of the total adsorption, however after applying vacuum and remeasuring the adsorption there is no difference from the value in the first run, indicating that this is a minor kinetic issue or an artifact created by the small aliquot size in the hydrogen storage measurement. At room temperature, all adsorption isotherms exhibit linear behavior however B150 appears to show saturation, possibly related to the decomposition of this material at the higher drying temperature reflected in the lower adsorption values for all 150 series materials. The B100 and B150 materials adsorb a significant amount of hydrogen at pressure 0 – 30 bar, unlike the vanadium hydrazides, which required pressures higher than 30 bar to achieve recognizable adsorption. Linear behavior without saturation at low pressure is not typical of physisorption and suggests a different mechanism of hydrogen storage is operative in these materials, which we have previously attributed to the involvement of the Kubas interaction.

The gravimetric adsorption of the B100 sample is 1.06 wt. % at 85 bar and 298 K while the true volumetric adsorption of this sample is 24.2 kg H_2/m^3, slightly higher than the true volumetric adsorption of B150 at 23.7 kg H_2/m^3. These amounts use the skeletal density in the calculation (see experimental for complete explanation) and represent the amount of hydrogen contained in and on the surface of the solid portion of the sample without the compressed gas in the void space. For comparison, the true volumetric adsorption of B100 is 3.53 times more than the volumetric of compressed hydrogen gas under the same conditions (6.86 kg/m^3 at 298 K and 85 bar for idea gas). At 77 K and 85 bar, the B100 sample adsorbs 1.31 wt. %, corresponding to a true volumetric adsorption of 30 kg H_2/m^3. Figure S10 shows the excess storage isotherms of a pellet of B100 compressed at 500 psi to eliminate excess void space. The bulk density measured for this sample of 1.5054 g/cm^3 provides excess volumetric storage capacities of 31.76 kg H_2/m^3 at 77 K, and 18.97 kg H_2/m^3 at 298 K determined from the gravimetric adsorption data at 77 K (2.11 wt%) and 298 K (1.26 wt%), respectively, of this sample. The volumetric performance of 31.76 kg H_2/m^3 is similar to that of MOF-177, which possesses an excess

volumetric storage of 32.0 kg H_2/m^3 at 77 K and an absolute volumetric adsorption (which contains an additional compressed gas component not included in our calculations of the Mn materials) at 77 K of 49.0 kg H_2/m^3.[30] From a comparison of the gravimetric adsorption data at 298 K and 77 K, the retentions of excess adsorption capacities can be calculated, and range from 90% to 35%. This is comparable to the values obtained for Cr hydrazides[19] and much higher than that of MOF-5 and carbon AX-21, which retain 5.5% and 13%, respectively, and once again suggests that the Kubas interaction is involved in the mechanism as confirmed by Raman spectroscopy for the Cr analogues. In fact, by comparing the loss in gravimetric adsorption between 77 K and 298 K to the surface areas of ca. 250 m^2/g, it appears that this quantity can be completely attributed to the physisorption component and that the remaining amount attributed to the Kubas interaction is constant from 77 K to 298 K.

These results establish that a mole ratio of 1:1 and heating temperature of 100 ^oC provides the best synthetic conditions for generation of manganese hydrazide gels for optimized hydrogen adsorption performance. Further discussion on the relationship between the synthesis conditions and physical properties of these materials provides useful insights. The elemental analysis results demonstrate that the Mn:hydrazine ratio of 2:1 is insufficient to remove enough alkyl groups to ensure high activity by reducing the steric profile around the metal center and lowering the system weight through substitution of trimethylsilylmethyl ligand for hydrazine. The lower hydrazine ratios also lead to a domination of hydrazine N bound to two or more Mn centers as confirmed by XPS, further increasing steric congestion about the Mn centers through excess clustering of the crucial metal centers. Conversely a Mn:hydrazine ratio of 1:2 leads to a material with a higher proportion of high oxidation state Mn unable to bind H_2. Excess hydrazine molecules also block coordination sites that would otherwise be available for H_2. Heating these materials to 150 ^oC causes an increase in skeletal densities and decrease of gravimetric adsorption capacities of all samples. The increase in density is likely due to the elimination of alkyl groups, a process that was confirmed by observation of the C-H stretch in the IR.

Table 4.2: Average number H_2 adsorbed per Mn site at 85 bar using TGA data.

Sample	Number of H_2/Mn at 77 K	Number of H_2/Mn at 298 K
A100	0.59	0.33
B100	0.58	0.47
C100	0.51	0.46
D100	0.34	0.23

Calculations based on the basis of gravimetric adsorption and the manganese content in each sample result in an average number of hydrogen molecules per manganese atom (Table 4.2) ranging from 0.34 – 0.59 H_2/V at 77 K and 0.23 – 0.47 H_2/V at 298 K. This compares to 1.8 H_2/Ti measured for benzyl Ti fragments on mesoporous silica[14] and 1.75 and 0.57 H_2/M for Cr[19] and V[18] hydrazides, respectively. The reason for the lower than expected number of active binding sites is possibly due to inhomogeneity in the hydrazide gel resulting in Mn(IV) and Mn(VII) centers that do not bind H_2 and other Mn centers that may not be sterically accessible. For comparison, a metal-organic framework system incorporating framework Mn^{2+}, prepared by ion-exchange, also show and enhancement in hydrogen adsorption.[31] Further computational research proved that in these Mn/MOFs, one Mn could adsorb up to 1 H_2/Mn center,[32] however these were shown to be bound through a simple σ-interaction.

In order to investigate the potential of these materials for multiple cycle hydrogen storage, 20 cycles of hydrogen adsorption/desorption were undertaken at 298 K with pressure up to 85 bar on sample B100 (Fig. S4.9). Initial cycles showed 1.06 – 1.10 wt% hydrogen adsorption while subsequent cycles yielded between 0.95 – 1.10 wt%, and the final adsorptions are at 1.01 – 1.00%, displaying a minor decrease in the materials' performance, which falls in the error range of the instrument at ± 0.05 wt%.

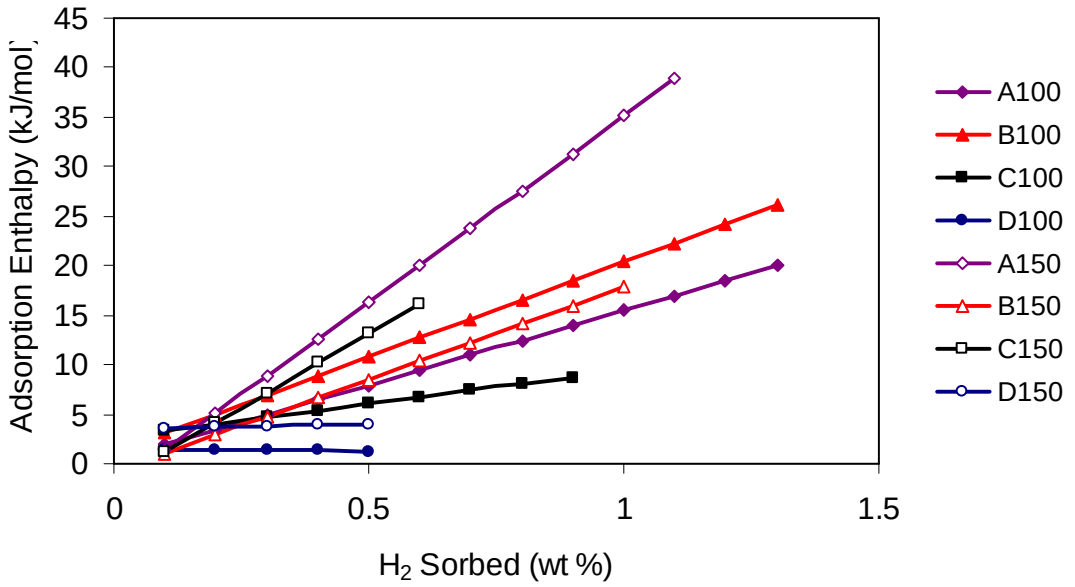

Figure 4.7: Heat of hydrogen adsorption on manganese hydrazide materials and carbon AX-21.

The isosteric heats of hydrogen adsorption to be calculated by fitting the adsorption isotherms at 77 K and 87 K into the Clausius – Clapeyron equation. The data for materials heated at 100 ^{o}C as well as that of carbon AX-21 as a standard was measured under the same conditions (Figure 4.7). This isosteric heat of adsorption of all manganese hydrazide materials rises from roughly 1.3 kJ/mol H_2 up to 39 kJ/mol H_2, contrasting strongly to the behavior of AX-21, which demonstrate decreasing enthalpies from 6 kJ/mol H_2 down to 3.3 kJ/mol H_2, typical of physisorption. The average value of the manganese hydrazides spans the range from 20 – 30 kJ/mol H_2, believed to be the ideal heat of hydrogen adsorption of suitable room temperature hydrogen storage materials.[9] The rising enthalpies with surface coverage, observed in all previous publications from our group concerning hydrogen storage on supported low-coordinate low-valence organometallic fragments, have been rationalized by computations using the Kubas interaction as a model. The results show that as subsequent H_2 units bind to a metal center through what is initially a predominantly σ-interaction the positive charge at the metal decreases and improves the π-bonding, which strengthens the M-H_2 interaction.[33] While these computations have centered around multiple H_2 binding to just one metal

center, we are currently investigating cooperative effects on adjacent metal centers and the involvement of metallic conductivity in distribution of electron density throughout the material in order to rationalize rising enthalpies in systems with lower H_2/M values.

In order to further confirm the metal – hydrogen interaction in this system, electron paramagnetic resonance (EPR) spectroscopic measurements were conducted on the B100 sample before and after hydrogen loading. Since Raman spectroscopy did not reveal any noticeable new signals in the Mn hydrazide sample at ambient pressure under H_2 or D_2, unlike Cr hydrazide gels[19] and V oxamide polymers,[23] we used electron paramagnetic spectroscopy (EPR) to probe the binding interaction. In previous work EPR was used to probe hydrogen binding in our vanadium hydrazide material and revealed that H_2 interacted with V (III) but not V (IV).[18] Prior to hydrogen addition, the X-band (9.4 GHz) EPR spectrum at room temperature shows a signal centered at 3411 G (g = 1.96), diagnostic of a high spin Mn^{II} centre ($3d^5$, S = 5/2), with no orbital contribution to the g-value. Whilst ^{55}Mn has I = 5/2 and is 100% naturally occurring, hyperfine coupling only tends to be observed in dilute single crystal experiments and at high concentrations EPR spectra are typically observed as broad unresolved singlets (Figure 4.8 (a)). In the current system, high Mn concentrations and short Mn…Mn internuclear distances anticipated for bridging hydrazides is likely to give rise to significant dipolar broadening. In addition the possibility of a range of Mn^{II} environments associated with the amorphous nature of the material may also lead to a distribution of g-values close to g = 2.0, affording some inhomogeneous line broadening. After addition of hydrogen gas to the sample, the EPR signal intensity (based on the double integral of the first derivative EPR spectrum) was enhanced by ~110% (Figure 4.8(b)). Subsequent removal of the hydrogen led to a restoration of the signal intensity. Similar behavior was observed at 77 K. At a qualitative level, these observations are consistent with weak and reversible sorption of hydrogen gas to the Mn centers. At a quantitative level, the increase in EPR spectral intensity, with no observation of additional features in the 500 – 6000 G region, is intriguing. Mn^{II} complexes are almost invariably high spin due to the large stabilizing exchange term associated with coparallel spins, even in the presence of strong field ligands such as Cp^-,[34] though CO ligands may stabilize the low spin configuration,[35] especially in the presence of strong π-electron-rich nitrogen bases including hydrazide.[35b] Indeed a number of

studies have been made on sequential deprotonation of hydrazines[36] as potential intermediates during enzymatic nitrogen fixation.[37] In the case of octahedral low spin Mn^{II} the ground state configuration is $^2T_{2g}$ although symmetry lowering and spin-orbit coupling typically lead to a range excited states close to the ground state which can assist rapid relaxation and broad, unresolved EPR lines down to low temperatures. When an EPR spectrum can be detected,[35b] residual spin-orbit coupling tends to give rise to g-values greater than 2.0 which are inconsistent with the observed g-value (1.96) characteristic of high spin Mn(II). The enhancement in EPR signal intensity is therefore unlikely to arise from a simple change in spin-state at the metal centre. Because of this further studies are necessary to resolve these observations.

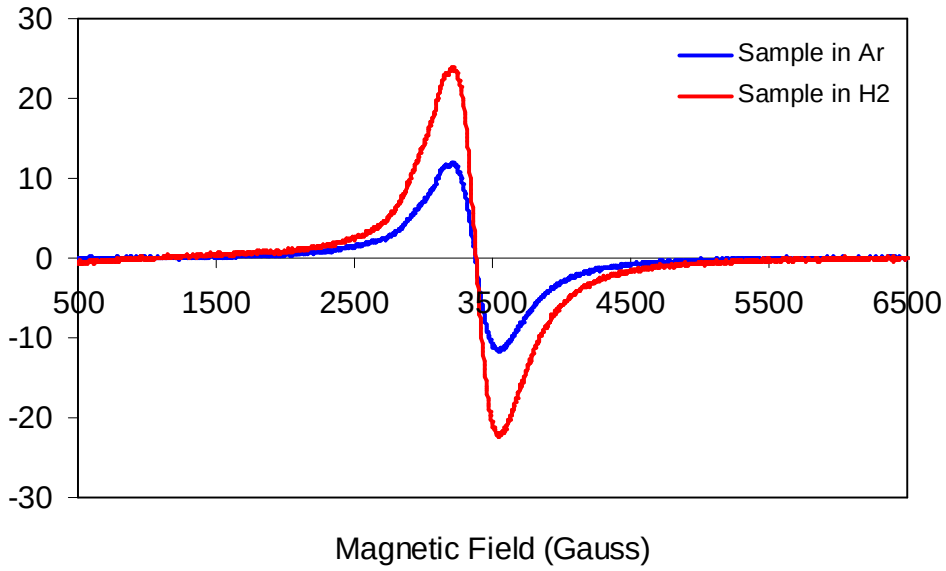

Figure 4.8: Room-temperature EPR spectra of manganese hydrazide gel B100, (a) prior to exposure to hydrogen gas, and (b) after exposure to hydrogen gas. *Experimental conditions:* frequency = 9.382 GHz, microwave power = 20 mW, time constant = 20.48 ms, modulation amplitude = 10 G, accumulation of four 42 s scans.

4.4 Conclusions

New amorphous framework materials consisting of an extended network of low valent manganese metal centers were designed for use of Kubas binding of hydrogen for hydrogen storage and synthesized by the reaction between bis(trimethylsilylmethyl)manganese with anhydrous hydrazine followed by heat treatment in vacuum. Hydrogen storage capabilities were demonstrated at 298 K up to 18.97 kg/m^3 and 1.26 wt % at 85 bar with hydrogen gas pressure as a toggle switch to load or release hydrogen. The samples showed multiple oxidation states by XPS, suggesting that further control over the polymerization reaction to maximize formation of the proposed Mn (II) active centers may further improve activity. The materials exhibited enthalpies that rise with surface coverage and EPR suggested coordination of hydrogen to Mn as a storage mechanism. Once further optimized, these materials could potentially be used under the same conditions as compressed gas, already the main method of hydrogen storage in vehicle prototypes, with significantly higher volumetric capacities.

Supporting Information Available: X-ray powder diffraction, elemental analysis tables, simulated X-ray photoelectron spectra for manganese and nitrogen, hydrogen adsorption isotherms at 77 K and 298 K for A, C, and D samples. Infrared red spectra of manganese hydrazide materials and the $Mg(CH_2SiMe_3)_2$ precursor, the and the cycling experiments on B100.

4.5 References

(1) a) Schlapbach, L.; Zuettel, A. *Nature*, **2001**, 414, 353; b) Seayad, A. M; Antonelli, D.M. *Adv. Mater.* **2004**, 16, 765; c) Yaghi, O. M.; O'Keeffe, M.; Ockwig, N. W.; Chae, H. K.; Eddaoudi, M.; Kim, J. *Nature* **2003**, 423, 705; d) Mark Thomas, K. *Dalton Trans*., **2009**, 1487; e) Wang, L.; Yang, R. T. *Energy Environ. Sci.*, **2008**, 1, 268; f) Lochan, R. C.; Head-Gordon, M.; *Phys. Chem. Chem. Phys*., **2006**, 8, 1357; g) Eberle, U.; Felderhoff, M.; Schueth, F. *Angew. Chem., Int. Ed*., **2009**, 48, 2; h) Cameron, J. M.; Hughes, R. W.; Zhao, Y.; Gregory, D. H. *Chem. Soc. Rev*. **2011**, 4099; i) Hamilton, C. W.; Baker, R. T.; Staubitz, A.; Manners, I. *Chem. Soc. Rev*. **2009**, 279.

(2) Aceves, S. M.; Espinosa-Loza, F.; Ledesma-Orozco, E., Ross, T. O., Weisberg, A. H., Brunner, T. C.; Kircher, O. *Inter. J. Hydrogen Energy* **2010**, 1219.

(3) a) Satyapal, S.; Petrovic, J.; Read, C.; Thomas, G.; Ordaz, G. *Catal. Today* **2007**, 120, 246; b) Liu, C.; Li, F.; Ma, L. –P, Cheng, H. –M. *Adv. Mater*. **2010**, 22, E28;

(4) a) Langmi, H. W.; Book, D.; Walton, A.; Johnson, S. R.; Al-Mamouri, M. M.; Speight, J. D.; Edwards, P. P.; Harris, I. R.; Anderson, P. A. *J. Alloy. Compd*. **2005**, 404–406, 637; b) Hirscher, M.; Panella, B. *Scr. Mater*. **2007**, 56, 809; c) Bénard, P.; Chahine, R. *Scr. Mater*. **2007**, 56, 803; d) Hu, Y. H.; Zhang, L. *Adv. Mater*. **2010**, 22, E1; e) Zhao, J.; Shi, J.; Zhang, X.; Cheng, F.; Liang, J.; Tao, Z.; Chen, J. *Adv. Mater*. **2010**, 22, 394; f) Wang, X.-S.; Ma, S.; Yuan, D.; Yoon, J. W., Hwang, Y. K.; Chang, J.-S; Wang, X.; Jørgensen, M. R.; Chen, Y. -S.; Zhou, H. -C. *Inorg. Chem*. **2009**, 7519.

(5) Graetz, J.; Reilly, J. J. *Scr. Mater*. **2007**, 56, 835.

(6) Farha, O. F.; Yazaydin, A. O.; Eryazici, I.; Malliakas, C. D.; Hauser, B. G.; Katnatzidis, M. G.; Nguyen, S. T.; Snurr, R. Q.; Hupp, J. T. *Nature Chemistry* **2010**, 2, 944.

(7) a) Vitillo, J. G.; Regli, L.; Chavan, S.; Ricchiardi, G.; Spoto, G.; Dietzel, P. D. C.; Bordiga, S.; Zecchina, A. *J. Am. Chem. Soc*. **2008**, 130, 8386; b) Dincă, M.; Long, J. R. *Angew. Chem. Int. Ed*. **2008**, 47, 6766.

(8) Hydrogen, Fuel Cells and Infrastructure Technologies Program: Multi-year Research, Development and Demonstration Plan: Planned Program Activities for 2005 – 2015. http://www1.eere.energy.gov/hydrogenandfuelcells/mypp/pdfs/storage.pdf Retrieved November 25th, 2011.

(9) Zhao, Y.; Kim, Y.; Dillon, A. C.; Heben, M. J.; Zhang, S. B. *Phys. Rev. Lett*. **2005**, 94, 155504.

(10) a) Yildirim, T.; Ciraci, S. *Phys. Rev. Lett*. **2005**, 175501; b) Íñiguez, J.; Yildirim, T.; Udovic, T. J., Sulic, M.; Jensen, C. M. Phys. Rev. B **2004**, 060101-1; c) Cha, M. -H.; Nguyen, M. C.; Choi, K.; Kim, M.; Ihm, J. Nano **2011**, 6, 225.

(11) Hoang, T. K. A.; Antonelli, D. M. *Adv. Mater*. **2009**, 21, 1787.

(12) a) Kubas, G. J.; Ryan, R. R.; Swanson, B. I.; Vergamini, P. J.; Wasserman, H. J. *J. Am. Chem. Soc*. **1984**, 106, 451; b) G. J. Kubas, *Chem. Rev*. **2007**, 107, 4152; b) Heinekey, D. M.; Lledós, A.; Lluch, J. M. *Chem. Soc. Rev*. **2004**, 33, 175.

(13) Hamaed, A.; Trudeau, M.; Antonelli, D. M. *J. Am. Chem. Soc*. **2008**, 130, 6992.

(14) Hamaed, A.; Hoang, T. K. A.; Trudeau, M.; Antonelli, D. M. *J. Organomet. Chem*. **2009**, 694, 2793.

(15) a) Hu, X.; Skadtchenko, B. O.; Trudeau, M.; Antonelli, D. M. *J. Am. Chem. Soc.* **2006**, 128, 11740; b) Hu, X.; Trudeau, M.; Antonelli, D. M. *Chem. Mater*. **2007**, 19, 1388.

(16) a) Hamaed, A.; Mai, H, V.; Hoang, T. K. A.; Trudeau, M.; Antonelli, D. M. *J. Phys. Chem. C* **2010**, 114, 8651; b) Hoang, T. K. A.; Hamaed, A.; Trudeau, M.; Antonelli, D. M. *J. Phys. Chem. C* **2009**, 113, 17240.

(17) Mai, H. V.; Hoang, T. K. A.; Hamaed, A.; Trudeau, M.; Antonelli, D. M. *Chem. Commun*. **2010**, 46, 3206.

(18) Hoang, T. K. A.; Webb, I. M.; Mai, H. V.; Hamaed, A.; Walsby, C. J.; Trudeau, M.; Antonelli, D. M. *J. Am. Chem. Soc*. **2010**, 132, 11792.

(19) Hamaed, A.; Hoang, T. K. A.; Moula, G.; Aroca, R.; Trudeau, M. L.; Antonelli, D. M. *J. Am. Chem. Soc*. **2011**, *133*, 15434.

(20) a) Fetter, N. R.; Bartocha, B. K. W. (U.S. Navy). U.S. Patent 3321503, April 3, 1962/May 23, 1967; Chem. Abstr. **1967**, *67*, 55828; b) Schmidt, E. W. Hydrazine and its Derivatives. Preparation, Properties, Application; John Wiley & Sons, Inc.: New York, 2001; pp 99 – 105.

(21) Alberola, A.; Blair, V. L.; Carrela, L. M.; Clegg, W.; Kennedy, A. R.; Klett, J.; Mulvey, R. E.; Newton, S.; Rentschler, E.; Russo, L. *Organometallics* **2009**, 28, 2112.

(22) Furukawa, H.; Miller, M. A.; Yaghi, O. *J. Mater. Chem*. **2007**, 17, 3197.

(23) Hoang, T. K. A.; Hamaed, A.; Moula, G.; Aroca, R.; Trudeau, M. L.; Antonelli, D. M. *J. Am. Chem. Soc*. **2011**, 133, 4955.

(24) Ansell, R.O.; Dickinson, T.; Povey, A. F. *Corros. Sci*. **1978**, 18, 245.

(25) Escard, J.; Mavel, G.; Guerchais, J. E.; Kergoat, R. *Inorg. Chem*. **1974**, 13, 695.

(26) Ivanov-Emin, B. N.; Nevskaya, N. A.; Zaitsev, B. E.; Ivanova, T. M. *Zh. Neorg. Khimii* **1982**, 27, 3101.

(27) Umezawa, Y.; Reilley, C. N. *Anal. Chem*. **1978**, 50, 1290.

(28) Nishimura, O.; Yabe, K.; Iwaki, M.; *J. Electron Spectrosc. Relat. Phemon*. **1989** 49, 335.

(29) Larkins, F. P.; Lubenfeld, A. *J. Electron Spectrosc. Relat. Phenom*. **1979**, 15, 137.

(30) Wong-Foy, A. G.; Matzger, A. J.; Yaghi, O. M. *J. Am. Chem. Soc.* **2006**, 128, 3494.

(31) Dincă, M.; Dailly, A.; Liu, Y.; Brown, C. M.; Neumann, D. A.; Long, J. R. *J. Am. Chem. Soc*. **2006**, 128, 16876.

(32) Sun, Y. Y.; Kim, Y.-H.; Zhang, S. B. *J. Am. Chem. Soc*. **2007**, 129, 12606.

(33) a) Skipper, C. V. J; Hamaed, A.; Antonelli, D.; Kaltsoyannis, N. *J. Am. Chem. Soc*. **2010**, 132, 17296; b) Skipper, C. V. J.; Hoang, T. K. A.; Antonelli, D. M.; Kaltsoyannis, N. *Chem. Eur. J*. **2011**, accepted.

(34) a) Switzer, M. E.; Wang, R.; Rettig, M. F.; Maki, A.H. *J. Am. Chem. Soc*. **1974**, 96, 7669; b) Ammeter, J. H.; Bucher, R.; Oswald, N. *J. Am. Chem.Soc*. **1974**, 96, 7833; c) Hebendanz, N.; Köhler, F. H.; Müller G.; Riede, J. *J. Am. Chem. Soc*. **1986**, 108, 3281.

(35) a) Snow, M. R.; Stiddard, M. H. B. *J. Chem. Soc., A* **1966**, 777; b) Gross R.; Kaim, W. *J. Chem. Soc., Faraday I* **1987**, 83, 3549.

(36) a) Sellman, D. *Angew .Chem. Int. Ed*. 197211, 534; b) Sellman, D.; Weiss, W. *Angew. Chem. Int. Ed*. **1977**, 16, 880; c) Sellman D.; Weiss, W. *Angew. Chem. Int Ed*. **1978**, 17, 269.

(37) a) Henderson, R. A.; Leigh, G. J.; Pickett, C. J. *Adv. Inorg. Chem Radiochem*, **1983**, 27, 197; b) Barrientos-Penna, C. F.; Einstein, F. W. B.; Jones, T.; Sutton, D. *Inorg. Chem*. **1982**, 21, 2578; c) Murray, R. C.; Schrock, R. R. *J. Am. Chem. Soc*. **1985**, 107, 4557.

Supplemental information for Chapter 4 – Multivalent Manganese Hydrazide Gels for Kubas Type Hydrogen Storage

Table S4.1: Elemental analysis results of synthetic manganese hydrazide samples.

Material	Manganese (%)	Carbon (%)	Hydrogen (%)	Nitrogen (%)	Manganese (%)[(a)]
A100	50.7	6.59	1.49	9.23	61.30
B100	41.9	5.36	1.40	9.58	61.74
C100	35.8	5.41	1.90	8.51	51.50
D100	28.7	6.75	2.39	7.67	43.56

(a): From thermo-gravimetric analysis.

Table S4.2: Proposed unit formula of synthetic materials.

Material	Proposed chemical formula	Manganese (%)	Hydrogen (%)	Nitrogen (%)
A100	MnN	79.68	0	20.31
B100	MnN_2H_2	64.66	2.37	32.97
C100	MnN_3H_4	54.40	3.99	41.61
D100	MnN_4H_6	46.95	5.17	47.88

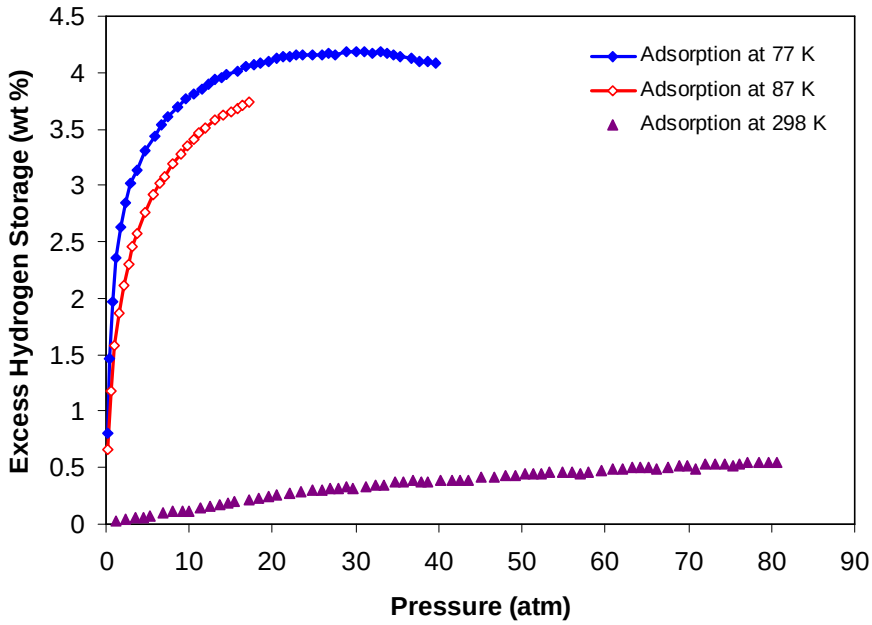

Figure S4.1: Hydrogen excess storage at 77 K, 87 K, and 298 K of carbon AX-21 up to 80 bar recorded on Advanced Materials PCI.

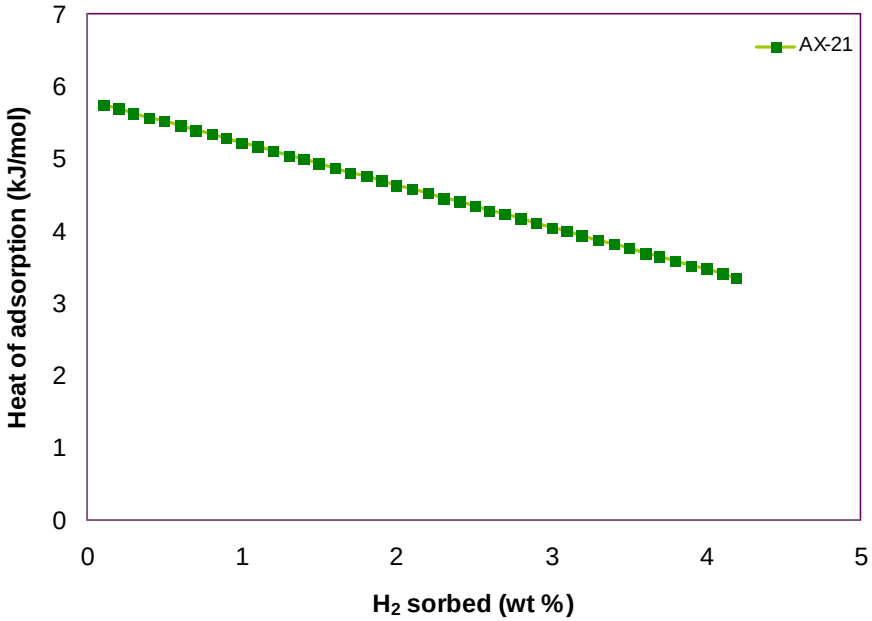

Figure S4.2: Heat of hydrogen adsorption of carbon AX-21 calculated from data in S1.

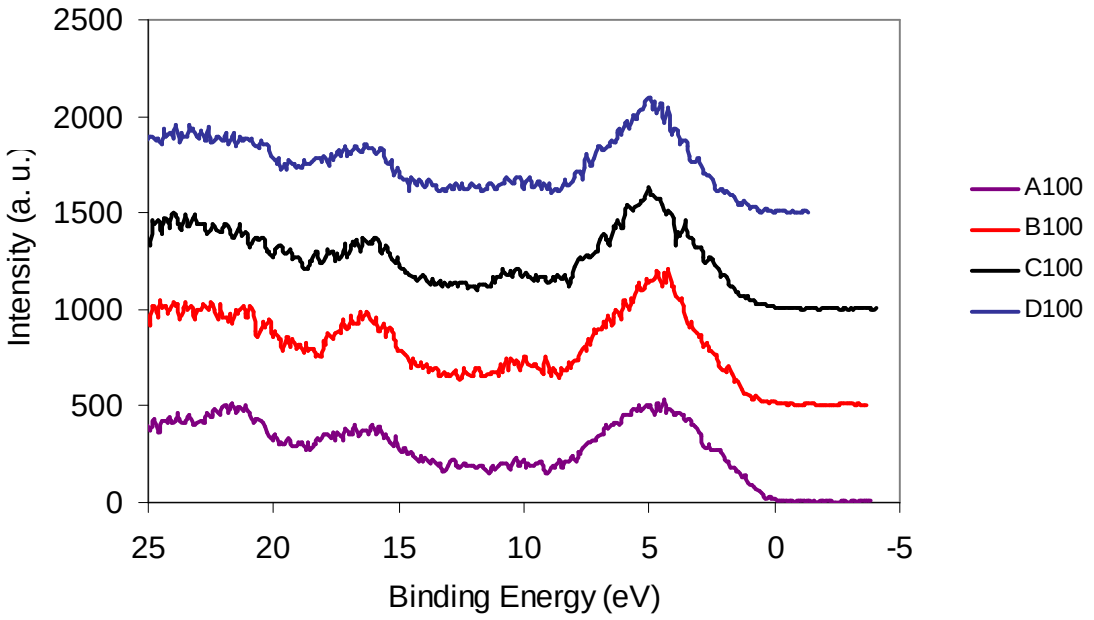

Figure S4.3: Valence region of XPS spectrum of manganese hydrazide materials heated to 100 °C. From top to bottom: D100, C100, B100, then A100.

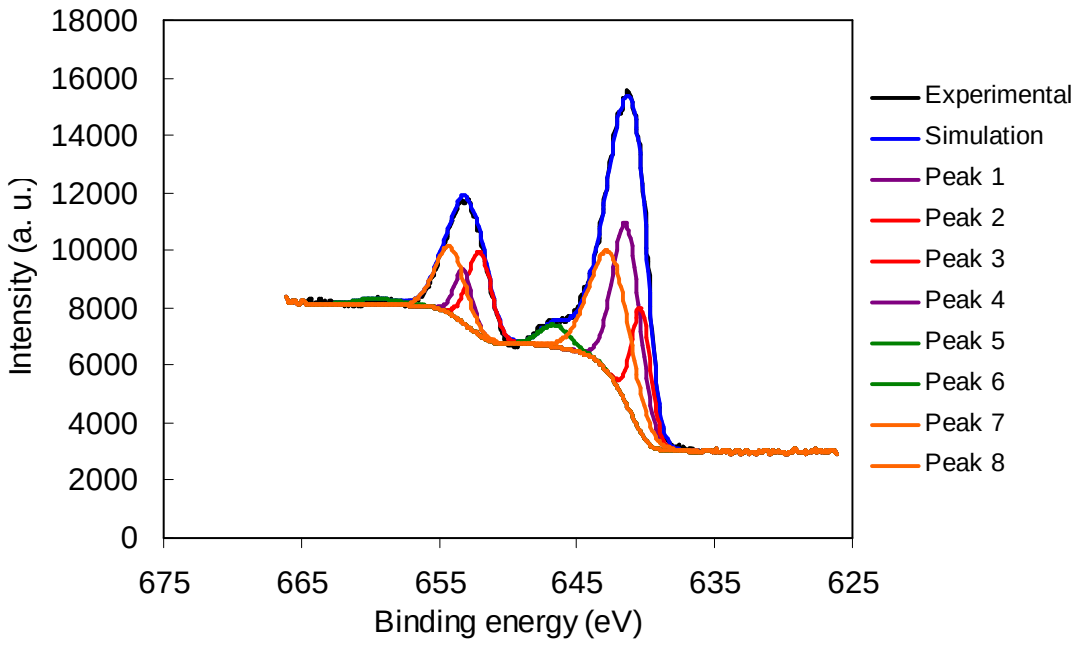

Figure S4.4a: Peak fitting of manganese 2p1/2 and 2p3/2 emissions in the XPS spectrum of A100 sample.

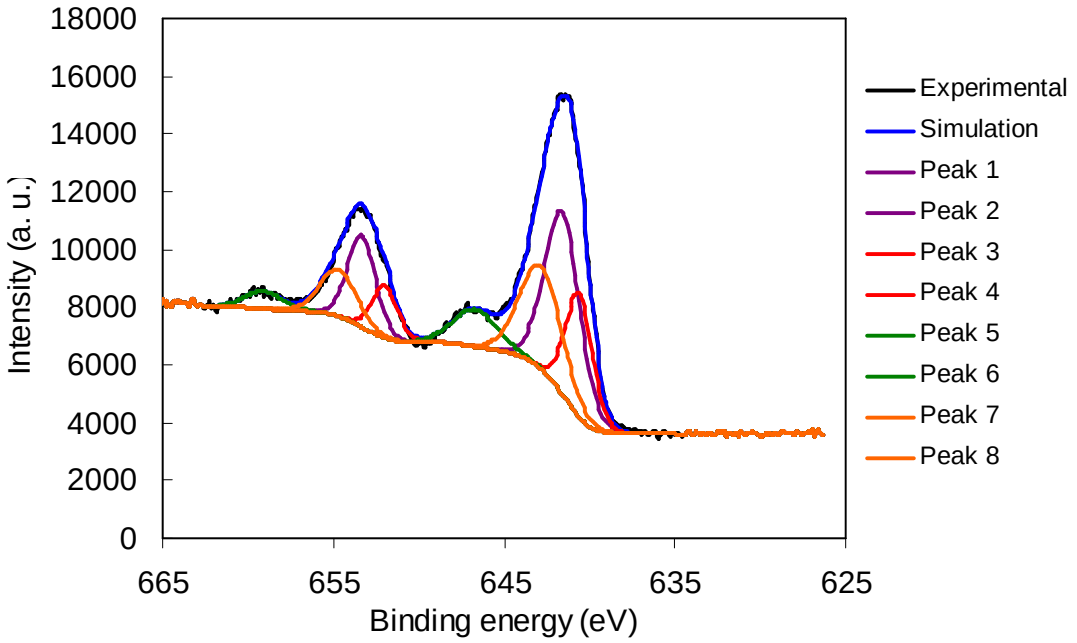

Figure S4.4b: Peak fitting of manganese 2p1/2 and 2p3/2 emissions in the XPS spectrum of B100 sample.

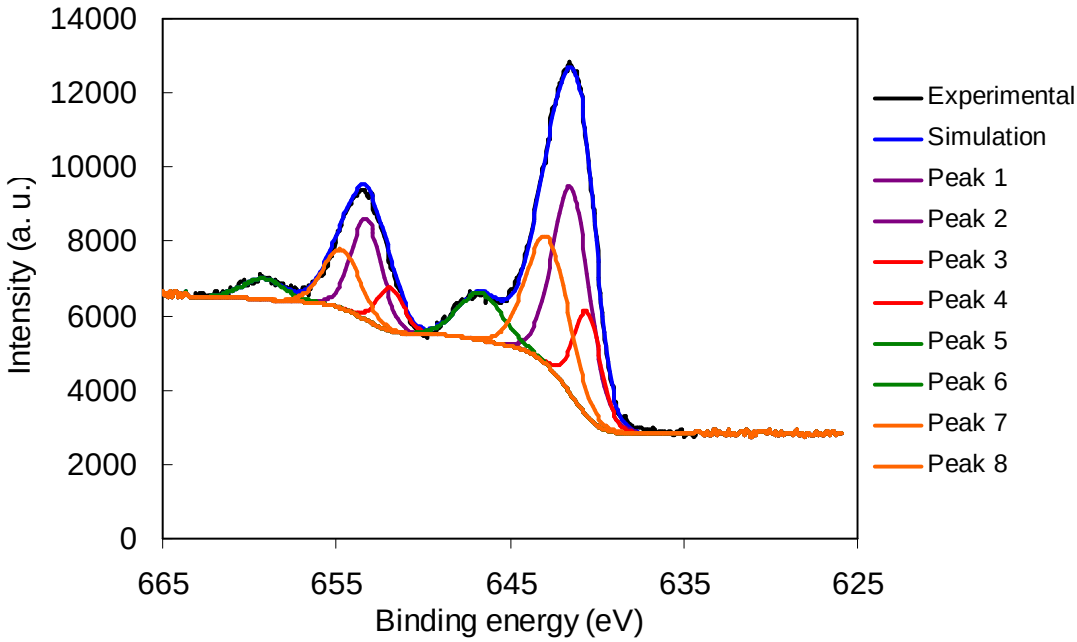

Figure S4.4c: Peak fitting of manganese 2p1/2 and 2p3/2 emissions in the XPS spectrum of C100 sample.

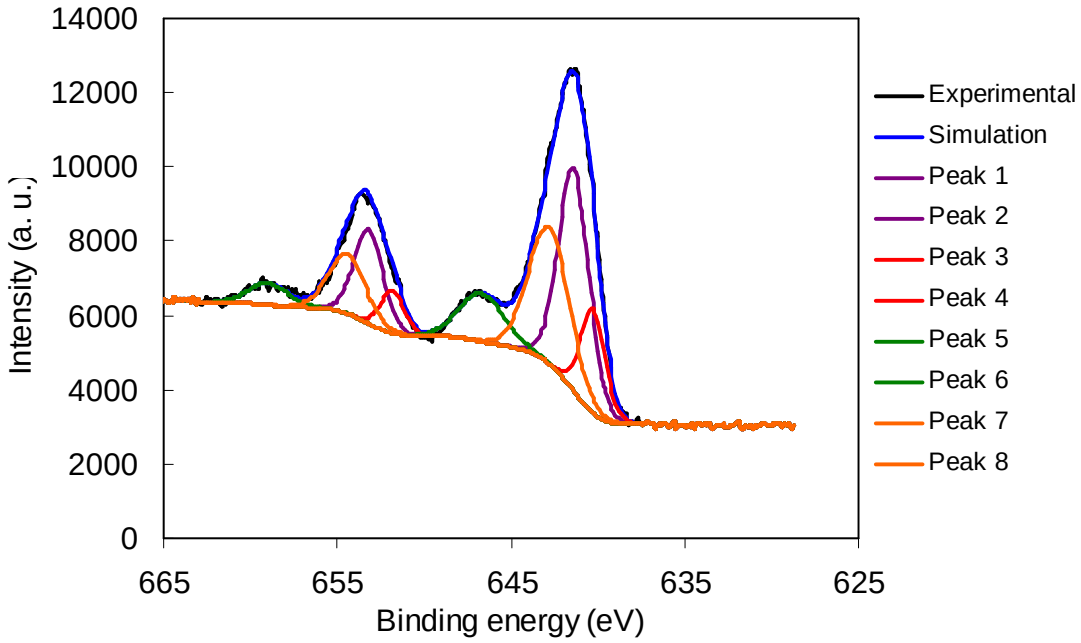

Figure S4.4d: Peak fitting of manganese 2p1/2 and 2p3/2 emissions in the XPS spectrum of D100 sample.

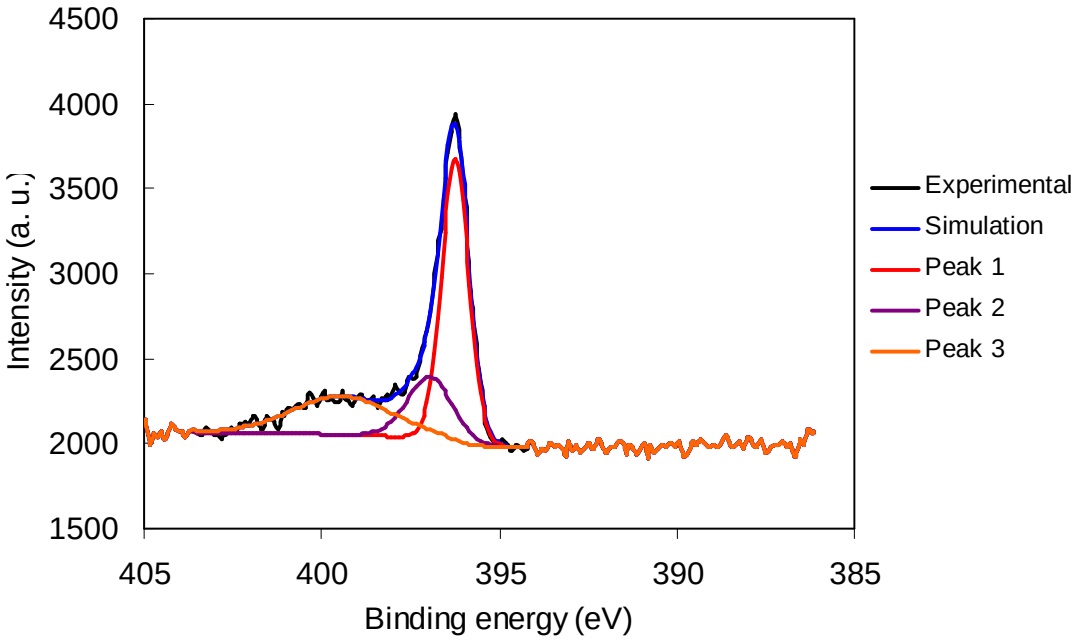

Figure S4.5a: Peak fitting of N 1S region of XPS Spectrum of A100 sample.

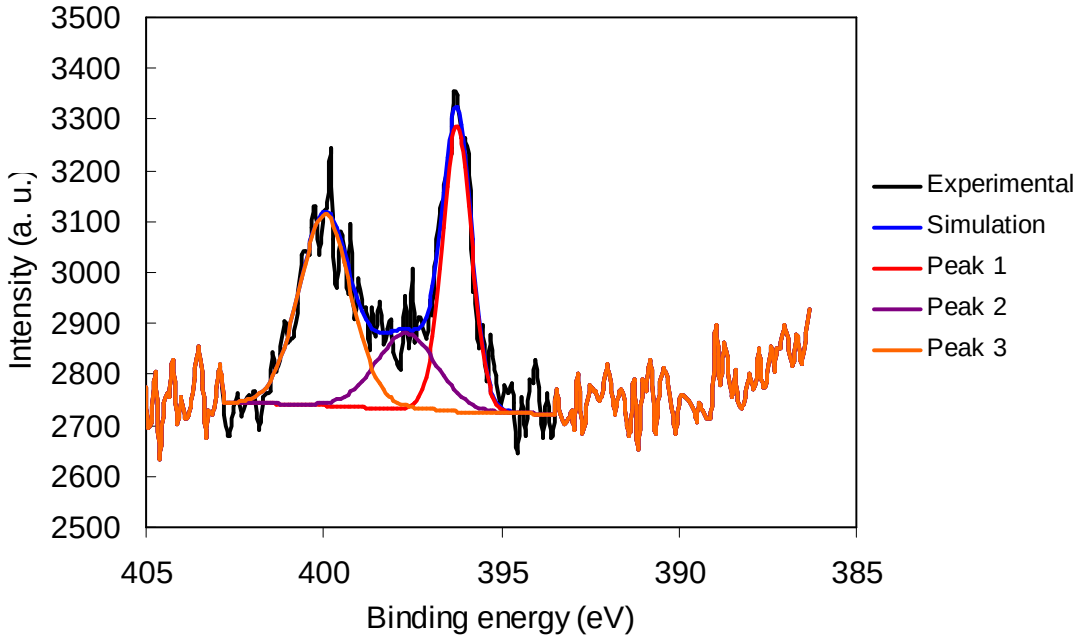

Figure S4.5b: Peak fitting of N 1S region of XPS Spectrum of B100 sample.

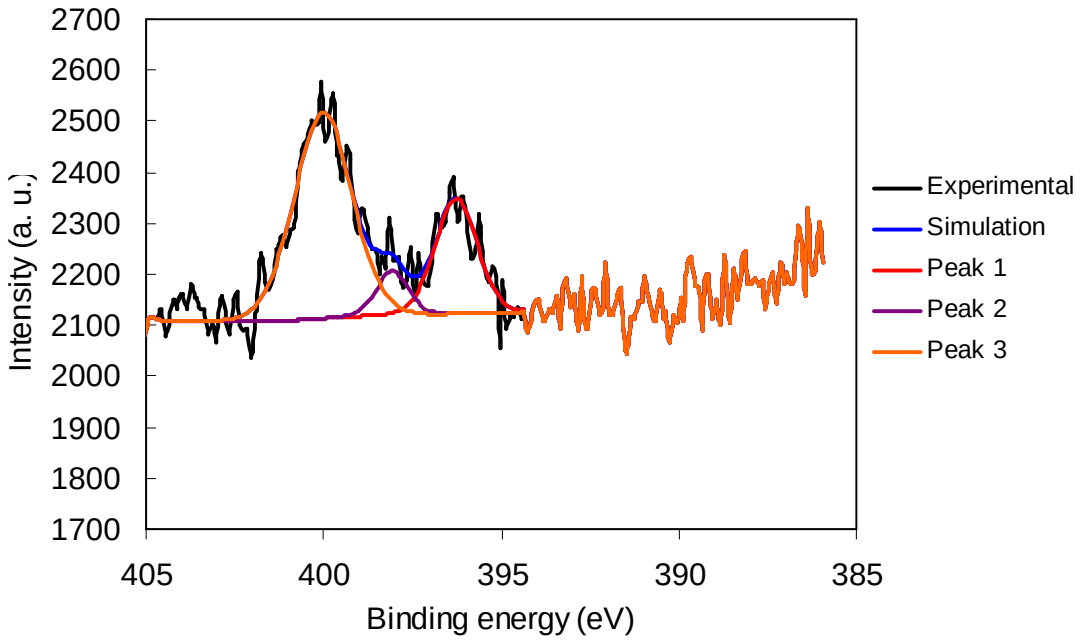

Figure S4.5c: Peak fitting of N 1S region of XPS Spectrum of C100 sample.

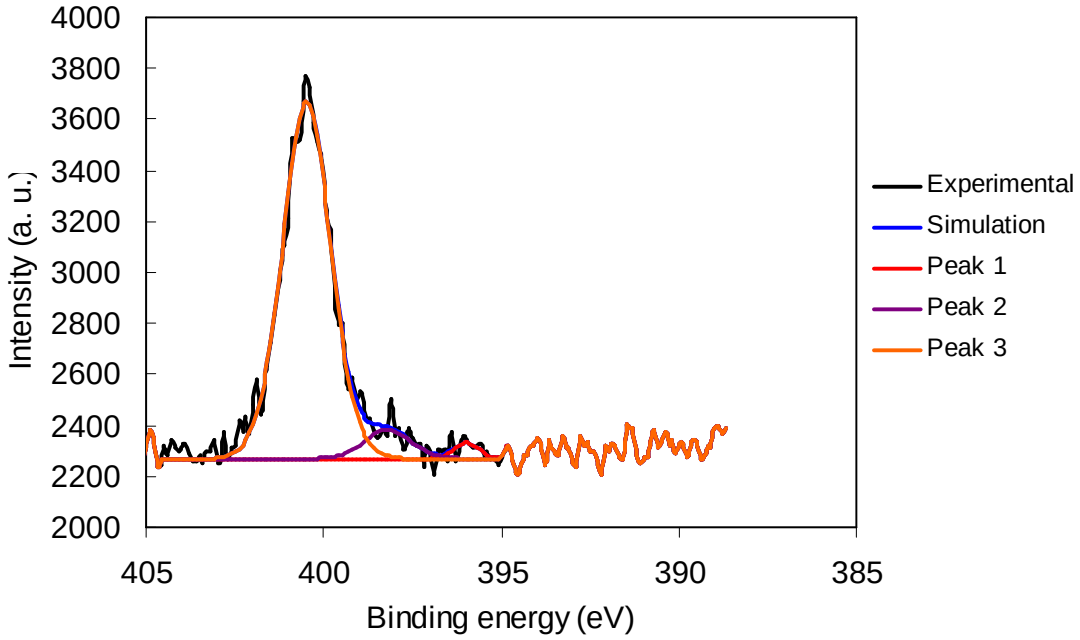

Figure S4.5d: Peak fitting of N 1S region of XPS Spectrum of D100 sample.

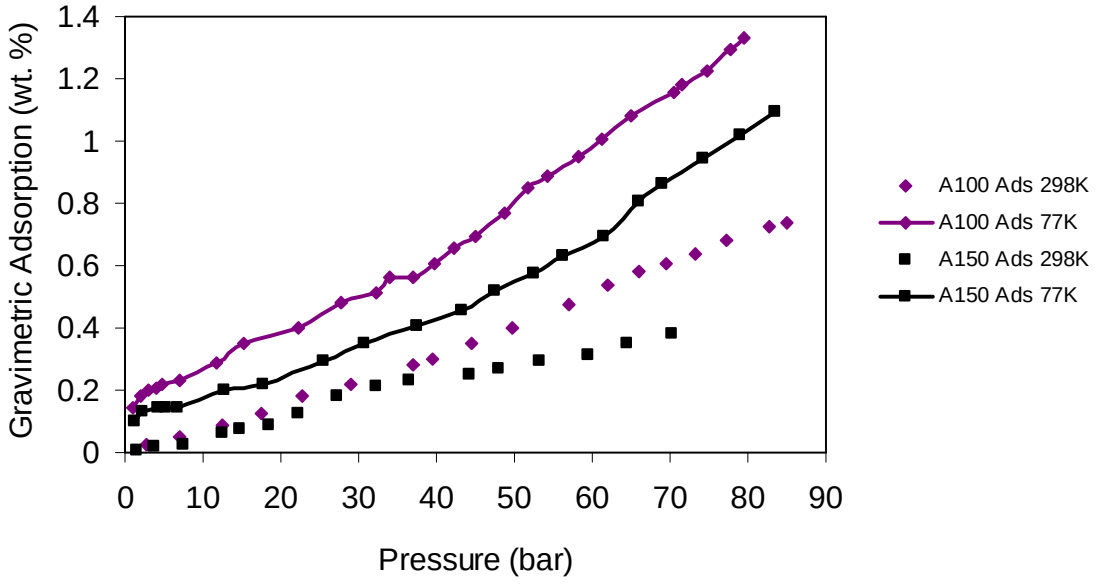

Figure S4.6: Hydrogen adsorption isotherms of A-series manganese hydrazide materials synthesized with a Mn:hydrazine ratio of 2:1. Desorption omitted for clarity.

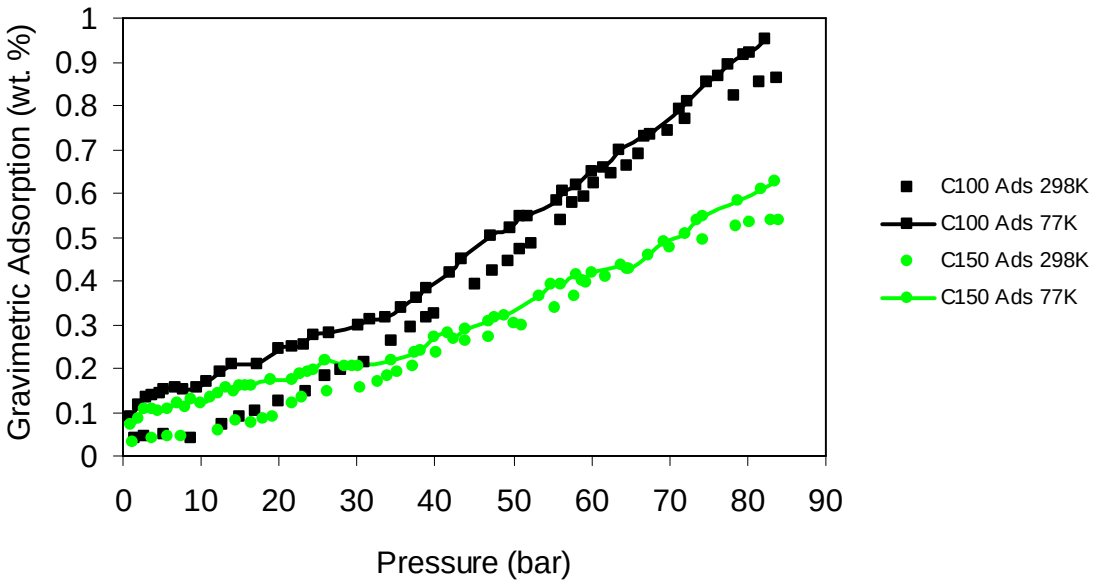

Figure S4.7: Hydrogen adsorption isotherms of C-series manganese hydrazide materials synthesized with a Mn:hydrazine ratio of 1:1.5. Desorption omitted for clarity.

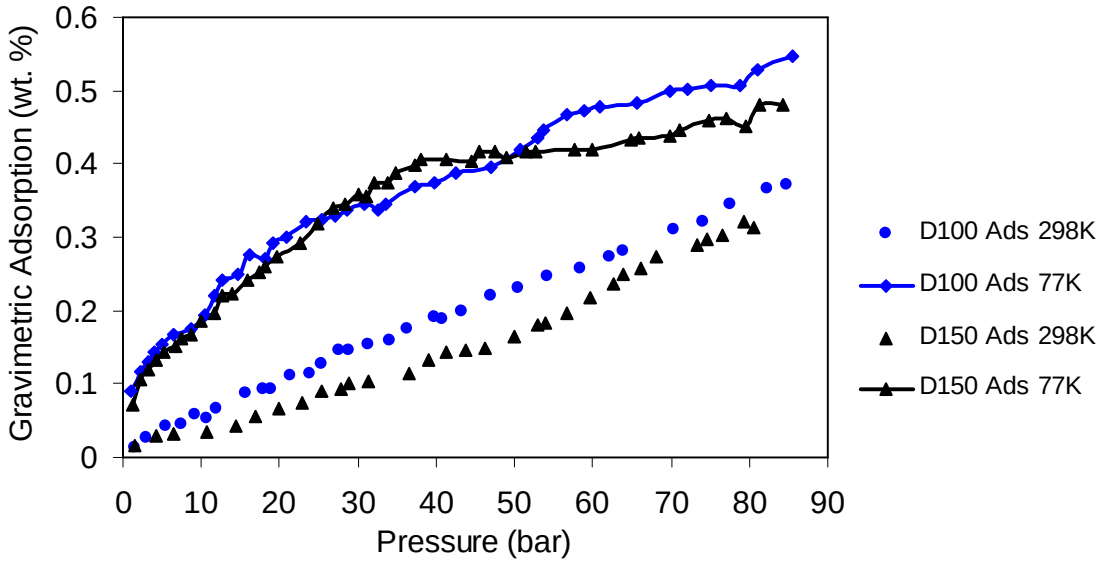

Figure S4.8: Hydrogen adsorption isotherms of D-series manganese hydrazide materials synthesized with a Mn:hydrazine ratio of 1:2. Desorption omitted for clarity.

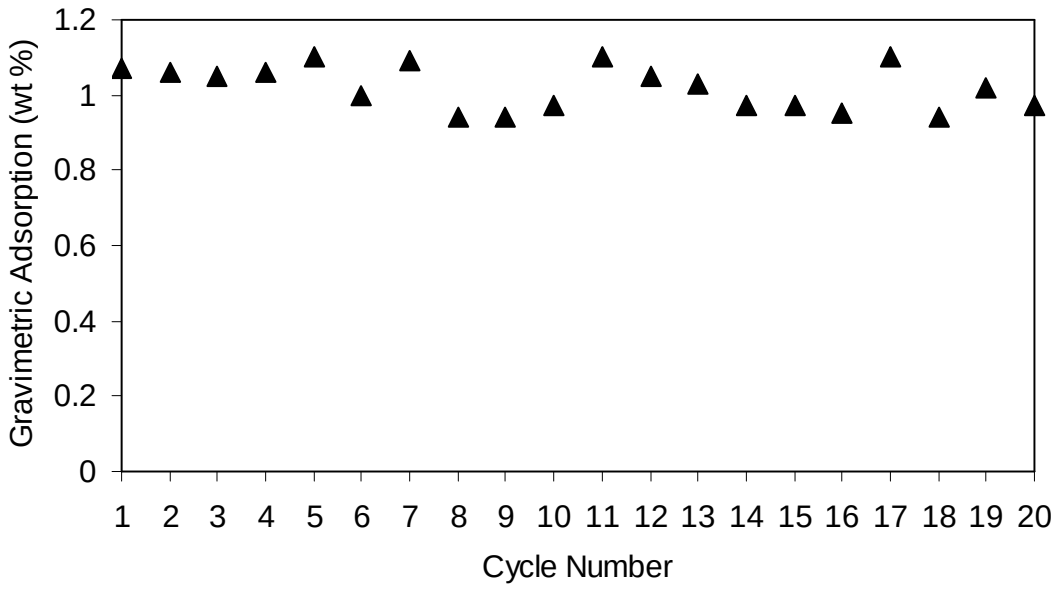

Figure S4.9: Hydrogen adsorption capacity at 298 K in a 20 cycle test to 85 bar of the B100 sample.

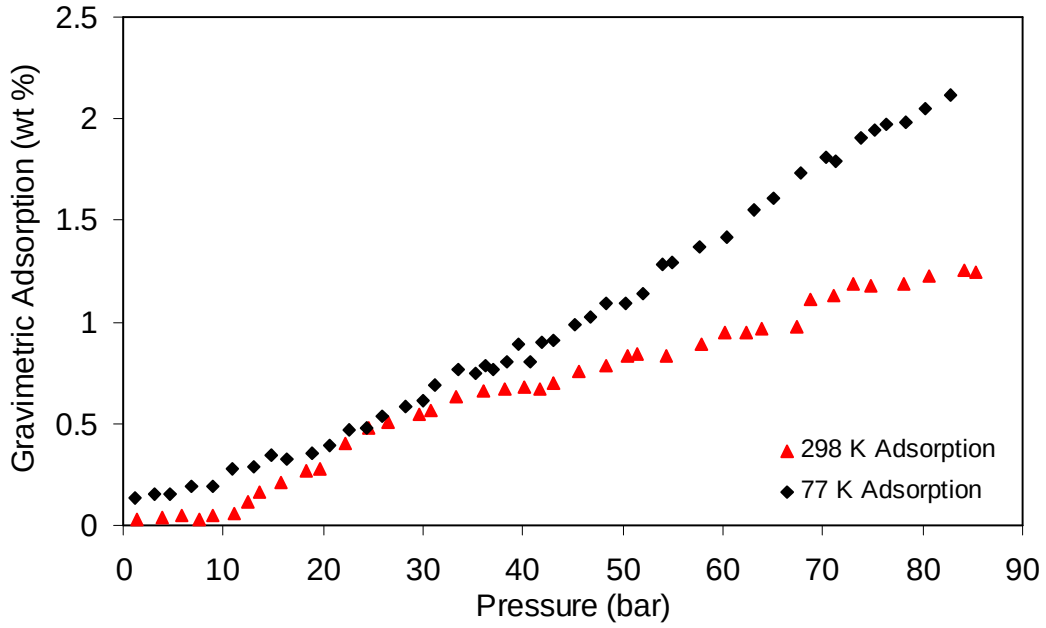

Figure S4.10: Excess storage isotherms at 298 K and 77 K of a pellet of the B100 material compressed at 500 Psi.

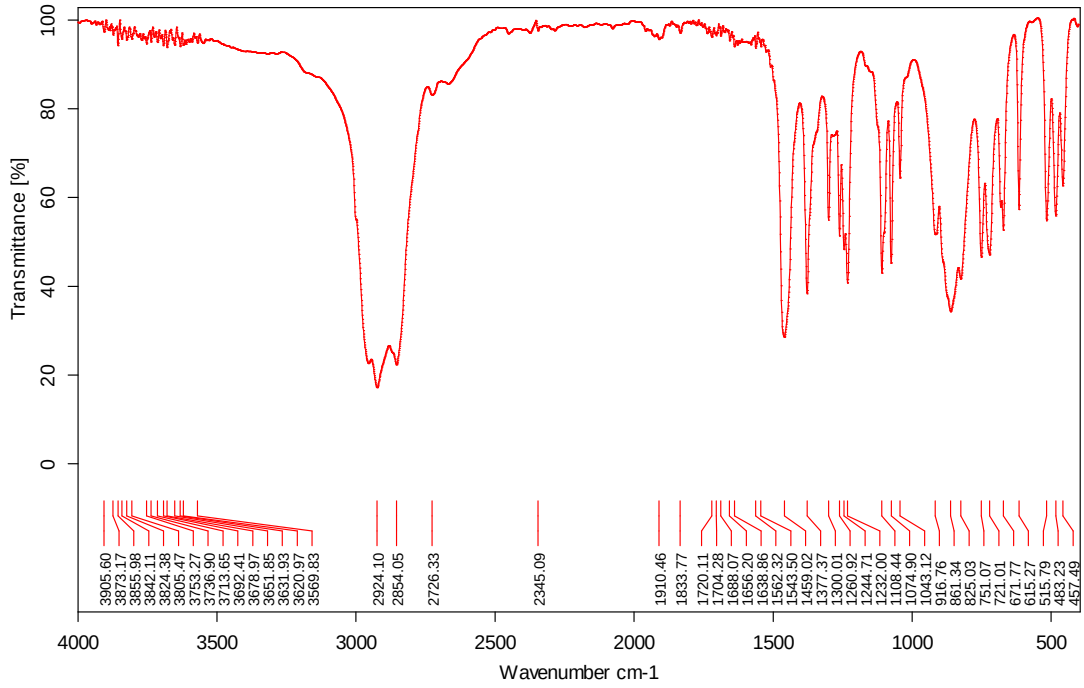

Figure S4.11a: Infrared spectrum of $Mg(CH_2SiMe_3)_2$ in Nujol.

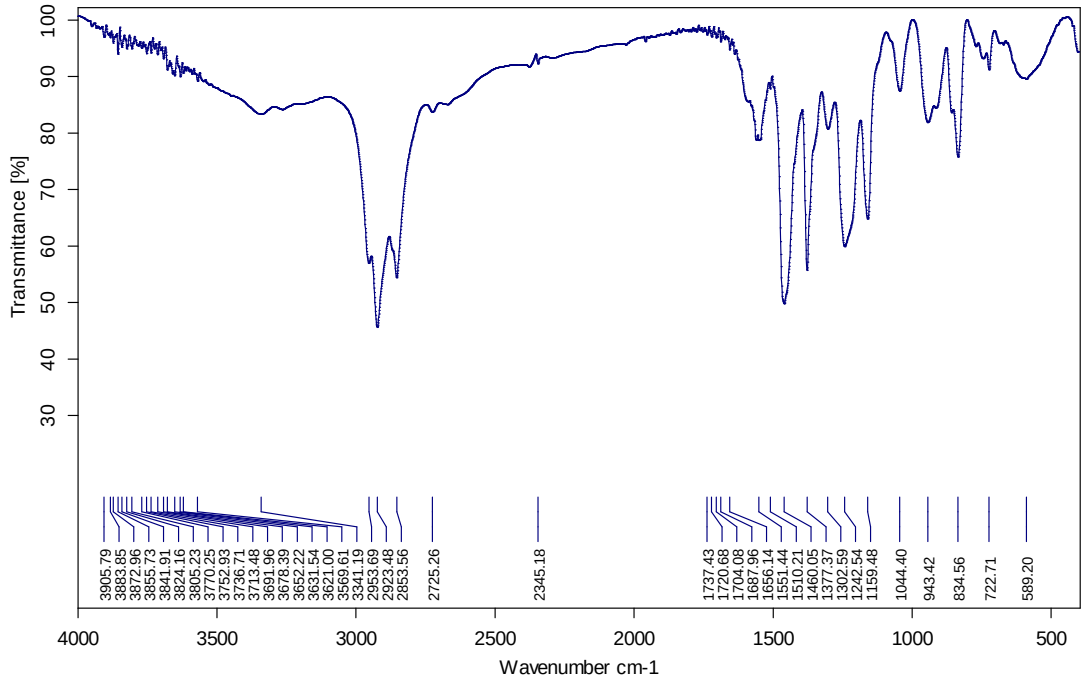

Figure S4.11b: Infrared spectrum of $[\{Mn(CH_2SiMe_3)_2\}_\infty]$ in Nujol.

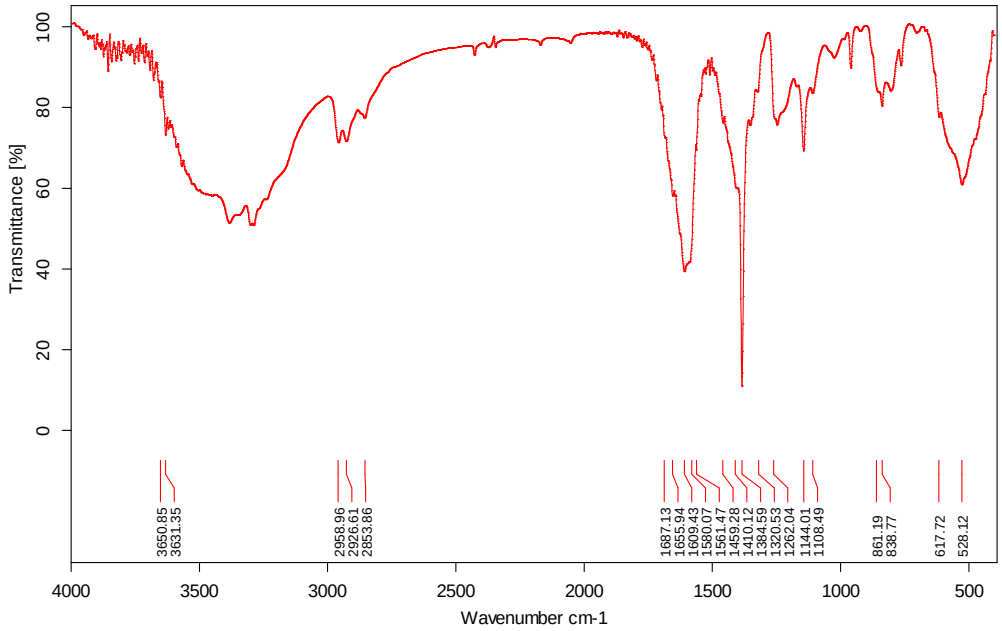

Figure S4.11c: Infrared spectrum of A100 in KBr.

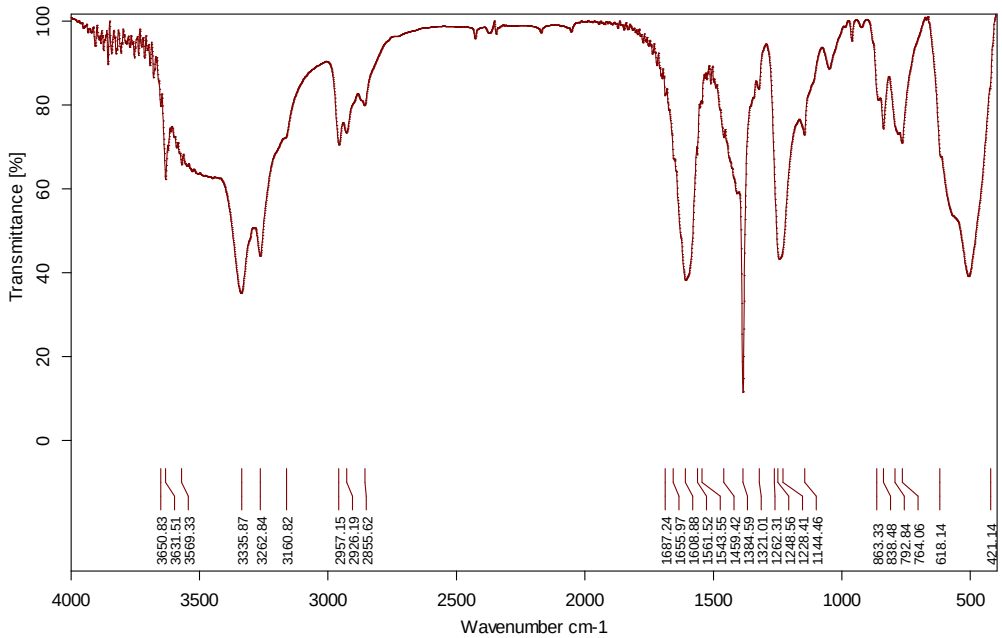

Figure S4.11d: Infrared spectrum of B100 in KBr.

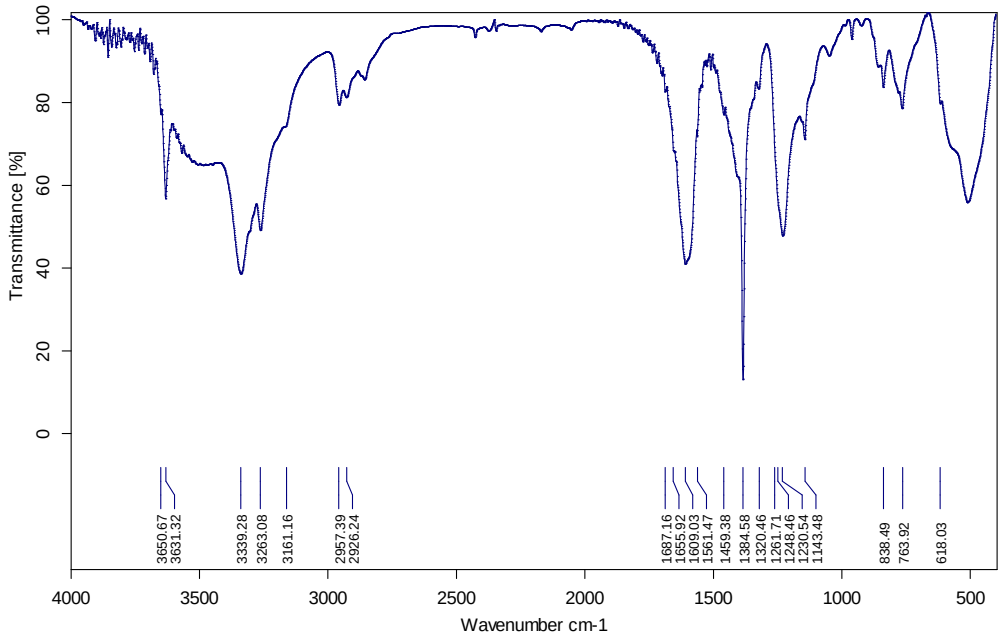

Figure S4.11e: Infrared spectrum of C100 in KBr.

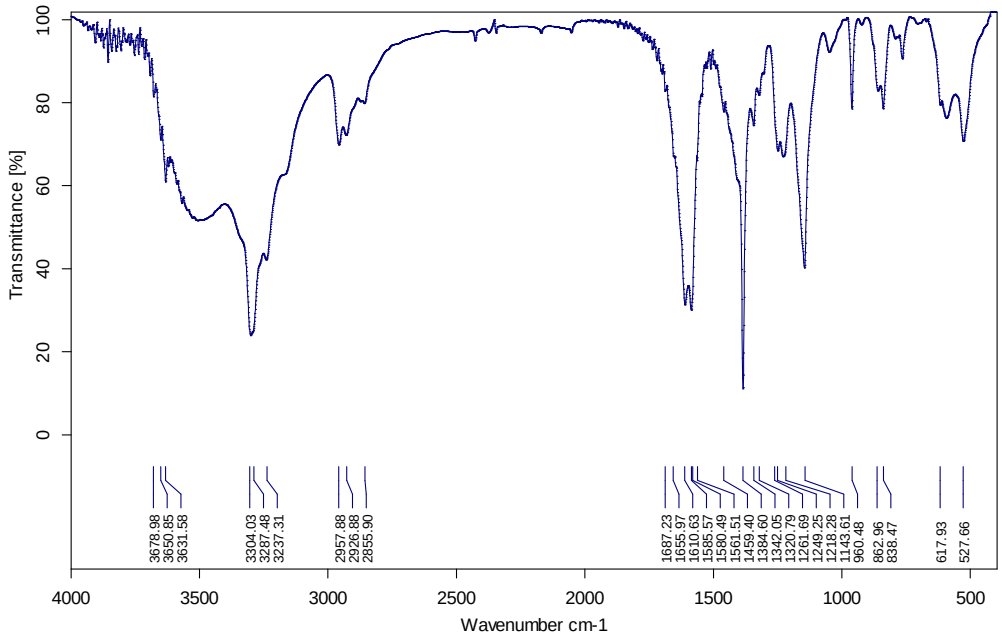

Figure S4.11f: Infrared spectrum of D100 in KBr.

Chapter 5 – Titanium Hydrazide Gels for Kubas-type Hydrogen Storage

5.1 Introduction

With chemical bond energies of 120 MJ/kg and water as the only combustion by product, hydrogen is the most promising alternative fuel, especially when used in a high-efficiency fuel cell. However, its density at 273 K and 1 atm of 0.089g/L is too low for economical use in an automobile. The search for solid state materials which store large amounts of hydrogen at room temperature and moderate pressure is therefore an area of much current interest.[1] The ideal enthalpy of hydrogen binding for room temperature storage has been calculated at 20-30 kJ/mol. This value is lower than usually observed for bulk metal hydrides, and higher than physisorption materials.[2-4] The Kubas interaction, a non-dissosciative ligation of H_2 to a transition metal, has been studied widely in organometallic chemistry[2] and generally possesses enthalpies in this range. Because of this, our group is currently pursuing the design and synthesize of solid state materials consisting of high concentrations of low valent early transition metal species expected to bind significant amounts of hydrogen via the Kubas interaction.[5-7] In previous work we explored cyclopentadienyl Cr,[6a] V,[6b] and Cr,[6c] hydrazide materials in which the hydrazide acts as a light weight support for an amorphous framework structure allowing diffusion of H_2 to the transition metal binding sites. Using this approach we have a achieved a maximum of 3.2 wt % and 40.8 kg/m^3 at 298 K and 170 bar without any kinetic barrier at an average enthalpy of 20 kJ/mol for Cr hydrazide hydrides.[6c] However, computations have predicted that Ti(III) hydrazide dihydride polymers, with a formula TiN_2H_5 can store 9.9 wt % of hydrogen by the Kubas interaction.[8] Since Ti is also a cheaper metal than Cr, the synthesis of Ti hydrazides is of obvious interest to the development of a room temperature hydrogen storage system. Early efforts by our group using tris(benzyl)titanium(III)[9] as a precursor for titanium hydrazides provided a best result of 4.5 wt% fully reversible adsorption at 298 K and 85 bar with 92 kg/m^3 with no significant kinetic barrier. However, tris(benzyl)titanium is extremely unstable and not isolable,[10] and every sample synthesized using this precursor gave different storage results. Because of this, we began to explore other Ti (III) alkyl precursors; although very few are stable or

even isolable. In this paper we use tris(bis(methylsilyl)methyl) titanium(III) as precursor for Ti hydrazides synthesized for use in H_2 storage.[11] The bulky alkyl group stabilizes Ti(III) center, hence allowing complete control of the synthesis conditions.

5.2 Experimental Section

All chemicals were purchased from Sigma-Aldrich and used as is. Diethyl ether and toluene were distilled over sodium/benzophenone to remove oxygen and moisture. Distilled solvents were transferred to a Schlenk flask using a canula. Dry Ar gas was bubbled through the flask for 30 min before transferring into a dry-box. Triethylamine was distilled over CaH_2 and bis(trimethylsilyl)methyl chloride was distilled over P_2O_5 before use. H_2 grade 6.0, N_2, Ar, and He were obtained from Praxair Canada. Manipulations were performed in an Ar glove box and on an Ar Schlenk line as low valence Ti species are extremely sensitive to air and moisture. Anhydrous hydrazine was distilled from hydrazine hydrate using a procedure described in chapter 3.[12] Hydrazine is toxic, flammable, explosive and must be handled with extreme care. $TiCl_3.0.67\{N(C_2H_5)_3\}$ was synthesized from the reaction of $TiCl_3$ and triethyl-amine. $LiCH(SiMe_3)_2$ was prepared from $(Me_3Si)_2CHCl$ and Li. $Ti\{CH(SiMe_3)_2\}_3$ was prepared from $TiCl_3.0.67\{N(C_2H_5)_3\}$ and $LiCH(SiMe_3)_2$ by a modified procedure obtained from Baker et al.[11] $Ti\{CH(SiMe_3)_2\}_3$ obtained from the previous reaction as a green viscous oil was quantified by weighing by difference and then dissolving in fresh distilled toluene before further use. The reactions with hydrazine ratios of 1:1 and 1:1.5 relative to Ti are described below. Higher and lower ratios than these were not explored because in previous work by our group these were shown in every case to negatively impact hydrogen storage results.[6]

5.2.1 Preparation of 1:1 titanium hydrazide gels. 50 ml of toluene was added to 3.00g (5.7 mmol) of $Ti\{CH(SiMe_3)_2\}_3$ with stirring. 0.18 mL (5.7 mmol) of hydrazine was then added dropwise into the solution. The resulting solution turned dark within minutes and was then stirred at room temperature for 24 h at 25 ^oC, and 100 ^oC for 72 h. The solution was then filtered and a solid product was obtained, which was then heated in vacuum for 8 h at room temperature followed by a further 8 h at 100 ^oC. This sample was named A100. Heating the freshly filtered material at 150 ^oC under vacuum for 8 h gives A150.

5.2.2 Preparation of 1:1.5 titanium hydrazide gels. The same procedure as above was applied, using 0.27 mL hydrazine. The sample heated at 100 ^{o}C for 8 h was labelled B100 and the sample heated at 150 ^{o}C for 8 h was named B150.

5.2.3 Hydrogenation of titanium hydrazide gels. 0.3000 g of A100 (or B100) was added to the Advanced Materials PCI sample chamber, which was connected to the Gas Reaction Controller. The sample was soaked with H_2 at 5 bar after which the temperature was raised to 150 ^{o}C before H_2 pressure was adjusted to 80 bar. After 2 h the hydrogen was evacuated, and heating was continued for another 2 hours. The hydrogenated product was given the annotation A100-H_2 (or B100-H_2).

5.2.4 Characterization. Powder X-ray diffraction (PXRD) was performed on Siemens D-500 diffractometer with a Cu Kα radiation (40 kV, 40 mA) source. The step size was 0.02° and the counting time was 0.3s for each step. Diffraction patterns were recorded in the 2θ range 1.5 - 52°. Samples for PXRD analysis were put in sealed glass capillary tube to protect sample from air and moisture during the experiment. Nitrogen adsorption and desorption data were collected on a Micromeritics ASAP 2010. All X-ray Photoelectron Spectroscopy (XPS) emissions were referenced to the carbon C-(C, H) emission at 284.8 eV, and the data were obtained using a Physical Electronics PHI-5500 spectrometer. Samples were loaded in an Ar glove box to maintain sample integrity. Elemental analysis (EA) was conducted using a Perkin – Elmer Series II CHNO/S 2400 Analyzer, calibrated with acetanilide standard. Samples for EA were loaded in an Ar glove box, using tin capsules. Infrared spectroscopy was conducted on a Bruker Vector 22 instrument using Nujol or KBr discs. Thermo-gravimetric analysis was conducted on a Mettler Toledo TGA SDTA 851e, using helium (99.99%) as purging gas with a rate of 30 mL/min. Samples were held at 25 ^{o}C for 30 min before heating to 550 ^{o}C at a rate of 5 ^{o}C/min.

5.2.5 Hydrogen adsorption measurements. Hydrogen adsorption isotherms were obtained by using a computer controlled commercial Gas Reaction Controller manufactured by Advanced Materials Corporation, Pittsburgh, PA, except in the case of the isotherm recorded at 298 K and 170 bar, which was obtained on a Hy-Energy PCT Pro. High purity hydrogen (99.9995% purity) was used as the adsorbent. All measurements were performed exactly as reported previously by our group to ensure

reproducibility.[13] Skeletal densities were collected using a Quantachrome Ultrapycnometer housed in an Ar glove box. This instrument was calibrated bi-monthly as per user manual, using a small sphere with a known volume of 0.0898 cm^3 to monitor the instrument's performance. The volume of an empty cell is collected over several running cycles using He until the values are within ± 2% difference. A pre-weighed portion of sample is loaded into the cell under inert conditions and the volume of the system (sample + cell) is then determined. The skeletal volume of the sample is the difference between volume of sample + cell and the volume of empty cell. Skeletal density is obtained by using the sample mass divided by the sample volume. Excess hydrogen storage measurements on a standard AX-21 sample (4.2 wt. % at 30 bar and 77 K, 0.55 wt. % at 80 bar and 298 K) were performed to ensure proper calibration (Figure S5.1, Supporting Information). Leak testing was also performed during each measurement by checking for soap bubbles at potential leak points. These measurements are all necessary to ensure the veracity of the isotherms. In the H_2 adsorption-desorption experiments a high level of reversibility was observed for all samples across the whole range of pressures. Samples were run at liquid nitrogen temperature (77 K), liquid argon temperature (87 K), and room temperature (298 K) to 85 bar on the Advanced Materials instrument. Isotherms were always measured first at room temperature and then at 77 K or 87 K and the temperature was kept constant by keeping the sample chamber in liquid N_2, liquid Ar, or water. In the Advanced Materials instrument the sample weight and skeletal density are used to determine the volume of the sample in the sample chamber, which is then subtracted from the sample chamber volume to provide an accurate void space volume. When the skeletal density is used for the gravimetric hydrogen uptake measurement, the compressed hydrogen within the pores is treated as part of the sample chamber volume and hence subtracted. Therefore only the hydrogen contained on or beneath the walls of the structure will be recorded by the PCI instrument. This gravimetric value is termed the adsorption or excess storage. When the bulk density is used the hydrogen in the pores of the sample is automatically included in the calculation without any further correction factors and the final value is termed the total storage or absolute storage,[6] which represents all hydrogen contained in the sample including the compressed gas in the voids and the hydrogen adsorbed on or beneath the walls of the

structure. Gravimetric densities are recorded as read from the isotherms while volumetric densities are calculated from the adsorption data and the skeletal or bulk density, depending on the desired value. The excess volumetric storage is typically calculated from the excess storage and the bulk density and gives a measure of the gas adsorbed on or in the solid phase of the material scaled across the entire volume occupied by the sample including the void space. In materials such as MOFs that posses a well-defined and constant ratio between mass and void space this value is often quoted. For compressible materials that may have variable ratios of solid mass and void space it can often help to scale the volumetric density to the solid phase alone as the void space will vary on sample preparation. For this purpose, we have defined the true volumetric adsorption[6,14] as the amount of hydrogen adsorbed on or in a given volume of the solid portion of the sample. This is calculated from the excess storage data and the skeletal density. This value neglects the void space and is useful in comparing volumetric densities of ball-milled powders and gels (materials with textural porosity only and no intrinsic pore structure) to pure solid phase materials such as metal hydrides. Since the materials in this study stand between hydrides and physisorption materials in their mechanism of storage, this value is important. It also allows us to compare volumetric adsorption values of the solid phase alone from one sample to another without having to correct for the different textural void space in each material. The absolute volumetric adsorption has also been defined[6,13] and is a representation of the sum of the excess volumetric storage plus the compressed gas in the void space. This can be calculated from the volumetric storage as measured from the instrument and the bulk density, or by taking the volumetric adsorption and adding the amount in the void space calculated from the pore volume and the ideal gas law.[13] The first method is only possible when using the Advanced Materials instrument. In this paper we have chosen not to calculate this value (or the total gravimetric storage) because the differences between the skeletal densities and bulk densities are much smaller than in MOFs and hence the void space compressed gas contribution is negligible and will also vary due to sample preparation.

Enthalpies of adsorption were calculated using a variant of the Clapeyron – Clausius I equation taking both 77 K and 87 K hydrogen excess storage data.[15] Pressure as a function of the amount adsorbed was determined by using exponential fit for each

isotherm; the first 10 – 11 points of the isotherms were picked up and fit to the exponential equation. This exponential equation provides an accurate fit over the pressure up to 1 MPa with the goodness of fit (R^2) above 0.97. The corresponding P_1 and P_2 values at a certain amount of H_2 adsorbed at both temperatures can be obtained by the simulated exponential equation. Inputting these numbers into equation 1, we then calculate the adsorption enthalpies. This technique is commonly used to measure enthalpies of amorphous carbons and MOFs. The enthalpy for carbon AX-21calculated using this method using hydrogen adsorption data measured on The Advanced Materials PCI as described above is shown in Figure S5.2. Since the enthalpy of a reaction does not vary with temperature, unlike Gibbs free energy, this method provides information on hydrogen binding that is meaningful over a wide temperature range.

5.2.6 H_2/Ti Calculations. Calculations on titanium hydrazide samples were based on %Ti values obtained from the thermo-gravimetric analysis data from Table S1. As an example calculation, A100-H_2 absorbs 1.55 wt % of hydrogen at 85 bar and 298 K. This corresponds to 0.0155 g or 0.00775 mol of H_2 for 1 g of sample. Based on the 55.28 wt% Ti in the sample from Table S1, this translates into an average of 0.67 molecules of H_2 per metal center.

5.3 Results and Discussions

Tris{bis(trimethylsilyl)methyl}titanium was stirred with anhydrous hydrazine in dry toluene for 24 h at 25 ^oC, and 72 h at 100 ^oC, yielding a dark air sensitive solid, which was then heated at 100 ^oC or 150 ^oC under vacuum. For a Ti{$CH(SiMe_3)_2$}:N_2H_4 ratio of 1:1 the resulting materials were given the annotations A100 and A150, respectively. The compounds prepared from a Ti/N_2H_4 ratio of 1:1.5 were named B100 and B150, respectively. In this reaction we propose that the hydrazine acts as a nucleophile and proton source to afford a titanium hydrazide monomer (Scheme 5.1), which polymerizes on further heating.

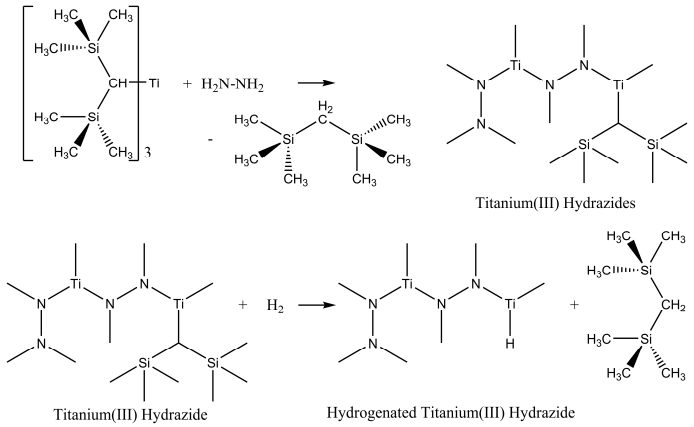

Scheme 5.1: Synthesis of titanium hydrazide gels.

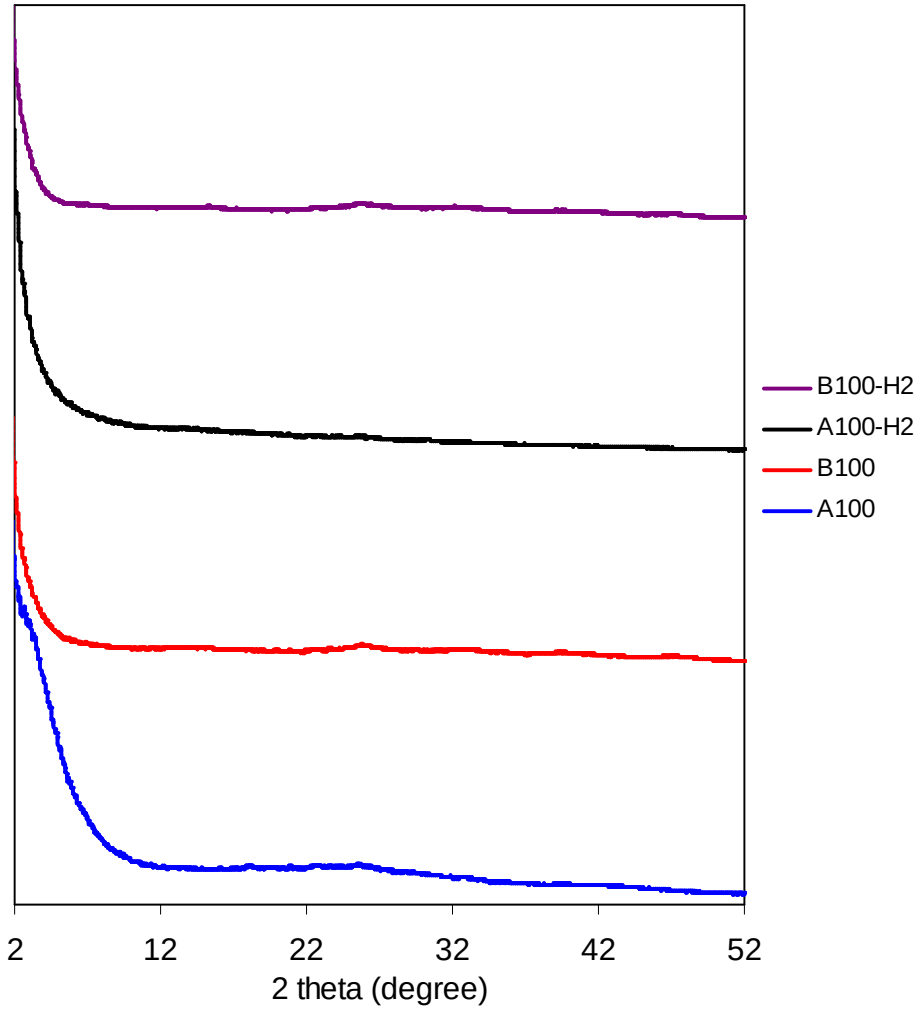

Figure 5.1: Powder X-ray diffraction of titanium hydrazide materials. From top to bottom: B100-H2, A100-H2, B100, and A100 samples.

The powder X-ray diffraction (PXRD) patterns for the titanium hydrazide materials heated at 100 ^{o}C are shown in Figure 5.1. All patterns were similar and no distinct reflection was detected, indicating a lack of long range order. The PXRD of the A100 material possesses a very broad peak from 3-5° 2-theta, possibly indicating a degree of mesoscopic order in this sample.

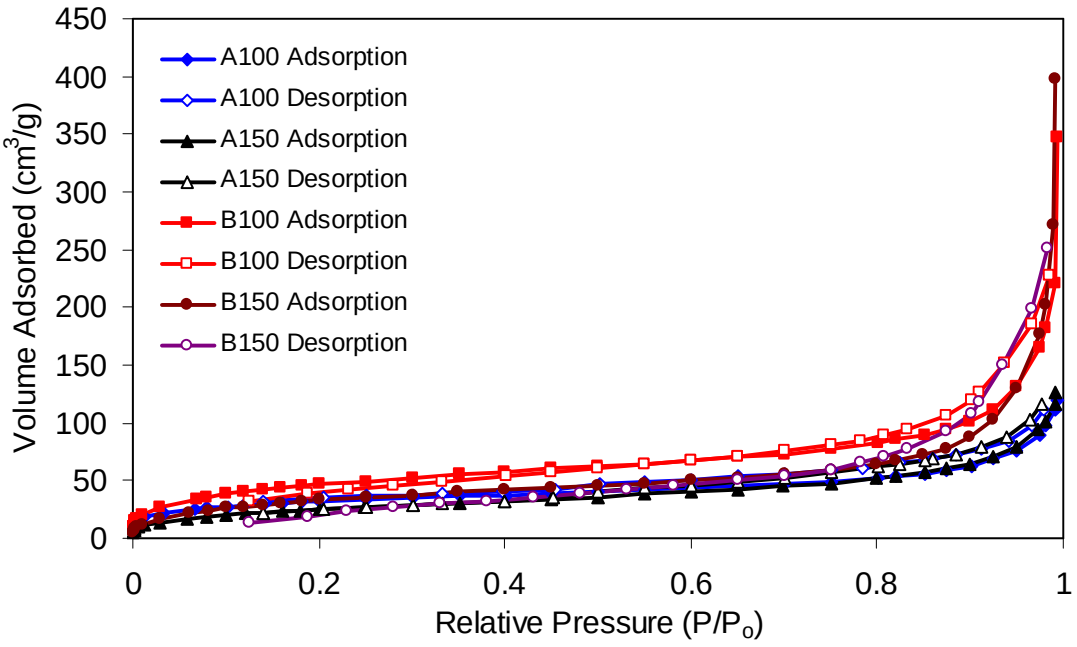

Figure 5.2a: Nitrogen adsorption – desorption isotherms of titanium hydrazide materials heated at 100 ^{o}C and 150 ^{o}C. Samples were measured on an ASAP-2010 instrument at 77 K.

Nitrogen adsorption isotherms recorded at 77 K are shown in Figure 5.2. These isotherms of the non-hydrogenated materials show a negligible amount of micro-porosity comprising only ca. 5% the total volume adsorbed, and can thus be classified as Type II. The specific surface areas of all materials decrease with increased drying temperature from 100 to 150 ^{o}C. For example, A100 possesses a Brunauer – Emmett – Teller (BET) surface area of 117 m^2/g, but after heating under vacuum to 150 ^{o}C to form A150, the surface area falls to 95 m^2/g, indicating a densification with loss of porosity. However, hydrogenation at 150 °C leads to a dramatic increase in BET surface areas, with the microporosity amounts increasing to ~30 %, and the adsorption isotherms on the cusp

between Type I and Type IV, suggesting that loss of bis trimethylsilyl methane from hydrogenation results in the creation of new porous pathways in the material.

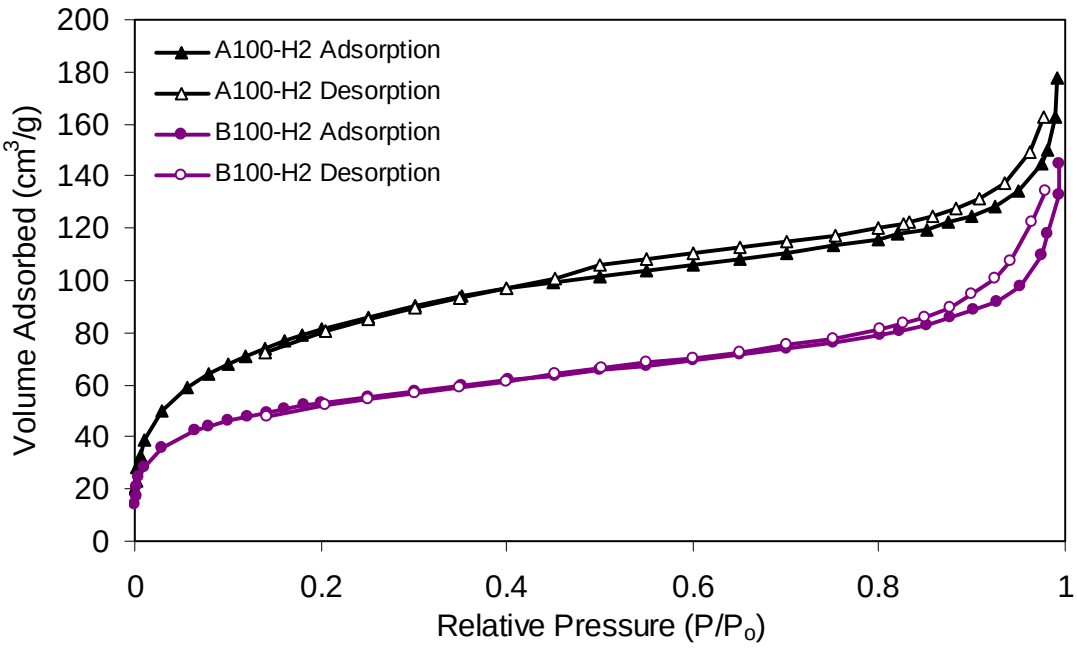

Figure 5.2b: Nitrogen adsorption – desorption isotherms of titanium hydrazide materials hydrogenated at 80 bar H_2, 150 ^{o}C, 2 h. Samples were measured on an ASAP-2010 instrument at 77 K.

The C, H, N elemental analysis data of the titanium hydrazide materials are shown in Table S5.1 (Supporting Information) and display the expected decreasing trend in carbon concentration from 20.18 wt% to 13.93 wt% with increasing hydrazine ratio for samples heated to 100 °C. A decrease in carbon concentrations with further heating and/or hydrogenation was also detected, although residual carbon was still remaining in all cases. The thermally driven loss of hydrocarbon was also observed in all previously published hydrazide materials, and can be accounted for by the thermally driven protolysis reaction between coordinated hydrazine and residual alkyl groups.[6] Taking the nitrogen adsorption results into account, hydrogenation appears to decrease hydrocarbon levels without collapse of the structure, a feature important for hydrogen diffusion kinetics to the active binding sites. Further heating to temperatures of 180 °C provided

further hydrocarbon elimination, however the N – N hydrazide bond was broken, and the structure of the materials collapsed as determined by the drop in BET surface area.

Figure 5.3 displays the thermo-gravimetric analysis plots of A100, B100, A100-H_2 and B100-H_2. After 30 minutes at 25 ^oC, the materials began to lose mass as the temperature gradually approached 400 – 550 ^oC. At the heating limit, sample A100-H_2 and B100-H_2 retained 92.24 % and 79.23 % of their original mass, respectively. Higher levels of weight loss were observed for A100 and B100, which retained 90.81 % and 72.68 %, respectively. The results for the Ti concentration based on these results are shown in Table S5.1 and are lower in all cases than expected on the basis of hypothetical formulas proposed in Table S5.2 for materials assuming complete loss of hydrocarbon.

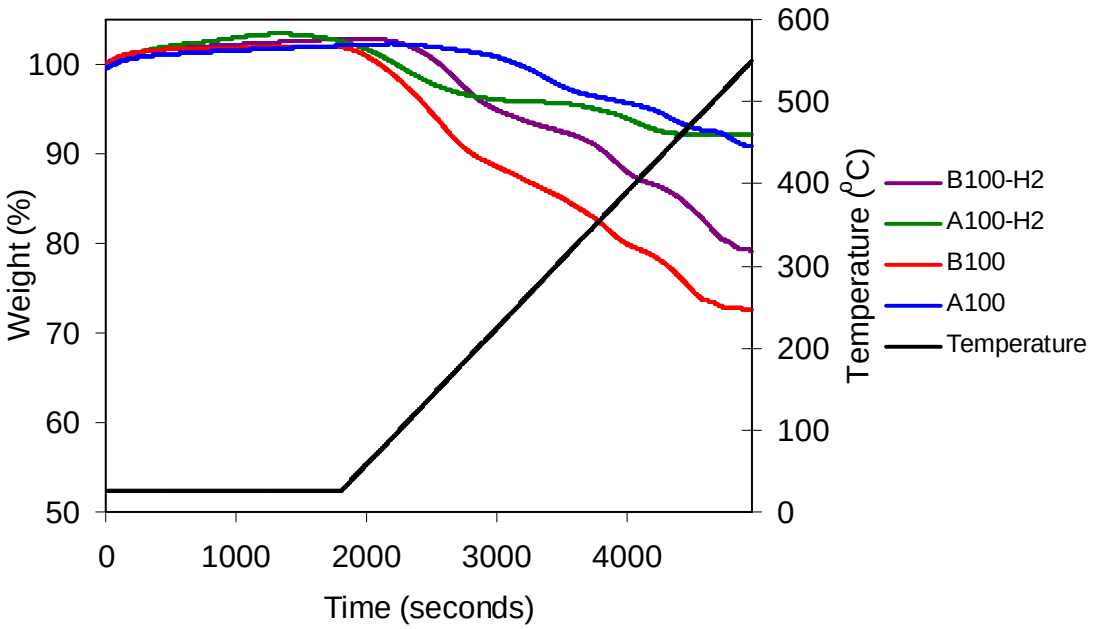

Figure 5.3: Thermo-gravimetric analysis results of titanium hydrazide materials.

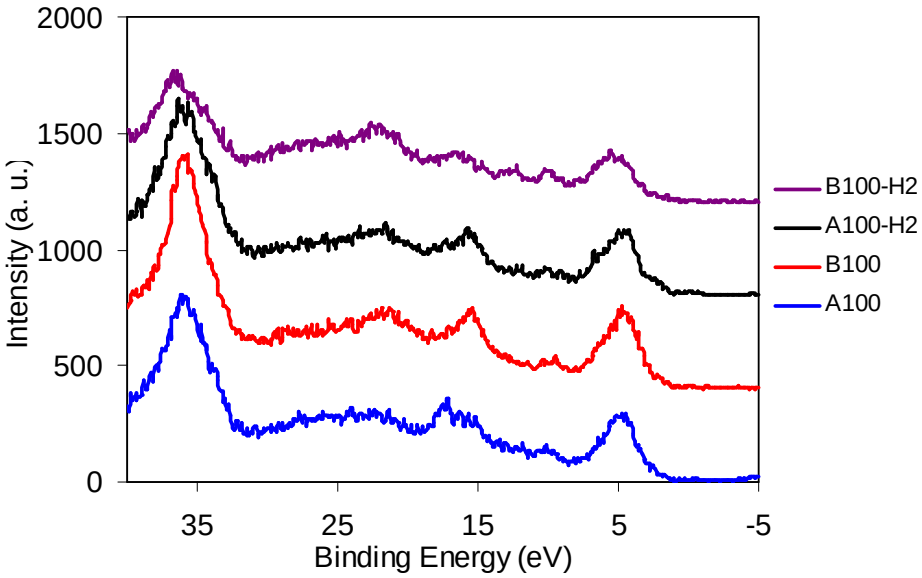

Figure 5.4: Valence region of XPS spectrum of titanium hydrazide materials heated to 100 °C. From top to bottom: B100-H2, A100-H2, B100, and then A100.

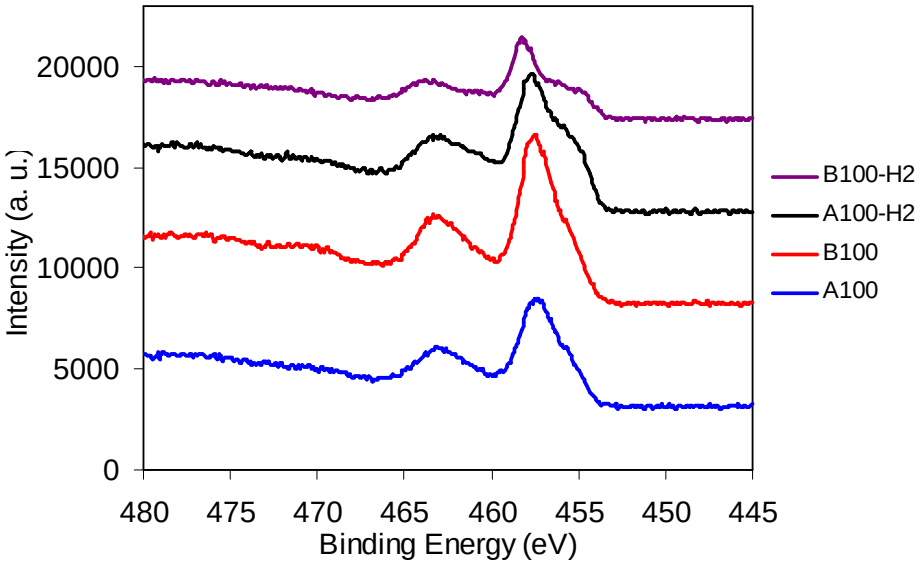

Figure 5.5: Titanium 2p1/2 and 2p3/2 region of XPS spectrum of titanium hydrazide materials heated to 100 °C and hydrogenated at 150 °C, 80 bar, 2 h. From top to bottom: B100-H2, A100-H2, B100, and then A100.

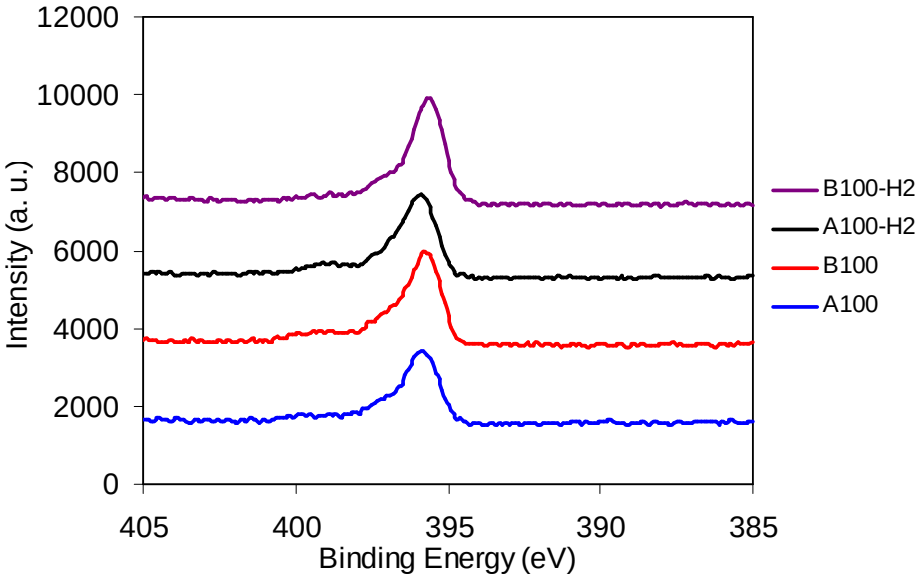

Figure 5.6: Nitrogen 1s region of XPS spectrum of titanium hydrazide materials heated to 100 °C and hydrogenated at 150 °C, 80 bar, 2 h. From top to bottom: B100-H2, A100-H2, B100, and then A100.

X-ray Photoelectron Spectroscopy (XPS) studies of the titanium hydrazides are shown in Figures 5.4 to 5.6. Emissions are observed close to the Fermi level, suggesting that these materials are semimetals or narrow bandgap semiconductors (Figure 5.4). Figure 5.5 shows the Ti 2p1/2 and 2p3/2 region. All spectra show two emissions corresponding to Ti (III) nitride,[14] one at 460.5 eV and 455.3 eV and a second at 457.3 eV and 463.0 eV (Figure S5.3a-d). Hydrogenation increases the emission at lower binding energy, and in the case of B100-H2, creates a new emission at 454.5 eV and 458.9 eV, also corresponding to Ti (III). In this case it is a TiH_3 species.[15] The lowering of binding energy with hydrogenation in these emissions is likely related to the removal of alkyl groups from the structure, although specific assignments in a non-stoichiometric amorphous material are often difficult. Figure 5.6 shows the the N 1s region of all materials. A major emission at 395.8 eV is observed in all materials with a minor second emission at 399.5 eV, the sum of which can be deconvoluted into 3 major peaks (fig. S5.4a-d). Because metal nitrides typically come at 396.4 eV[16] and protic nitrogen species such as ammonia appear at 398.8 eV,[17] the first simulated emission at 395.6 eV likely

corresponds to an N bound directly to two Ti centers. The second emission located at ~396.7 eV likely represents a H-N-Ti species, while the third emission at 399 eV can be assigned to a terminal -NH_2 species. The intensities of the 399 eV emissions are small, as expected for terminal groups in a polymer. The presence of NH in the material was confirmed by a broad IR band observed from 3400 – 3500 cm^{-1} (Figure S5.9d-i).

The excess storage isotherms of non-hydrogenated samples are shown in figure S5.5 – S5.7. These 77 K isotherms show an initial rise at low pressure consistent with a small amount of physisorption expected from the surface areas in the 95 – 176 m^2/g range, followed by a linear region up to 85 bar without saturation to 2.22 wt%. This overall shape was also observed on vanadium hydrazides[3b] and chromium hydrazides.[3c] The desorption isotherms of A100 and B100 are also shown in Figure S5.5 and show small hysteresis from 40 – 0 bar, with amounts of irreversibility equivalent to approximately one quarter of the total adsorption. If short vacuum[3] is applied after desorption, or if the sample is warmed to room temperature, the full adsorption capacity will be obtained in a successive measurement. At room temperature, all adsorption isotherms exhibit linear behavior without saturation at 85 bar. Higher hydrogen adsorption performance is expected at higher pressure and this linear behavior without saturation at low pressure is not typical of physisorption, suggesting a different mechanism of hydrogen storage is operative in these materials, which we have previously attributed to the involvement of the Kubas interaction.

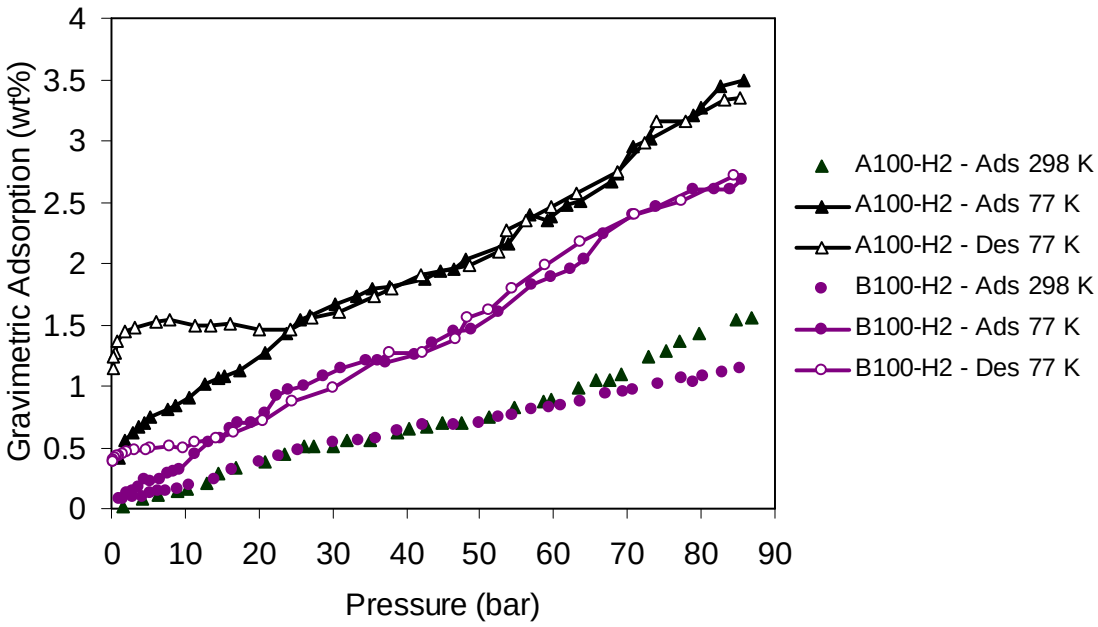

Figure 5.7: Gravimetric hydrogen adsorption – desorption isotherms of hydrogenated titanium hydrazide materials synthesized with a Ti:hydrazine ratio of 1:1 and 1:1.5.

Figure 5.7 depicts the hydrogen adsorption of hydrogenated materials and table 5.1 summarizes the hydrogen adsorption data of synthetic samples. The gravimetric adsorption of the A100-H_2 sample is 1.55 wt. % at 85 bar and 298 K and its true volumetric adsorption (see experimental for full explanation) is 21.6 kg H_2/m^3, slightly lower than the true volumetric adsorption of the best vanadium hydrazide under these same conditions (23.2 kg H_2/m^3), however this is attributable to the higher density of the V material, which possesses a lower gravimetric storage under these conditions (298 K and 85 bar). Considering H_2 as ideal gas, a 1 m^3 cylinder could store 6.86 kg H_2 at 85 bar and 298 K; a volumetric adsorption of 21.6 kg/m^3 is 3.15 times higher. At 77 K and 85 bar, the A100-H_2 sample adsorbs 3.49 wt. %, corresponding to a true volumetric adsorption of 48.7 kg H_2/m^3. Figure S5.8 shows the excess storage isotherms of a pellet of A100-H_2 compressed at 500 psi to eliminate excess void space. At 85 bar the pellet adsorbs 1.82 wt% and 3.87 wt % at 298 K and 77 K, respectively. The bulk density measured for this sample of 1.0130 g/cm^3 provides excess volumetric storage capacities of 18.44 kg H_2/m^3 at 298 K, and 39.20 kg H_2/m^3 at 77 K. The excess volumetric

performance of 39.20 kg H_2/m^3 is higher than that of MOF-177, which possesses an excess volumetric storage of 32.0 kg H_2/m^3 at 77 K.[18] From a comparison of the gravimetric adsorption data at 298 K and 77 K, the retentions of excess adsorption capacities can be calculated in the range from 44% to 64%. This is comparable to the values obtained for V hydrazides[3b] and much higher than that of MOF-5 and carbon AX-21, which retain 5.5% and 13%, respectively. When comparing the loss in gravimetric adsorption between 77 K and 298 K to the surface areas of ca. 310 m^2/g, this loss can be attributed to the physisorption component, which would be diminished with increasing temperature to ambient conditions, while the adsorption amount at room temperature could be attributed to the Kubas interaction, which remains constant from 77 K to 298 K.

These results establish that A100-H_2, prepared at a mole ratio of 1:1 and heating temperature of 100 ^oC, followed by hydrogenation at 150 ^oC, 80 bar H_2 for 2 hours provides the best synthetic conditions for generation of titanium hydrazide gels for optimized hydrogen storage.

Calculations based on the basis of gravimetric adsorption and the titanium content in each sample result in an average number of hydrogen molecules per titanium atom (Table 5.2) ranging from 0.87 – 1.51 H_2/Ti at 77 K and 0.54 – 0.67 H_2/Ti at 298 K. This compares to 1.8 H_2/Ti measured for benzyl Ti fragments on mesoporous silica[5b] and 1.75 and 0.57 H_2/M for Cr[6c] and V[6b] hydrazides, respectively. The reason for the lower than expected number of active binding sites (ca. 5H_2/Ti) is possibly due to inhomogeneity in the hydrazide gel caused by the steric hindrance of the remaining alkyl ligand, making some centers inaccessible. While computations show that 9.9 wt% H_2 can bind to a Ti (III) hydrazide dihydride, this is based on 4 H_2 per Ti on a tetrahedral Ti center with two N ligands and two H ligands.[8] For a tetrahedral Ti (III) hydrazide with 4 N ligands, the maximum number that could bind was 2 H_2/Ti. We have also observed up to 4 H_2 per Ti on benzyl Ti fragments on silica at 77 K and 85 bar.[5b] Other theoretical computations have shown that titanium decorated nanotubes can adsorb 8 wt% hydrogen,[4] and 12 wt% for Ti decorated polymers,[19] In both case, each Ti atom was proposed to hold up to 5 hydrogen molecules in a Kubas type interaction.

Table 5.1: Summary of excess storage results on titanium hydrazide materials and carbon AX-21. Data recorded at 85 bar.

Material	BET Surface Area (m^2/g)	Skeletal Density (g/cm^3)	Gravimetric Adsorption (wt%)	True Volumetric Adsorption (kg/m^3)	Retention (%)
A100	117	1.3228	1.99 (at 77 K) 1.28 (at 298 K)	26.3 (at 77 K) 16.9 (at 298 K)	64
A150	95	1.4045	2.22 (at 77 K) 1.24 (at 298 K)	31.2 (at 77 K) 17.4 (at 298 K)	56
B100	176	1.4856	2.02 (at 77 K) 0.99 (at 298 K)	30.0 (at 77 K) 14.7 (at 298 K)	49
B150	129	1.6827	1.79 (at 77 K) 1.11 (at 298 K)	30.1 (at 77 K) 18.73 (at 298 K)	62
A100-H2	301	1.3944	3.49 (at 77 K) 1.55 (at 298 K)	48.7 (at 77K) 21.6 (at 298 K)	44
B100-H2	190	1.7914	2.68 (at 77 K) 1.15 (at 298 K)	48.0 (at 77 K) 20.6 (at 298 K)	43
AX-21	3225	2.1030	4.2 (at 77 K, 65 bar) 0.55 (at 298 K)	14 (at 77 K, 65 bar) -	13
MOF-5	3534		5.10 (at 77 K) 0.28 (at 298 K)		5.5

The isosteric heats of hydrogen adsorption were calculated by fitting the adsorption isotherms at 77 K and 87 K into the Clausius – Clapeyron equation. The data for all six materials are shown in Figure 5.8. The data for carbon AX-21 measured under the same conditions and calculated using the same method is shown in Figure S5.1 and S5.2. This isosteric heat of adsorption rise from a low of 3 kJ/mol H_2 for A100 up to a high of 28 kJ/mol H_2 for A150, contrasting strongly to the behavior of AX-21, which demonstrate decreasing enthalpies from 6 kJ/mol H_2 down to 3.3 kJ/mol H_2, typical of physisorption. While replacement of an alkyl group with a hydride usually leads to an increase in binding enthalpies for Kubas H_2 ligands,[8] there seemed to be no regular trend relating the

enthalpies to the synthetic method or hydrogen storage performance. However the average value of the titanium hydrazides approach and the ideal range of 20 – 30 kJ/mol H_2, believed to be the ideal heat of hydrogen adsorption of suitable room temperature hydrogen storage materials.[5] The rising enthalpies with surface coverage on materials containing low valent Ti have been observed elsewhere, and were rationalized by computations using the Kubas interaction as a model.[5,6,8] Rising enthalpies illustrate the advantage of multi-molecule adsorption on one center as the second H_2 will be adsorbed more easily than the first H_2. Computations have shown that this is because the positive charge of the adsorption centers decrease with subsequent H_2 ligation, leading to improvement of the π-back-bonding in to the H-H σ^* orbital, which in turn strengthens the M-H_2 interaction.[8]

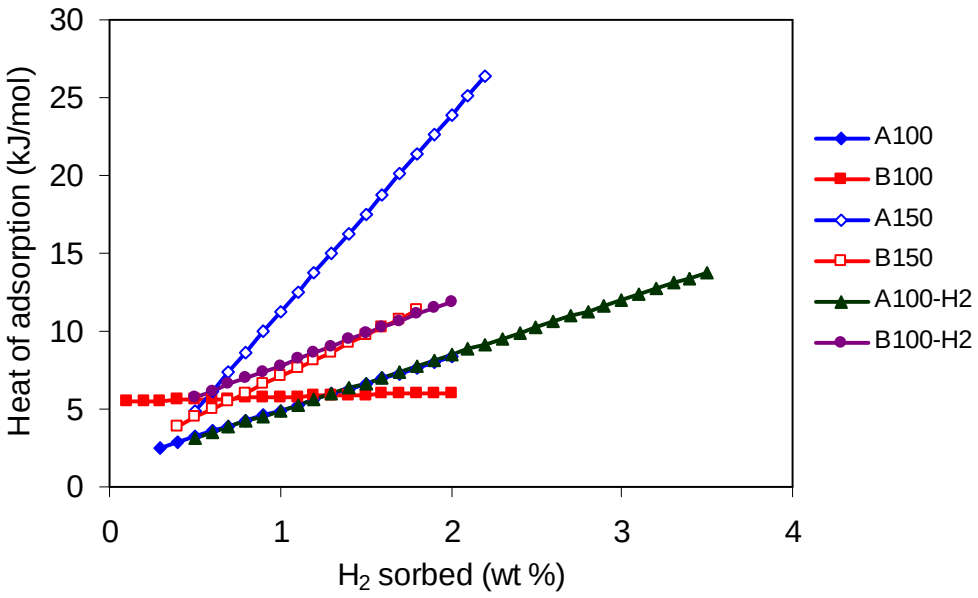

Figure 5.8: Heat of hydrogen adsorption on titanium hydrazide materials.

The mechanism of H_2 binding was explored by ESR and Raman using D_2/H_2 experiments. While we were unable to observe any perturbations in the spectra on treatment with H_2 or D_2, this may be due to the small amounts absorbed at 1 bar pressure and 298 K. Previous work on V[6b] and Mn hydrazides (chapter 4) showed signal changes in the ESR for the metal on exposure to H_2, while Raman studies revealed the expected

bathochromic shift for Kubas bound H_2 and D_2 for Cr hydrazides[6c] and V oxamide polymers.[6d] Since the materials all displayed the unusual rising enthalpies, it appears that the observance of this trend in the present study strongly implies the role of the Kubas interaction in storage at higher pressure than 1 bar.

Table 5.2: Average number H_2 adsorbed per Ti site at 85 bar using TGA data

Sample	Number of H_2/Ti at 77 K	Number of H_2/Ti at 298 K
A100	0.87	0.56
B100	1.11	0.54
A100-H_2	1.51	0.67
B100-H_2	1.35	0.58

5.4 Conclusions

Titanium hydrazide materials were synthesized from tris{bis(trimethylsilyl)methyl} titanium and anhydrous hydrazine and optimized for Kubas-type hydrogen storage, exploiting the interaction of low valent Ti with intact hydrogen molecules. Hydrogen storage capabilities were demonstrated at 298 K up to 18.44 kg/m^3 and 1.82 wt % at 85 bar with hydrogen gas pressure as a toggle switch to load or release hydrogen. The samples showed enthalpies that rise with surface coverage. Once further optimized closer to the predicted 9.9 wt% H_2 storage performance, these materials could potentially be used in the association with traditional compressed gas technology with the advantage of more than three fold enhancement in the total storage.

5.5 References

(1) a) Schlapbach, L.; Zuettel, A. *Nature*, **2001**, 414, 353; b) Seayad, A. M; Antonelli, D.M. *Adv. Mater.* **2004**, 16, 765; c) Yaghi, O. M.; O'Keeffe, M.; Ockwig, N. W.; Chae, H. K.; Eddaoudi, M.; Kim, J. *Nature* **2003**, 423, 705; d) Mark Thomas, K. *Dalton Trans*., **2009**, 1487; e) Wang, L.; Yang, R. T. *Energy Environ. Sci.*, **2008**, 1, 268; f) Lochan, R. C.; Head-Gordon, M.; *Phys. Chem. Chem. Phys*., **2006**, 8, 1357; g) Eberle, U.; Felderhoff, M.; Schueth, F. *Angew. Chem., Int. Ed*., **2009**, 48, 2; h) Cameron, J. M.; Hughes, R. W.;

Zhao, Y.; Gregory, D. H. *Chem. Soc. Rev*. **2011**, 4099; i) Hamilton, C. W.; Baker, R. T.; Staubitz, A.; Manners, I. *Chem. Soc. Rev*. **2009**, 279.

(2) a) Kubas, G. J.; Ryan, R. R.; Swanson, B. I.; Vergamini, P. J.; Wasserman, H. J. *J. Am. Chem. Soc*. **1984**, 106, 451; b) G. J. Kubas, *Chem. Rev*. **2007**, 107, 4152; b) Heinekey, D. M.; Lledós, A.; Lluch, J. M. *Chem. Soc. Rev*. **2004**, 33, 175; c) Hoang, T. K. A.; Antonelli, D. M. *Adv. Mater*. **2009**, 21, 1787.

(3) Zhao, Y.; Kim, Y.; Dillon, A. C.; Heben, M. J.; Zhang, S. B. *Phys. Rev. Lett*. **2005**, 94, 155504.

(4) a) Yildirim, T.; Ciraci, S. *Phys. Rev. Lett*. **2005**, 175501; b) Íñiguez, J.; Yildirim, T.; Udovic, T. J., Sulic, M.; Jensen, C. M. Phys. Rev. B **2004**, 060101-1.

(5) a) Hamaed, A.; Trudeau, M.; Antonelli, D. M. *J. Am. Chem. Soc*. **2008**, 130, 6992; b) Hamaed, A.; Hoang, T. K. A.; Trudeau, M.; Antonelli, D. M. *J. Organomet. Chem*. **2009**, 694, 2793; c) Hamaed, A.; Mai, H, V.; Hoang, T. K. A.; Trudeau, M.; Antonelli, D. M. *J. Phys. Chem. C* **2010**, 114, 8651; d) Hoang, T. K. A.; Hamaed, A.; Trudeau, M.; Antonelli, D. M. *J. Phys. Chem. C* **2009**, 113, 17240.

(6) a) Mai, H. V.; Hoang, T. K. A.; Hamaed, A.; Trudeau, M.; Antonelli, D. M. *Chem. Commun*. **2010**, 46, 3206; b) Hoang, T. K. A.; Webb, I. M.; Mai, H. V.; Hamaed, A.; Walsby, C. J.; Trudeau, M.; Antonelli, D. M. *J. Am. Chem. Soc*. **2010**, 132, 11792; c) Hamaed, A.; Hoang, T. K. A.; Moula, G.; Aroca, R.; Trudeau, M. L.; Antonelli, D. M. *J. Am. Chem. Soc*. **2011**, *133*, 15434; d) Hoang, T. K. A.; Hamaed, A.; Moula, G.; Aroca, R.; Trudeau, M. L.; Antonelli, D. M. *J. Am. Chem. Soc*. **2011**, 133, 4955.

(7) Cha, M. -H.; Nguyen, M. C.; Choi, K.; Kim, M.; Ihm, J. *Nano* **2011**, 6, 225.

(8) Skipper, C. V. J.; Hoang, T. K. A.; Antonelli, D. M.; Kaltsoyannis, N. *Chem. Eur. J*. **2012**, accepted.

(9) Maksimov, N. G.; Nesterov, G. A.; Zakharov, V. A.; Stchastnev, P.V.; Anufrienko, V. F.; Yermakov, Y. I. *J. Mol. Catal*. **1978**, 4, 167.

(10) Jacob, K.; Thiele, K. H.; Dimitrov, V. *Z. Anorg. Allg. Chem*. **1978**, 447, 136

(11) Baker, B. K.; Lappert, M. F.; Howard, J. A. K. *J. Chem. Soc. Dalton* **1978**, 734.

(12) a) Fetter, N. R.; Bartocha, B. K. W. (U.S. Navy). U.S. Patent 3321503, April 3, 1962/May 23, 1967; Chem. Abstr. **1967**, *67*, 55828; b) Schmidt, E. W. Hydrazine and its Derivatives. Preparation, Properties, Application; John Wiley & Sons, Inc.: New York, 2001; pp 99 – 105.

(13) a) Furukawa, H.; Miller, M. A.; Yaghi, O. *J. Mater. Chem*. **2007**, 17, 3197; b) Hu, X.; Skadtchenko, B. O.; Trudeau, M.; Antonelli, D. M. *J. Am. Chem. Soc.* **2006**, 128, 11740; c) Hu, X.; Trudeau, M.; Antonelli, D. M. *Chem. Mater*. **2007**, 19, 1388.

(14) Badrinarayanan, S.; Sinha, S.; Mandalae, A. B. *J. Electron Spectrosc. Relat. Phenom*. **1989** 49, 303 and reference there in.

(15) Lisowski, W.; van den Berg, A. H. J.; Leonard, D.; Mathieu, H. J. *Surf. Interface Anal*. 2000, 29, 292.

(16) Nishimura, O.; Yabe, K.; Iwaki, M.; *J. Electron Spectrosc. Relat. Phenom*. **1989** 49, 335.

(17) Larkins, F. P.; Lubenfeld, A. *J. Electron Spectrosc. Relat. Phenom*. **1979**, 15, 137.

(18) Wong-Foy, A. G.; Matzger, A. J.; Yaghi, O. M. *J. Am. Chem. Soc.* **2006**, 128, 3494.

(19) a) Lee, H.; Choi, W. I.; Ihm, J. *Phys. Rev. Lett*. **2006**, 97, 056104. b) Lee, H.; Choi, W. I.; Nguyen, M. C.; Cha, M. H.; Moon, E.; Ihm, J. *Phys. Rev. B* **2007**, 76, 195110.

Supplemental Information for Chapter 5 – Titanium Hydrazide Gels for Kubas Type Hydrogen Storage

Table S5.1: Elemental analysis results of synthetic titanium hydrazide samples.

Material	Carbon (%)	Hydrogen (%)	Nitrogen (%)	Titanium (%)[(a)]
A100	20.18	4.28	12.97	54.42
A150	6.18	1.34	10.41	N/A
B100	13.93	3.27	15.01	43.56
B150	5.54	0.87	7.45	N/A
A100-H_2	9.83	2.47	12.69	55.28
B100-H_2	12.92	3.20	14.85	47.48

(a): From thermo-gravimetric analysis.

Table S5.2: Proposed unit formula of synthetic materials assuming complete loss of hydrocarbon.

Material	Proposed chemical formula	Titanium (%)	Hydrogen (%)	Nitrogen (%)
A100	TiN_2H_2	61.45	2.59	35.96
B100	TiN_3H_4	50.97	4.29	44.74
A100-H_2	TiN_2H_2	61.45	2.59	35.96
B100-H2	TiN_3H_4	50.97	4.29	44.74

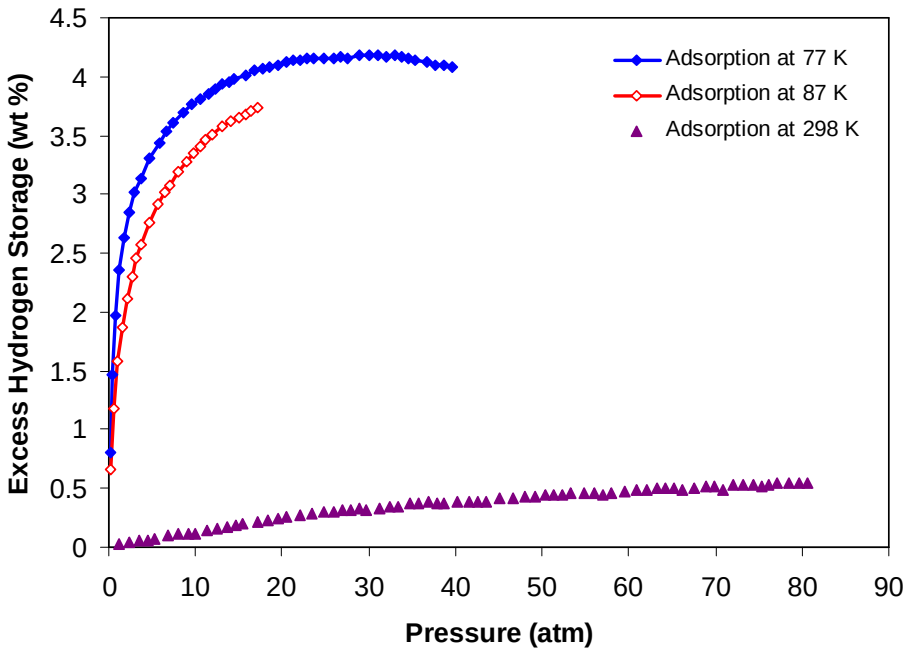

Figure S5.1: Hydrogen excess storage at 77 K, 87 K, and 298 K of carbon AX-21 up to 80 bar recorded on Advanced Materials PCI.

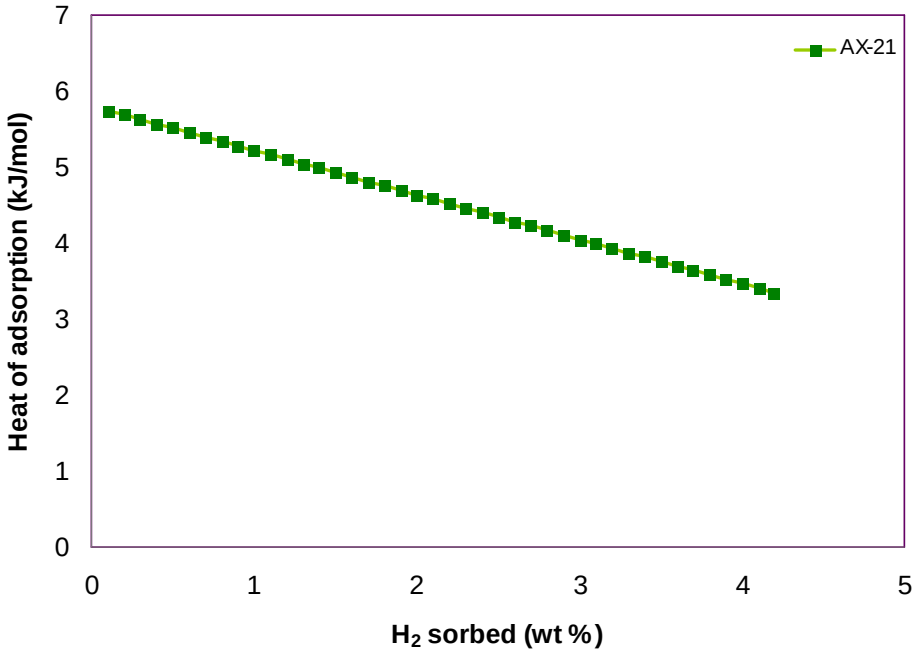

Figure S5.2: Heat of hydrogen adsorption of carbon AX-21 calculated from data in S1.

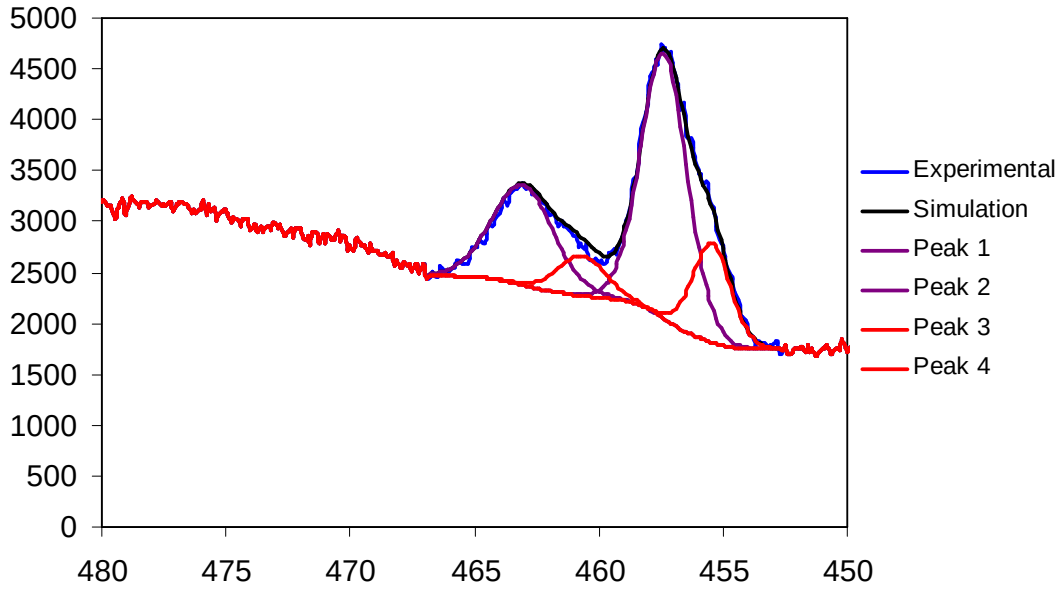

Figure S5.3a: Peak fitting of titanium 2p1/2 and 2p3/2 emissions in the XPS spectrum of A100 sample.

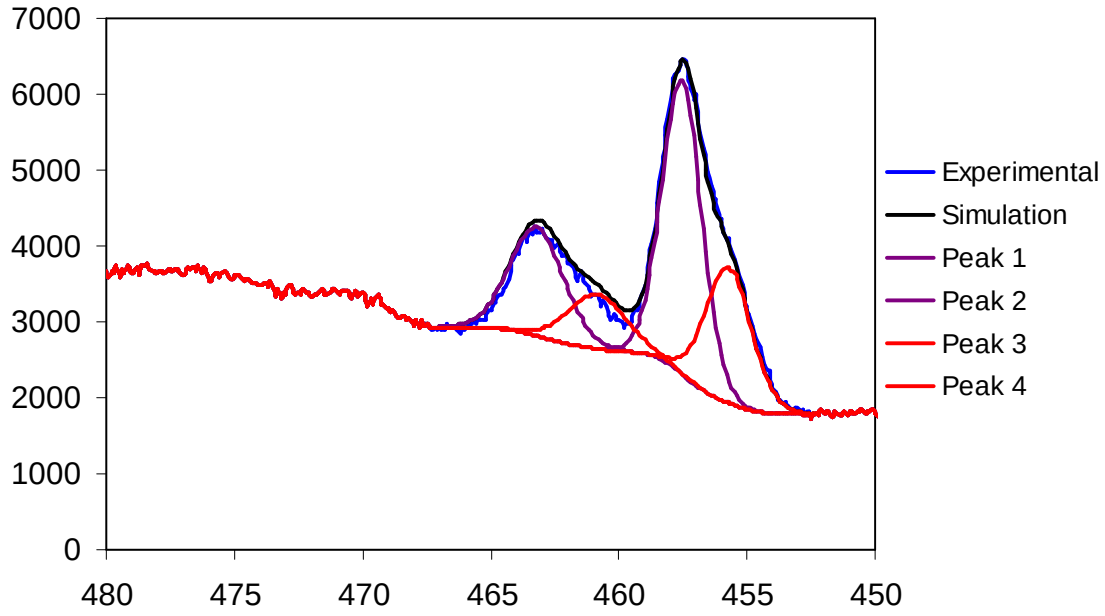

Figure S5.3b: Peak fitting of titanium 2p1/2 and 2p3/2 emissions in the XPS spectrum of B100 sample.

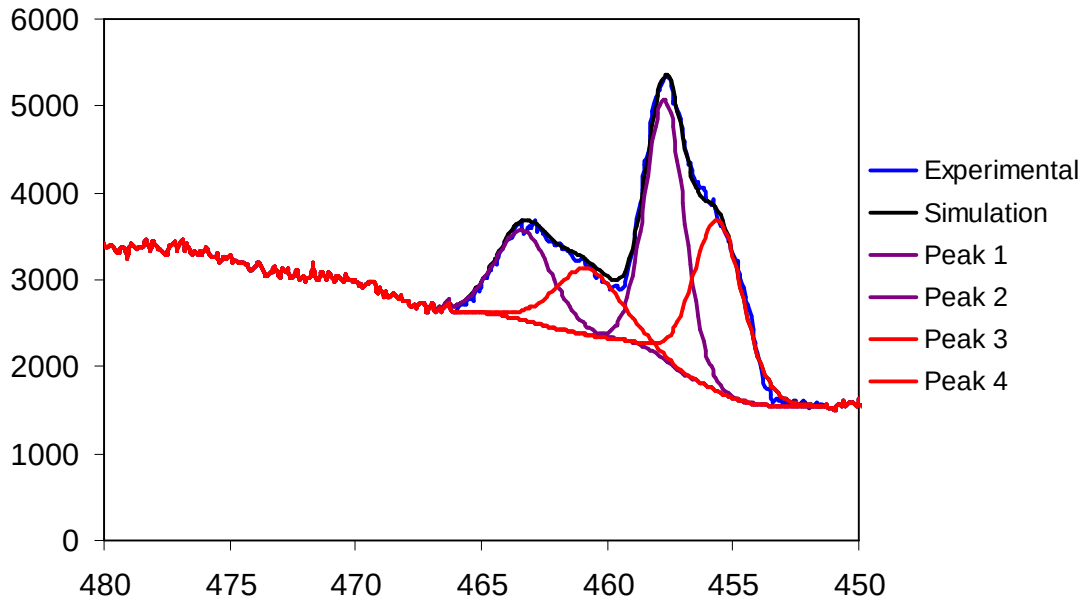

Figure S5.3c: Peak fitting of titanium 2p1/2 and 2p3/2 emissions in the XPS spectrum of A100-H_2 sample.

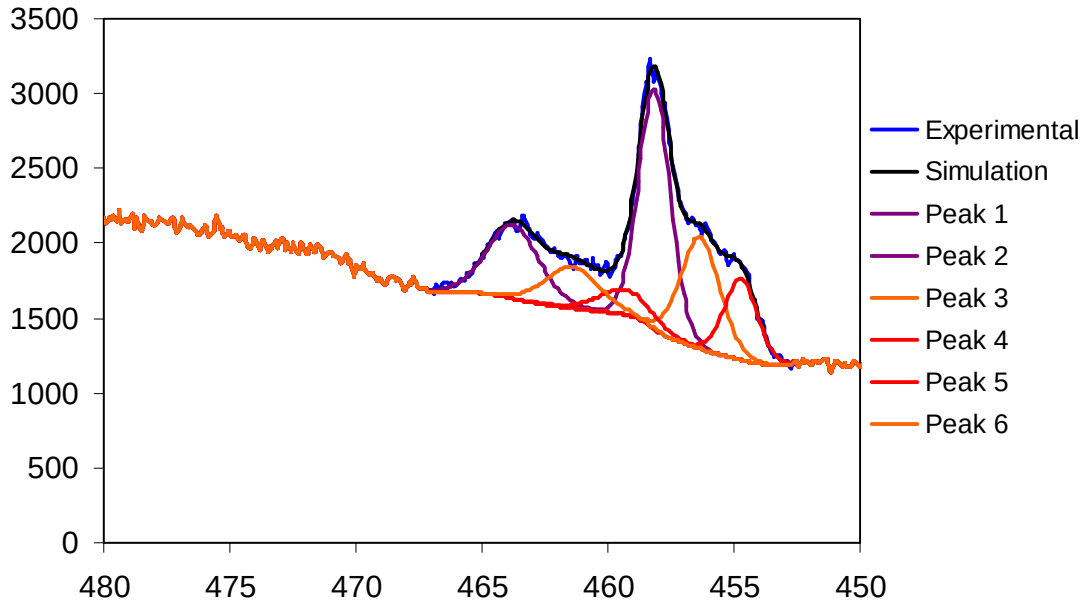

Figure S5.3d: Peak fitting of titanium 2p1/2 and 2p3/2 emissions in the XPS spectrum of B100-H_2 sample.

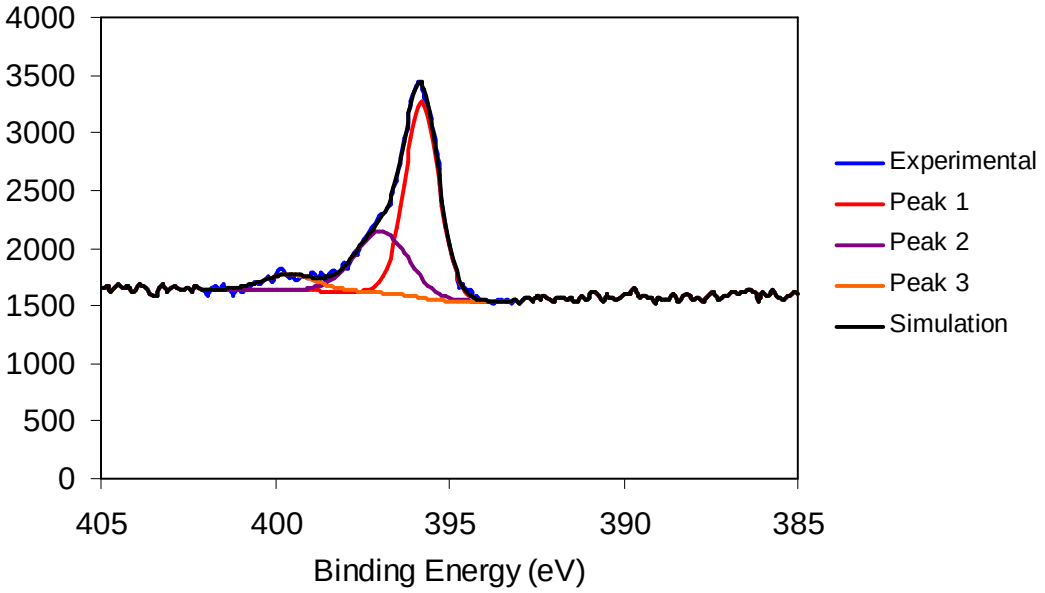

Figure S5.4a: Peak fitting of N 1S region of XPS Spectrum of A100 sample.

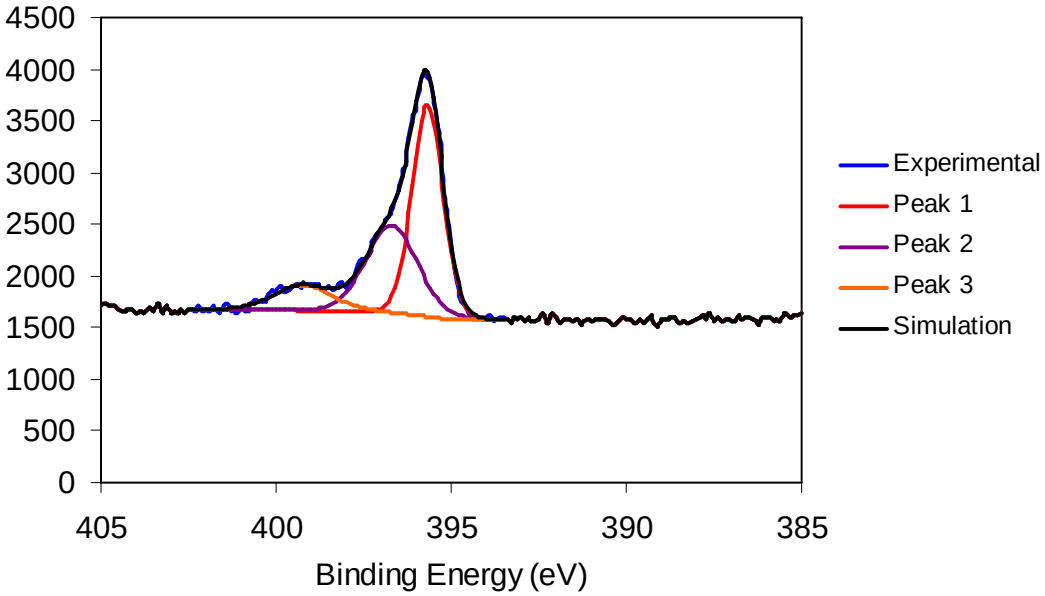

Figure S5.4b: Peak fitting of N 1S region of XPS Spectrum of B100 sample.

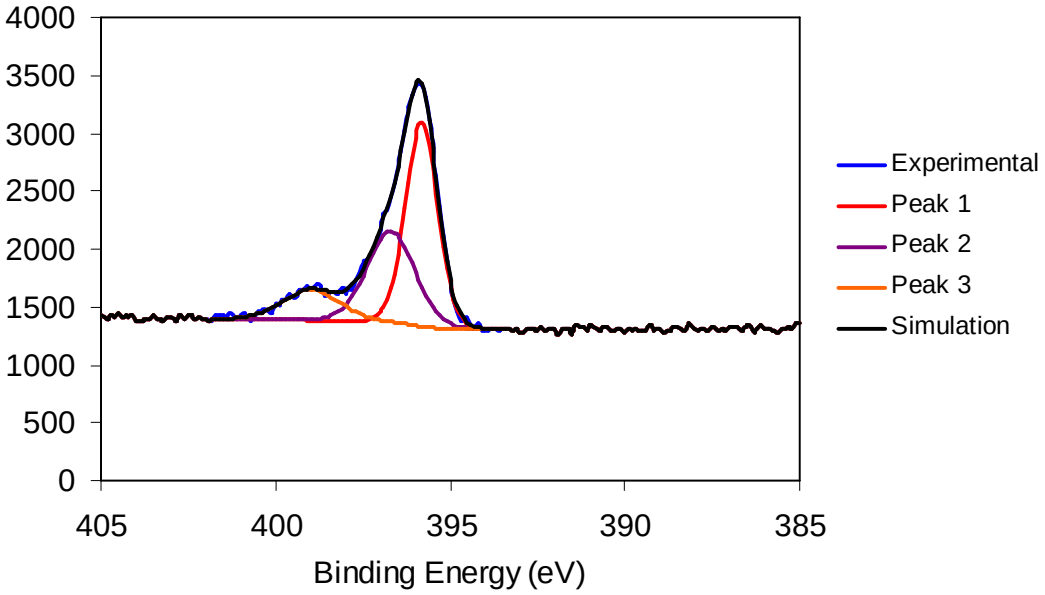

Figure S5.4c: Peak fitting of N 1S region of XPS Spectrum of A100-H_2 sample.

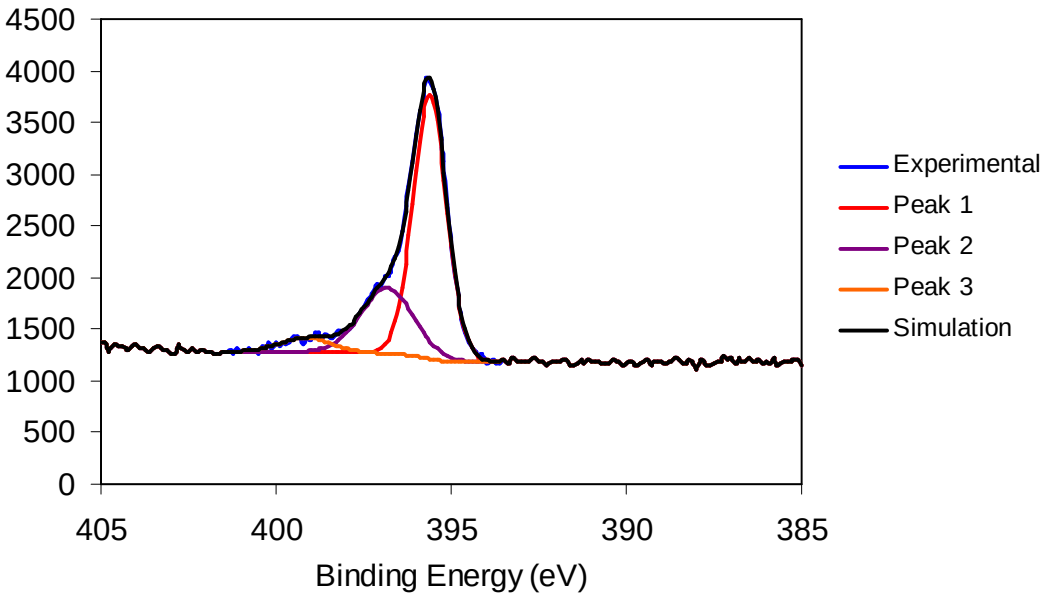

Figure S5.4d: Peak fitting of N 1S region of XPS Spectrum of B100-H_2 sample.

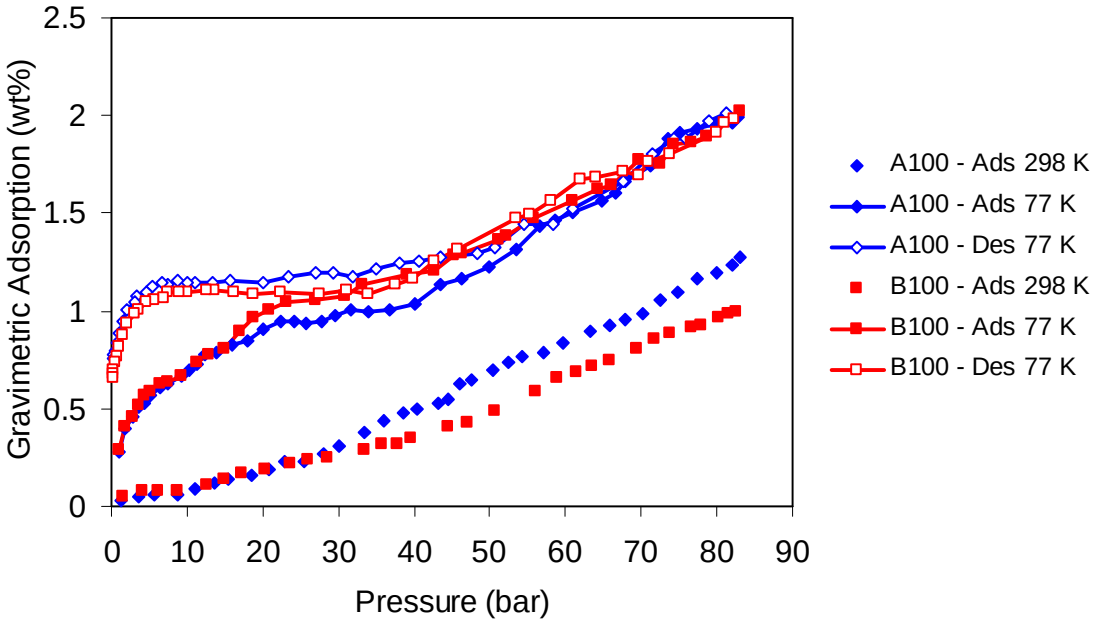

Figure S5.5: Excess storage isotherms of A100 and B100 materials. Desorption of 298 K isotherms omitted for clarity.

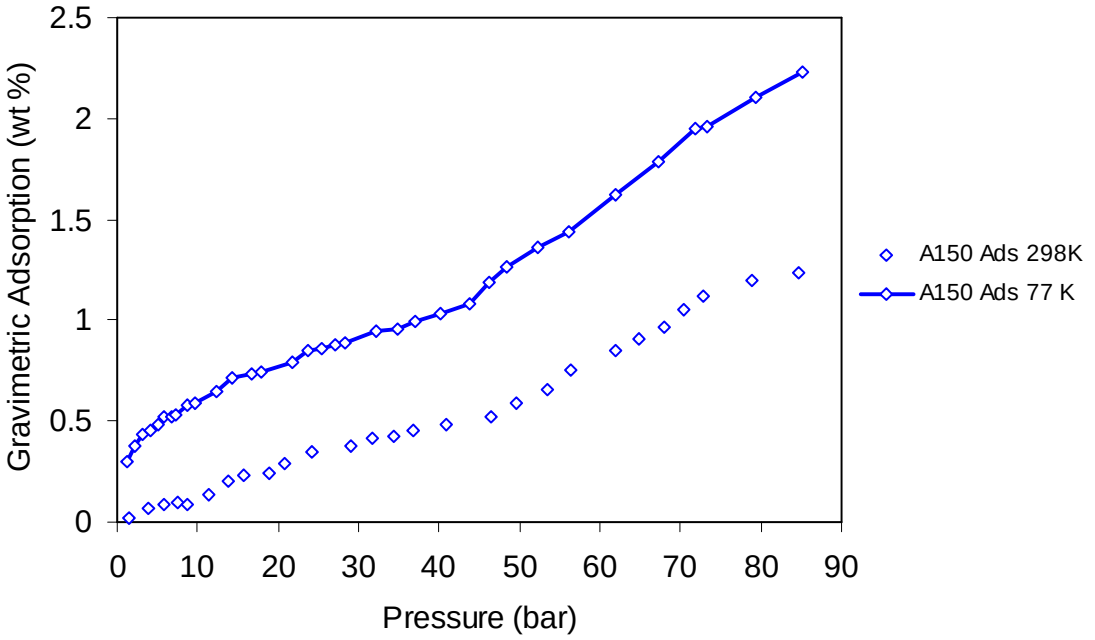

Figure S5.6: Excess storage isotherms of A150 materials.

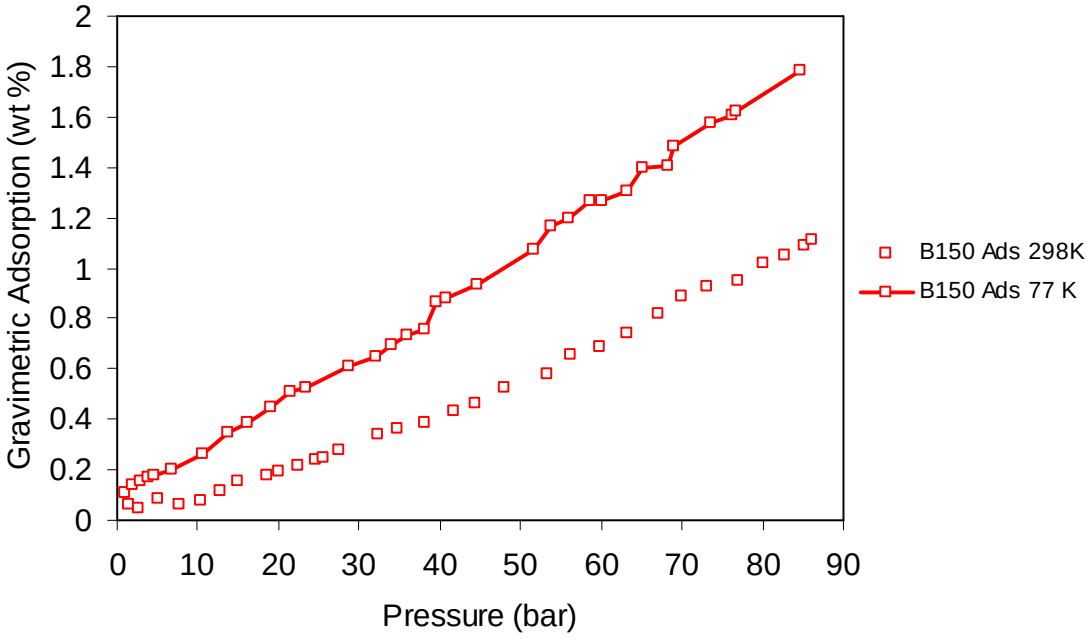

Figure S5.7: Excess storage isotherms of B150 materials.

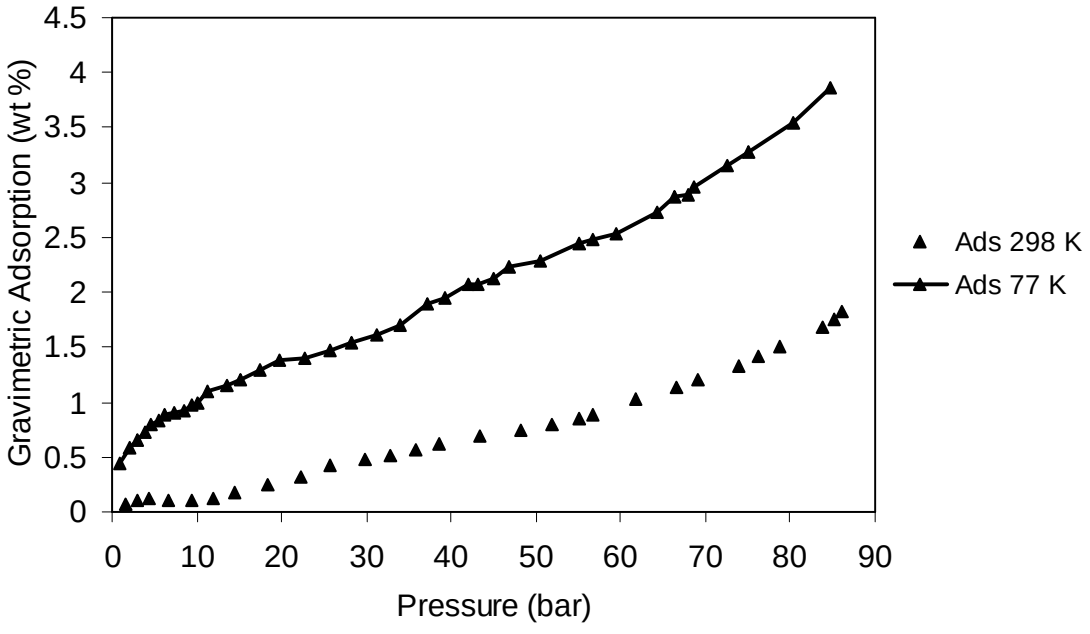

Figure S5.8: Excess storage isotherms at 298 K and 77 K of a pellet of the A100-H_2 material compressed at 500 Psi.

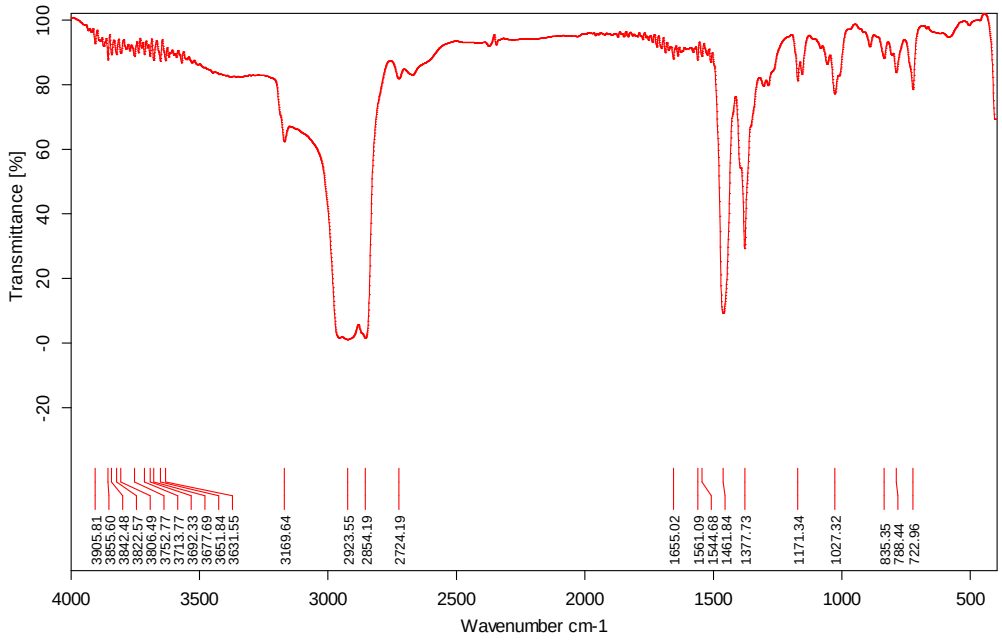

Figure 5.9a: Infrared spectrum of $TiCl_3.0.67\{N(C_2H_5)_3\}$

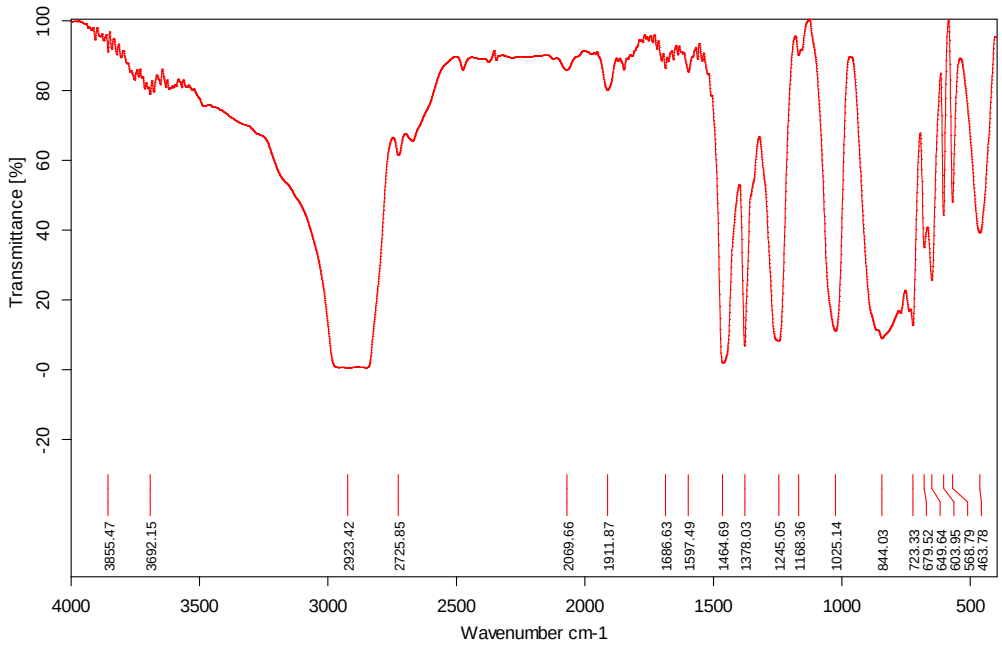

Figure S5.9b: Infrared spectrum of $LiCH(SiMe_3)_2$ in Nujol.

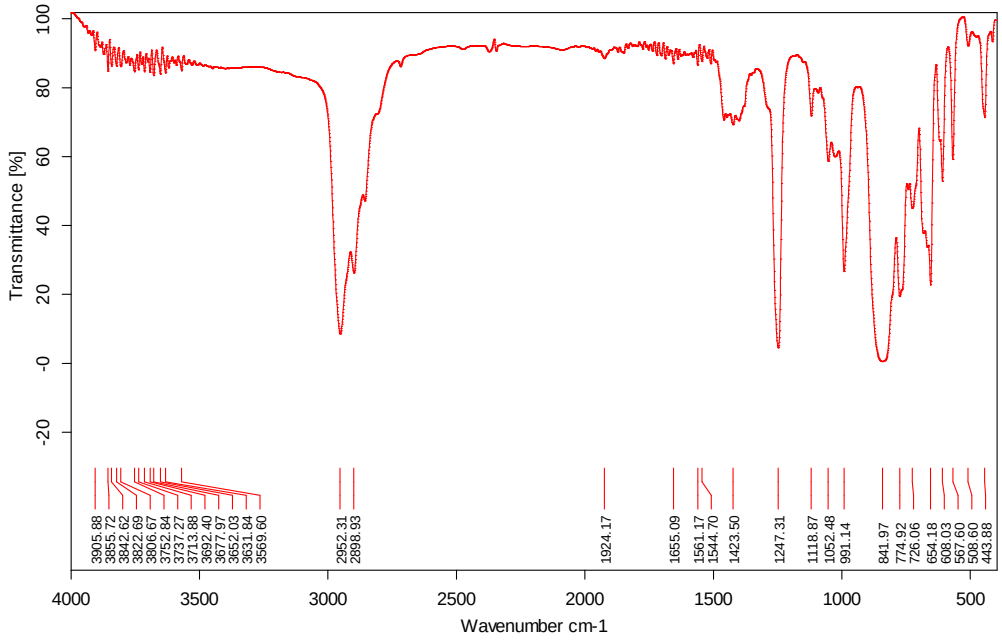

Figure S5.9c: Infrared spectrum of Ti{(CH(SiMe$_3$)$_2$}$_3$ in Nujol.

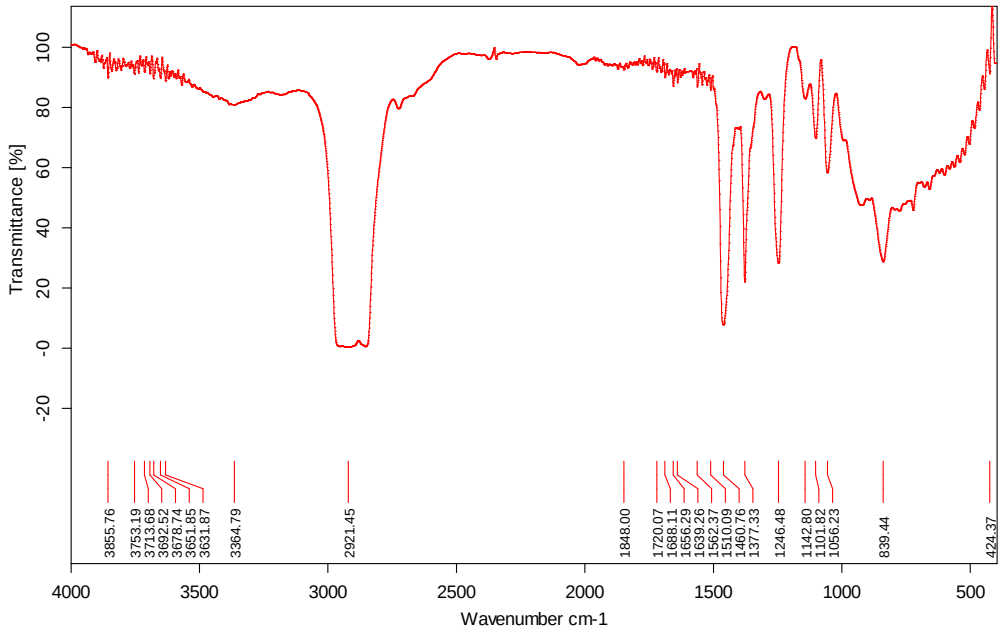

Figure S5.9d: Infrared spectrum of A100 in Nujol.

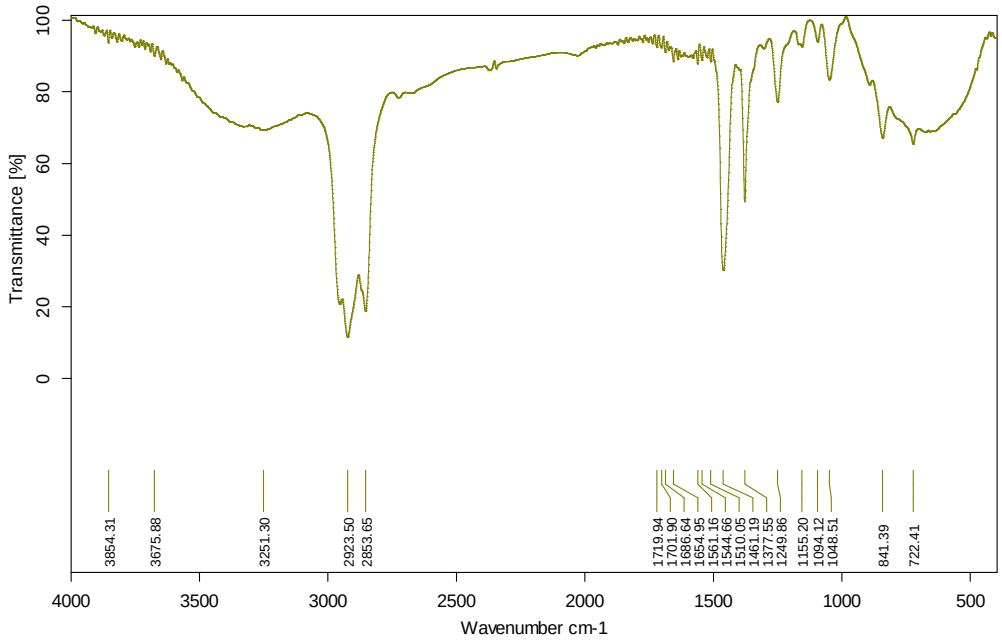

Figure S5.9e: Infrared spectrum of A150 in Nujol.

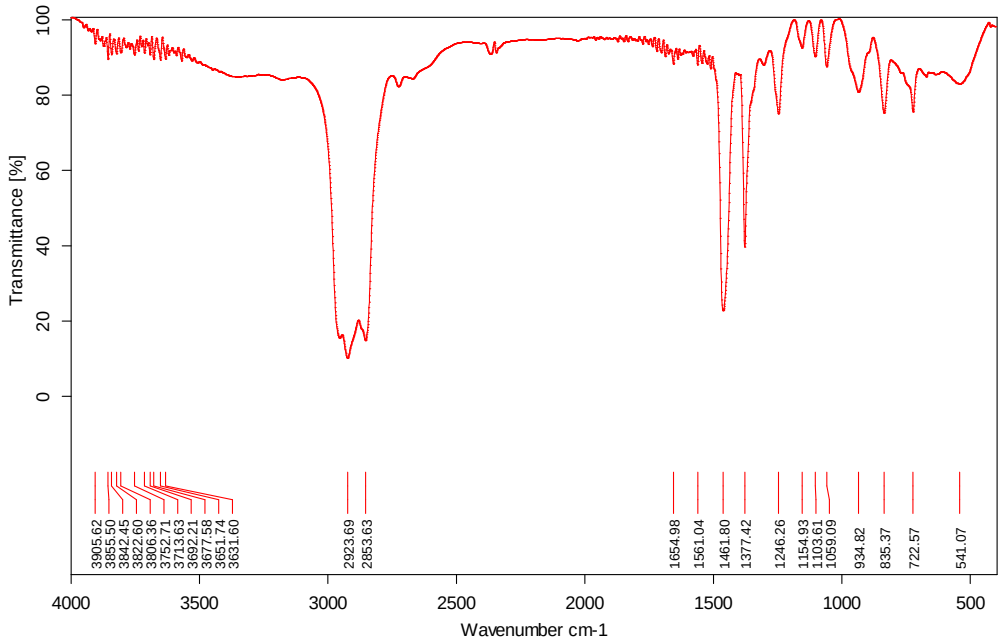

Figure S5.9f: Infrared spectrum of B100 in Nujol.

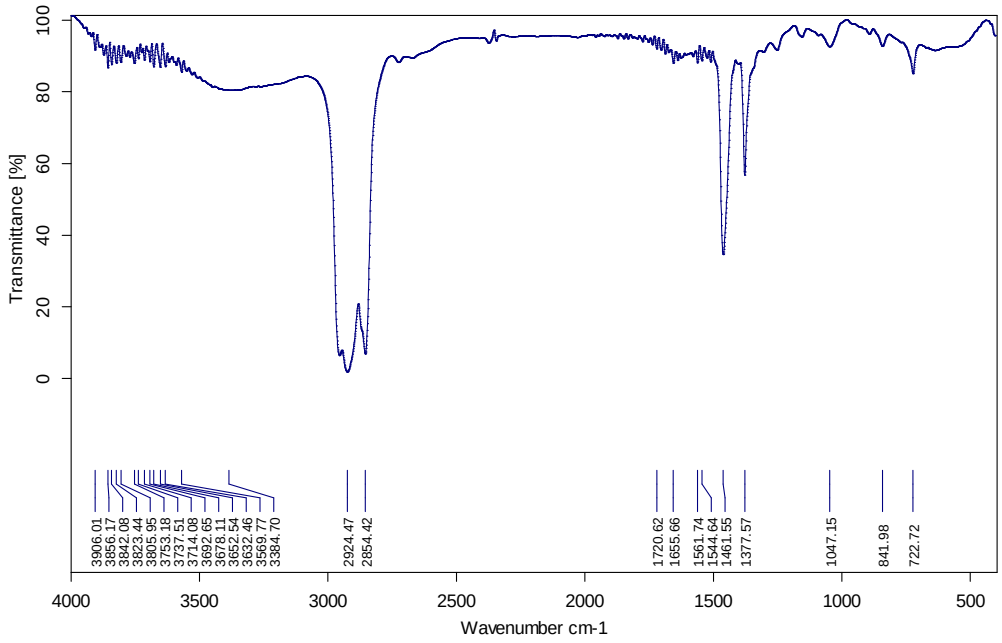

Figure S5.9g: Infrared spectrum of B150 in Nujol

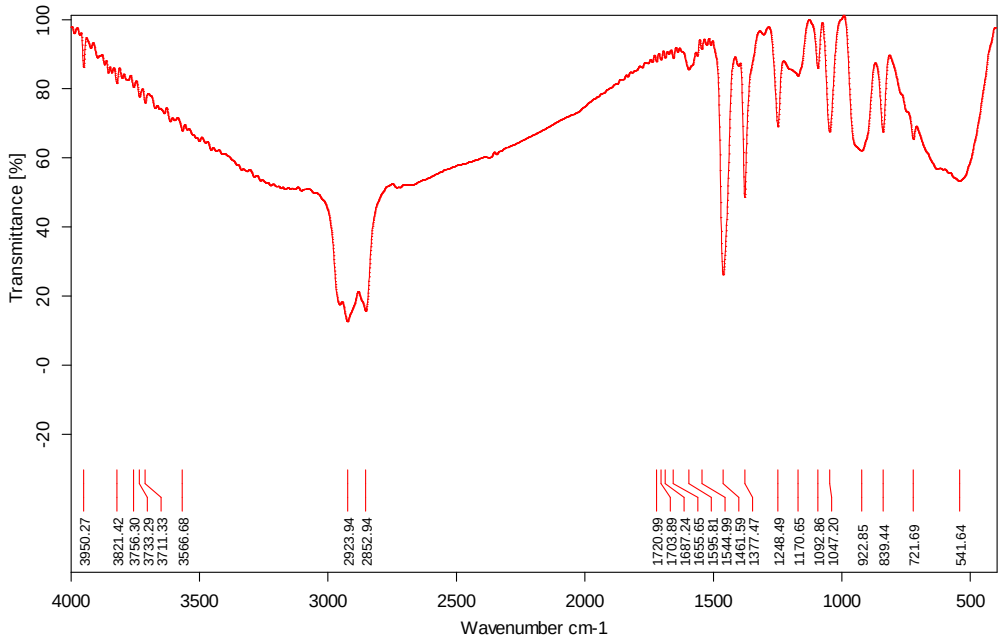

Figure S5.9h: Infrared spectrum of A100-H_2 in Nujol.

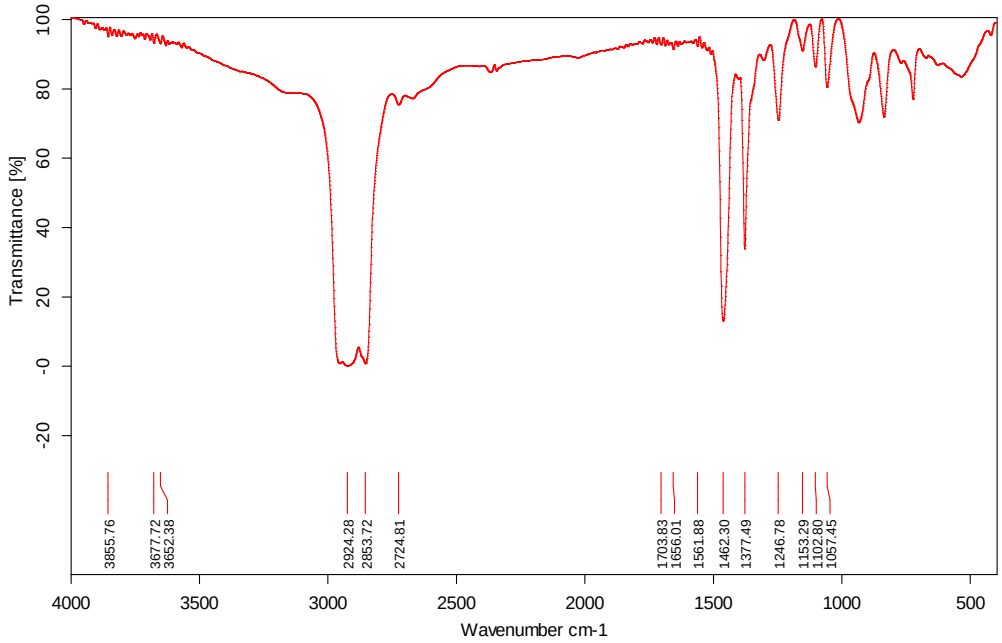

Figure S5.9i: Infrared spectrum of B100-H2 in Nujol.

Chapter 6 – Kubas-Type Hydrogen Storage in V(III) Polymers Using Tri- and Tetradentate Bridging Ligands

6.1 Introduction

Hydrogen is one of the best candidates for an alternative energy carrier and currently could be stored in compressed cylinders, which is not efficiently enough to be applied in mobile applications economically until researchers have improved storage technologies.[1] Extensive research has been carried out using a variety of systems as chemical carriers based around physisorption[2] and metal hydrides,[3] however these approaches have so far fallen short of the U. S. Department of Energy (DOE) 2017 system target[4] of 5.5 wt % and 40 kg/m^2 H_2 at 298 K. Some chemical hydrides, which possess high adsorption enthalpies in the 70 kJ/mol range, contain enough hydrogen to satisfy the ultimate DOE target,[5] however, the kinetics of charging and discharging hydrogen and the heat management issues prevent them from practical usage.[6] Catalyzed hydrogen spillover for hydrogen storage,[7] another method employing dissociative hydrogen adsorption, is considered promising, however it too has yet to meet the stringent DOE goals. Physisorption materials, such as carbon[8] and metal-organic frameworks (MOFs)[9] possess much lower binding enthalpies (5-13 kJ/mol) and demonstrate excellent hydrogen uptake with no kinetic barrier and little heat management issues at 77 K and moderate pressure. For example, the total hydrogen uptake of MOF-177 and NOTT-122 surpasses the DOE 2017 system target under these conditions,[10] however the cost of cooling still makes this technology prohibitive. To improve performance at higher temperatures, some MOF materials have been synthesized with active metal sites in hopes to exploit the role of open metal sites[11] or Kubas interaction,[12] a type of hydrogen binding to transition metals with enthalpies in the 20-50 kJ/mol range.[13-15] While there has yet to be conclusive spectroscopic evidence of the Kubas interaction in MOFs, it has been observed by vibrational spectroscopy in Cu-ZSM-5.[16] Extensive studies of metal binding sites have also been carried out by our group on Ti, V, Cr supported silica systems using different oxidation states, ligand types, preparation methods, and doping levels.[17,18] In these studies, Ti(III), V(III), Cr(II), and Cr(III) were identified as the best metal hosts for what

was believed to be Kubas interaction with hydrogen at room temperature and moderate pressure on the basis of rising enthalpies with surface covereage.[19] Subsequent computational studies have supported this assignment,[20] however no spectroscopic evidence has yet been obtained due to the small amounts of hydrogen absorbed by the 5% metal in these systems. In order to maximize the number of potential Kubas sites per unit volume, cyclopentadienyl chromium hydrazide gels[21] and vanadium hydrazide gels[22] were synthesized by the reaction of low valent organometallic precursors with anhydrous hydrazine. Hydrazine was used as a linker because of its low molecular weight and ability to bridge two metal centers, providing a diffusion pathway for hydrogen without creating excess void space, while also maintaining the low ligation number of the metal coordination sphere. These X-ray amorphous materials possess linear isotherms at both 77 K and 298 K that do not saturate at 80 bar, ideal adsorption enthalpies in the 20-40 kJ/mol range and maintain up to 49 % of their performance at 298 K as compared to 77 K. The volumetric adsorption of the vanadium material at 77 K and 80 bar (60 kg/m^3) surpasses all MOFs as well as the 2017 DOE target. At room temperature, this material demonstrates a volumetric adsorption of 23.2 kg/m^3 H_2, approaching the 2010 DOE target. While transition metal hydrazides show enormous promise, hydrazine has many safety issues and can also bind in multiple coordination modes, leading to amorphous systems that are difficult to characterize. Because of this we are continuing to explore other low-molecular weight ligands that support low-coordinate metal sites useful for Kubas binding. In this work, trismesitylvanadium (III)•THF was treated with various commercially available multi-proton, multi-dentate chelating ligands capable of bridging two metal centers in a controlled stoichiometric fashion, with the aim of creating new materials for hydrogen storage. The one-to-one metal-to ligand stoichiometry used in this study should also favor a 1-d system with much more flexibility around the tetrahedral metal center than more rigid 3-d systems such as zeolites,[23] which do not possess a high number of active and strong adsorption centers per unit volume, to optimize the orbital geometries for H_2 coordination.

6.2 Experimental section

All chemicals, unless otherwise stated, were obtained from Aldrich. H_2 grade 6.0, N_2, Ar, and He were obtained from Praxair Canada. All solvents were dried by distillation in argon atmosphere, using sodium/benzophenone to remove moisture and oxygen. Distilled solvent was transferred to a schlenk flask using a canula. Dry argon gas was bubbled through the flask for 30 minutes, followed by degassing before transferring into a dry box.

Preparation of $V(Mes)_3{\cdot}THF$: 33.33 ml of dry tetrahydrofuran (THF) was added to 50 ml of mesityl magnesiumbromide 1M (MesMgBr) solution in THF, followed by the portion-by-portion addition of 6.22 g of $VCl_3{\cdot}3THF$ 97%. The obtained solution was stirred vigorously at room temperature for 2 hours and a clear blue solution was obtained. 21.66 ml of dioxane was then added to the solution with stirring. After 2 more hours, stirring was ceased and the solution was left to settle before filtration. The filtrate was collected and concentrated in vacuum until crystals formed. 16.67 ml of diethylether was then added and the remaining product precipitated out. The solid product was then collected by filtration and washed several times with a solution of THF and ether (THF : ether = 1:3 by volume) before drying in vacuum.[24]

6.2.1 Preparation of V-Oxamide100 and V-Oxamide150: V-Oxamide100 was synthesized as follows: $V(Mes)_3{\cdot}THF$ (3 g, 6.24 mmol) was dissolved in 75 ml of dry toluene at room temperature in an Erlenmeyer flask. 0.5608 g (6.24 mmol) of oxamide was then added with vigorous stirring. The solution was capped and stirring was continued for 12 hours. The solution was then heated to 100 ^oC for 3 hours with stirring. After this, the system was filtered and a black solid was obtained. The filtrate was colorless, indicating complete reaction of the V precursor. This solid was transferred to an air-free tube and was then dried under vacuum (10^{-2} mmHg) for 12 hours, followed by heating at 60 ^oC under vacuum (10^{-2} mmHg) for a period of 6 hours and another 6 hours at 100 ^oC under vacuum(10^{-2} mmHg) . V-Oxamide150 was obtained by continuing to heat V-Oxamide100 at 150 ^oC for 6 hours in vacuum (10^{-2} mmHg).

6.2.2 Preparation of V-Oxalate150, V-Glycolate150, and V-Glycolamide150: V-Oxalate150 was synthesized by the same method as V-Oxamide150, using 0.5618 g (6.24 mmol) of oxalic acid instead of oxamide. V-Glycolate150 and V-Glycolamide150 were also synthesized in this same way, using glycolic acid (0.4973 g; 6.24 mmol) and glycolamide (0.4780 g; 6.24 mmol), respectively. The filtrate was colorless in each case, indicating complete reaction of the V precursor.

6.2.3 Preparation of H2-V-Oxalate and H2-V-Glycolate: V-Oxalate150 and V-Glycolate150 were treated with hydrogen at 150 ^{o}C and 85 bar for 3 hours and the resulting materials were then collected and stored under Ar.

6.2.4 Characterization. Powder X-ray Diffraction (PXRD) was performed on a Siemens diffractometer D-500 with Cu Kα radiation (40 KV, 40 mA) source. The step size was 0.02° and the counting time was 0.3 s for each step. Diffraction patterns were recorded in the 2θ range of 2.3^{o} to 52°. Samples for PXRD analysis were put in a sealed capillary glass tube to protect sample from air and moisture during experiment.

Nitrogen adsorption and desorption data were collected on a Micromeritics ASAP 2010. All XPS studies were conducted using a Physical Electronics PHI-5500 spectrometer using charge neutralization and emissions were referenced to the carbon C-(C, H) peak at 284.8 eV. Elemental analysis was performed by Galbraith Labs, Knoxville Tennessee. Thermogravimetric analysis was conducted on a Mettler Toledo TGA SDTA 851e, using helium (99.99%) as purging gas with the rate of 30 mL/min. Samples were held at 25 ^{o}C for 20 min before being heated to 550 ^{o}C at rate of 5 ^{o}C/min.

FT-IR was conducted on all synthesized materials using a Bruker Vector 22 instrument. In a typical experiment, 2 mg of sample was mixed with 500 mg of dry KBr, and a compressed disc was made in an inert atmosphere. The discs were then transferred outside, and the measurements were conducted immediately. Since this technique was primarily used to identify the hydrocarbon in the sample, which would not oxidize on exposure to air, rigorously air-free conditions were not employed.

6.2.5 Hydrogen – deuterium exchange experiment: 100 mg of V-Oxamide150 was placed in a Schlenk tube connected to a bubbler and a deuterium cylinder. A deuterium stream was passed over the sample for seven days at a rate of one liter per hour. After this, the deuterium treated sample was left under vacuum for 6 hours. The original and deuterium treated materials were then studied by infrared spectroscopy using a Bruker Tensor 27 instrument. 3 mg of material was mixed with 500 mg of KBr and a compressed disc was made in inert atmosphere. The discs were transferred outside and the measurements were conducted immediately.

6.2.6 Raman experimental details: Samples were loaded in NMR tubes fitted with J – Young valves and spectra recorded at 1 atm pressure of H_2, D_2, or Ar. For the samples recorded after vacuum, the samples were left for 1 h under H_2 or D_2 and then placed under vacuum for ten minutes before back filling with Ar. All micro-Raman scattering experiments were conducted using a Renishaw InVia system, with laser excitation at 514.5 nm, and powers of 10-20 μW at the sample. Each scan was duplicated to ensure that any features observed were reproducible. All measurements were made in a backscattering geometry, using a 20x microscope objective with a numerical aperture value of 0.40, providing scattering areas of ~20 μm^2. Single-point spectra were recorded with 4 cm^{-1} resolution and 50 s accumulation times. Data acquisition and analysis were carried out using the WIRE software for windows and Galactic Industries GRAMS™ C software.

6.2.7 Hydrogen adsorption measurements: Hydrogen adsorption isotherms were obtained by using an Advanced Materials PCI and the same method described in our previous publications on metal hydrazides.[21,22] Adsorption enthalpies were calculated from adsorption isotherms at 77 and 87 K, using a method described elsewhere.[25] True volumetric adsorption of all materials were calculated on the basis of gravimetric adsorption and skeletal densities of materials while absolute volumetric adsorption was calculated based on gravimetric adsorption using bulk densities.[25, 26]

6.3 Results and Discussions

In this work, tris(mesityl) vanadium(III)·THF was treated with one molar equivalent of either oxamide, oxalic acid, glycolic acid, and glycolamide to create polymers with V – O and V – N linkages through protonolysis of the mesityl groups. The samples were then dried at either 100 °C or 150 °C (to create, for example, V-Oxamide100 or V-oxamide150, respectively) and their hydrogen storage properties tested. Since the materials dried at 150 °C possessed superior hydrogen storage performance the majority of this paper focuses on these samples. The proposed reaction of $V(Mes)_3$·THF with the various ligands are shown in Scheme 6.1.

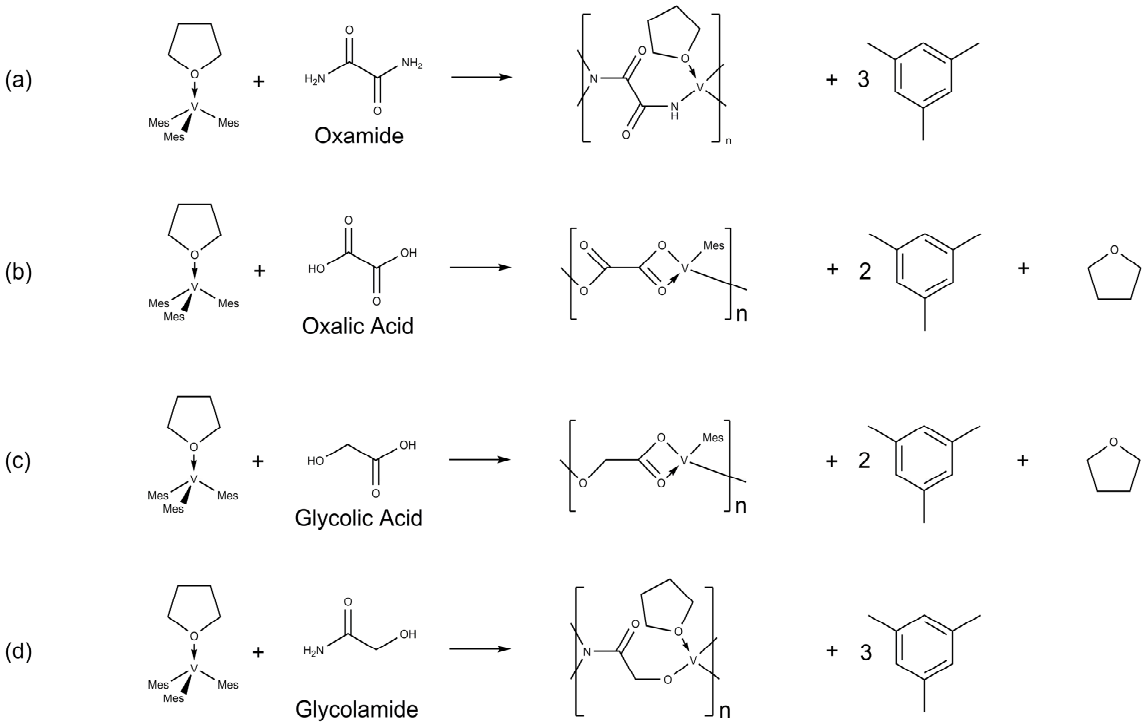

Scheme 6.1: Proposed reaction between $V(Mes)_3$·THF with various ligands. a) oxamide, b) oxalic acid, c) glycolic acid, d) glycolamide.

The four protons present in oxamide are enough to eliminate three mesityl groups with one proton remaining, putatively resulting in a tetrahedral V (III) center bound to 2 O and 2 N atoms from oxamide, capable of binding 3 H_2 according to the 18-electron rule.[27] Since the expected weight of the V-oxamide monomer is 136 g/mol, this corresponds to 4.41 wt% H_2, close to the 2017 DOE goal of gravimetric adsorption (5.5 wt%). Oxalic

acid has only two protons per ligand so one remaining mesityl is expected in V-oxalate, resulting in a five-coordinate environment with the 4 oxalate oxygens, while in the glycolate material there are only two available protons and three ligating atoms, so retention of one aryl group to create a 4-coordinate center V (III) is expected. In the glycolamide material there are three protons available and three ligating atoms per ligand, however elimination of all three mesityls would result in a three-coordinate V center, which is not likely. Therefore it is possible that there is a remaining aryl functionality on the V-center with a proton still remaining on the ligand, or conversely that all mesityls have been eliminated and the extra coordination site is taken up by THF, which could be clarify by XPS and IR spectroscopy.

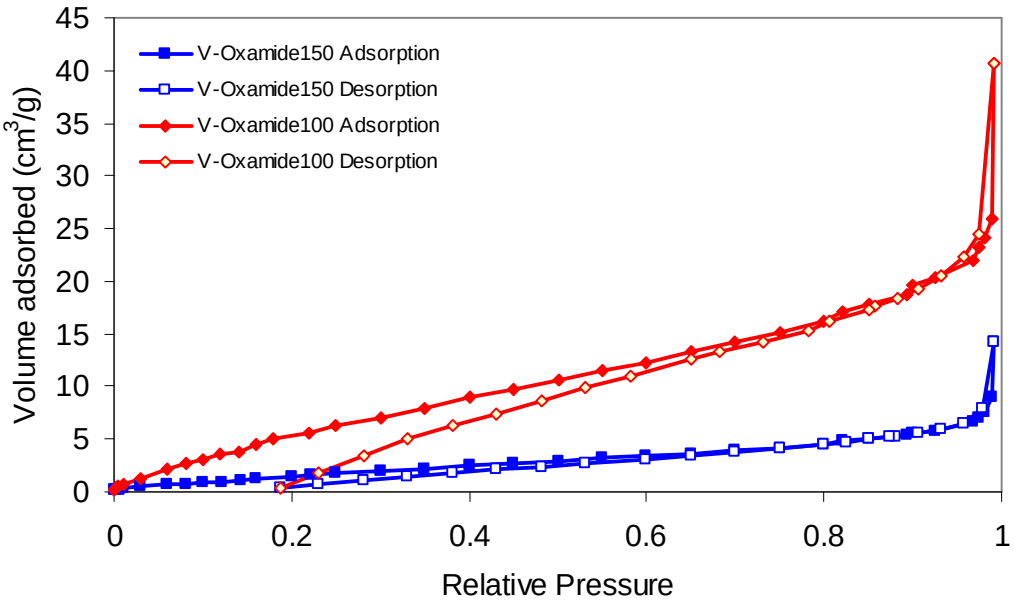

Figure 6.1: Nitrogen adsorption – desorption isotherms of V-Oxamide100, V-Oxamide150. Samples were measured on an ASAP-2010 instrument at 77K.

The PXRD pattern (Figure S6.1a-f; Supporting Information) of V-Oxamide150 showed a wide reflection at $2\theta < 5^{o}$, suggesting possible mesoscopic periodicity with no long-range order in the material. Similar XRD patterns were obtained with vanadium hydrazide gels, which were synthesized by employing the same $V(Mes)_3$.THF precursor, but with

anhydrous hydrazine as linking agent.[22] The materials synthesized from oxalic acid, glycolic acid, or glycolamide, do not possess any distinct XRD feature and appear to be completely amorphous. Nitrogen adsorption and desorption isotherms for these materials displayed Brunauer – Emmett – Teller (BET) surface areas in the range of 9 – 220 m^2/g (Figure. 6.1-6.2). The isotherms were all type II, representing non-porous materials with most of the surface area arising from textural porosity.[28] Similar isotherms and surface areas were observed for V- and cyclopentadienyl Cr-hydrazide gels studied previously by our group.[21,22] The isotherms for the V-Oxamide materials show anomalies in the desorption branch passing under the adsorption branch, which can be attributed to the very low surface areas of these materials (9 and 28 m^2/g) approaching the detection limit of the instrument on the sample sizes used in the measurement.

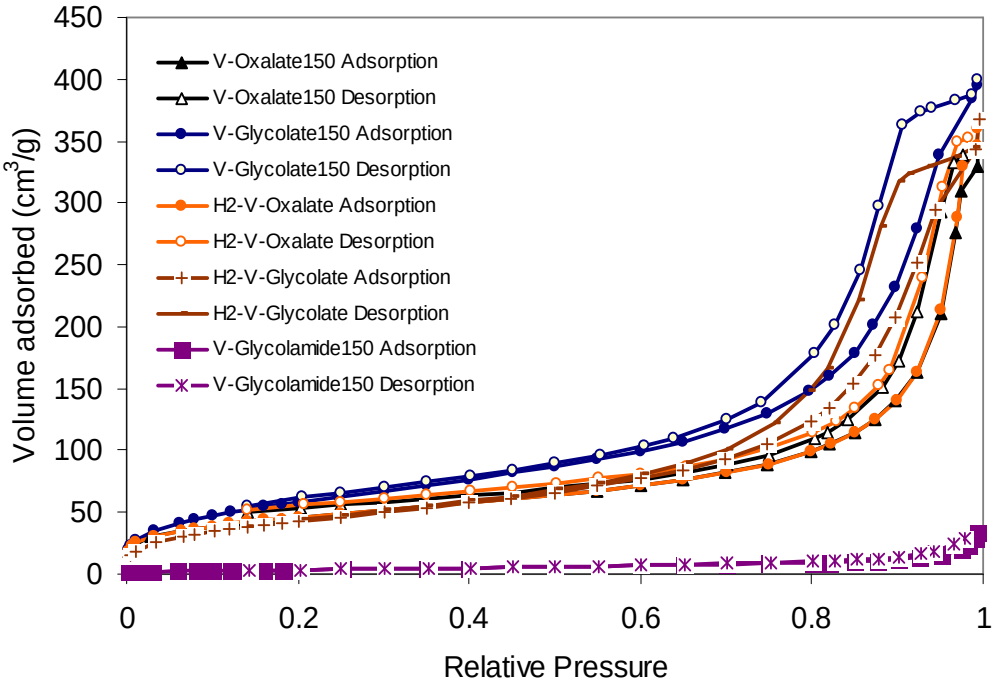

Figure 6.2: Nitrogen adsorption – desorption isotherms of V-Oxalate150, V-Glycolate150, H2-V-Oxalate150, H2-V-Glycolate150, and V-Glycolamide150.

The C, H, N, and V elemental analysis data of these materials are shown in Table S1 and the expected molecular formulas and compositions of the stoichiometric products are shown in Table S6.2 (Supporting Information). The high carbon values for the oxamide

and glycolamide samples indicate that the reaction did not go to completion, either due to retention of THF or incomplete protolysis of the mesityl groups. In contrast, the carbon values for the oxalic acid and glycolic acid samples were lower than expected, perhaps due to incomplete combustion of the material during the elemental analysis process leading to carbide formation. The V values are systematically low, potentially due to incomplete reaction stoichiometries or error in the elemental analysis process due to incomplete digestion of the V species in HF, so these values may not reflect the true V content in the materials. Repeat analysis yielded similar results so this may reflect the limitations of this technique on these materials.

Infrared spectroscopy (IR) was also used to characterize the materials. All samples show strong stretches for metal-coordinated carbonyl groups at ca. 1600 cm^{-1}. The elimination of hydrocarbon was supported by the decrease in intensity of the C – H stretches at 2850 – 2950 cm^{-1} in the spectrum of the products as compared to $V(Mes)_3 \cdot THF$ (Figure S6.2; Supporting Information). Because V-glycolate150 and V-glycolamide150 contain methylene protons in the σ-carbon to the carbonyl it is not possible to distinguish the C-H stretches arising from these functionalities from those of residual mesitylene. The C-C aromatic stretches expected at 1500 cm^{-1} in all materials are obscured by other bands and are therefore not useful in this study. The IR spectrum of the V-Oxamide150 shows an unusual feature at 2200 cm^{-1} that can be assigned to a V-H.[29] The presence of this species must arise from migration of the additional hydrogen atom from the organic ligand to the V center through an σ-hydrogen migration.[30] Since only three of the four oxamide protons are used in eliminating the aryl groups, the remaining proton, not present in the other three ligands, is free to migrate to the V (III) center.

XPS studies of the synthetic materials were conducted, and the results are shown in Figures S6.3 – S6.6 (Supporting Information). In general these spectra support the formulations suggested by the IR spectra, but expand on our knowledge of the oxidation states and binding modes present in each material. Multiple oxidation states of vanadium were detected in the vanadium 2p 1/2, 3/2 regions of all samples (Figure S6.3; Supporting Information). For V-Oxamide150, a small amount of a V(I) species is detected at 513.8 eV and 519.7 eV, assigned by comparison with literature values.[31] Emissions at 515.1 eV

and 521.9 eV can be assigned to V(III).[32] V(IV) species are also present at 516.2 eV and 523.4 eV.[33] V(V) is detected with emissions at 517.6 eV and 524.9 eV.[34] Similar disproportionation was observed for vanadium hydrazides studied by our group and is common in the chemistry of lower oxidation sates of this element. Four oxidation states of vanadium were also detected in V-Oxalate150 and V-Glycolate150, but the emissions are slightly shifted to higher binding energies with ~ 0.3 eV difference. The V-glycolamide150 material also has multiple oxidation states but there appear to be no V(I) species present. The reason for this is not understood but may be related to the relative disproportionation pathways open to the metals in the different ligand environments.

The O 1s region of the XPS spectra of all materials is shown in Figure S4. The emission at 530.4 eV, which is very strong in the case of V-Oxamide150 and moderately strong in the case of V-Glycolamide150, can be attributed to coordinated THF on the basis of our previous work on vanadium hydrazides, which show a substantial amount of THF retention.[22] This is consistent with the EA of these materials, which exhibits a higher amount of carbon than expected. The fact that the THF is not observed in the glycolate or oxalate samples is consistent with the presence of the one remaining sterically demanding mesityl group expected by proton stoichiometry. The emission at 532 eV can be attributed to V-bound oxygen in the amide carbonyl or carboxylate group in all four species on the basis of previous XPS spectra of metal coordinated carboxylate species,[35,36] while the small emission at 533.8 eV corresponds to an oxygen with two single bonds in either C-O-V or C-O-H species.[37] The latter would be expected in the oxamide and glycolamide materials due to tautomerization of the amide functionality. The N 1S XPS spectrum of V-Oxamide150 shows a large peak, which can be simulated as three emissions at 396.8 eV, 398.8 eV, and 400.3 eV (Figure S6.5; Supporting Information). Compared with the values reported for monomeric compounds, the emission at 400.3 eV could be attributed to a bound nitrogen from a –(C=O)-NH_2 species.[38] The emission at 398.8 eV can be assigned to the nitrogen in –(C=O)-NH- species on the basis of previous XPS on metal coordinated amides,[35,39] The small emission at 396.7 eV can be attributed to a free amino N bound directly to two vanadium centers,[40] possibly formed through a small amount of reductive C-N cleavage due to decomposition. The high intensity of the central emission being assigned to a proton-free

N species is consistent with three of the four oxamide protons being used to eliminate the aryl group. The XPS of the N 1s region of V-Glycolamide150 can be simulated as two peaks at 400.2 eV and 398.8 eV and can thus be assigned to analogous –(C=O)-NH_2 and –(C=O)-NH- species by comparison to the oxamide species. The presence of N-H is consistent with incomplete elimination of the aryl group. No emission is detected at 396.8 eV, indicating that there are no free amino groups in the materials. This can be further confirmed by IR, as there are N-H stretches present from 3400 – 3500 cm^{-1} in V-Oxamide150 but not in the IR of the other materials. XPS of all samples in the valence region were also obtained (Figure S6.6; Supporting Information). All materials with the exception of V-Oxamide150 display a high density of states at the Fermi level consistent with metallic behavior in these samples. This was confirmed by the fact that charge neutralization was only required on the oxamide sample.

In order to gain further insight into the composition of these materials we performed thermogravimetric analysis (TGA), which is often used as a compliment to elemental analysis. The TGA curves for all four samples are shown in the supplemental section (Figure S6.7) and show a steady drop in mass with heating at a rate of 5 °C/min from 200 °C to 350 °C, followed by a more gradual decrease to 550 °C. For V-oxamide150 45.09% mass was remaining at the end of the experiment. Assuming complete conversion to V_2O_5, the %V in the original sample would be 25.26%. If the molecular formula of this material was $C_2HN_2O_2V$, then 37.46% of the sample would be V, with 66.87% mass remaining after stoichiometric conversion to V_2O_5. If 1 THF per V center is included, as suggested by the IR and XPS, then the material would have a formula of $C_6H_9N_2O_3V$, with 24.48% V and 43.7% mass remaining after conversion to V_2O_5. The TGA data is thus more consistent with the later formulation of this material as a THF adduct as given in Table S6.2. Likewise, V-Glycolamide150 can be formulated more accurately as a THF adduct on the basis of 50.95% mass remaining after combustion, while the remaining glycolic and oxalic acid materials appear to be correctly formulated as described in Scheme 6.1, with 49.13% and 42.01% mass remaining, respectively, after combustion in the TGA experiment. The %V as derived from TGA is shown for all materials in Table S6.1 and in all cases more closely matches the expected values listed in Table S6.2 than the EA results.

Figure 6.3 shows the excess hydrogen adsorption and desorption isotherms at 77 K and excess hydrogen adsorption at 298 K of the V-Oxamide100 and V-Oxamide150 materials. The hydrogen storage results for this and other samples are summarized in Table 6.1. At 77 K, there is an initial sharp rise to ~ 0.5 wt % at the beginning of adsorption process, followed by linear region up to 85 bar. The cyclopentadienyl chromium hydrazide materials synthesized by our group possess similar adsorption isotherms with an sharp rise at low pressure.[21] This can be attributed to a small amount of physisorption arising from the relatively low surface area of the material and the adsorption of hydrogen molecules on the outermost adsorption centers, which are coordinatively unsaturated and exposed. At 85 bar, V-Oxamide100 adsorbs 2.25 wt % hydrogen at 77 K and 0.51 wt % at 298 K (Table 6.1). Increasing the activation temperature up to 150 ^{o}C affords a material with 3.49 wt % adsorption at 77 K and 85 bar. From 0 to 30 bar, this material adsorbs up to 0.55 wt % at 298 K. After that, the isotherm is linear up to 85 bar and an adsorption capacity of 0.87 wt % is achieved. These results correspond to a true volumetric density of 51 kg/m^3 at 77 K and 13 kg/m^3 at room temperature. The true volumetric density was quoted previously by our group for vanadium hydrazide gels and is defined as the product of the skeletal density and the excess storage.[22] While it is not typical in the physorption of carbons and MOFs to use the skeletal densities in calculating the volumetric density, this is because of the large amount of void space in these materials and the correspondingly large discrepancy between the bulk density and skeletal density. In our polymeric materials the void space has been minimized to optimize the amount of adsorption arising from Kubas sites, so there is only a small difference in skeletal density and bulk density. The absolute volumetric adsorption of V-Oxamide150 material was obtained by using a pre-weighed portion of material, which was compressed at 500 psi pressure to remove void spaces between particles. The compressed material possesses a bulk density of 0.9739 g/cm^3. At 85 bar it adsorbs 2.25 wt% of hydrogen at 77 K and 0.99 wt% at 298 K. This corresponds to an absolute volumetric adsorption of 21.91 kg/m^3 and 9.6 kg/m^3, respectively, at 77 K and 298 K. This compares to an absolute volumetric adsorption of 30 kg/m^3 for MOF 177 and a volumetric storage of MOF-177, including the compressed gas, of 50.3 kg/m^3 at 77 K and 8 kg/m^3 at 298 K.[26] Since V-Oxamide150 adsorbs hydrogen in a linear

fashion without saturation at 80 bar and 298 K, this indicates that higher adsorption results could be expected at higher pressures.

Table 6.1: Summary of excess storage data on various vanadium materials and carbon AX-21. Data are taken at 85 bar. MOF adsorption data obtained from [41].

Material	BET Surface Area (m^2/g)	Skeletal Density (g/cm^3)	Gravimetric Adsorption (wt %)	Volumetric Adsorption (kg/m^3)	Retention (%)
V-Oxamide100	28	1.2308	2.25 (at 77 K) 0.51 (at 298 K)	28 (at 77 K) 6.2 (at 298 K)	23
V-Oxamide150	9	1.4636	3.49 (at 77 K) 0.87 (at 298 K)	51 (at 77 K) 13 (at 298 K)	25
V-Oxalate150	168	1.6452	1.10 (at 77 K) 0.23 (at 298 K)	18 (at 77 K) 3.8 (at 298 K)	21
H_2-V-Oxalate	169	1.4581	1.40 (at 77 K) 0.44 (at 298 K)	20 (at 77 K) 6.4 (at 298 K)	32
V-Glycolate150	220	1.4407	1.60 (at 77 K) 0.28 (at 298 K)	23 (at 77 K) 4.0 (at 298 K)	17
H_2-V-Glycolate	163	1.3110	1.70 (at 77 K) 0.35 (at 298 K)	22 (at 77 K) 4.9 (at 298 K)	22
V-Glycol-amide150	15	1.2390	1.40 (at 77 K) 0.37 (at 298 K)	17 (at 77 K) 4.6 (at 298 K)	27
AX-21	3225	2.103	4.2(at 77 K, 65 bar) 0.55 (at 298 K)	14 (at 77 K, 65 bar) -	13
MOF-5[(*)]	3534	-	5.1 (at 77 K) 0.28 (at 298 K)		5.5

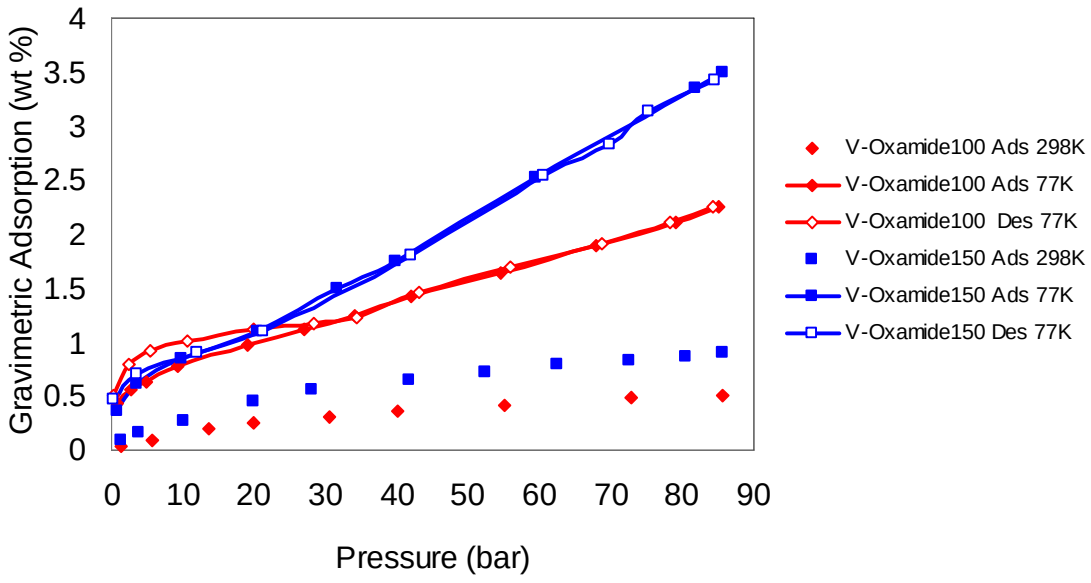

Figure 6.3: Excess hydrogen adsorption isotherms at 77 K, 298 K of V-Oxamide100, V-Oxamide150. Desorption at 298 K is left out for clarity.

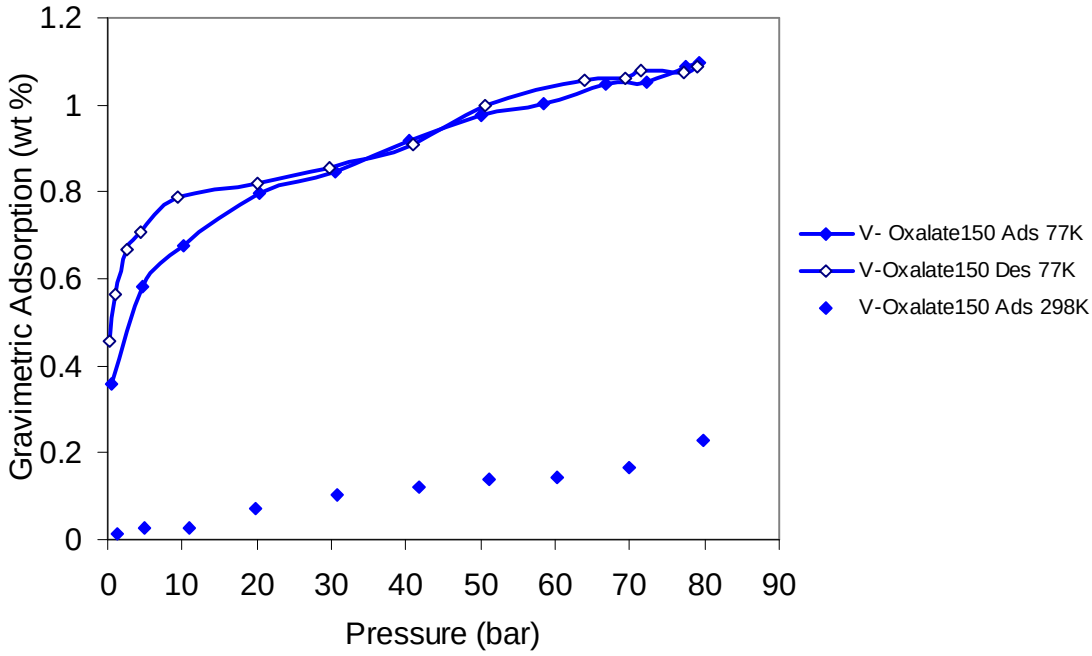

Figure 6.4: Hydrogen adsorption properties at 77 K, 298 K of V-Oxalate150. Desorption at 298 K left out for clarity.

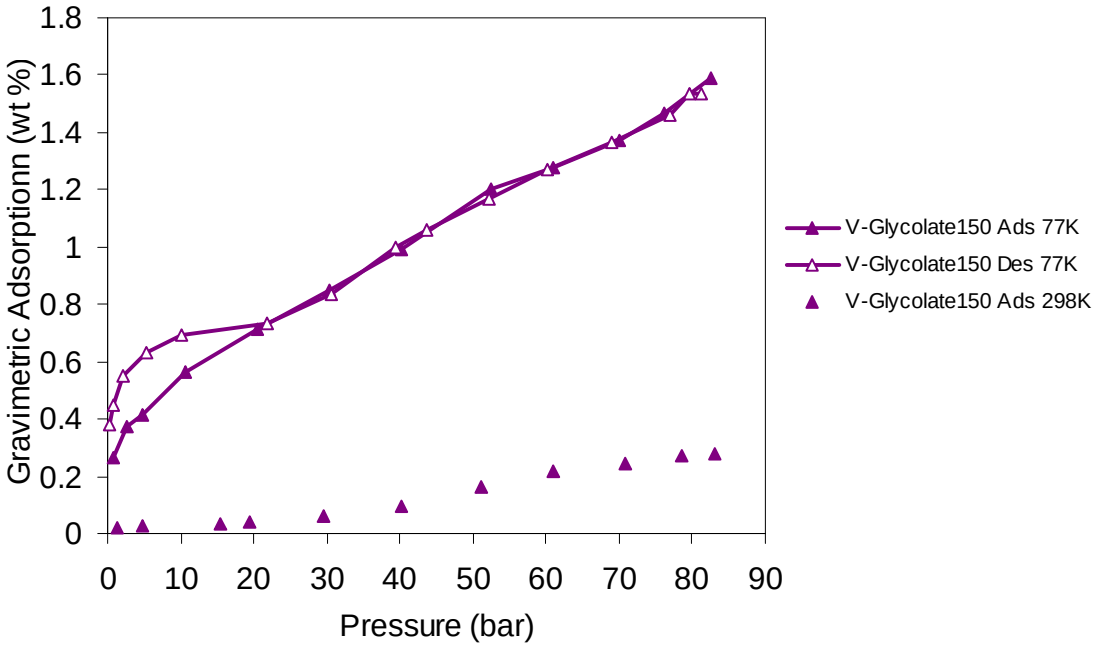

Figure 6.5: Hydrogen adsorption properties at 77 K, 298 K of V-Glycolate150. Desorption at 298 K left out for clarity.

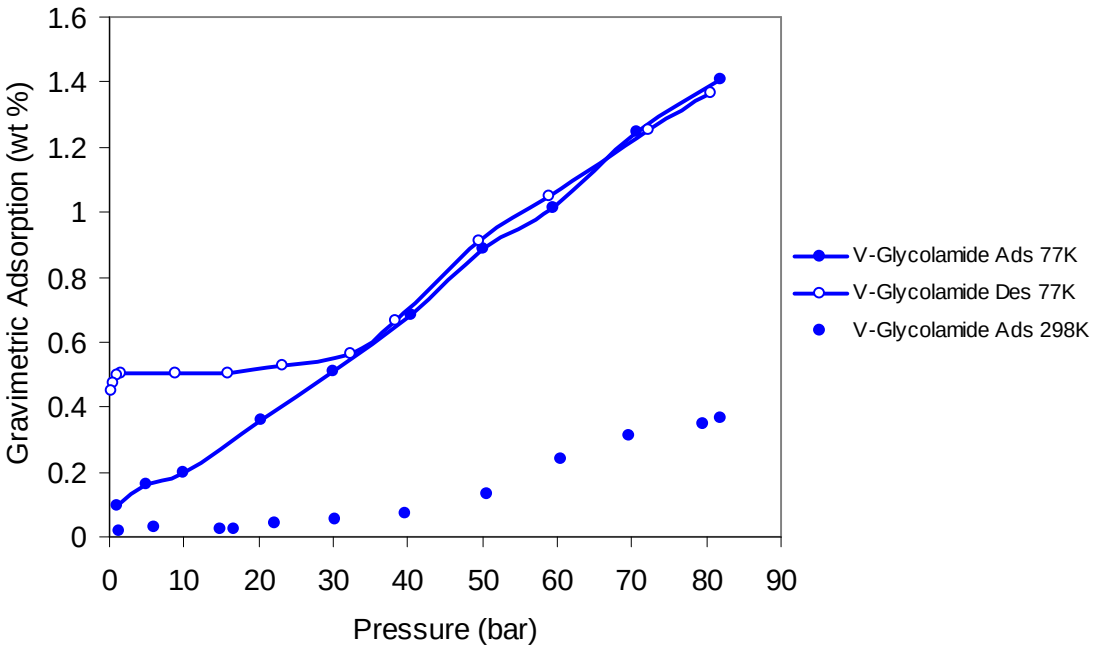

Figure 6.6: Hydrogen adsorption properties at 77 K, 298 K of V-Glycolamide150. Desorption at 298 K is left out for clarity.

The excess storage isotherms of V-Oxalate150, V-Glycolate150, and V-Glycolamide150 are shown in Figure 6.4, 6.5, and 6.6, respectively. At 77 K, a sharp initial rise up to 0.65 wt % from 1 to 10 bar is observed in V-Oxalate150. This is attributed to physisorption and is followed by a linear region increasing up to 1.1 wt % at 85 bar (Fig. 2). A similar rise up to 0.5 wt % for V-Glycolate150, followed by linear adsorption up to 1.6 wt % is also observed (Fig. 6.3).

At room temperature and 85 bar, V-Oxalate150 and V-Glycolate150 adsorb 0.23 wt % and 0.28 wt % of hydrogen, respectively (Figure 6.4-6.5). The V-Glycolamide150 materials does not exhibit a sharp physisorption increase at low pressure and 77 K, and the adsorption isotherm is linear in the pressure range up to 85 bar, at which it absorbs 1.4 wt% hydrogen. A sharp increase is observed in the desorption, however, as it plateaus at 0 bar and 0.5 wt % hydrogen (Figure 6.6). Placing the sample under vacuum after the desorption cycle removes this hysteresis as the second adsorption cycle is then identical to the first. The reason why this behavior is not observed in V-Oxamide150 is not understood, but may be related to different pore structures in the material. This would introduce a slight kinetic barrier to initial adsorption and desorption at low pressure in this material, due to the low porosity and energy required for hydrogen diffusion through the void space within the materials.[42] Moreover, at 298 K and 85 bar, V-Glycolamide150 adsorbs 0.37 wt % hydrogen, which is higher than that of H_2-V-Glycolate materials, even though the V-Glycolamide150 possesses a much smaller nitrogen surface area. According to XPS results, V-Glycolamide150 possesses the second highest concentration of V(III) in the sample series and these active species are account for the hydrogen adsorption capacity, physisorption in this case represents minor adsorption capacity contribution.

Hysteretic adsorption – desorption were also observed in V-Oxalate150, and V-Glycolate150, however, to a much lower degree. At room temperature, V-Glycolamide150 adsorbs up to 0.37 wt % at 85 bar, which is higher than that of V-Oxalate150 and V-Glycolate150, but lower than observed in the V-Oxamide series. By comparing the gravimetric adsorption capacities at 298 and 77 K, the retention of excess adsorption capacities are calculated and range from 17 to 32 %. These values are higher than those of MOF-5, which retains 5.5 %;[37] and carbon AX-21, which retains 13 %.[21]

Table 6.2: V concentration of various vanadium materials and average number of hydrogen molecules adsorbed on each vanadium site at 85 bar. Numbers calculated from experimental TGA results.

Material	Number of H_2/V at 77K	Number of H_2/V at 298K
V-Oxamide150	3.50	0.88
V-Oxalate150	1.19	0.25
H_2-V-Oxalate	1.42	0.45
V-Glycolate150	1.81	0.31
H_2-V-Glycolate	1.41	0.29
V-Glycolamide150	1.25	0.33

To summarize these results, V-oxamide150 possesses both the lowest surface area and the highest excess storage capacities. The combination of low surface area and a high concentration of Kubas binding sites in this material minimize physisorption allowing the majority of adsorption to arise via the Kubas interaction. This is clearly seen in Table 6.2, which shows the comparison of H_2/V in the materials studied. On the basis of the TGA results, the oxamide material absorbs 3.5 H_2/V at 77 K and 0.88 H_2/V at 298 K while the other materials range from 0.25 – 0.45 H_2/V (Table 2). By comparison the vanadium hydrazides range in 1.13 – 1.96 H_2/V center,[22] the value of 3.5 H_2/V at 77 K reflects the presence of a component of physisorption in the total amount absorbed, introducing a systematic error in the H_2/V values. This accounts for the fact that the maximum allowable by the 18 electron rule with THF coordination is 2 H_2/V. Thus a value of 2 H_2/V is more reasonable and compares to a value of 2.18 H_2/V at 77 K for a compressed pellet of this material (Figure S6.8). So, while not entirely accurate, these values are still useful benchmarks in comparing the relative efficiency of H_2 adsorption in these materials. Thus, while these materials posses lower gravimetric and volumetric capacities of the best vanadium hydrazide materials,[22] which exhibit 1.17 wt% and 23.2 kg H_2/m^3, the more controlled coordination environment around the V centers afforded by the oxamide ligand as compared to hydrazine, which can bond and bridge in several ways, may make these materials easier to study and characterize.

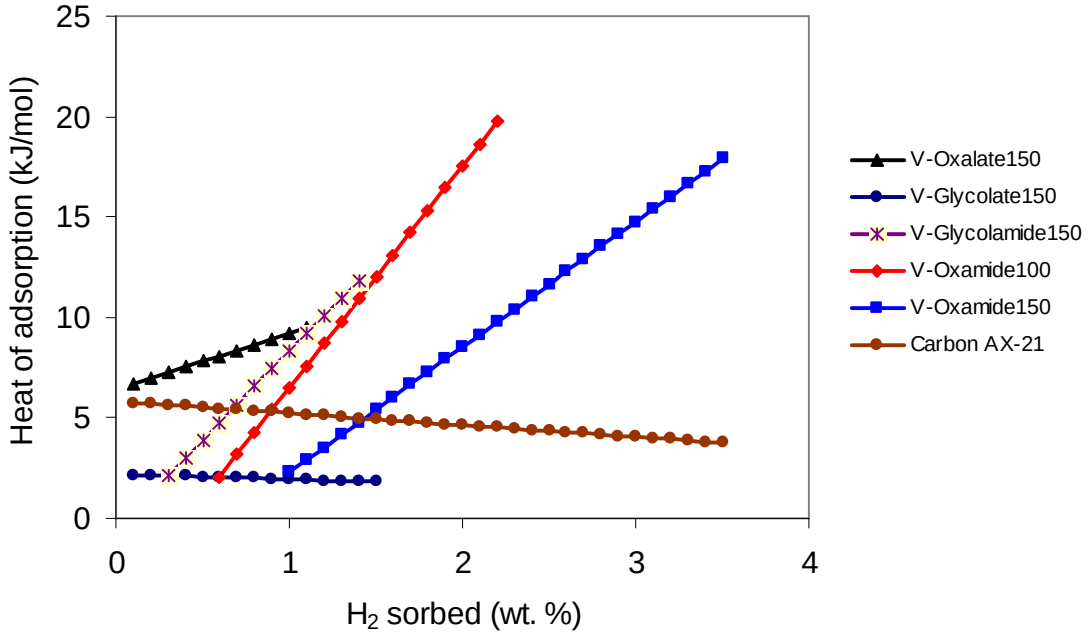

Figure 6.7: Hydrogen binding enthalpies of V-Oxamide100, V-Oxamide150, V-Oxalate150, V-Glycolate150, V-Glycolamide150, and carbon AX-21.

Using a variant of Clausius – Clapeyron I equation, the hydrogen adsorption enthalpies were calculated by employing two sets of adsorption data at 77 and 87 K. V-Oxamide100 and V-Oxamide150 possess adsorption enthalpies that rise versus surface coverage and from 2.3 – 19.8 kJ/mol H_2, approaching the 20 – 30 kJ/mol H_2 range, believed to be the ideal hydrogen adsorption enthalpy (Figure 6.7).[13] This rising enthalpy trend has been observed in all materials studied in our group involving reduced early transition metal species, where the Kubas interaction is believed to be operative as an adsorption mechanism.[15] This phenomenon been predicted in calculations on Sc-coated buckyballs[14] and evidence for the Kubas interaction in these and related materials was provided by recent ESR work on V-hydrazide gels.[22] V-Oxalate150 and V-Glycolamide150 exhibit adsorption heat in the range of 6.6 – 9.5 kJ/mol H_2 and 2.1 – 11.9 kJ/mol H_2, respectively. The lower enthalpies correspond with the lower hydrogen adsorption of these samples at 77 K and 298 K. V-Glycolate150 possesses the lowest adsorption enthalpy at ~ 2 kJ/mol with traditional physisorption behavior that decreases with hydrogen concentration. This indicates that there is little or no Kubas binding in the mechanism of adsorption of this material.

A 20-cycle adsorption run with pressure up to 85 bar was carried out on the V-Oxamide150 sample. The result shows no significant loss of excess adsorption capacity through cycling (Figure S6.9, Supporting Information). The adsorption results range randomly between 0.82 wt% and 0.91 wt %, falling within the instrument error (± 0.05%, instrument's user manual) and the average adsorption capacity of this 20-cycle run is 0.87 wt %.

Hydrogenation was carried out on V-Oxalate150 and V-Glycolate150 according to Scheme 6.2 in order to replace residual mesityl groups with hydride ligands, using experimental conditions developed previously by our group.[19] Theoretical studies on the interaction of hydrogen with different ligands showed that transition metal species with hydride ligands possess higher heat of adsorption than those with alkyl, allyl, aryl, or benzyl groups.[20] This is because alkyl, allyl, aryl, or benzyl groups are stronger π-acceptors and exhibit more steric hindrance than hydride. Moreover, the removal of carbon will lead to a decrease in the sample weight and a concomitant increase in gravimetric hydrogen storage capacity. Thus, hydrogenation at 85 bar and 150 °C of V-Oxalate150 and V-Glycolate150 decreases the carbon concentration from 28.14 to 23.99 % for V-Glycolate while V-oxalate150 showed very little change. There was also an increase in vanadium concentration from 19.64 to 21.60 wt % in the V-Glycolate150 material, while again the V-Oxalate150 sample showed little change. The TGA results (Figure S7) showed 44.87% remaining mass after combustion for the hydrogenated V-Oxalate material as compared to 42.01% in the parent material, indicating that only a small amount of hydrocarbon had been removed. Likewise, 54.83% mass remained for the hydrogenated V-Glycolate as compared to 49.13% in the starting material. If complete hydrogenation had occurred, TGA would show 65.39% and 72.18% mass remaining for the V-Oxalate and V-Glycolate materials, respectively. Hydrogenation of V-Glycolate150 led to a detectable decrease in surface area (from 220 m^2/g to 163 m^2/g), but no significant change was observed in the surface area of the hydrogenated V-Oxalate150 material. The IR spectra of these materials both show a very minor decrease in the C-H stretch indicating that only a small change has occurred in both samples. There was also little detectable change in the XPS spectra of either material. The

difficulty in hydrogenating off the mesityl group from V was observed previously in silica supported vanadium mesityl fragments.[19]

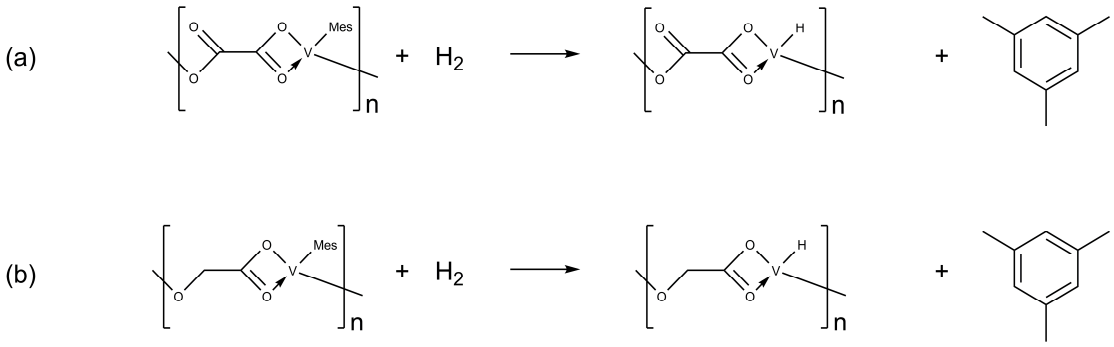

Scheme 6.2: Proposed hydrogenolysis reactions of (a) V-Oxalate150 and (b) V-Glycolate150.

Hydrogenation has more pronounced effect in the hydrogen adsorption performance of V-Glycolate150 than that of V-Oxalate150 on the basis of elemental analysis and thermo-gravimetric analysis. H_2-V-Oxalate and H_2-V-Glycolate possess linear hydrogen adsorption isotherms from 0 – 85 bar at room temperature with better linearity than those of V-Oxalate150 and V-Glycolate150. The excess storage isotherms of H_2-V-Oxalate and H_2-V-Glycolate are shown on Figure 6.8 and 6.9, respectively. H_2-V-Oxalate demonstrated a rise to 0.7 wt % at 77 K and low pressure, after which the isotherm became linear and rose to 1.4 wt % at 85 bar, which is 0.3 wt % higher than the adsorption capacity of the non-hydrogenated V-Oxalate material. A 0.1 wt % adsorption increment with respect to the non-hydrogenated sample was observed at 77 K and 85 bar in H_2-V-Glycolate. The two hydrogenated materials possess linear adsorption isotherms at room temperature, H_2-V-Oxalate and H_2-V-Glycolate adsorbing up to 0.44 wt % and 0.35 wt %, respectively. Increasing the hydrogenation reaction temperatures led to further decrease of carbon content for the V-Glycolate150 sample, but no enhancement of hydrogen adsorption capacities.

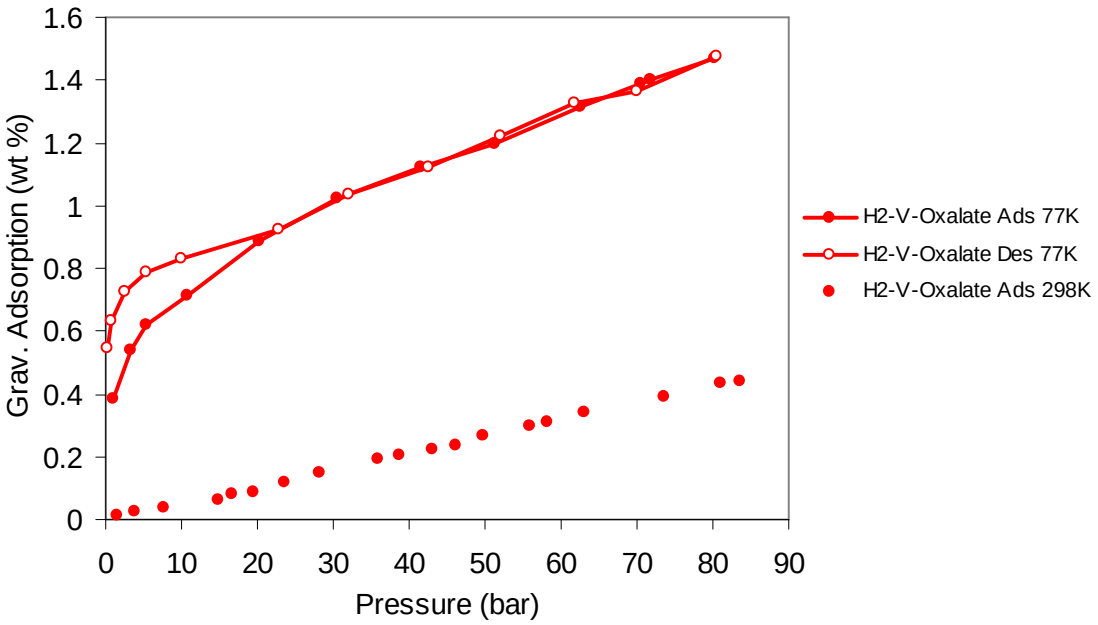

Figure 6.8: Hydrogen adsorption properties at 77 K, 298 K of H2-V-Oxalate. Desorption at 298 K is left out for clarity.

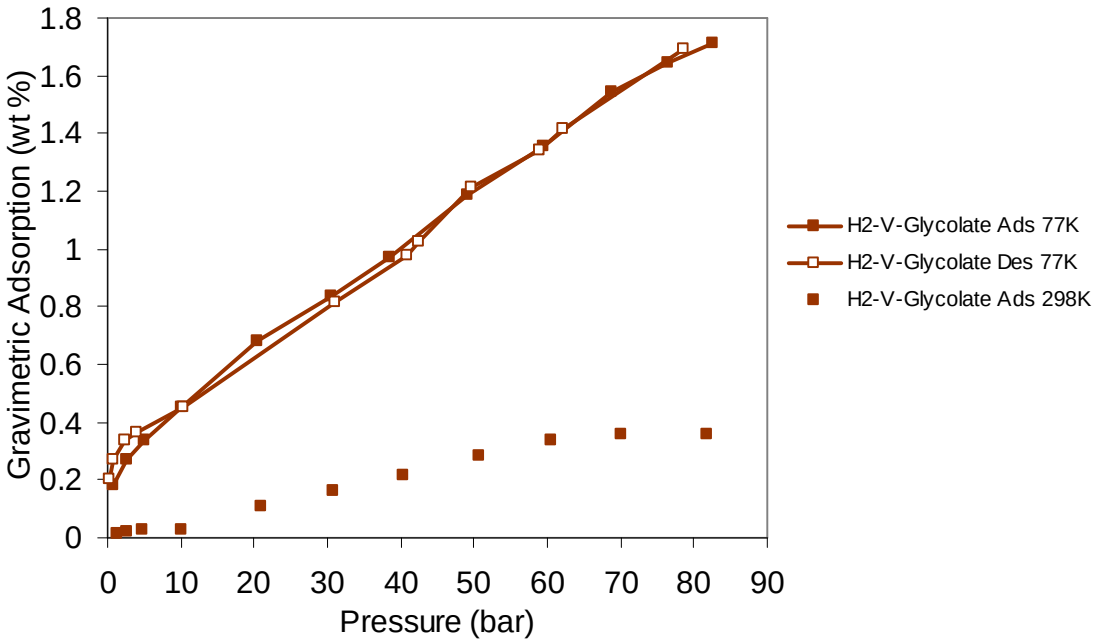

Figure 6.9: Hydrogen adsorption properties at 77 K, 298 K of H2-V-Glycolate. Desorption at 298 K is left out for clarity.

Heats of hydrogen adsorption of these two samples are calculated using adsorption isotherms at 77 and 87 K and shown in Figure 6.10. In line with the negligible change in H_2-V-Oxalate on hydrogenation, there was little change in the enthalpy behavior or magnitude in this sample. In the case of H_2-V-Glycolate, however, hydrogenation leads to a dramatic increase in enthalpy, now rising from 2.2 to 17.3 kJ/mol H instead of falling from 2.0 kJ/mol. The change in enthalpy behavior corresponds to a noticeable change in hydrogen adsorption capacity at 77 K and 85 bar (1.6 to 1.8 wt%) and the change in this material's composition. The enhancement of adsorption performance of H_2-V-Glycolate at 298 K and 85 bar (0.28 to 0.35 wt%) is smaller but still noticeable. The most likely reason for the increase in enthalpy and absorption is the opening up of new more active V centers on loss of hydrocarbon ligand as evidenced by the EA results. However, this adsorption performance is much less than that of V-Oxamide150 because there are a limited number of Kubas hydrogen coordination sites available in V-Glycolate150 to begin with, so opening up a small amount of sites of higher enthalpy only leads to a moderate change in gravimetric adsorption.

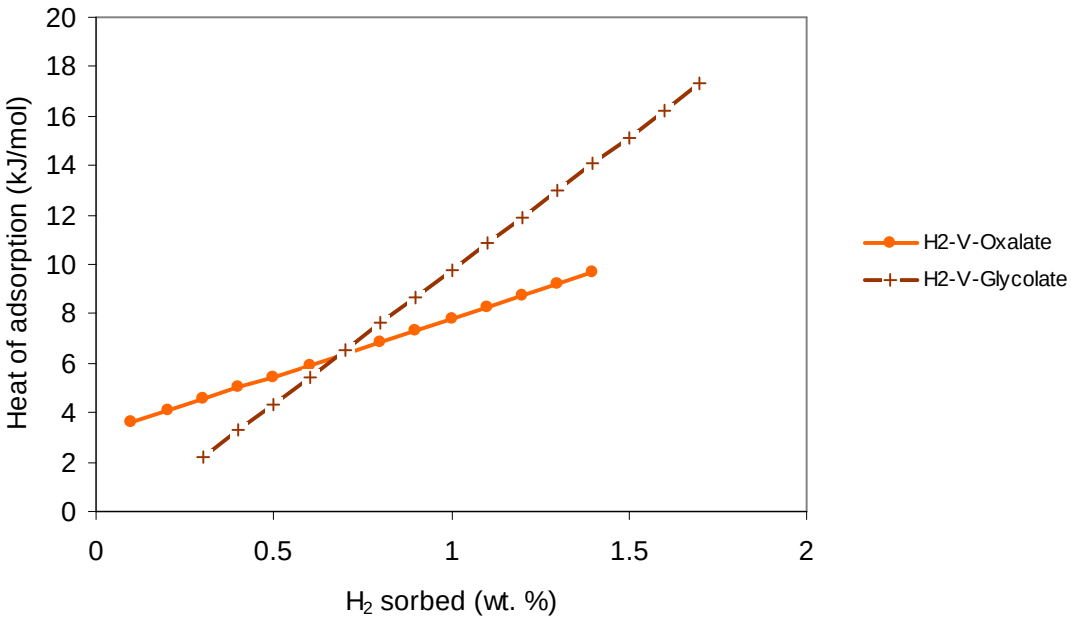

Figure 6.10: Hydrogen binding enthalpies of H2-V-Oxalate150, H2-V-Glycolate150.

Vibrational spectroscopy studies were carried out in order to clarify the interaction between hydrogen and the adsorption centers. In previous work on vanadium hydrazides we used ESR to confirm that V (III) was interacting with H_2 at room temperature.[22] Vibrational spectroscopy is a more traditional method of studying Kubas binding to metals because it potentially provides more direct information on the mode of hydrogen interaction with the metal and the length of the H-H bond can be used to gauge the strength of the binding interaction.[43] A free H-H stretch is Raman active, but IR inactive while coordinated M(H-H), which becomes formally IR allowed due to polarization along the M(H-H) axis, is weak or invisible unless coupled to other bands such as M(CO), and typically appears in the region from 2100-2700 cm^{-1}.[43] This band loses intensity and shifts to 1700-1900 cm^{-1} in the case of the D_2 analogue, demonstrating a smaller net isotope effect than observed for M-H(D).[43] In accordance with these expectations, V-Oxamide 150 shows no change in the IR on treatment with H_2 or D_2 at 1 bar for 1 h before sample preparation. After treatment with D_2 for several days, however, V-Oxamide150 exhibits a weaker intensity of the V – H band at 2200 cm^{-1} (Figure S9; Supporting Information), suggesting that a small amount of deuterium substitution has occurred.[29] This phenomenon could be attributed to the formation of a metastable $VH(D_2)$ complex, which could yield either V – D or the original V – H after the sample is evacuated.

Figure 6.11 shows the Raman spectrum of V-Oxamide150 under H_2 followed by the same sample after evacuation, this evacuated sample under D_2, and finally this D_2 sample after vacuum. The sample prior to any treatment with H_2 or D_2 is also shown for reference. The strong band at 2553 cm^{-1} disappears under vacuum and after treatment with D_2 a new broader and less intense band appears at 1927 cm^{-1}, which also disappears after vacuum. These results are consistent with Raman studies on previous Kubas compounds[43] and demonstrate for the first time that the rising enthalpies are indeed related to the Kubas interaction, as the ESR evidence in a previous report on V-hydrazides shows only that H_2 is interacting with the V(III) center, but does not give any information on the intimate nature of this interaction. The position and lower intensity of the ν(D-D) is expected on the basis of previous studies in the literature.[43] This is thus the first Raman evidence of the Kubas interaction in an extended solid in which the metals are a part of the framework structure. Previous work on MOFs with open metal sites suggested Kubas interactions

but only coulombic interactions were observed,[44-46] however all Raman spectra showed little or no bathochromic shift expected for this bonding mode, all of the ν(H-H) appearing above 4000 cm^{-1}.[44] Raman spectroscopy has been performed on Cu-exchanged ZSM-5[16] and has shown a ν(H-H) of 3079 cm^{-1} and 3130 cm^{-1}, indicative of a weak Kubas interaction, however the Cu is not a part of the framework in this material and ν(H-H) values are relatively high compared to the majority of Kubas compounds in the literature.[43] Furthermore, in the design of materials exploiting the Kubas interaction for hydrogen storage it is important that the metal comprises as large a fraction as possible of the overall weight of the system and is not just an ion or metal complex exchanged onto the surface of a much heavier structure that does not absorb H_2 in a Kubas fashion.

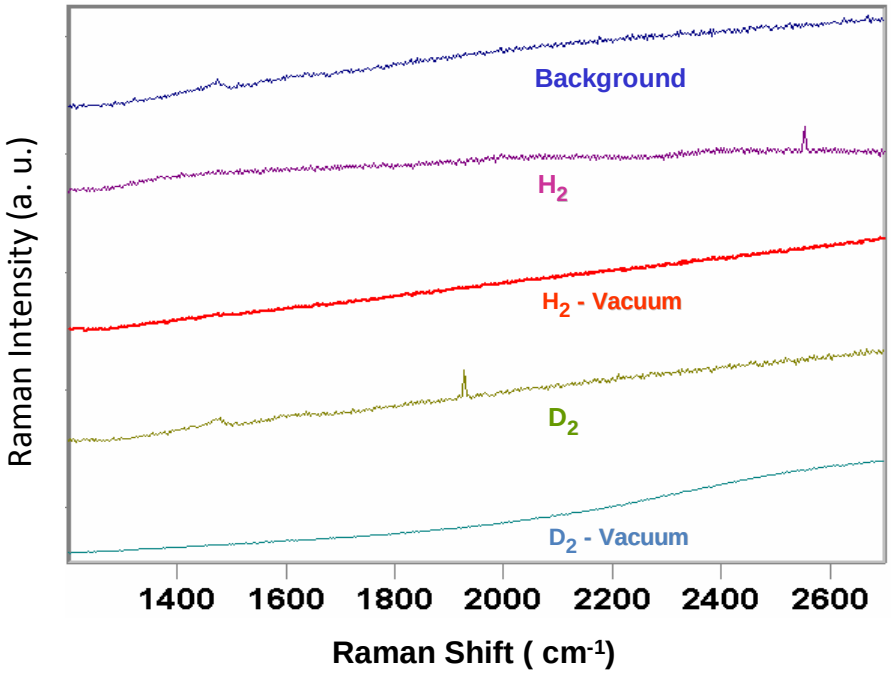

Figure 6.11: Raman spectra of V-Oxamide150 under H_2 and D_2.

6.3 Conclusions

In summary, a series of new polymeric solids were synthesized by the reaction between $V(Mes)_3$·THF with various polyprotic multidentate ligands. These polymers were designed with the aim of creating well-defined Kubas sites for hydrogen storage that could be studied by spectroscopy and gas sorption techniques. The V-Oxamide150

sample showed the highest performance with adsorption value of 3.49 wt % with adsorption enthalpy of 17.9 kJ/mol H_2 at 77 K. At 298 K, the materials adsorb 0.87 wt % at 85 bar with linear isotherms without reaching saturation, which increases the value of these materials at higher pressure. While these values fall short of the DOE goals, they are on par with the best MOFs at 298 K and 80 bar. Raman spectroscopy and deuterium labeling confirmed the presence of Kubas binding in these solids, for the first time unequivocally tying the rising enthalpy trends observed previously in our systems based on low-valent metals to the Kubas interaction. The DOE guidelines specify a maximum pressure of 100bar, however, commercial pressure vessels for hydrogen transport are normally rated at 200 bar or higher, and our materials possess linear isotherms that do not saturate at 298 K and 80 bar. We thus anticipate further gains not only on applying this strategy to different metal systems, but also recording isotherms at higher pressures.

Supporting Information Available. XRD, BET surface areas, IR spectroscopy and XPS of all samples dried at 150 ^{o}C, elemental analysis, TGA, adsorption of V-Oxamide150 compressed pellet, and 20-cycle hydrogen adsorption run of V-Oxamide150 are available.

6.4 References

(1) a) Schlapbach, L.; Zuettel, A. *Nature*, **2001**, 414, 353; b) Seayad, A. M; Antonelli, D.M. *Adv. Mater.* **2004**, 16, 765; c) Yaghi, O. M.; O'Keeffe, M.; Ockwig, N. W.; Chae, H. K.; Eddaoudi, M.; Kim, J. *Nature* **2003**, 423, 705; d) Mark Thomas, K. *Dalton Trans*., **2009**, 1487; e) Wang, L.; Yang, R. T. *Energy Environ. Sci.*, **2008**, 1, 268; f) Lochan, R. C.; Head-Gordon, M.; *Phys. Chem. Chem. Phys*., **2006**, 8, 1357; g) Eberle, U.; Felderhoff, M.; Schueth, F. *Angew. Chem., Int. Ed*., **2009**, 48, 2; h) Satyapal, S.; Petrovic, J.; Read, C.; Thomas, G.; Ordaz, G. *Catal. Today* **2007**, 120, 246; i) Liu, C.; Li, F.; Ma, L. –P, Cheng, H. –M. *Adv. Mater*. **2010**, 22, E28.

(2) a) Langmi, H. W.; Book, D.; Walton, A.; Johnson, S. R.; Al-Mamouri, M. M.; Speight, J. D.; Edwards, P. P.; Harris, I. R.; Anderson, P. A. *J. Alloy. Compd.* **2005**, 404–406, 637; b) Hirscher, M.; Panella, B. *Scr. Mater.* **2007**, 56, 809; c) Bénard, P.; Chahine, R. *Scr. Mater.* **2007**, 56, 803; d) Hu, Y. H.; Zhang, L. *Adv. Mater*. **2010**, 22, E1; e) Zhao, J.; Shi, J.; Zhang, X.; Cheng, F.; Liang, J.; Tao, Z.; Chen, J. *Adv. Mater*. **2010**, 22, 394.

(3) a) Orimo, S.; Nakamori, Y.; Eliseo, J. R.; Zuettel, A.; Jensen, C. M. *Chem. Rev*. **2007**, 107, 4111; b) Sandrock, G. *J. Alloys Comp*. **1999**, 293, 877; c) Bogdanovic, B.; Eberle, U.; Felderhoff, M.; Schueth, F. *Scr. Mater*. **2007**, 56, 809.

(4) Hydrogen, Fuel Cells and Infrastructure Technologies Program: Multi-year Research, Development and Demonstration Plan: Planned Program Activities for 2005 – 2015. http://www1.eere.energy.gov/hydrogenandfuelcells/mypp/pdfs/storage.pdf Retrieved September 16th, 2009.

(5) Dornheim, M.; Doppiu, S.; Barkhordarian, G.; Boesenberg, U.; Klassen, T.; Gutfleisch, O.; Bormann, R. *Scr. Mater*. **2007**, 56, 841.

(6) Graetz, J.; Reilly, J. J. *Scr. Mater*. **2007**, 56, 835.

(7) Yang R. T.; Wang, Y. *J. Am. Chem. Soc*. **2009**, 131, 4224.

(8) a) Strobel, R.; Garche, J.; Moseley, P. T.; Jorissen, L.; Wolf, G. *J. Power Sources* **2006**, 159, 781;

(9) a) Wong-Foy, A. G.; Matzger, A. J.; Yaghi, O. M. *J. Am. Chem. Soc*., **2006**, 128, 3494; b) Dailly, A.; Vajo, J. J.; Ahn, C. C. *J. Phys. Chem. B* **2006**, 110, 1099; c) Kaye, S. S.; Long, J. R. *J. Am. Chem. Soc*. **2005**, 127, 6506; d) Rosi, N. L.; Eckert, J.; Eddaoudi, M.; Vodak, D. T.; Kim, J.; O'Keeffe, M.; Yaghi, O. M. *Science* **2003**, 300, 1127.

(10) Yan, Y.; Lin, X.; Yang, S.; Blake, A. J.; Dailly, A.; Champness, N. R.; Hubberstey, P.; Schroeder, M. *Chem. Commun*. **2009**, 1025.

(11) a) Zhou, W.; Yildirim, T. *J. Phys. Chem. C* **2008**, 112, 8132; b) Dincă, M.; Dailly, A.; Liu, Y.; Brown, C. M.; Neumann, D. A.; Long, J. R. *J. Am. Chem. Soc*. **2006**, 128, 12876.

(12) a) Kubas, G. J.; Ryan, R. R.; Swanson, B. I.; Vergamini, P. J.; Wasserman, H. J. *J. Am. Chem. Soc*. **1984**, 106, 451; b) G. J. Kubas, *Chem. Rev*. **2007**, 107, 4152; b) Heinekey, D. M.; Lledós, A.; Lluch, J. M. *Chem. Soc. Rev*. **2004**, 33, 175.

(13) a) Vitillo, J. G.; Regli, L.; Chavan, S.; Ricchiardi, G.; Spoto, G.; Dietzel, P. D. C.; Bordiga, S.; Zecchina, A. *J. Am. Chem. Soc*. **2008**, 130, 8386; b) Dincă, M.; Long, J. R. *Angew. Chem. Int. Ed*. **2008**, 47, 6766.

(14) Zhao, Y.; Kim, Y.; Dillon, A. C.; Heben, M. J.; Zhang, S. B. *Phys. Rev. Lett*. **2005**, 94, 155504.

(15) Hoang, T. K. A.; Antonelli, D. M. *Adv. Mater*. **2009**, 21, 1787.

(16) Georgiev, P.A.; Albinati, A.; Mojet, B.L.; Ollivier, J.; Eckert, J. *J. Am. Chem. Soc*. **2007**, 129, 8086.

(17) Hamaed, A.; Trudeau, M.; Antonelli, D. M. *J. Am. Chem. Soc*. **2008**, 130, 6992.

(18) a) Hoang, T. K. A.; Hamaed, A.; Trudeau, M.; Antonelli, D. M. *J. Phys. Chem. C* **2009**, 113, 17240; b) Hu, X.; Trudeau, M.; Antonelli, D. M. *Chem. Mater*. **2007**, 19, 1388; c) Hamaed, A.; Hoang, T. K. A.; Trudeau, M.; Antonelli, D. M. *J. Organomet. Chem*. **2009**, 694, 2793.

(19) Hamaed, A.; Mai, H, V.; Hoang, T. K. A.; Trudeau, M.; Antonelli, D. M. *J. Phys. Chem. C* **2010**, 114, 8651.

(20) Skipper, C.; Hamaed, A.; Antonelli, D.; Kaltsoyannis, N. *J. Am. Chem. Soc.* **2010**, 132, 17296.

(21) Mai, H. V.; Hoang, T. K. A.; Hamaed, A.; Trudeau, M.; Antonelli, D. M. *Chem. Commun*. **2010**, 46, 3206.

(22) Hoang, T. K. A.; Webb, I. M.; Mai, H. V.; Hamaed, A.; Walsby, C. J.; Trudeau, M.; Antonelli, D. M. *J. Am. Chem. Soc*. **2010**, 132, 11792.

(23) Langmi, H. W.; Walton, A.; Ah-Mamouri, M. M.; Johnson, S. R.; Book, D.; Speight, J. D.; Edwards, P. P.; Gameson, I.; Anderson, P. A.; Harris, I. R. *J. Alloys and Compounds* **2003**, 356-357, 710.

(24) Seidel, V. W.; Kreisel, G. *Z. Anorg. Allg. Chem*. **1977**, 435, 146.

(25) Hu, X.; Skadtchenko, B. O.; Trudeau, M.; Antonelli, D. M. *J. Am. Chem. Soc.* **2006**, 128, 11740.

(26) Furukawa, H.; Miller, M. A.; Yaghi, O. *J. Mater. Chem*. **2007**, 17, 3197.

(27) Seidel, W.; Kreisel, G. *Z. Chem*. **1974**, 14, 25.

(28) Gregg, S. J.; Sing, K. S. W. Adsorption, Surface Area and Porosity. 2nd ed., Academic Press, London 1982, p41-42.

(29) Heinekey, D. M.; Oldham Jr, W. J. *Chem. Rev*. **1993**, 93, 913.

(30) Antonelli, D. M.; Schaefer, W. P., Parkin, G.; Bercaw, J. E. *J. of Organomet. Chem.* **1993**, *462*, 213.

(31) Groenenboom, C. J.; Sawatzky, G.; Meijer, H. J. D.; Jellinek, F. *J. Organometal. Chem*. **1974**, 76, C4 – C6.

(32) Horvath, B.; Strutz, J.; Geyer-Lippmann, J.; Horvath, E. G. *Z. Anorg. Allg. Chem*. **1981**, 483, 181.

(33) Kasperkiewicz, J.; Kovacich, J. A.; Lichtman, D. *J. Electron Spectrosc. Relat. Phenom*. **1983**, 32, 123.

(34) Wagner, C. D.; Riggs, W. M.; Davis, L. E.; Moulder, J. F.; Muilenberg, G. E. *Handbook of X-Ray Photoelectron Spectroscopy: Physical Electronics Division*, Perkin-Elmer Corp.: Eden Prairie, MN, 1979.

(35) Whelan, C. M.; Cecchet, F.; Baxter, R.; Zerbetto, F.; Clarkson, G. J.; Leigh, D. A.; Rudolf, P. *J. Phys. Chem. B* **2002**, 106, 8739.

(36) Sivastava, S.; Badrinarayanan, S.; Mukhedkar, A.J. *Polyhedron* **1985**, 4, 409.

(37) Batich, C. D.; Donald, D. S. *J. Am. Chem. Soc*. **1984**, 106, 2758.

(38) Gervais, M.; Douy, A.; Gallot, B.; Erre, R. *J. Colloid Interface Sci*. **1988**, 125, 146.

(39) Larkins, F. P.; Lubenfeld, A. *J. Electron Spectrosc. Relat. Phenom*. **1979**, 15, 137.

(40) Kafizas, A.; Hyett, G.; Parkin, I. P. *J. Mater. Chem*. **2009**, 19, 1399.

(41) Panella, B.; Hirscher, M.; Puetter, H.; Mueller, U. *Adv. Funct. Mat*. **2006**, 16, 520.

(42) a) Kang, J.; Wei, S. –H.; Kim, Y. –H. *J. Am. Chem. Soc*. **2010**, 132, 1510; b) Yamada, K.; Tanaka, H.; Yagashita, S.; Adachi, K.; Uemura, T.; Kitagawa, S.; Kawata, S. *Inorg. Chem*. **2006**, 45, 4322.

(43) Bender, B. R.; Kubas, G. J.; Jones, L. H.; Swanson, B. I.; Eckert, J.; Capps, K. B.; Hoff, C. D. *J. Am. Chem. Soc*. **1997**, 119, 9179.

(44) Murray, L. J.; Dincă, M.; Long, J. R. *Chem. Soc. Rev*. **2009**, 38, 1294.

(45) Kaye, S. S.; Long, J. R. *J. Am. Chem. Soc*. **2008**, 130, 806.

(46) Centrone, A.; Siberio-Pérez, D. Y.; Millward, A. R.; Yaghi, O. M.; Matzger, A. J.; Zerbi, G. *Chem. Phys. Lett.* **2005**, *411*, 516.

Supplemental Information for Chapter 6 – Kubas-Type Hydrogen Storage in V(III) Polymers Using Tri- and Tetradentate Bridging Ligands

Table S6.1: Elemental analysis results of synthetic vanadium samples.

Material	Vanadium (%)	Carbon (%)	Hydrogen (%)	Nitrogen (%)	Vanadium (%)[(a)]
V-Oxamide150	17.56	27.26	2.83	14.40	25.26
V-Oxalate150	18.34	33.21	3.09	N/A	23.53
H_2-V-Oxalate	18.36	32.63	3.18	N/A	25.13
V-Glycolate150	19.64	28.14	3.08	N/A	22.61
H_2-V-Glycolate	23.16	23.99	2.85	N/A	30.71
V-Glycolamide150	21.60	26.67	3.51	11.15	28.54

(a): From thermo-gravimetric analysis.

Table S6.2: Proposed unit formula of synthetic materials.

Material	Proposed chemical formula	Vanadium (%)	Carbon (%)	Hydrogen (%)	Nitrogen (%)
V-Oxamide150	$C_6H_9N_2O_3V$	24.48	34.63	4.35	13.46
V-Oxalate150	$C_{11}H_{11}O_4V$	19.73	51.18	4.30	N/A
*H_2-V-Oxalate	C_2HO_4V	36.39	17.16	0.72	N/A
V-Glycolate150	$C_{11}H_{13}O_3V$	20.86	54.11	5.37	N/A
*H_2-V-Glycolate	$C_2H_3O_3V$	40.43	19.07	2.40	N/A
V-Glycolamide150	$C_6H_{10}NO_3V$	26.11	36.94	5.17	7.18

* Hypothetical formulation based on complete hydrogenation of mesityl group from parent material.

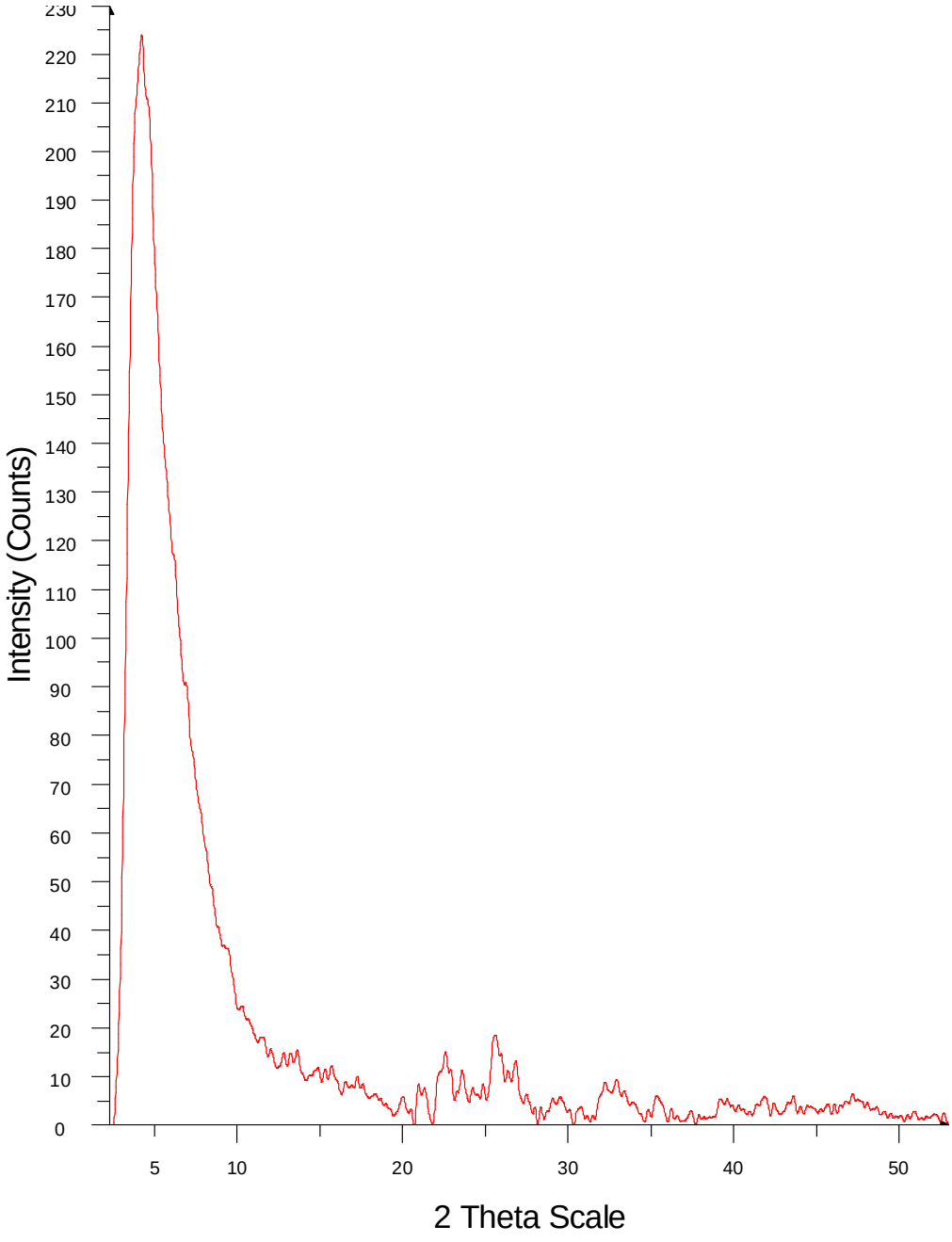

Figure S6.1a: Powder X-ray diffraction pattern of V-Oxamide150.

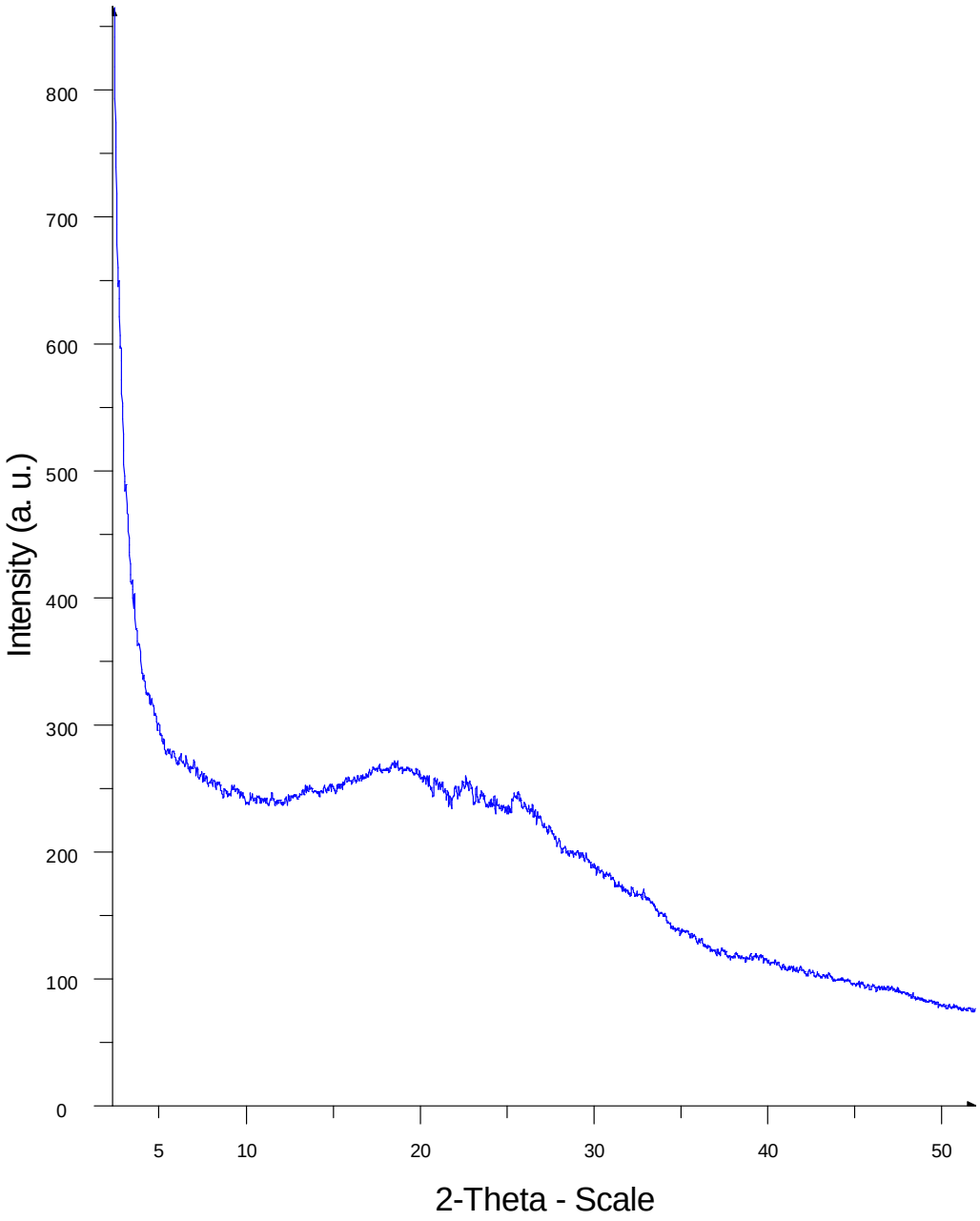

Figure S6.1b: Powder X-ray diffraction pattern of V-Oxalate150.

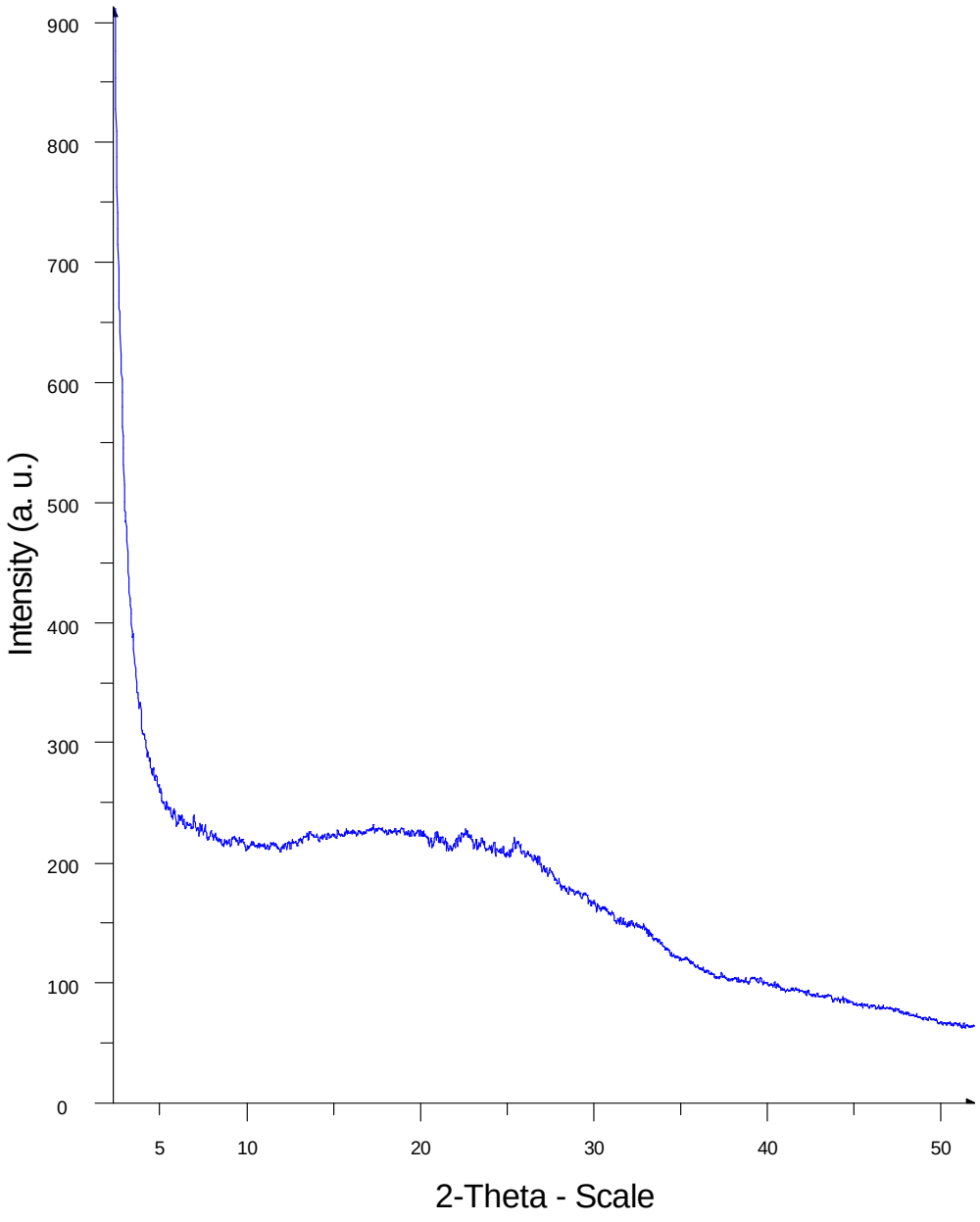

Figure S6.1c: Powder X-ray diffraction pattern of H_2-V-Oxalate150.

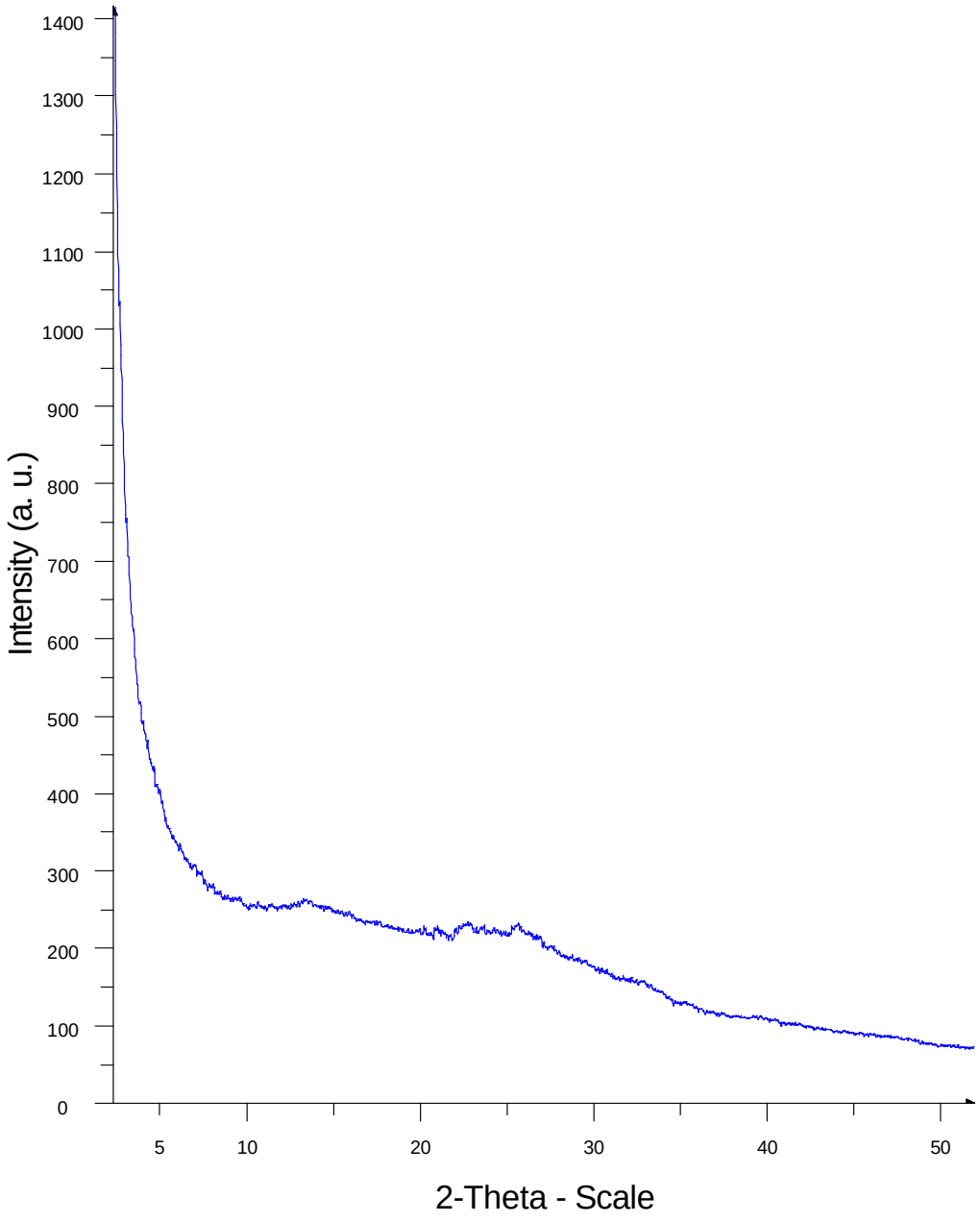

Figure S6.1d: Powder X-ray diffraction pattern of V-Glycolate150.

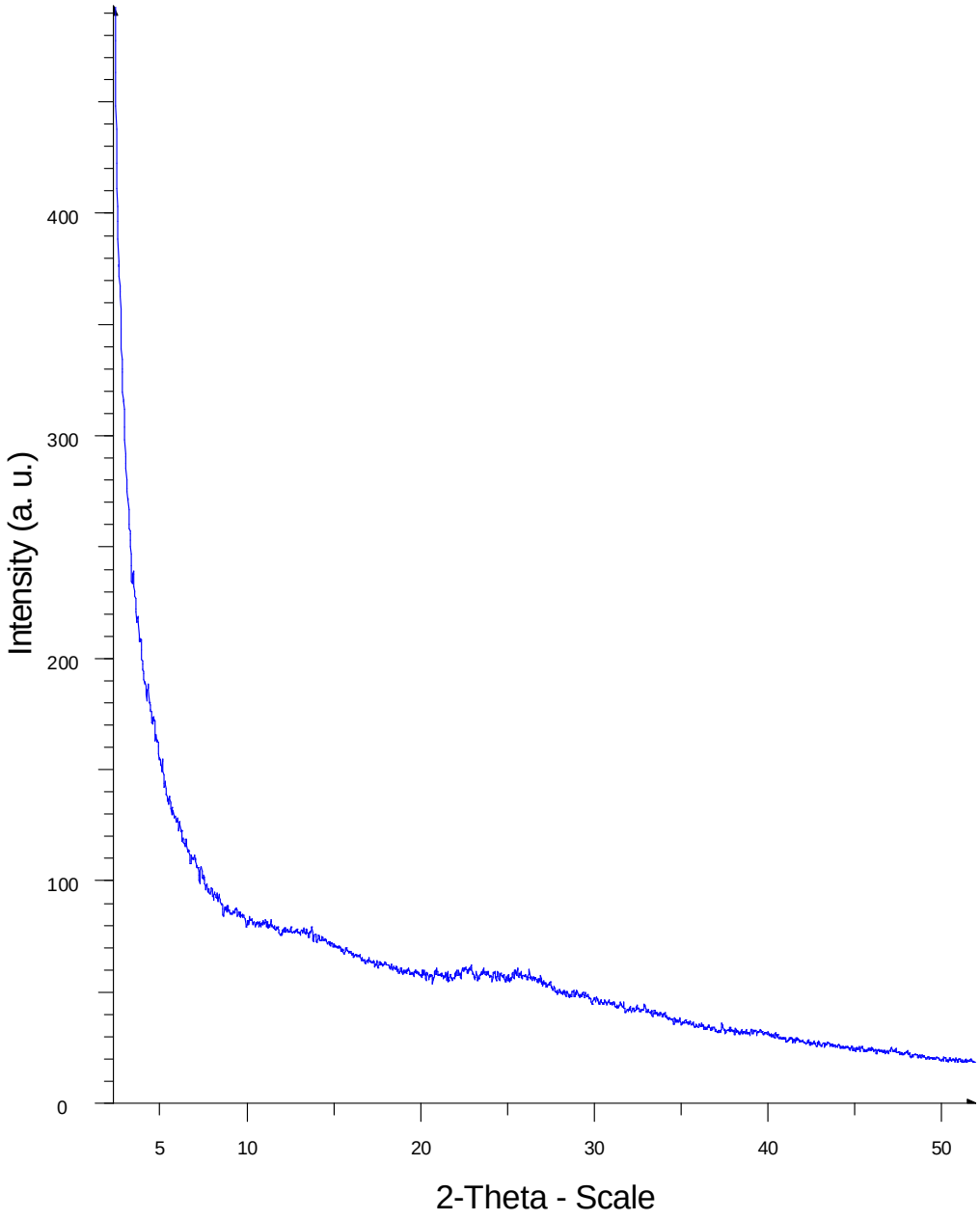

Figure S6.1e: Powder X-ray diffraction pattern of H_2-V-Glycolate150.

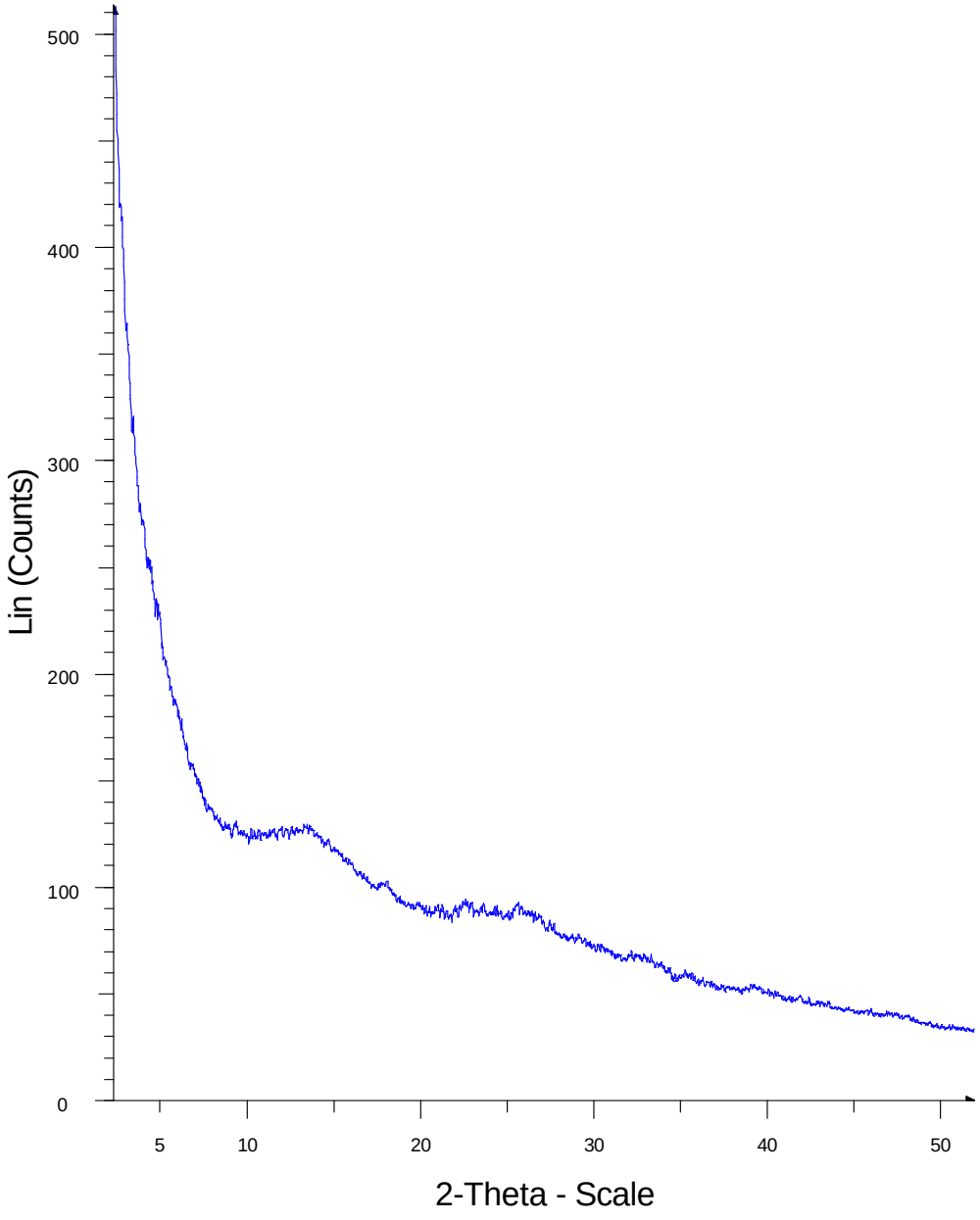

Figure S6.1f: Powder X-ray diffraction pattern of V-Glycolamide150.

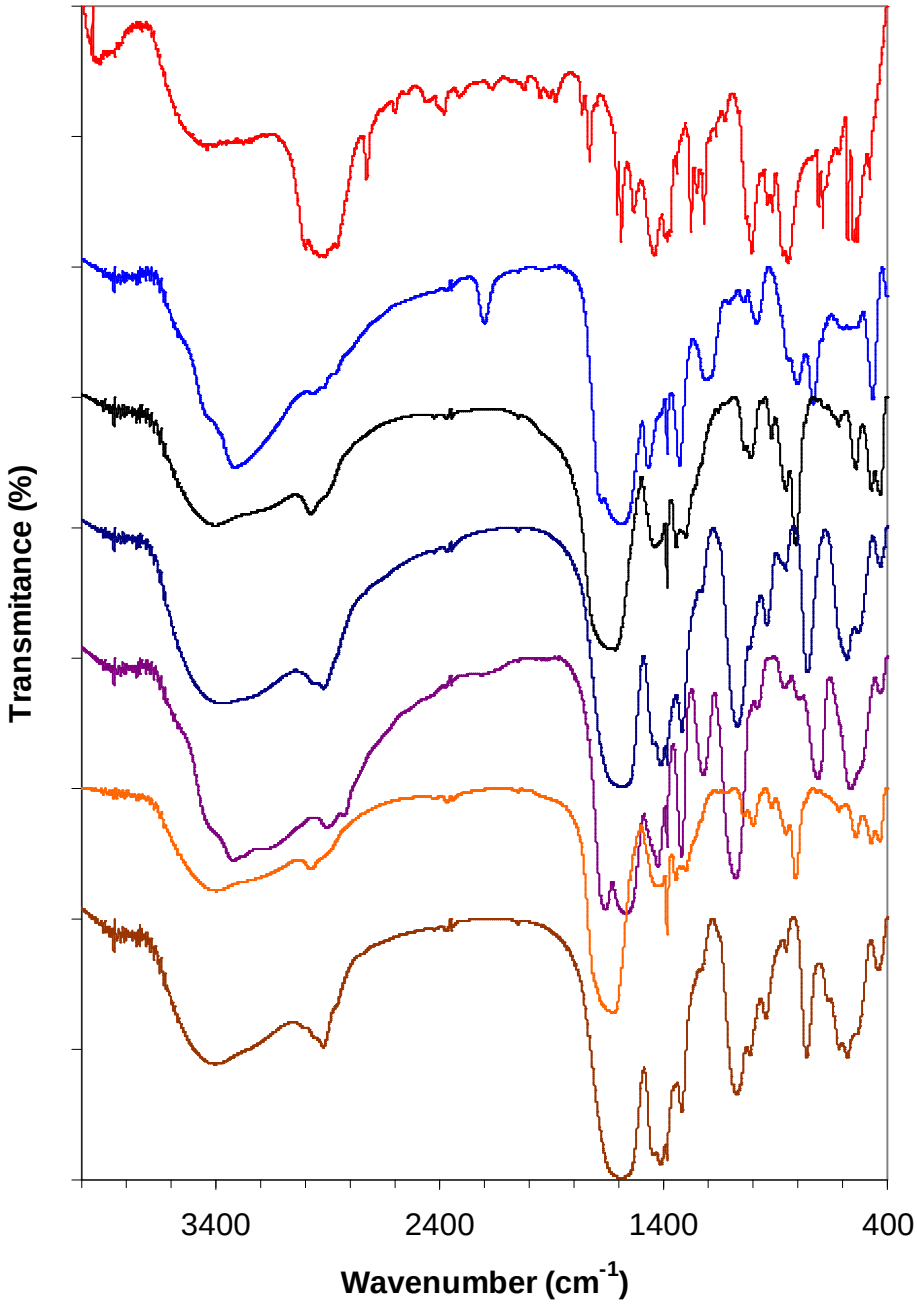

Figure S6.2: IR of all samples, from top to bottom: $V(Mes)_3$.THF, V-Oxamide150, V-Oxalate150, V-Glycolate150, V-Glycolamide150, H_2-V-Oxalate150, and H_2-V-Glycolate150.

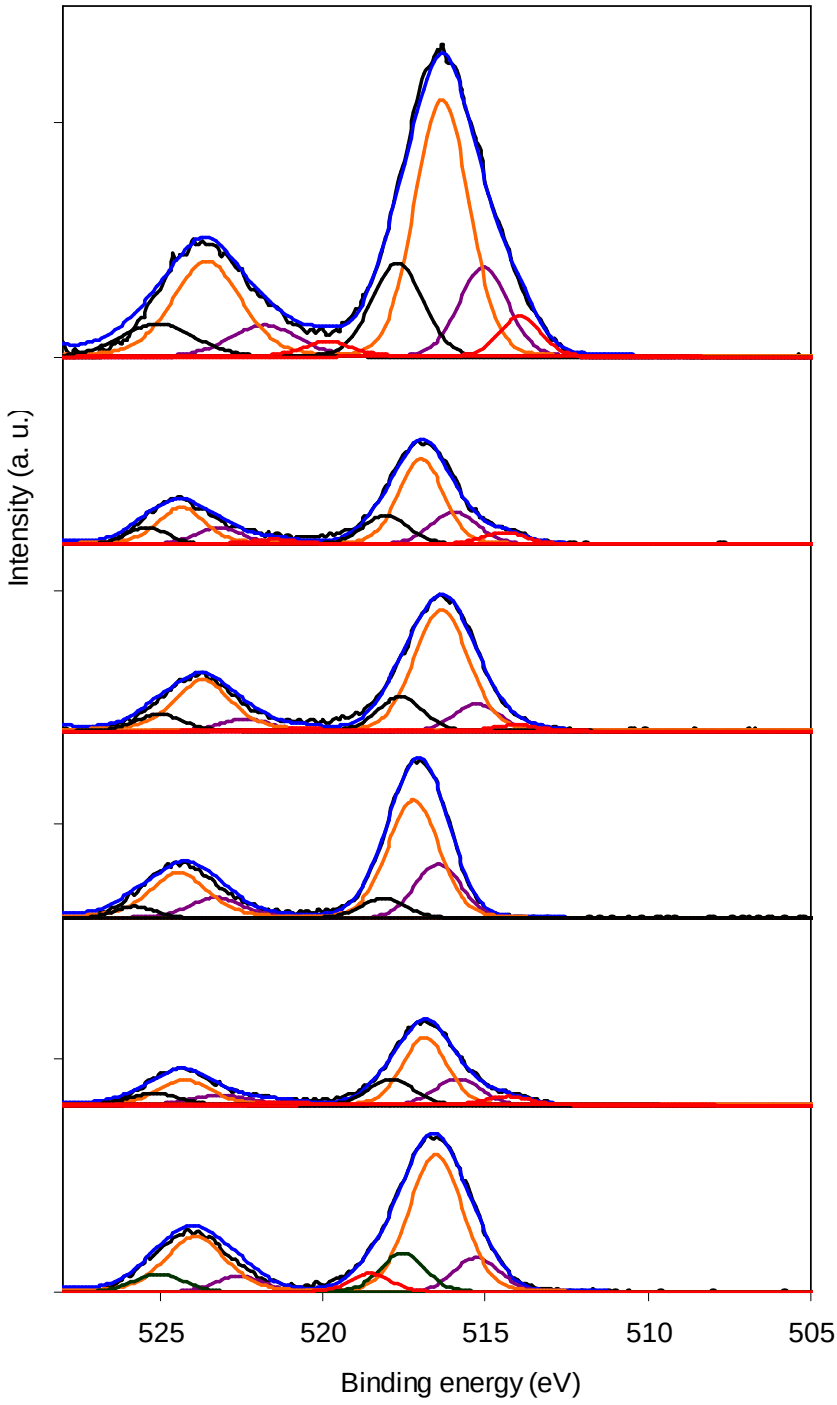

Figure S6.3: XPS of V 2p region of all samples, from top to bottom: V-Oxamide150, V-Oxalate150, V-Glycolate150, V-Glycolamide150, H_2-V-Oxalate150, and H_2-V-Glycolate150.

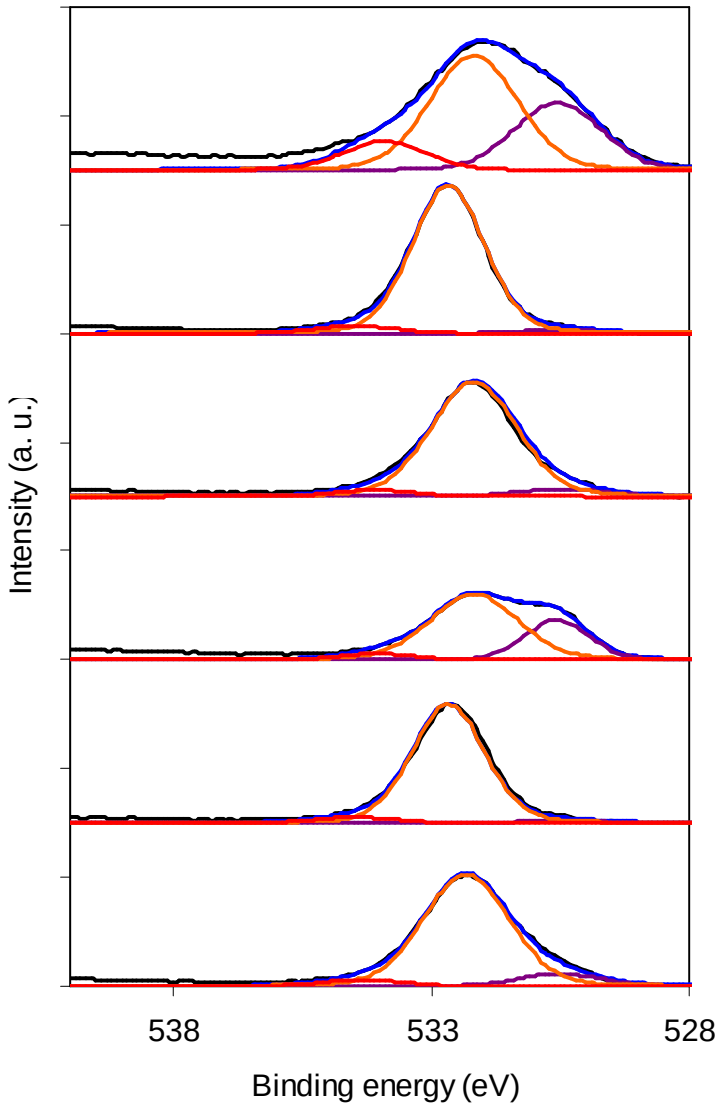

Figure S6.4: XPS of O 1s region of all samples, from top to bottom: V-Oxamide150, V-Oxalate150, V-Glycolate150, V-Glycolamide150, H_2-V-Oxalate150, and H_2-V-Glycolate150.

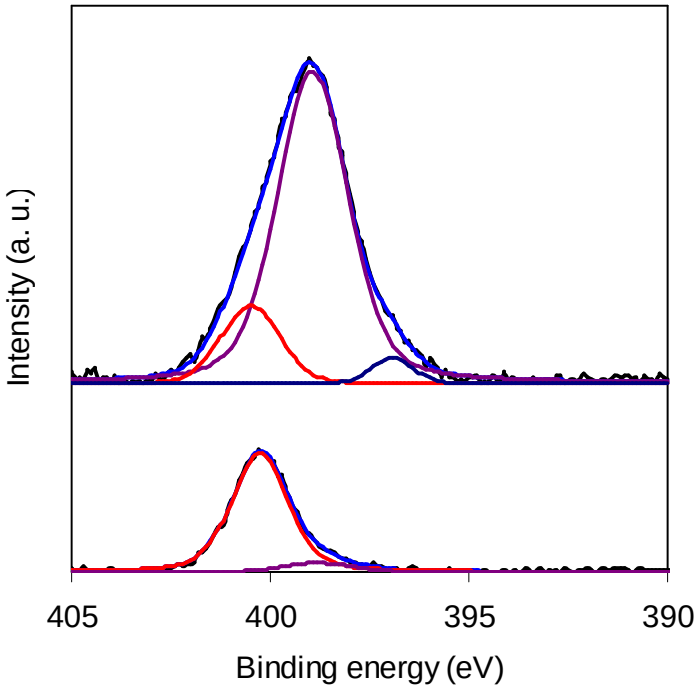

Figure S6.5: XPS of N 1s region of V-Oxamide150 (upper) and V-Glycolamide150 (lower).

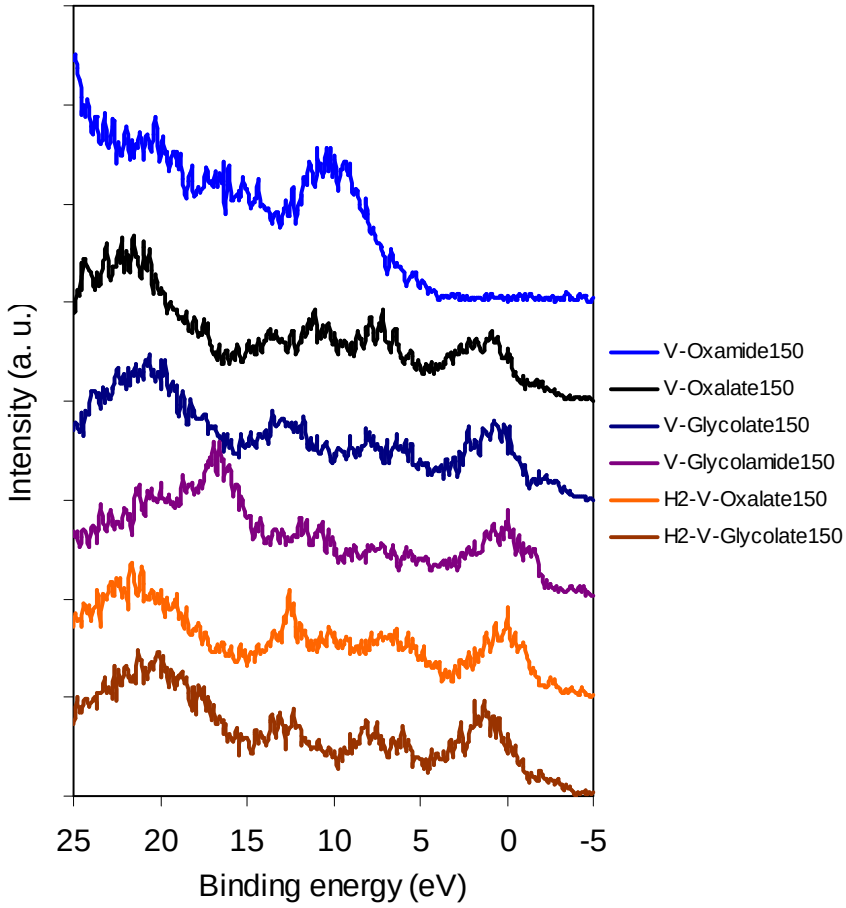

Figure S6.6: XPS at valence region of all samples activated at 150 ^{o}C in vacuum.

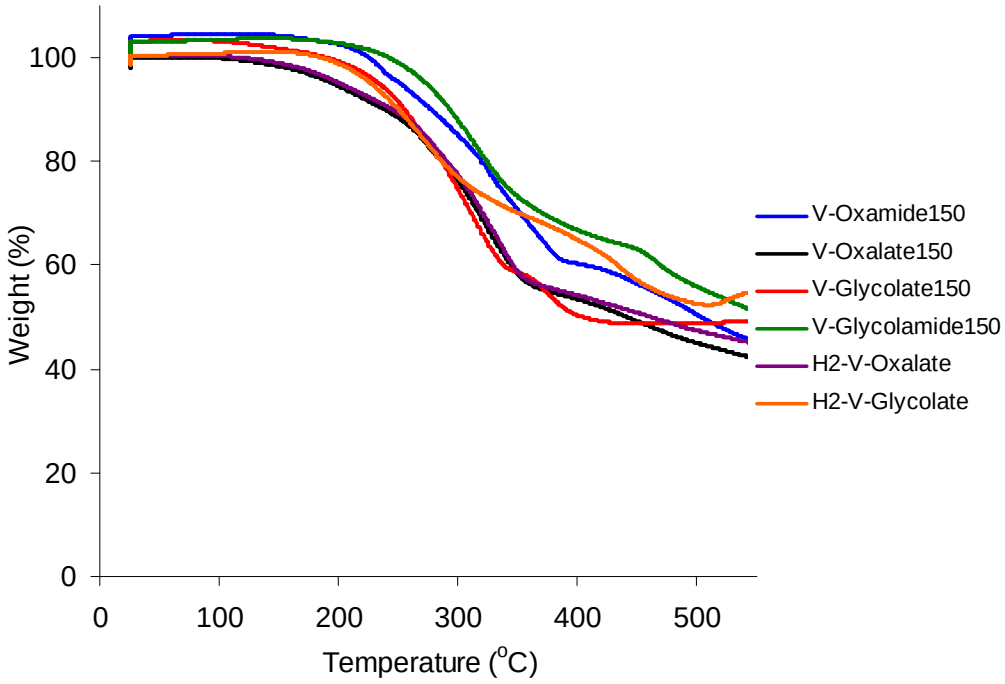

Figure S6.7: Thermo-gravimetric analysis results

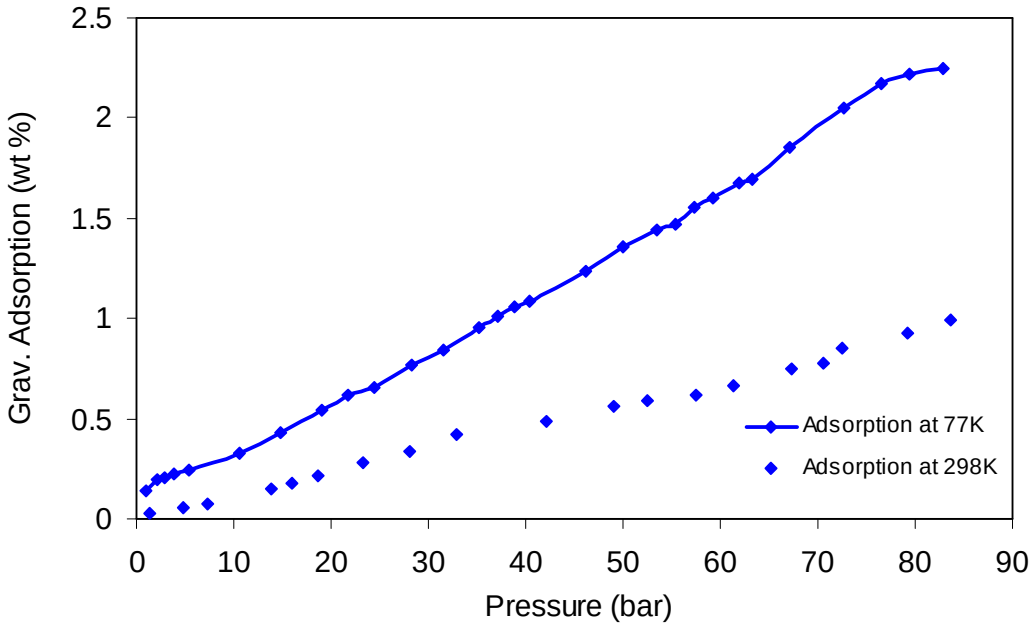

Figure S6.8: Adsorption of V-Oxamide150 compressed pellet.

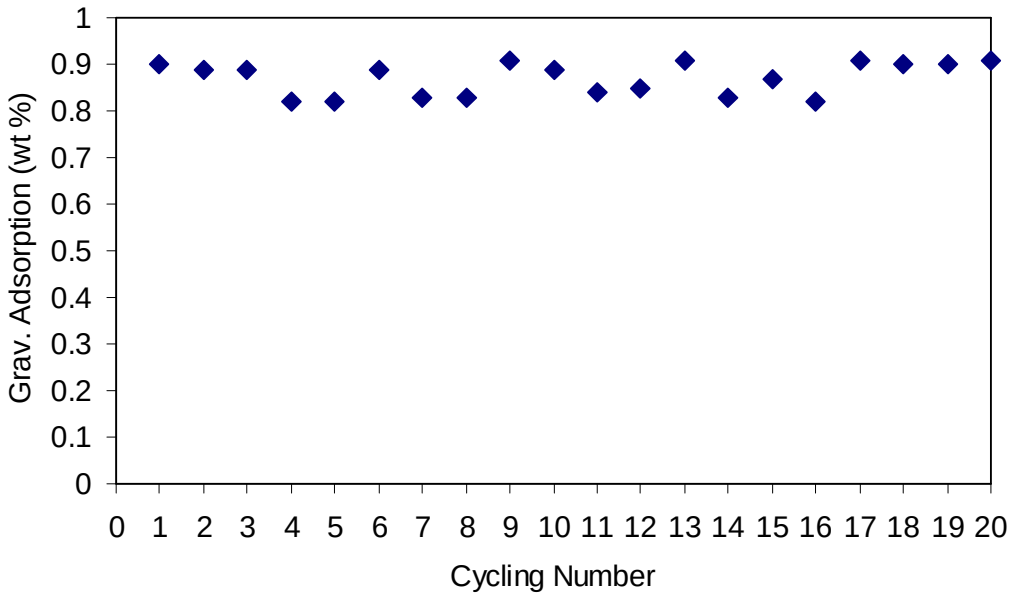

Figure S6.9: 20-cycle hydrogen adsorption run at room temperature of V-Oxamide150.

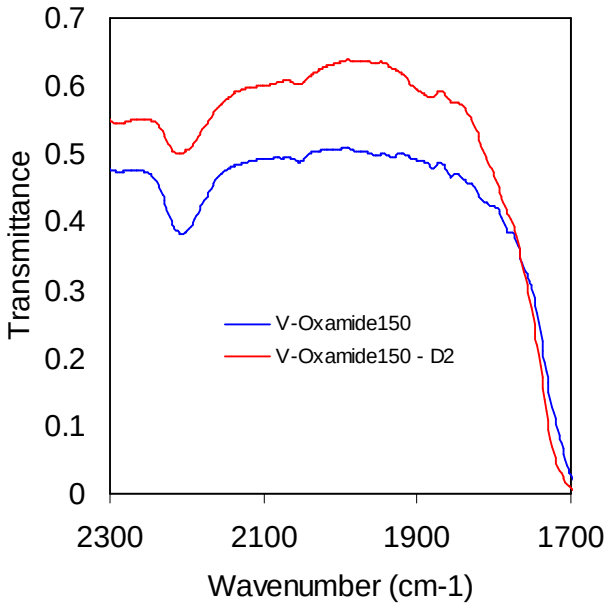

Figure S6.10: IR V-Oxamide150 before and after treatment with D_2.

Chapter 7 – The role of TiH_5 and TiH_7 in Ti(III) hydride gels for Kubas-type hydrogen storage

7.1 Introduction

Hydrogen is an ideal fuel because it is clean and renewable and possesses the highest amount of energy per gram (120 MJ/kg) of any chemical substance, and three times higher than that of conventional gasoline (44.4 MJ/kg).[1] However, methods for the safe and economical storage of hydrogen still remains elusive.[2] Many metal hydrides[3] contain enough hydrogen to satisfy the 2017 gravimetric (5.5 wt%) and volumetric (40 kg/m^3) targets established by the US Department of Energy (DOE), however sluggish kinetics and problems due to high enthalpies of adsorption (70 kJ/mol) pose a formidable challenge for these materials to be commercialized. New breakthrough in NH_3-BH_3 regeneration time of 24 hours by reaction with hydrazine in liquid ammonia is promising although is still higher than the refueling time demanded by the DOE (several minutes).[4] On the other hand, high surface area physi-sorbents absorb significant quantities of hydrogen at 77 K. For example the newly reported NU-100 adsorbs 9.05 wt % of hydrogen without any of the kinetic problems.[5] However, because of low heat of adsorption (≤ 10 kJ/mol), hydrogen molecules do not adhere strongly enough to the surface and thus up to 90% of the activity is lost at 298 K.[6] Because of the limitations of these technologies, researchers have begun to explore the potentials of weak chemisorption mechanisms, which provide an energy of H_2 interaction in the range of 20 – 30 kJ/mol, i. e. Kubas interaction,[7-11] or hypervalent main group hydrides.[12-15] Electron paramagnetic resonance (EPR) probed the existence of GeH_3, GeH_5, SiH_3, and SiH_5 at low temperature.[12] Theoretical studies on SiH_5, SiH_5^+, SiH_5^-, GeH_5^+ and GeH_7^+ hypervalent hydrides have suggested possible uses in hydrogen storage. For example, if converted to GeH_7, GeH_3 possesses a hydrogen adsorption performance of 5.0 wt %, close to the DOE 2017 goal. However this species cannot be synthesized in bulk, and to the best of our knowledge, GeH_9 or GeH_9^+ does not exist, clouding the hope of even higher hydrogen storage performance from hypervalent Ge hydrides. However, hypervalent hydrides of transition metals may offer new hope in this area. On the basis of

18 electron rule, a TiH_3 or VH_3 species could bind up to 5 intact hydrogen molecules, corresponding to 16.4 wt % or 15.6 wt%, respectively. These number are more than double the ultimate DOE goal (at 7.5 wt %). Traditional high pressure thermal treatment of metals do not allow the synthesis of hydrides in micro or mesoporous structures, which allow a minimal degree of void space while maintaining an effective diffusion rate of hydrogen in and out of the material lattices to the active binding sites. For this purpose, tris(alkyl) titanium (III) was chosen as precursor, because it is the only known Ti (III) alkyl stable at room temperature. From this compound, high surface area TiH_3 could be generated by the reaction between alkyl titanium(III) and hydrogen gas and tested for hydrogen storage as described in this chapter.

7.2 Experimental Section

All chemicals were purchased from Sigma-Aldrich and used as is. Diethyl ether and toluene were distilled over sodium/benzophenone to remove oxygen and moisture. Distilled solvents were transferred to a Schlenk flask using a canula. Dry Ar gas was bubbled through the flask for 30 min before transferring into a dry-box. Triethylamine was distilled over CaH_2 and bis(trimethylsilyl)methyl chloride was distilled over P_2O_5 before use. H_2 grade 6.0, N_2, Ar, and He were obtained from Praxair Canada. Manipulations were performed in an Ar glove box and on an Ar Schlenk line as low valent Ti species are extremely sensitive to air and moisture. $TiCl_3.0.67\{N(C_2H_5)_3\}$ was synthesized from the reaction of $TiCl_3$ and triethyl-amine.[1] $LiCH(SiMe_3)_2$ was prepared from $(Me_3Si)_2CHCl$ and Li. $Ti\{CH(SiMe_3)_2\}_3$ was prepared from $TiCl_3.0.67\{N(C_2H_5)_3\}$ and $LiCH(SiMe_3)_2$ as described from chapter 5. $Ti\{CH(SiMe_3)_2\}_3$ obtained from the previous reaction as a green viscous oil was quantified by weighing by difference.

7.2.1 Preparation of alkyl titanium hydride $TiH_{3-x}R_x$. 50 ml of toluene was added to 3.00g (5.7 mmol) of $Ti\{CH(SiMe_3)_2\}_3$ and stirring was started to create a green solution. Hydrogen gas grade 6.0 was passed over the solution at room temperature. The color changed to black after 24 h and dark green particles appeared. After 96 h, stirring was ceased, the system was filtered, and a solid was obtained, which was placed under vacuum at room temperature for 8 h at room temperature to give A25. A25 was heated

under vacuum for 8 h at 100 ^{o}C to yield A100. A150 was obtained by heating A100 material at 150 ^{o}C under vacuum for 8 h.

7.2.2 Hydrogenation of alkyl titanium hydride. 0.3000 g of A100 was added to the Advanced Materials PCI sample chamber, which was connected to the Gas Reaction Controller. Sample was soaked with H_2 at 5 bar and the temperature was raised to 150 ^{o}C before the H_2 pressure was adjusted to 80 bar. If these conditions were maintained for 2h (or 6h), the resulting materials were given annotation H150-2h (or H150-6h). The sample H180-2h was obtained using a similar process, during which temperature was kept at 180 ^{o}C for 2h. The times and conditions were chosen by monitoring the infrared spectra and using the 600 – 610 cm^{-1} asymmetric stretch of Ti - C bond and wagging vibration of C – Si bond at 835 – 845 cm^{-1} as a measure of hydrocarbon loss. After all hydrogenations vacuum was applied and the heating was continued for another 2h at 150 ^{o}C.

7.2.3 Characterization. Powder X-ray diffraction (PXRD) was performed on Siemens D-500 diffractometer with a Cu Kα radiation (40 kV, 40 mA) source. The step size was 0.02° and the counting time was 0.3s for each step. Diffraction patterns were recorded in the 2θ range 1.5 - 52°. Samples for PXRD analysis were placed in sealed glass capillary tube to protect samples from air and moisture during the experiment. Nitrogen adsorption and desorption data were collected on a Micromeritics ASAP 2010. All X-ray Photoelectron Spectroscopy (XPS) emissions were referenced to the carbon C-(C, H) emission at 284.8 eV, and the data were obtained using a Physical Electronics PHI-5500 spectrometer. Samples were loaded in an Ar glove box to maintain sample integrity. Elemental analysis (EA) was conducted using a Perkin – Elmer Series II CHNO/S 2400 Analyzer, calibrated with acetanilide standard. Samples for EA were loaded in a glove box, using tin capsules. Infrared spectroscopy was conducted on a Bruker Vector 22 instrument using Nujol. Thermo-gravimetric analysis was conducted on a Mettler Toledo TGA SDTA 851e, using helium (99.99%) as purging gas with the rate of 30 mL/min. Samples were held at 25 ^{o}C for 30 min before heating to 550 ^{o}C at a rate of 5 ^{o}C/min.

7.2.3 Hydrogen adsorption measurements. Measurement of hydrogen adsorption and enthalpy calculation are implemented exactly the same with chapter 5.

7.2.5 H_2/Ti Calculations. Calculations on titanium hydride samples were based on % Ti values obtained from the thermo-gravimetric analysis data from Table S7.1. As an example calculation, H150-2h absorbs 1.84 wt % of hydrogen at 85 bar and 298 K. This corresponds to 0.0184 g or 0.0092 mol of H_2 for 1 g of sample. Based on the 57.83 wt% Ti in the sample from Table S1, this translates into an average of 0.76 molecules of H_2 per metal center.

7.3 Results and Discussions

The materials studied in this paper were prepared by the reaction between tris{bis(trimethylsilyl)methyl}titanium(III) with hydrogen in dry toluene (Scheme 7.1). After 96 h stirring, the reaction mixture was filtered to obtain a black solid. This air and moisture sensitive material was placed under vacuum at 25 ^{o}C, 100 ^{o}C or 150 ^{o}C and the resulting materials named A25, A100 and A150, respectively. A100 materials were placed under 80 bar hydrogen pressure at 150 ^{o}C for 2 h or 6 h periods; or at 180 ^{o}C for 2 h before evacuation at 150 °C for 2 h. Prepared materials were given annotations H150-2h, H150-6h, or H180-2h,respectively.

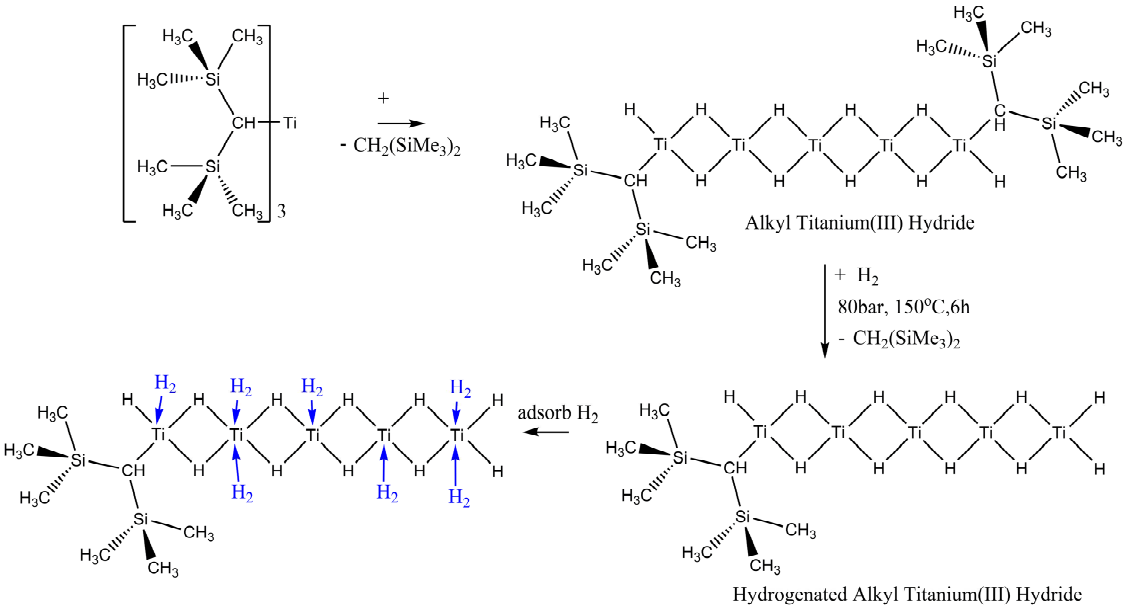

Scheme 7.1: Reaction between tris{bis(trimethylsilyl)methyl}titanium with hydrogen and hydrogenation of alkyl titanium hydrides.

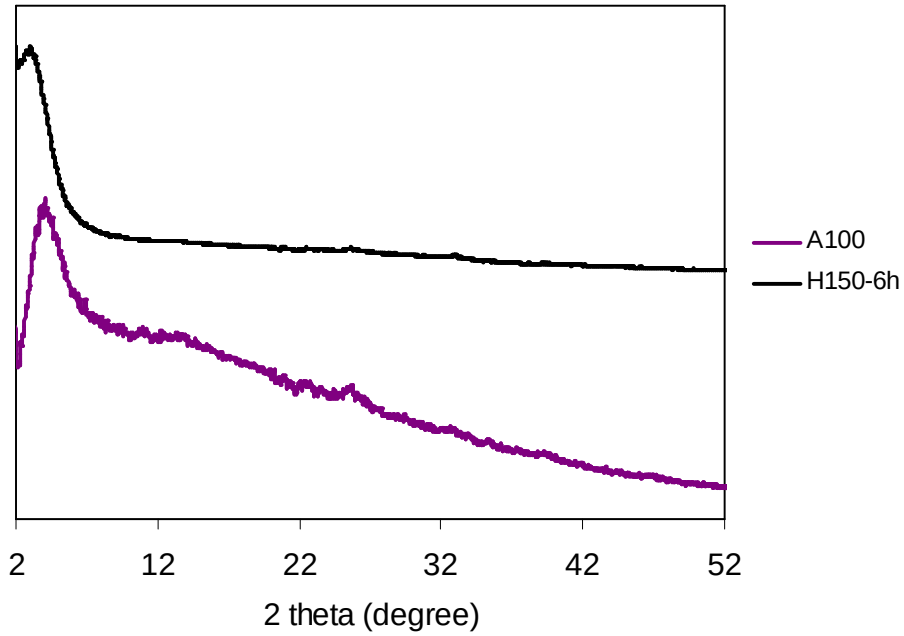

Figure 7.1: Powder X-ray diffraction of A100 and H150-6h materials

The powder x-ray diffraction (PXRD) patterns for the A100 and H150-6h are shown in Figure 7.1. Two patterns are similar and exhibit a single broad diffraction peak between 2θ of 3 – 5°, corresponding to a $d_{spacing}$ of 2.19 nm for A100 and 2.91 nm for H150-6h. The position and broadness of this reflection suggests nanoscopic periodicity, possibly related to microporosity, with a lack of long-range order. There are small broad reflections from 20-25 °2θ, likely due to crystalline TiH_3 that has begun to form from heating, however these reflections could not be indexed to any known pattern.

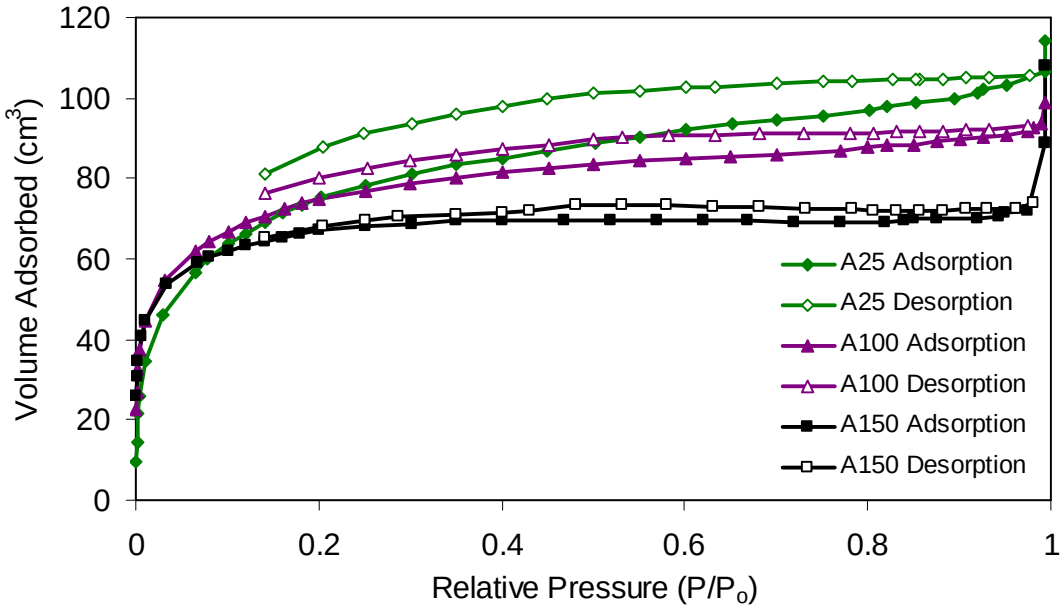

Figure 7.2a: Nitrogen adsorption – desorption isotherms of alkyl titanium hydride materials. Samples were measured on an ASAP-2010 instrument at 77 K.

Nitrogen adsorption isotherms recorded at 77 K are shown in figure 7.2. These isotherms confirm that both materials before and after hydrogenation are microporous, as reflected in the steep increases in volume adsorbed at low P/P_o relative pressure. The specific surface areas of all materials decrease with increasing the drying temperature from 25 to 150 ^oC. For example, A25 possesses a Brunauer – Emmett – Teller (BET) surface area of 276 m^2/g, but when heated under vacuum to 150 ^oC, the surface area decreases to 232 m^2/g. However, hydrogenation leads to enhancements of BET. For example, the A100 possesses a BET of 265 m^2/g, which increases to 499 m^2/g after hydrogenation at 80 bar hydrogen pressure, 150 ^oC, and 2 hours. However prolonged heating to 6h under these conditions leads to lowering of surface area to 310 m^2/g. This is consistent with hydrogenation opening up pore space by eliminating bulky alkyl groups, followed by slow structural collapse due to excessive thermal treatment.

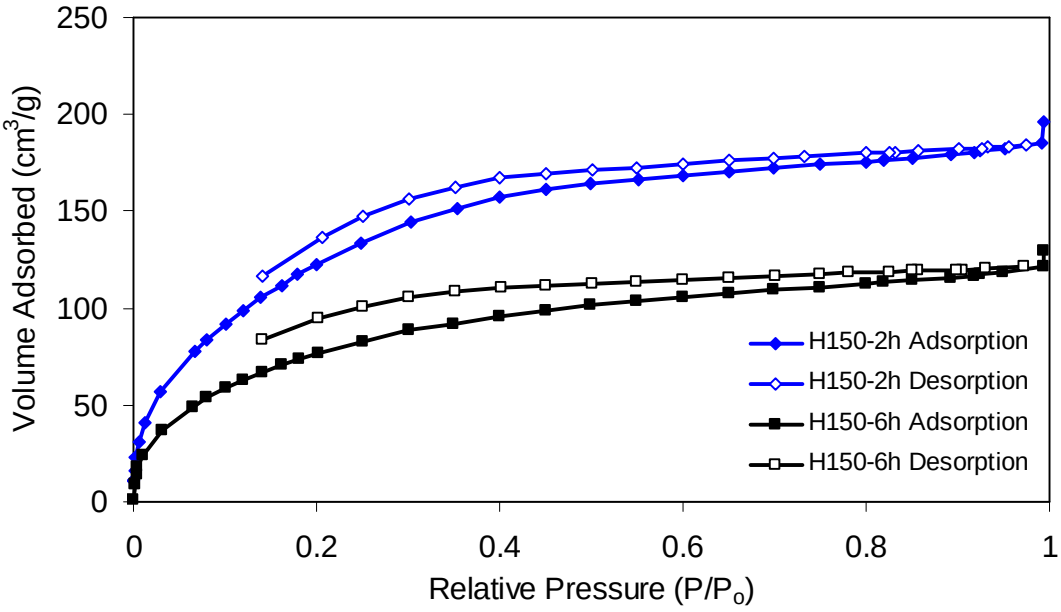

Figure 7.2b: Nitrogen adsorption – desorption isotherms of hydrogenated alkyl titanium hydride materials. Samples were measured on an ASAP-2010 instrument at 77 K.

Heating the sample under vacuum leads to progressive alkyl elimination as monitored by IR spectroscopy (ν_{as}(Ti-C) at 600 – 610 cm^{-1}), presumably by thermally driving the σ-bond metathesis reaction between tris{bis(trimethylsilyl)methyl}titanium(III) and hydrogen further towards completion. A broad band at 1600 - 1655 cm^{-1} is also observed, corresponding to a Ti-H. Previous studies on TiH, TiH_2, TiH_3, and TiH_4 made by high-energy laser ablation provided a Ti-H for TiH_3 at 1580.6 cm^{-1}.[16] This is different from our result, suggesting the amorphous porous structure in our study is different than that of the close packed TiH_3 synthesized in this previous report. The C, and H elemental analysis (EA) data of titanium materials are shown in table S7.1. Titanium concentration was determined by thermo-gravimetric analysis (TGA), which is discussed below. Table S7,2 provides the formulas and C, H, and Ti percentages of the hydrogenated materials in addition to those of representative stoichiometric compounds, including pure TiH_3 and starting material. From these data it can be determined that H150-6h has a chemical formula of $Ti\{CH(SiMe_3)_2\}_{0.22}H_{2.78}$, with roughly one alkyl group remaining for every five Ti centers. By comparison A100 retains 0.45 alkyl groups per Ti, consistent with a lower degree of hydrogenation. Thermo-gravimetric analysis (TGA) results of A100 and

H150-6h are presented in figure 7.3. A slight oxidation leading to weight gain of ~2 – 5 wt% was observed initially during the iso-thermal period before the mass began to decrease with temperature ramping. When heating was finished at 550 °C, H150-6h retains 96.59 wt% while A100 retains 66.45 wt%. These results were expected on the basis of the EA and IR, which show that A100 contains significantly more hydrocarbon than H150-6h.

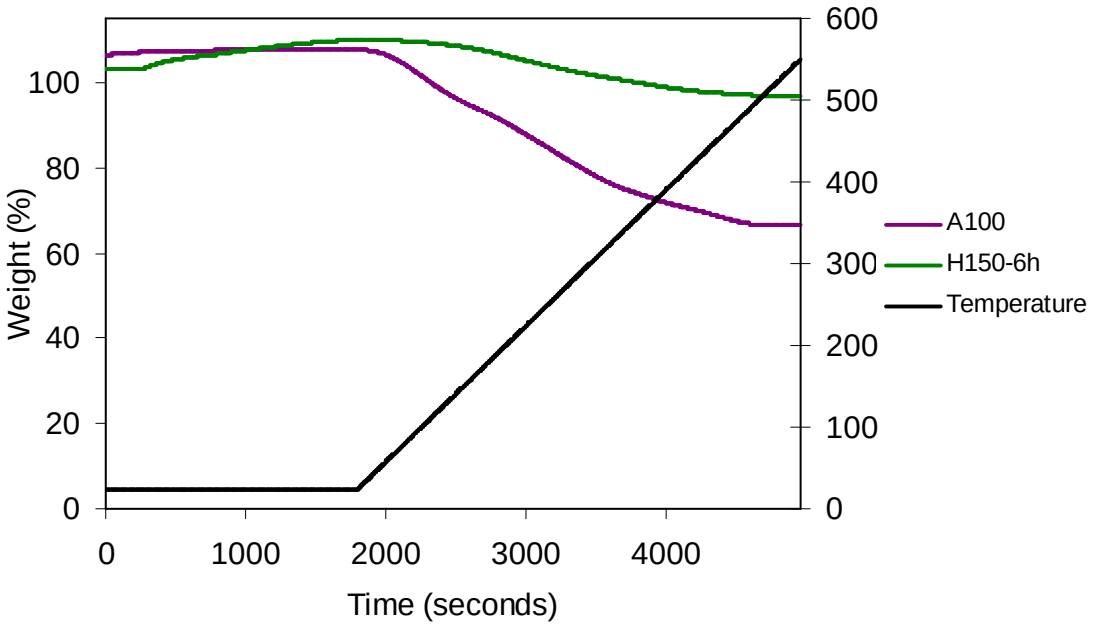

Figure 7.3: Thermo-gravimetric analysis results of A100 and H150-6h materials.

X-ray Photoelectron Spectroscopy (XPS) studies of the titanium containing materials were conducted and the results are shown in figure 7.4 and S7.3, S7.4. No charge neutralization was required and emissions are observed close to the Fermi level, suggesting that these materials are semi-metals or semiconductors (Figure S7.3). Two major emissions are observed in the Ti 2p region, which could be deconvoluted into two species for A100 and three species for H150-6h (Figure S7.4). By comparison with literature values, the emissions at 458.0 eV and 463.5 eV correspond to Ti(III) species, possibly with only two hydride ligands, consistent with 0.22 and 0.45 alkyl groups remaining for H150-6h and A100, respectively; while the emission at 456.1 eV and 460.9 eV can be assigned to a Ti(III) species in which all three alkyl groups have been replaced

by a hydride. These assignments are reasonable for several reasons. First, all Ti(IV) species have the main XPS emission of Ti 2p 3/2 at above 480.3 eV;[17] second, the Ti 3p emission of Ti(IV) falls at 37.5 eV[18] while an emission at 36.5 eV was observed for A100 and H1506h (Fig. S6); third, Ti – H emission is observed in the IR of both A100 and H150-6h at 1600 cm^{-1} (Fig. S10e-h). The third emission observed on H150-6h materials at 454.5 eV and 458.8 eV could be assigned to a second Ti hydride, possibly terminal rather than bridging.[19]

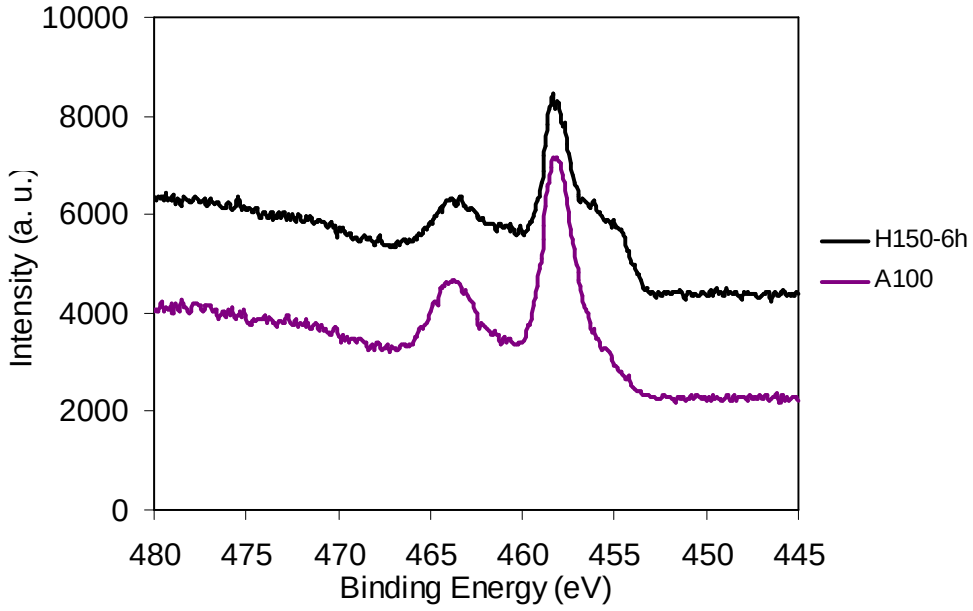

Figure 7.4: Titanium 2p1/2 and 2p3/2 region of XPS spectrum of A100 and H150-6h materials.

The excess gravimetric storage isotherms of A-series materials are shown in figure S7.5 and those of H-series materials are shown in figure 7.5. Linear adsorption behavior versus pressure was observed for all materials in A- and H-series, both at 77 K and 298 K, which is considered not a typical for physisorption and has been observed and described in previous work by our group on transition metal hydrazides.[20] The gravimetric and volumetric adsorption without saturation of H150-6h is 1.84 wt. % at 85 bar and 298 K, with a volumetric density of 23.4 kg H_2/m^3. This value is over three times that of compressed gas under the same conditions. At 77 K, this sample adsorbs 2.80 wt. %, and 36 kg H_2/m^3. This volumetric performance is greater than that of MOF-177, which is at

32 kg/m^3.[21] Hysteresis were observed on all samples in H-series at 77 K (but not 298 K) and vacuum was required to drive out the ~35% adsorption capacity remaining at the end of adsorption – desorption cycles. Generally, hydrogenation at 150 ^oC for 2 – 6 h at 80 bar hydrogen pressure, followed by a 2 h evacuation at 150 ^oC provides materials with the best adsorption performance. By comparing the gravimetric adsorption at 298 K and 77 K, the retentions of excess adsorption capacities can be calculated, and range from 39-88 %. This is much higher than that of MOF-5 and carbon AX-21, which retain 5.5 % and 13.2 %, respectively, and compares to the levels of Cr hydrazides in which the Kubas interaction was shown to be responsible for adsorption.[22]

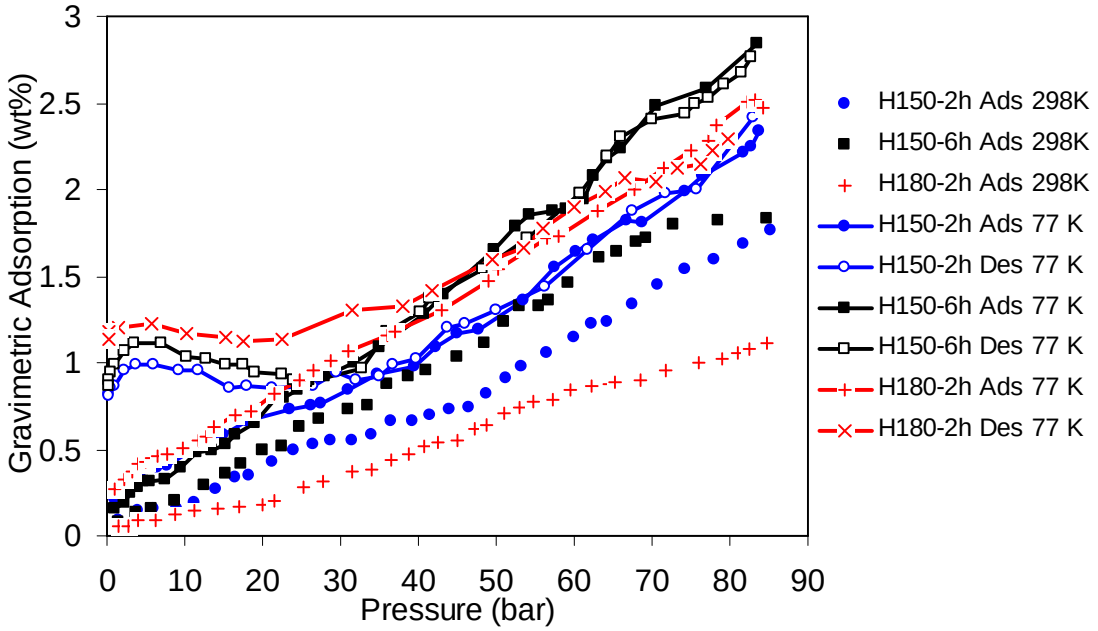

Figure 7.5: Hydrogen adsorption – desorption excess storage isotherms of H-series materials. Samples at 77 K run immediately after samples at 298 K.

Void space was removed from H150-6h sample by a compression at 500 psi and the compressed materials exhibit 1.34 wt% or 2.63 wt% at 298 K or 77 K and 85 bar, respectively, demonstrating that compression does not lead to enhanced performance as it does for the hydrazides, possibly because of loss of surface area or collapse of the structure. Calculations on the basis of gravimetric adsorption and the titanium content in each sample result in an average number of hydrogen molecules per titanium atom (table 7.2) ranging from 1.16 – 1.39 H_2/Ti at 77 K and 0.64 – 0.76 H_2/Ti at 298 K and 85 bar.

These are lower than the values observed for silica-supported titanium,[23] vanadium,[24] and chromium[25] species, but comparable with that of vanadium and chromium hydrazide materials.[20,22]

Table 7.1: Summary of Excess Storage Results of A-series and H-series materials and Carbon AX-21, MOF-5.

Material	BET Surface Area (m^2/g)	Skeletal Density (g/cm^3)	Gravimetric Adsorption (wt. %)	True Volumetric Adsorption (kg/m^3)	Retention (%)
A25	276	1.4120	1.13 (at 77 K) 1.00 (at 298 K)	16 (at 77 K) 14.1 (at 298 K)	88
A100	265	1.3308	2.32 (at 77 K) 1.06 (at 298 K)	31 (at 77 K) 14.1 (at 298 K)	46
A150	232	1.5730	1.72 (at 77 K) 1.03 (at 298 K)	27 (at 77 K) 16.2 (at 298 K)	60
H150-2h	499	0.9879	2.34 (at 77 K) 1.77 (at 298 K)	23 (at 77 K) 17.5 (at 298 K)	76
H150-6h	310	1.2703	2.80 (at 77 K) 1.84 (at 298 K)	36 (at 77 K) 23.4 (at 298 K)	66
H180-2h	N/A	1.1237	2.76 (at 77 K) 1.09 (at 298 K)	31 (at 77 K) 12.2 (at 298 K)	39
AX-21	3225	2.1030	4.2 (at 77 K, 65 bar) 0.55 (at 298 K)	14 (at 77 K, 65 bar) -	13
MOF-5	3534		5.10 (at 77 K) 0.28 (at 298 K)		5.5

Excess storage isotherms up to 140 bar for H160-6h recorded on a PCT-Pro are shown in Figure 7.6 and show 3.49 wt % at 298 K, rising in a linear fashion without any evidence of saturation. This corresponds to a volumetric density of 44.3 kg/m^3, 3.88 times higher than compressed hydrogen at the same conditions (11.4 kg/m^3 according to ideal gas law). Taking into account 57.83 % Ti in the materials, we can calculate an average

number of H_2 per Ti center of 1.44 H_2/Ti under these conditions. Considering further gains could be made by eliminating the remaining hydrocarbon, on the basis of the difference in molar mass between TiH_3 and H150-6h, a value of 5.8 wt% without saturation could be expected at 298 K and 140 bar on the basis of weight difference alone, disregarding any other effects of removing the last traces of hydrocarbon.

Table 7.2: Average number H_2 adsorbed per Ti site at 85 bar using TGA data.

Sample	Number of H_2/Ti at 77 K	Number of H_2/Ti at 298 K
A100	1.39	0.64
A150-6h	1.16	0.76

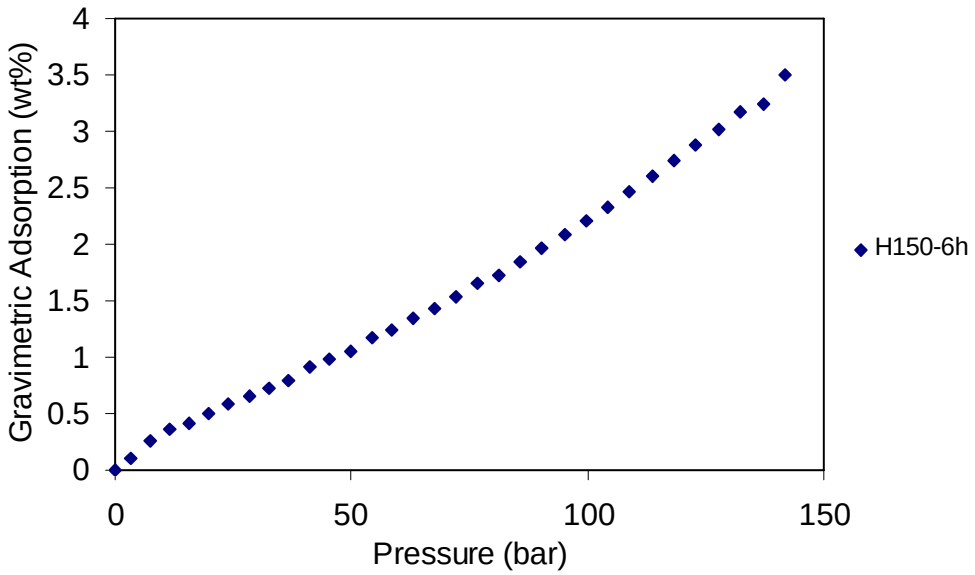

Figure 7.6: Adsorption up to 140 bar of H150-6h materials on a PCT-Pro instrument.

By fitting the adsorption isotherms at 77 K and 87 K into the Clapeyron – Clausius equation, the isosteric heats of hydrogen adsorption can be calculated for both A- and H-series materials (figure 7.2) as well as that of carbon AX-21 as an external standard measured under the same conditions (figure S7.1-7.2) to ensure the highest level of veracity in the measurements.[26,27] The isoteric heat of adsorption of all materials rises from a low of ~3 kJ/mol H_2 for A25 up to a maximum of 32 kJ/mol H_2 for A100, contrasting strongly to the behavior of AX-21, which has enthalpies which decrease from 6 kJ/mol H_2 to 3.3 kJ/mol H_2, typical of physisorption. The average value of V, Cr, and

Mn hydrazide materials made in our group falls in the range of 20 – 30 kJ/mol H_2,[20, 22, 28] which was believed to be the ideal range of adsorption enthalpy for suitable room temperature hydrogen storage.[7] The rising enthalpies with surface coverage were observed in all previous publications from our group concerning hydrogen storage on both supported organometallic fragments and transition metal hydrazides. This behavior was attributed to the Kubas interaction on the basis of Raman and ESR evidence for V[20] and Cr[22] hydrazides, respectively. Computational work has demonstrated that partial charges on metal centers play an indispensable role.[29] After the adsorption of the first hydrogen molecule through Kubas bonding, this partial charge is diminished and thus more backbonding from the metal d system into the H-H antibonding orbital is more favorable, strengthening the interaction for subsequent hydrogens.[30]

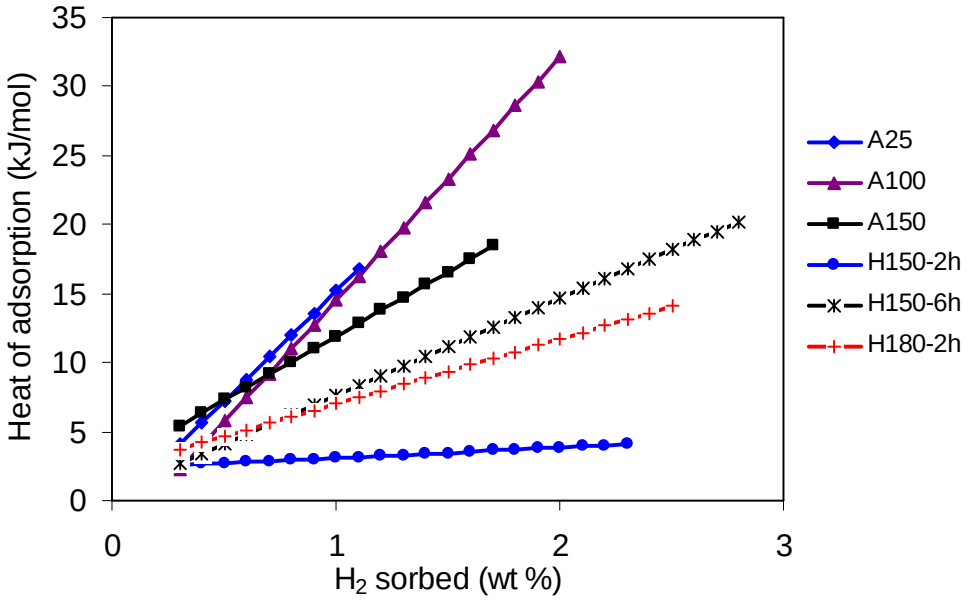

Figure 7.7: Heat of hydrogen adsorption on A-series and H-series materials.

Spectroscopies for the elucidating of the adsorption mechanism are being conducted. At 85 bar and 298 K 0.76 H_2 are absorbed, suggesting the presence of hypervalent TiH_5 under these conditions, since absorption is attributed to reversible non-dissociative binding of H_2 to the Ti centers. At 77 K and 85 bar, or 140 bar and 298 K, more than one H_2 per Ti is absorbed, invoking the presence of TiH_7 in some regions of the sample under these conditions, assuming reversible binding of a second H_2 to the Ti center. This is

reasonable on the basis of calculations demonstrating up to 5 H_2/Ti(III) in some cases. The existence of metastable hypervalent transition metal hydrides is exciting, given that such species have been confined to main group systems, and predominantly in the gas phase, or as transient entities only.

7.4 Conclusions

Titanium (III) hydride gels constitute a new class of hydrogen storage materials distinct from traditional hydrides or physi-sorbents. In this structure the hydride ligands are a lightweight structural feature as opposed to a source of stored hydrogen, and additional hydrogen can bind via the Kubas interaction to access hypervalent TiH_5 and TiH_7 species, to our knowledge the first solid state hypervalent hydrides ever isolated. Our best materials could adsorb up to 3.49 wt % of hydrogen, approaching the DOE 2017 target at 5.5 wt %. This adsorption performance can possibly be enhanced at a higher adsorption pressure or further optimization of synthetic pathway to arrive in materials with lower hydrocarbon content and higher concentration of Ti while maintaining the microporous structure. Moreover, by extending this class of materials to other transition metal hydrides with different 3d electron structures and different oxidation states, better hydrogen storage materials could be discovered and developed and it is likely that higher storage capacities will be realized. Since the pressures used in this study fall short of the 200 bar normally used in the hydrogen transport industry, it is likely that higher pressures at room temperature will lead to performance closer to the ultimate DOE goals. Furthermore, the calculated enthalpies of these hydrides favor room temperature hydrogen binding and are not too strong to create heat management issues. These materials can potentially be used in commercially available compressed hydrogen gas tanks and operate under the same working conditions of these tanks; with three to four times higher in storage capacities. Since hydrogen storage has been identified as the key problem in realizing the widespread use of hydrogen as a fuel, this new class of materials may show applications in the implementation into actual vehicles and power systems.

Supporting Information Available. X-ray powder diffraction, elemental analysis tables, simulated X-ray photoelectron spectra for titanium and nitrogen, hydrogen adsorption

isotherms at 77 K and 298 K for non-hydrogenated samples, infrared red spectra of titanium hydrazide materials and the $LiCH(SiMe_3)_2$ precursor, $Ti\{CH(SiMe_3)_2\}_3$.

7.5 References

(1) Hoffmann, P. Tomorrow's Energy Hydrogen, Fuel Cells, and the Prospects for a Cleaner Planet. The MIT Press Cambridge, Massachusetts and London, England (2001).

(2) Schlapbach, L.; Zuettel, A. *Nature* **2001**, 414, 353.

3. Orimo, S., Nakamori, Y., Eliseo, J. R., Zuettel, A., Jensen, C. M. *Chem. Rev*. **2007**, 107, 4111.

(4) Sutton, A. D.; Burrell, A. K.; Dixon, D. A.; Garner III, E. B.; Gordon, J. C.; Nakagawa, T.; Ott, K. C.; Robinson, P.; Vasiliu, M. *Science* **2011**, 331, 1426.

(5) Farha, O. F.; Ozgur Yazaydin, A.; Eryazici, I.; Malliakas, C. D.; Hauser, B. G.; Katnatzidis, M. G.; Nguyen, S. T.; Snurr, R. Q.; Hupp, J. T. *Nature Chemistry* **2010**, 2, 944.

(6) Yan, Y., Lin, X., Yang, S., Blake, A. J., Dailly, A., Champness, N. R., Hubberstey, P., Schroeder, M. *Chem. Commun*. **2009**, 1025.

(7) Vitillo, J. G., Regli, L., Chavan, S., Ricchiardi, G., Spoto, G., Dietzel, P. D. C., Bordiga, S., Zecchina, A. *J. Am. Chem. Soc*. 2008, 130, 8386.

(8) Kubas, G. *Chem. Rev*. **2007**, 107, 4152.

(9) Zhao, Y., Kim, Y., Dillon, A. C., Heben, M. J., Zhang, S. B. *Phys. Rev. Lett*. 2005, 94, 155504.

(10) Hoang, T. K. A., Antonelli, D. M. *Adv. Mater*. **2009**, 21, 1787.

(11) Heinekey, D. M., Oldham Jr, W. J. *Chem. Rev*. **1993**, 93, 913.

(12) Nakamura, K.; Masaki, N.; Okamoto, M.; Sato, S.; Shimokoshi, K. *J. Chem. Phys*. **1987**, 86, 4949.

(13) Schreiner, P. R.; Schaefer III, H. F.; Von Ragué Schleyer, P. *J. Chem. Phys*. **1994**, 101, 2141.

(14) Carroll, M. T.; Gordon, M. S.; Windus, T. L. *Inorg. Chem*. **1992**, 31, 825.

(15) So, S. P. *J. Phys. Chem*. **1996**, 100, 8250.

(16) Chertihin, G. V.; Andrews, L. *J. Am. Chem. Soc*. 1994, 116, 8322.

(17) Bender H.; Chen W.; Portillo J.; Van den Hove L.; Wandervorst W. *Appl. Surf. Sci*. **1989**, 38, 37.

(18) Riga J.; Tenret- Noël C.; Pireaux J. J.; Caudano R.; Verbist J. J.; Gobillon, Y. *Phys. Scripta* **1977**, 16, 35.

(19) Lisowski, W.; van den Berg, A. H. J.; Leonard, D.; Mathieu, H. J. *Surf. Interface Anal*. **2000**, 29, 292.

(20) Hoang, T. K. A.; Webb, I. M.; Mai, H. V.; Hamaed, A.; Walsby, C. J.; Trudeau, M.; Antonelli, D. M. *J. Am. Chem. Soc*. **2010**, 132, 11792.

(21) Wong-Foy, A. G.; Matzger, A. J.; Yaghi, O. M. *J. Am. Chem. Soc*. **2006**, 128, 3494.

(22) Hamaed, A.; Hoang, T. K. A.; Moula, G.; Aroca, R.; Trudeau, M.; Antonelli, D. M. *J. Am. Chem. Soc*. **2011**, 133, 15434.

(23) Hamaed, A.; Hoang, T. K. A.; Trudeau, M.; Antonelli, D. M. *J. Organomet. Chem*. **2009**, 694, 2793.

(24) Hamaed, A.; Mai, H. V.; Hoang, T. K. A.; Trudeau, M.; Antonelli, D. M. *J. Phys. Chem. C* **2010**, 114, 8651.

(25) Hoang, T. K. A., Hamaed, A., Trudeau, M., Antonelli, D. M. *J. Phys. Chem. C* **2009**, 113, 17240.

(26) Furukawa, H., Miller, M. A., Yaghi, O. *J. Mater. Chem*. **2007**, 17, 3197.

(27) Hu, X.; Skadtchenko, B. O.; Trudeau, M.; Antonelli,D. M. *J. Am. Chem. Soc*. **2006**, 128, 11740.

(28) Hoang, T. K. A.; Rawson, J. M.; Trudeau, M. L.; Antonelli, D. M. Manuscript in Preparation.

(29) Skipper, C. V. J.; Hamaed, A.; Antonelli, D. M.; Kaltsoyannis, N. *J. Am. Chem. Soc*. **2010**, 132, 17296.

(30) Skipper, C. V. J.; Hoang, T. K. A.; Antonelli, D. M.; Kaltsoyannis, N. Chem. Eur. J. **2012**, accepted.

Supplemental Information for Chapter 7 – The role of TiH_5 and TiH_7 in Ti(III) hydride gels for Kubas type hydrogen storage

Table S7.1: Elemental analysis results of synthetic titanium

Material	Carbon (%)	Hydrogen (%)	Titanium (%)[(a)]
A100	27.74	6.41	39.82
H150-6h	18.55	4.25	57.83

(a): From thermo-gravimetric analysis.

Table S7.2: Unit formula and molecular weights of stoichiometric and synthetic materials.

Material	Proposed chemical formula	Formula molecular weight	Titanium (%)	Carbon (%)	Hydrogen (%)
TiH_3	TiH_3	50.89	94.06	0	5.94
$Ti\{CH(SiMe_3)_2\}_3$	$C_{21}H_{57}Si_6Ti$	526.06	9.10	47.94	10.92
$Ti\{CH(SiMe_3)_2\}H_2$	$C_7H_{21}Si_2Ti$	209.28	22.87	40.17	10.11
$Ti\{CH(SiMe_3)_2\}_{0.45}H_{2.55}$ (A100)	$C_{3.15}H_{11.1}Si_{0.9}Ti$	122.17	(a)39.82	30.96	9.16
$Ti\{CH(SiMe_3)_2\}_{0.22}H_{2.78}$ (H150-6h)	$C_{1.54}H_{6.96}Si_{0.44}Ti$	85.71	(a)57.83	21.57	8.16

[(a)]from thermogravimetric analysis results in Table S7.1.

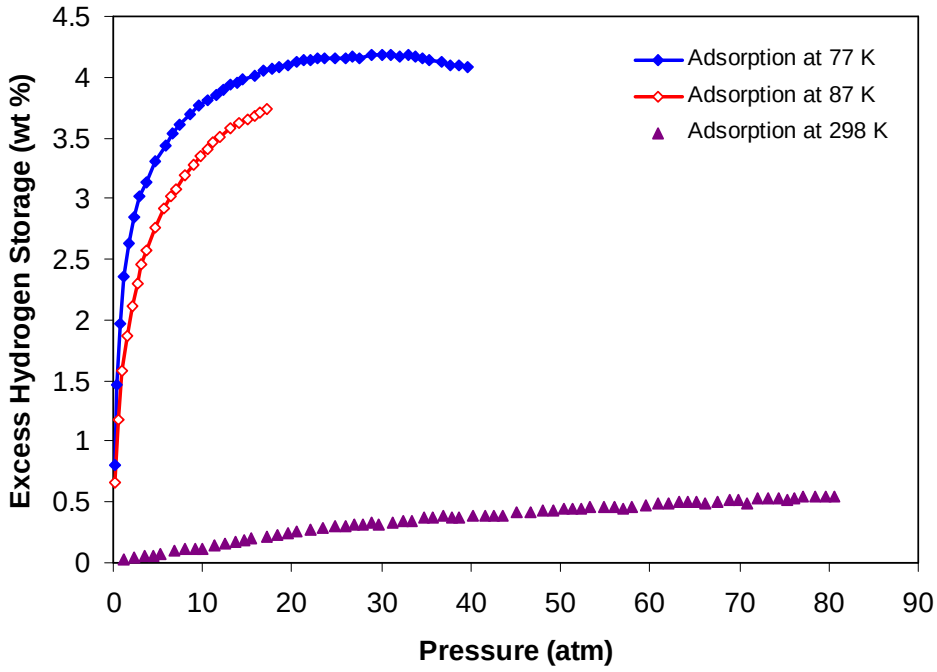

Figure S7.1: Hydrogen excess storage at 77 K, 87 K, and 298 K of carbon AX-21 up to 80 bar recorded on Advanced Materials PCI.

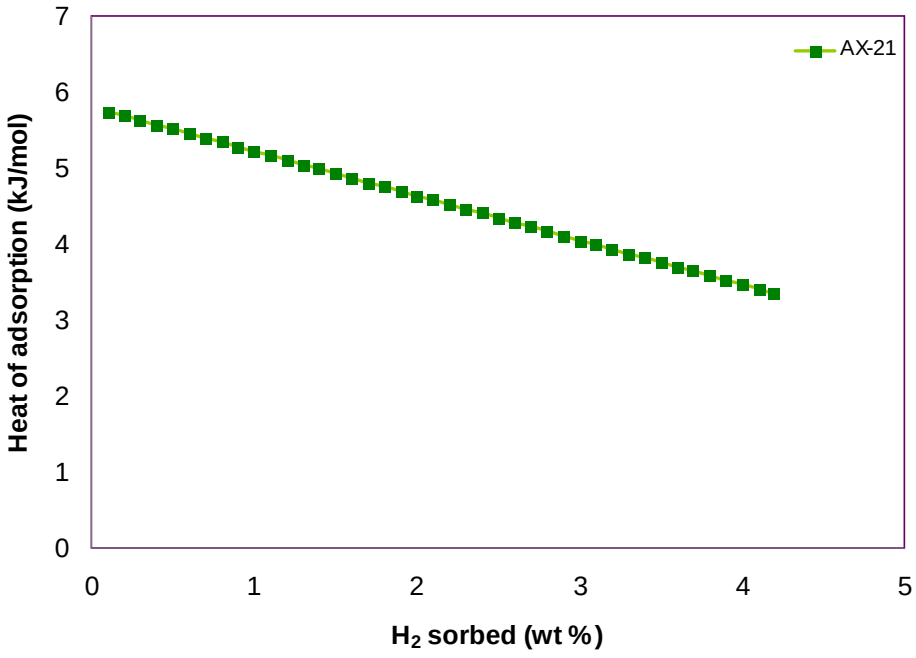

Figure S7.2: Heat of hydrogen adsorption of carbon AX-21 calculated from data in S1.

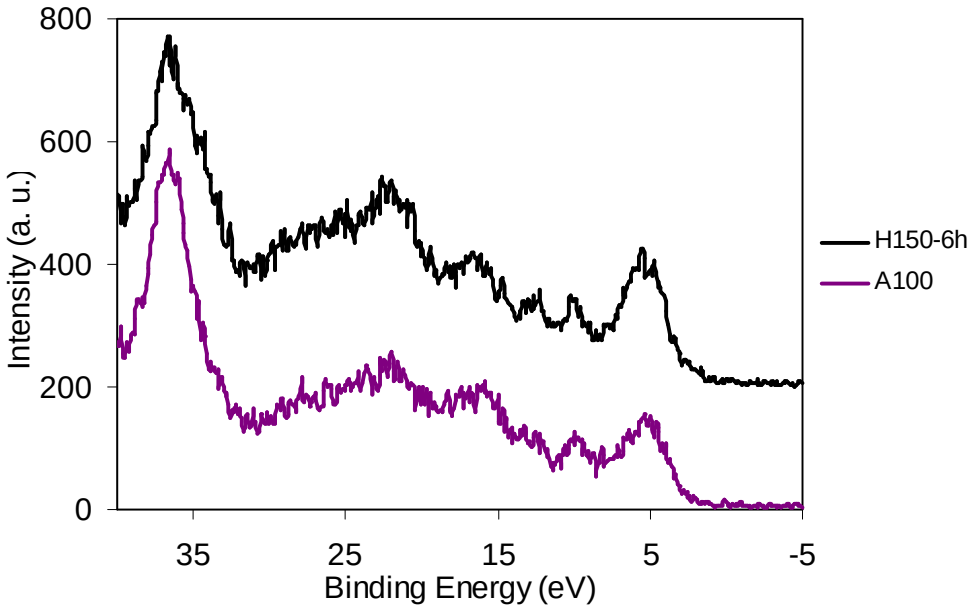

Figure S7.3: Valence region of XPS spectrum A100 and H150-6h.

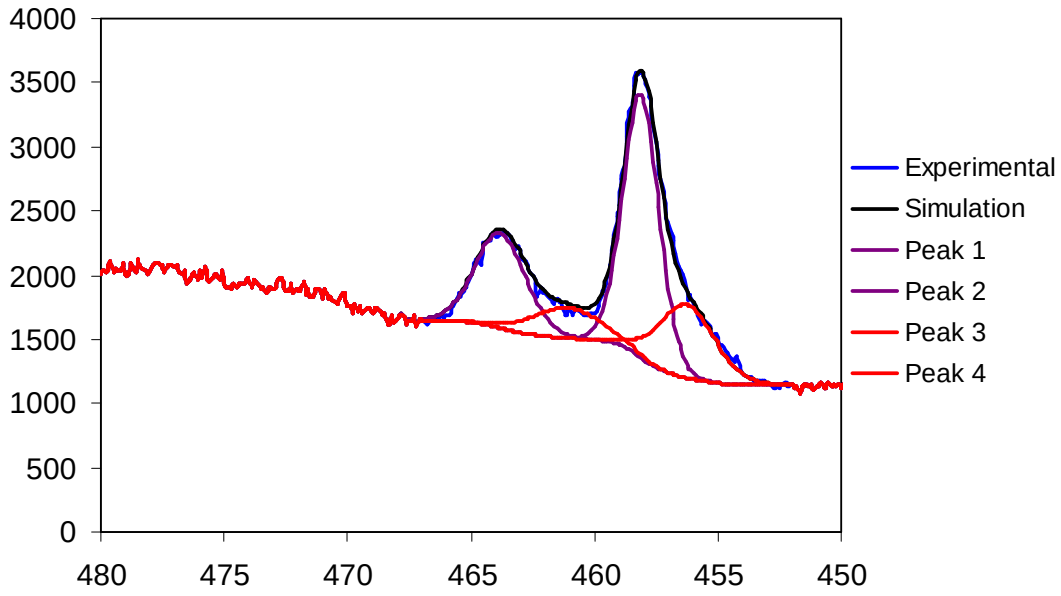

Figure S7.4a: Peak fitting of titanium 2p1/2 and 2p3/2 emissions in the XPS spectrum of A100 sample.

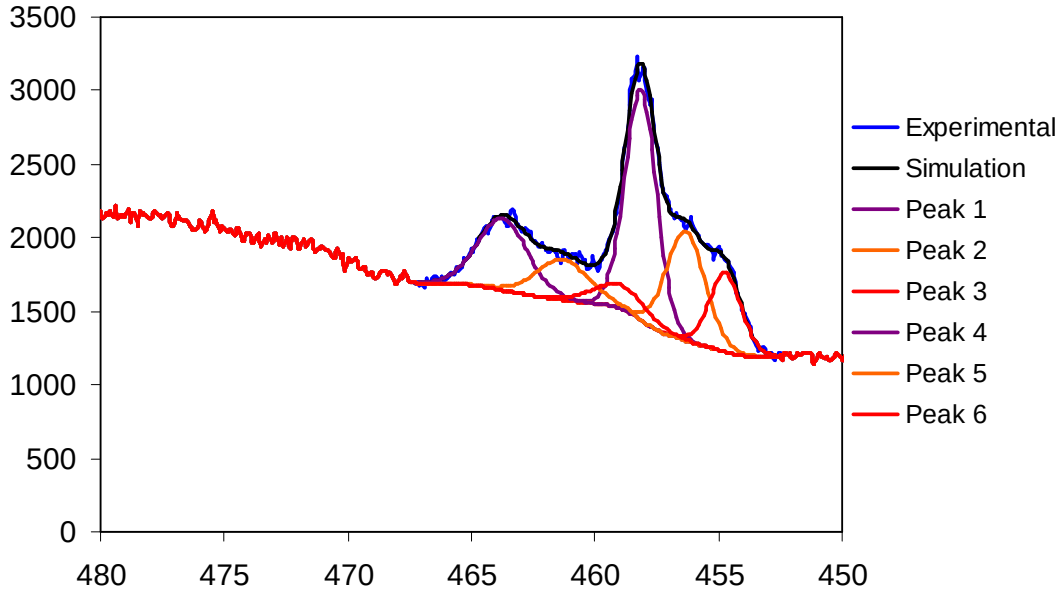

Figure S7.4b: Peak fitting of titanium 2p1/2 and 2p3/2 emissions in the XPS spectrum of H150-6h sample.

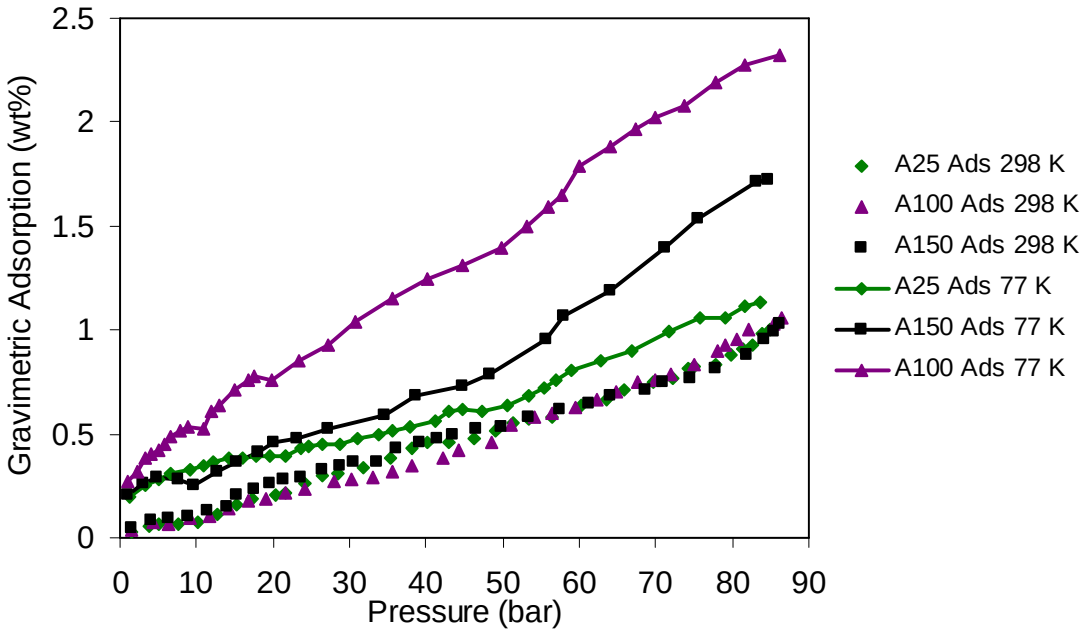

Figure S7.5: Hydrogen adsorption isotherms of A-series materials. Desorption omitted for clarity.

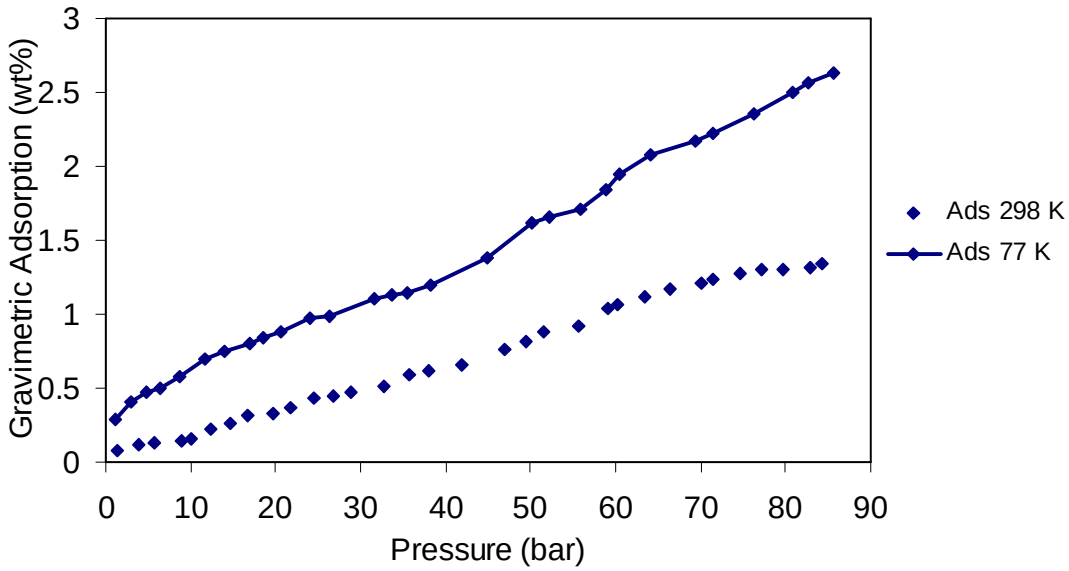

Figure S7.6: Excess storage isotherms at 298 K and 77 K of a pellet of the H150-6h material compressed at 500 Psi.

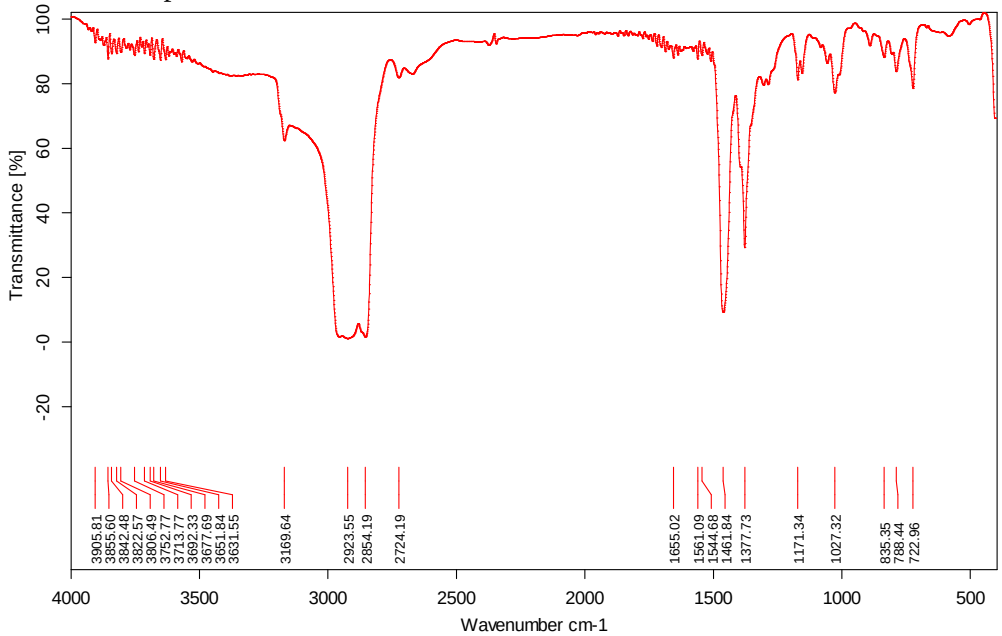

Figure S7.7a: Infrared spectrum of $TiCl_3.0.67\{N(C_2H_5)_3\}$ in Nujol.

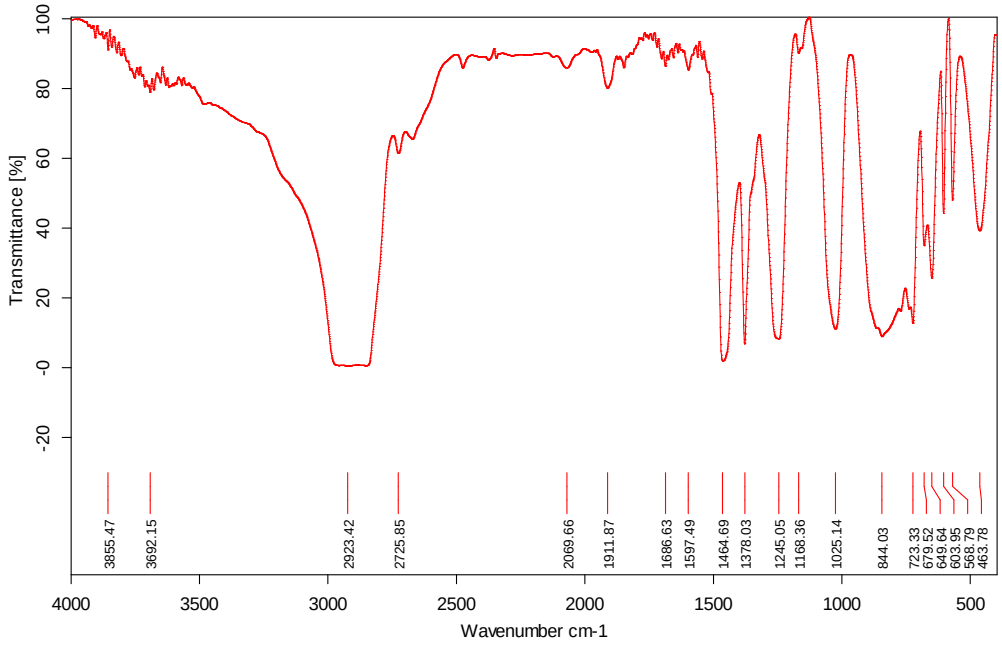

Figure S7.7b: Infrared spectrum of $LiCH(SiMe_3)_2$ in Nujol.

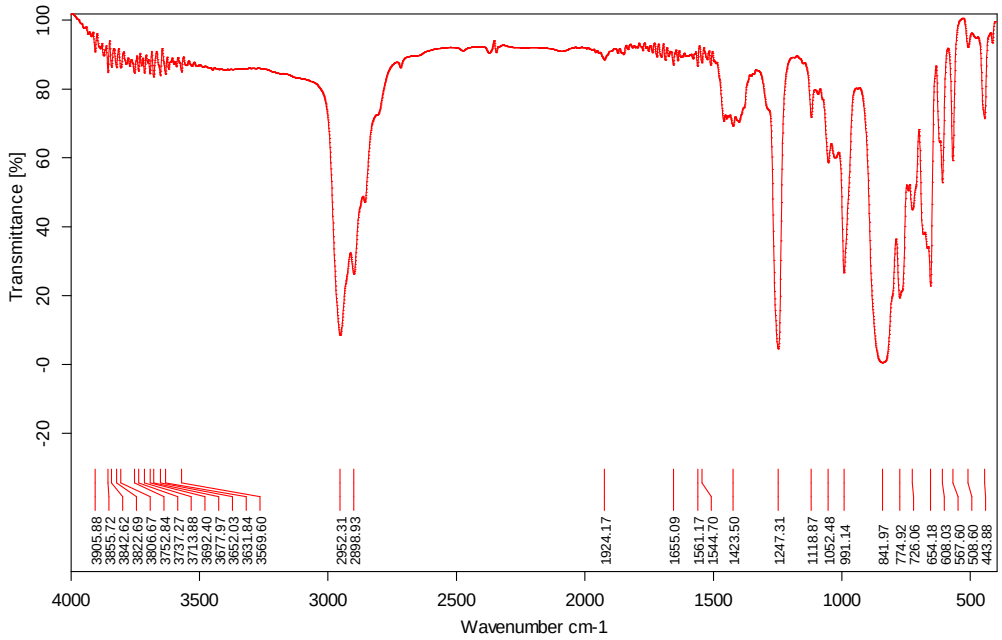

Figure S7.7c: Infrared spectrum of $Ti\{(CH(SiMe_3)_2\}_3$ in Nujol.

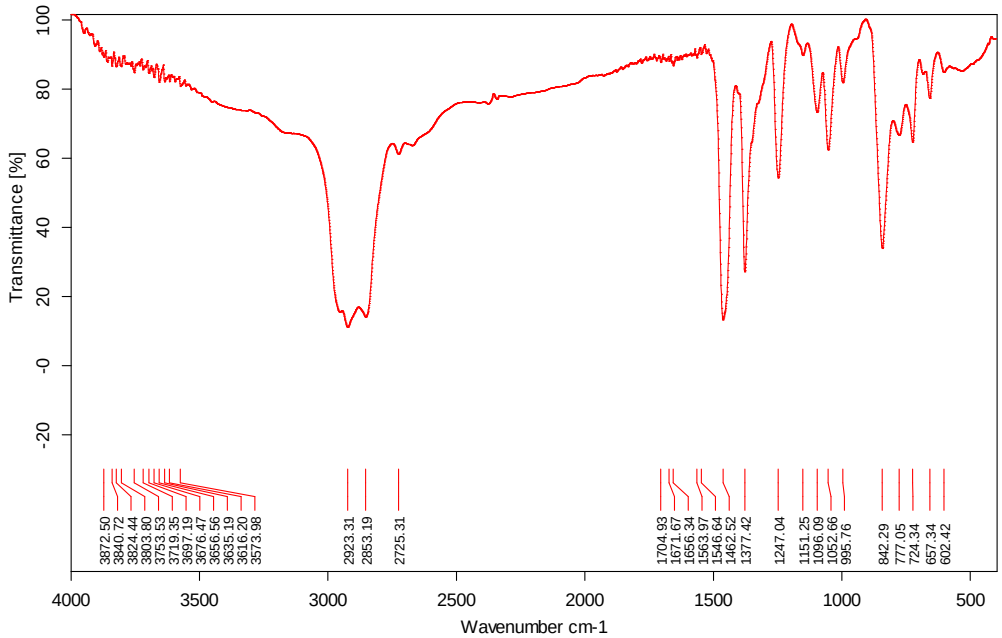

Figure S7.7d: Infrared spectrum of A25 in Nujol.

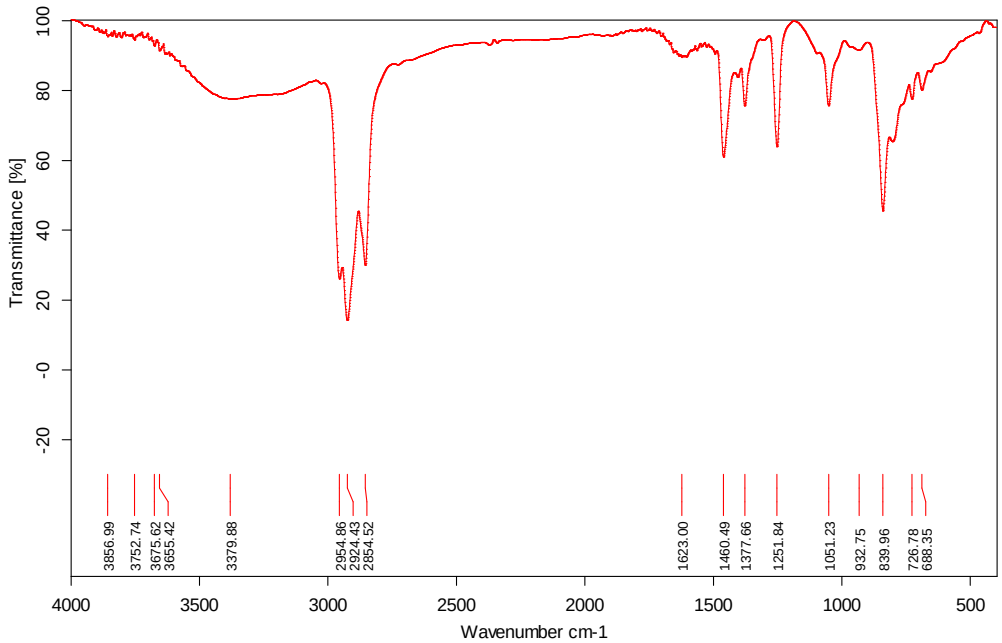

Figure S7.7e: Infrared spectrum of A100 in Nujol.

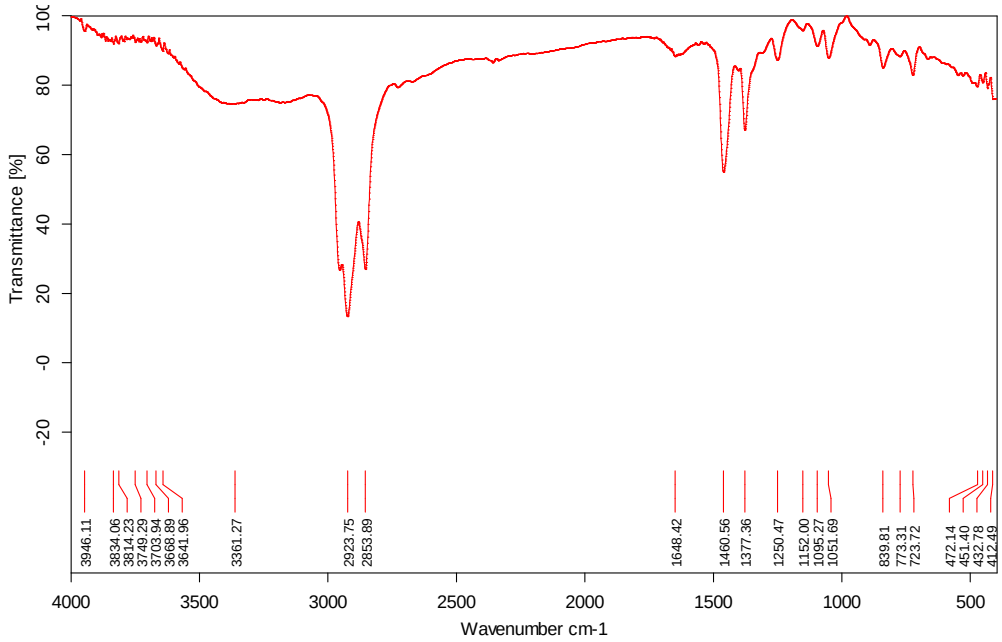

Figure S7.7f: Infrared spectrum of A150 in Nujol.

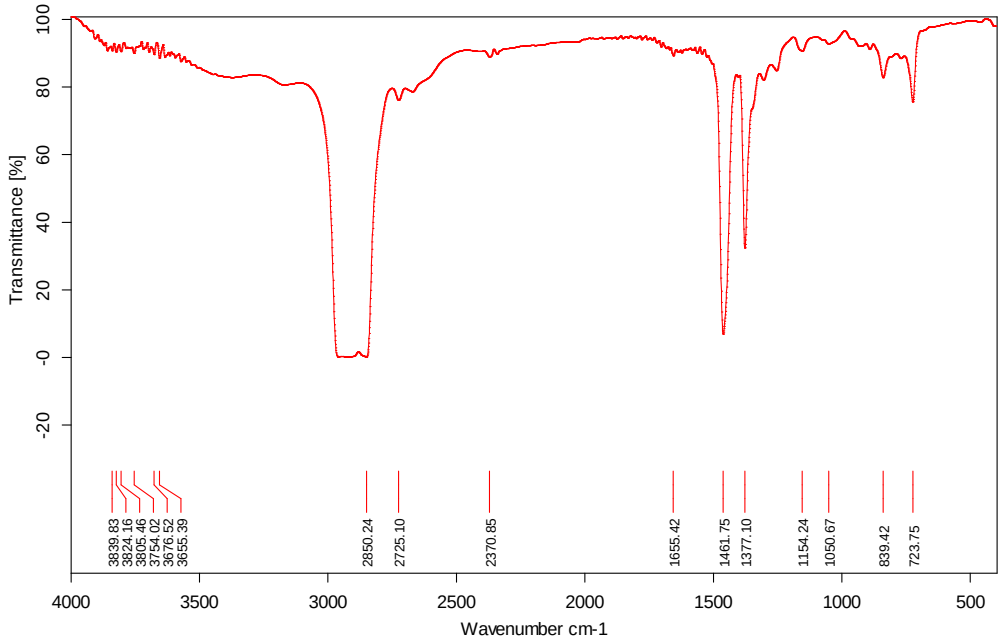

Figure S7.7g: Infrared spectrum of H150-2h in Nujol

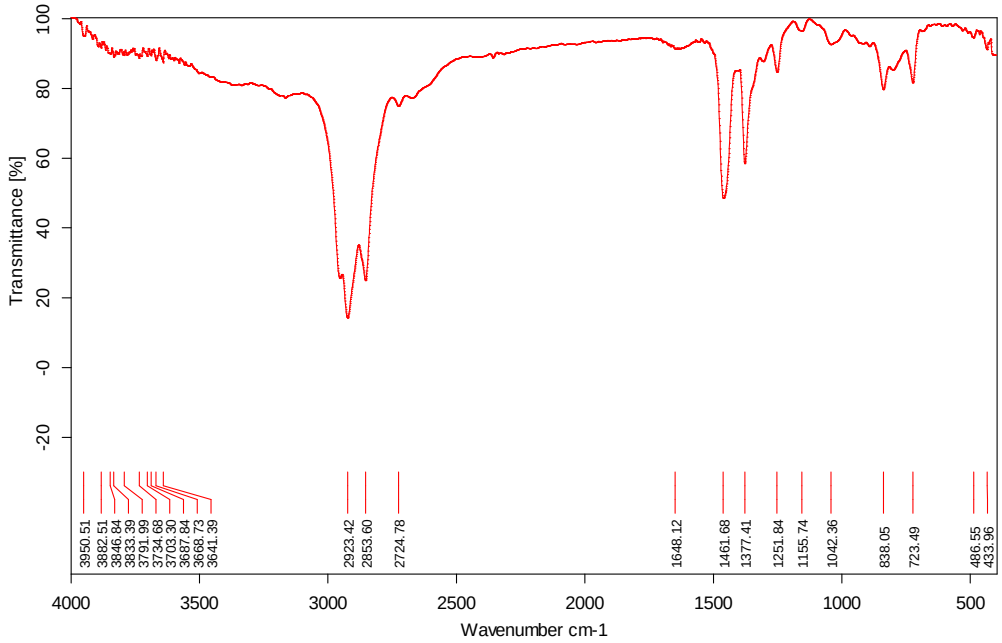

Figure S7.7h: Infrared spectrum of H150-6h in Nujol.

Chapter 8 – Conclusion and outlook

8.1 Brief Restatements and Conclusions

The world demand for energy is always rising with the steady increase of world's population. While fossil fuel, currently the main energy resource, is diminishing, the urgent demands for alternative energy resources are slowly being implemented. Wind, hydrogen, biomass, tide … are all great candidates to replace crude oil, charcoal, and uranium to supply energy for industry, transportation, and household consumption. Among the alternative energy sources, hydrogen is probably the best candidate because it doesn't involve CO_2 in its working cycle. While most hydrogen is currently produced from fossil fuels, technologies are available to produce H_2 and O_2 efficiently from solar energy. In addition to this, fuel cell technologies advanced over the last decade aim to use hydrogen gas and air to produce electricity, with water as the only by product. Thus thee only bottleneck remaining in to implement hydrogen technology is hydrogen storage.[1] As soon as an efficient and safe hydrogen storage method is discovered with a performance that surpasses the US Department of Energy system target,[2] hydrogen technologies could begin to be realized and commercialized.

Chemisorption materials, such as metal hydrides[3] and amino borane,[4] show great promise in both their gravimetric and volumetric hydrogen densities. However, because of high heat of adsorption, implementing these materials necessitates the use of a heat management system. On top of this, the kinetics of hydrogen release as well as the regeneration time and possible degradation of the hydride are remaining challenges, demanding great research efforts to improve and further realize them as practical technologies. Recent work regarding the regeneration of amino borane from hydrazine provides a great hope in improving the overall reversible performance of these materials,[4] however this process cannot be practically carried out in an on-board system and so further hurdles remain for this technology.

In contrast to chemical hydrides, recently designed physisorbents, such as MOF-177,[5] NU-100,[6] or NOTT-122 [7] show great promises under cryogenic conditions because their

gravimetric adsorption performances are in line with the ultimate DOE target (7.5 wt%) and their volumetric densities are higher than the DOE 2017 target of 40 kg/m^3.[2] Moreover, there are no great adsorption/desorption kinetics or charging/discharging problems with these materials. However, because of low heats of adsorption, implementing these technologies also means the association of a cryogenic system to prevent boil off and energy must be spent to cool the system down. Despite these weaknesses, researchers are incorporating highly active species with higher binding enthalpies into these physisorbents and their hydrogen storage capacities are improving.[8]

Of the known methods for hydrogen storage which possess the most suitable heats of hydrogen adsorption are those employing the Kubas interaction. This method of storing hydrogen relies on the adsorption and desorption of hydrogen without breaking the H-H bond into a dihydride with heats of adsorption often in the 20 – 30 kJ/mol range.[9] This interaction is common in organometallic chemistry, but the heavy weights of organometallic compounds and the molecular nature of the compounds makes them unattractive as hydrogen storage materials. For this reason researchers have begun to think of ways of using the Kubas interaction in solid-state materials more suitable for hydrogen storage systems. The first such systems were based on "fantasy molecules" studied by computational chemistry, which, although they could not be synthesized, shed light on the promise of this new approach, allowing subsequent experimental work to emerge.

The functioning mechanism of these systems stem from the early discovery of dihydrogen complexes by Gregory Kubas.[10] In his discovery, H_2 molecules could bind to a 16 electron $W(CO)_3\{P(\text{-}iPr)_3\}_2$ complex to create a stable 18 electron $H_2\text{-}W(CO)_3(P(iPr)_3)_2$ complex at room temperature. Hydrogen molecules could then be removed by applying vacuum. Later, other dihydrogen complexes of late transition metals (Ru, Re, Ir …) were discovered and characterized.[11] The enthalpy of H_2 binding to $W(CO)_3\{P(\text{-}iPr)_3\}_2$ was identified at 70 kJ/mol by theoretical chemistry and at 80 kJ/mol by experiment. While the gravimetric storage of such a system would be far too low for practical use, and the implementation of a molecular crystalline solid into an on-board storage system also a challenge, these enthalpies are also too high for reversible hydrogen storage at room

temperature and moderate pressures. The fact that vacuum is needed to drive off adsorbed hydrogen molecules also places a barrier into the direct application of these compounds as onboard hydrogen storage medium. Ideally, in room temperature hydrogen storage, pressure would be used as a toggle and materials could adsorb multiple hydrogen molecules with an increase in pressure and desorb when pressure is decreased from the system, thus releasing hydrogen gas in a controllable manner.

However, it has been predicted that low-valent early transition metals may bind H_2 with smaller adsorption enthalpies in the range of 20 – 30 kJ/mol, proven ideal for room temperature hydrogen storage.[9, 12] Low valent Sc and Ti supported on various carbon or hydrocarbon materials, such as single wall carbon nanotubes, multiple wall carbon nanotubes, Buckminster fullerene, ethylene, acetylene, polyacetyle, etc. were shown by computation to provide excellent hydrogen storage materials.[9, 12, 13] All of these materials would function in theory via the Kubas interaction. Each metal center could also bind multiple H_2 molecules. Maximum binding could reach 5 H_2/Ti, 5 H_2/Sc, or 4 H_2/V in some cases. Successively experimental works published in 2005 – 2010 provided evidence of the potential reality and practicability of these systems.[14] By laser ablation, Phillips and Shivaram prepared transition metal ethylene complexes in spectroscopic quantities, reaching 12 – 14 wt% hydrogen storage in the case of the Ti ethylene complex, matching well with theoretical work of Yildirim and co-workers.[15] This performance was achieved when titanium was doped into ethylene at a maximum concentration. Thus, higher concentrations of low valent early transition metal species lead to higher hydrogen storage capacities.

Early work from our group on chemically reduced mesoporous Ti oxide suggested the role of the Kubas interaction through increased storage performance and unusual rising enthalies on reduction from Ti (IV) to Ti(II).[16e] Later work from our group and other groups[8,16-18] suggested that low valent low coordination metal species supported on silica or in metal-organic frameworks (MOFs) enhance the hydrogen adsorption performance compared to the non treated materials. Theoretical[18] and experimental[17] results agreed that each Mn(II) center in a Mn-MOF[17] could adsorb up to 1 H_2/Mn center with the heat of adsorption ~ 10 kJ/mol. Organotitanium supported on carbon or silica materials

achieved 4 H_2/Ti at 77 K and 85 bar with maximum binding energy in the 20 – 30 kJ/mol, the ideal range for hydrogen storage.[16] At room temperature 1.96 H_2/Ti was observed at 85 bar with no kinetic barrier. Increasing enthalpies with surface coverage were also observed in this system, but spectroscopy was needed to ascertain the role of the Kubas interaction and the binding enthalpies of individual sites.

In chapter 2, the abilities of low valent V and Cr to provide hosts for multiple hydrogen bonding were studied.[16d] This was proven by doping bis(benzene) bis(cyclopentadienyl) V and Cr on hexagonally packed mesoporous silica at low loading level (5%). By acquiring adsorption isotherms up to 60 bar and 77 K, distinct enhancements of adsorption on the doped materials were observed. Pristine silica adsorbed 1.22 wt% while bis(cyclopentadienyl) Cr doped silica demonstrates 1.60 wt%, bis(cyclopentadienyl)V doped silica possesses 1.40 wt% and bis(benzene) V doped silica provides 1.30 wt%. On the basis of these adsorption results, it was identified that each Cr could be a host for an average of 2.1 H_2 and each V could accommodate 1.73 H_2 at 60 bar and 77 K. From the XPS results, Cr(II) and Cr(III) were identified as the main species in the Cr supported on silica sample. This sample also exhibits great stability by retaining 100% of its adsorption capacity after three months storage. Further work from our group again confirmed the active roles of Cr(II) and Cr(III) in hydrogen adsorption by treating silica with bis(trimethylsilylmethyl) Cr(II) and tris{bis(trimethylsilyl)methyl} Cr(III). Silica treated with other species, such as organometallic V(III), also showed a hydrogen adsorption increase. All of these systems showed the unusual rising enthalpy trend with surface coverage but the percentage of metals in each and the high pressures of storage made spectroscopy difficult.

On the basis of hydrogen adsorption, several early transition metal fragments with identified oxidation states and ligand environments were recognized by their superior hydrogen binding capacities.[16] However, low doping levels hindered spectroscopic studies on the (η^2 - H_2) – metal interaction to light as well as guaranteeing low overall storage performance. As stated previously, a successful hydrogen storage material should possess a very high concentration of a light weight metal. As an example bis titanium ethylene contains 77.34 wt% of Ti.[14, 15] Moreover, all the Ti must be free to interact with

hydrogen and not clustered together. For this reason, we decided to employ hydrazine, a low molecular weight compound containing four hydrogen atoms which could be substituted by metal in a protolysis reaction with a metal alkyl complex similar to a sol gel reaction between water and a metal alkoxide. Thus, the reaction between hydrazine with low coordinate Cr(II), Cr(III), Ti(III), or V(III) alkyl species results in hydrazide gels possessing a very high concentration of metals in preserved low valent states, suitable for hydrogen adsorption.

In chapter 3, vanadium hydrazide gels were synthesized by the reaction between $V(Mes)_3$.THF and anhydrous hydrazine. Reaction conditions (temperature, time, heating periods, reactant concentrations, and reactant ratios) were optimized in regard to maximize the hydrogen adsorption capacities. Anhydrous toluene was determined to be the best solvent for this reaction because it offered several advantages. First, anhydrous hydrazine could be prepared and quantified easily using syringe. Second, limited solubility of hydrazine in toluene allows the protolysis reaction to run smoothly without over heating, which is not favourable in the early steps of a sol-gel synthesis process. When heating the as-synthesized materials in vacuum, residual toluene evaporated and left behind some degree of porosity enhancing the ability for multiple hydrogen molecules to diffuse in and out of the lattice of the materials. At 77 K and 85 bar, the optimized vanadium hydrazide gels possess a true volumetric density of 80 kg/m^3 and an excess volumetric adsorption of 60.01 kg/m^3. These results are in line with the volumetric density stated in ultimate DOE system targets. Under these conditions, each vanadium center could bind an average of 1.96 H_2 molecules. At 298 K and 85 bar, an average of 0.57 H_2/V was observed, which was calculated based on the gravimetric adsorption of 1.17 wt% (or 23.2 kg/m^3 density) and 52.25 wt% of V in the materials. While these results are lower than those obtained from the transition metal fragments on silica, they are surprisingly high considering that residual THF remained bound to the V in the final gel. When void space was removed by compression, the compressed vanadium hydrazide exhibits an excess volumetric adsorption of 17.43 kg/m^3 at 85 bar and 298 K. This value suggests if one fills a $1m^3$ cylinder with the compressed vanadium hydrazide material and supplies 85 bar of H_2 pressure at 298 K, the mass of the cylinder would increase by 17.43 kg due to H_2 adsorption. The Kubas mechanism was suggested to be in operative by the

observation of an EPR change of signal when changing the sample atmosphere from Ar gas to H_2 gas. Hence, an EPR feature representing V(III) reversibly vanished on the replacement of Ar by H_2. This was the first evidence linking the rising enthalpy trend, also observed in this system, to the Kubas interaction, although further studies were obviously needed.

The inability of hydrazine to cleave off THF from the vanadium hydrazide stimulated the synthesis of other metal hydrazides that could be made from metal alkyl precursors free of a stabilizing Lewis base. In chapter 4, bis(trimethylsilylmethyl) manganese(II) was synthesized and employed as Mn(II) source to react with hydrazine. At room temperature and 85 bar, the best materials possesses a Mn concentration of 61.74 wt% and a volumetric hydrogen adsorption of 24.2 kg/m^3, corresponding to an average of 0.47 H_2/Mn. Under these same conditions, an excess volumetric hydrogen adsorption of 18.97 kg/m^3 was obtained from a compressed manganese hydrazide sample. A broad EPR feature was observed on exposure of the manganese hydrazide to Ar, which was enhanced when Ar was replaced by H_2. The results proved the interaction between H_2 guest and high spin Mn(II) hosts.

The replacement of bis(trimethylsilylmethyl)manganese(II) precursor with tris{bis(trimethylsilyl)methyl}titanium(III) in the reaction with hydrazine lead to the formation of titanium(III) hydrazide gels, which were described in chapter 5. The as-synthesized titanium hydrazide gels still possessed recognizable concentrations of hydrocarbon, which were partially removed by hydrogenation at 150 °C with an enhancement of hydrogen adsorption capacity. At 77 K and 85 bar the hydrogenated materials demonstrated an H_2 adsorption capacity of 3.49 wt% and 48.7 kg/m^3. At 298 K and 85 bar, the performance was 1.55 wt% and 21.6 kg/m^3, corresponding to 0.76 H_2/Ti. Saturation was not achieved at either temperature, suggesting even better performance is possible. The compressed materials demonstrated 1.82 wt% gravimetric and 18.44 kg/m^3 excess volumetric adsorption at 298 K and 85 bar. Spectroscopic studies to elucidate the (η^2 - H_2) – metal interaction are currently being exploited.

Efforts to replace anhydrous hydrazine by commercially available organic compounds because of the extreme air sensitive nature of all hydrazides studied were explored in chapter 6. Thus, oxamide, oxalic acid, glycolic acid, and glycolamide were employed to cleave off the mesityl groups of $V(Mes)_3$.THF by protolysis to make 1-d polymers with open coordination sites for Kubas binding of hydrogen. The residual mesityl groups in the vanadium containing polymers were partially exchanged with hydride via hydrogenolysis reaction at high pressure and temperature. At 85 bar a room temperature adsorption of 0.87 wt% and 13 kg/m^3 was observed on the product of $V(Mes)_3$.THF treated with oxamide. Direct evidence of a Kubas interaction between H_2 and the V center was clarified by means of Raman spectroscopy. When sample was under H_2 atmosphere, a signal was collected at 2553 cm^{-1} while it is at 1927 cm^{-1} if H_2 was replaced by D_2. This bathochromic shift was also observed in Cr (II) hydrazide gels, directly relating the rise in enthalpies on surface coverage to the Kubas interaction for the first time.

The success in cleaving the Ti – C bond in tris{bis(trimethylsilyl)methyl} titanium(III) with hydrogen gas resulted in the formation of new alkyl titanium hydrides for hydrogen storage. These materials were studied in detail in chapter 7, and offer a lightweight alternative to the use of hydrazine without the problems related to oxidative decomposition of the hydrazide in these air sensitive species. After treating a toluene solution of tris{bis(trimethylsilyl)methyl} titanium(III) with hydrogen, a black precipitate was obtained, with the formula $Ti\{CH(SiMe_3)_2\}_{0.45}H_{2.55}$ determined by thermo-gravimetric analysis and elemental analysis methods. Enhancement of hydrogen adsorption was achieved by increasing the titanium concentration via a gas-solid hydrogenation reaction to remove excess alkyl. A solid state material with the formula $Ti\{CH(SiMe_3)_2\}_{0.22}H_{2.78}$ was obtained demonstrating an adsorption up to 3.49 wt % and 44.3 kg/m^3 on a PCT Pro Sieverts apparatus at 298 K and 141 bar without saturation. At this pressure, stoichiometry suggests that the Ti exists as a hypervalent Ti hydride in the form of TiH_5 and TiH_7, which desorbs hydrogen by releasing of pressure. These species are the first examples of solid state hypervalent hydrides and could store up to ca. 8 wt% (based on TiH_7) if the system could be optimized. The operating mechanisms are currently being investigated.

Adsorption enthalpies were established for all of the materials by fitting the adsorption isotherms at 77 K and 87 K into the Clapeyron Clausius I equation. The enthalpies go down with surface coverage as expected for physisorbents, but only for the materials with a negligible concentration of low valent metal fragments or too much void space. In samples with high number of active Ti(III), V(III), or Cr(II), rising enthalpies were *always* observed, some of which approaching or surpassing the ideal range of 20 – 30 kJ/mol. Experimental artifacts were ruled out by running AX-21 as an external standard, demonstrating proper calibration of our instrument. Rising enthalpy indicates that the adsorption of a second H_2 molecule is easier than the first H_2. This was observed computationally on Sc decorated bulky balls and low valent Ti(III), V(III), Cr(III) supported silica as well as reduced mesoporous Ti oxides. This phenomenon was explained through extensive calculations by the reduction of charge on metal species after the first hydrogen molecule was adsorbed leading to more effective back bonding of H_2.[19]

8.2 Hydrogen adsorption at high pressures

Lack of saturation was observed on all hydrazides and the hydride materials and this gives rise to questions regarding their ultimate saturation pressures. Since in no case have the H_2/M calculations come close to the 4/H_2 per metal predicted by calculation, it seems much higher performance is possible. However, this cannot be answered at this moment because the Advanced Materials PCI instrument in our lab only allows adsorption to a maximum of 85 bar. Other instruments, such as The PCT-Pro offered by Setaram, allow adsorption up to higher pressures, so isotherms on these instruments may provide more information as to the ultimate performance envelope. In the case of the vanadium hydrazide, the V center could adsorb ~ 2 H_2/V at 77 K and just 0.57 H_2/V at 298 K and 85 bar without saturation. Increasing pressure or removing THF should result in higher adsorption if the pressure is high enough (ca. 300 bar) to allow each V to host the 2 H_2 observed at 77 K and 85 bar. The volumetric performance of vanadium hydrazides would thus surpass the Ultimate DOE system target. Likewise, both computational and experimental chemistry proved that each unsaturated Mn(II) center could adsorb up to 1 H_2/Mn in Mn hydrazides[17,18] However, we only observed 0.47 H_2/Mn at 85 bar and 298 K. Again, the adsorption isotherm at room temperature is linear and no saturation is

observed, so it is expected that at 181 bar, each Mn could serve as a host for 1 H_2 molecule giving a true volumetric adsorption would be 51.5 kg/m^3, surpassing the DOE2017 system target.

Low valent Ti species may be the best hosts since experimental and computational studies proved multiple binding of hydrogen molecules to this metal. Thus, each Ti center is capable of accommodating 4 – 5 H_2/Ti. In the case of titanium(III) hydrazide (or titanium hydride), each Ti just adsorbs an average of 0.67 H_2 (or 0.76 H_2) without saturation, far below its expected performance. Increase pressure up to ca. 500 bar should allow titanium hydrazide to achieve its maximum volumetric adsorption performance at 129 kg/m^3, which means an average of 4 H_2/Ti. In the case of hypervalent Ti hydrides, it is predicted that at 450 bar, the volumetric should be 123 kg/m^3 on the basis of 4 H_2 molecules were adsorbed on every Ti center. This would result in an adsorption of 16 wt%. While this pressure may be too high for a conformable tank, a pressure of half this (225 bar) is close to the transportation pressure of 200 bar used for hydrogen cylinders and would still lead to a performance of 8 wt%, higher than the ultimate DOE goal. Compression of this material and further loss of hydrocarbon would increase the density and further increase the volumetric performance at this pressure of 61.5 kg/m^3. With no kinetic barrier and ideal thermodynamics of adsorption these materials seem very promising at this early stage.

8.3 Research Outlook

Transition metal hydrazide, hydride, and metal containing polymers first explored in this dissertation are newly designed synthetic materials for the purpose of hydrogen storage. Their rich chemistry and engineering potential are to be studied and explored in the future. However further spectroscopy could be applied to elucidate the (η^2 - H_2) – metal interactions involved. Raman spectroscopy was applied successfully in demonstrating the Kubas interaction between (η^2 - H_2) – metal in the vanadium oxamide polymer and chromium hydrazide gels, while EPR suggested an (η^2 - H_2) – metal interaction in vanadium hydrazide gels and manganese hydrazide gels. In light of the wealth of techniques available, other methods are required to compliment and verify the current

results. The behaviour of different types of adsorption centers, for example, centers with different ligand environments, may be examined by means of inelastic neutron scattering (INS). INS does not work well in systems with low concentrations of active species, such as the organotransition metal fragments supported on silica, but may be capable of shedding light on the interaction between hydrogen and each metal environment existing in the transition metal hydrazides. Raman spectroscopy or EPR could be at important in probing multiple binding of hydrogen molecules to metal centers. However, on the basis of adsorption at room temperature up to 85 bar, a metal center in these materials can bind far less than one H_2/metal. To probe multiple H_2/metal, one may need to run the experiment under cryogenic conditions and high pressure or at room temperature with pressure from 200 – 400 bar. Beside spectroscopy works, the exploitation of other hydrazides or hydrides could be important. Hydrazides of later transition metals, such as Fe, Co, Ni … might be synthesized and hydrides of V, Cr, or Mn may be prepared for use in Kubas-type hydrogen storage, or be applied to other chemical or physical applications.

8.4 References

(1) a) Schlapbach, L.; Zuettel, A. *Nature*, **2001**, 414, 353; b) Seayad, A. M; Antonelli, D.M. *Adv. Mater.* **2004**, 16, 765.

(2) Hydrogen, Fuel Cells and Infrastructure Technologies Program: Multi-year Research, Development and Demonstration Plan: Planned Program Activities for 2005 – 2015. http://www1.eere.energy.gov/hydrogenandfuelcells/mypp/pdfs/storage.pdf Retrieved November 25th, 2011.

(3) a) Orimo, S.; Nakamori, Y.; Eliseo, J. R.; Zuettel, A.; Jensen, C. M. *Chem. Rev*. **2007**, 107, 4111; b) Sandrock, G. *J. Alloys Comp*. **1999**, 293, 877; c) Bogdanovic, B.; Eberle, U.; Felderhoff, M.; Schueth, F. *Scr. Mater*. **2007**, 56, 809.

(4) Sutton, A. D.; Burrell, A. K.; Dixon, D. A.; Garner III, E. B.; Gordon, J. C.; Nakagawa, T.; Ott, K. C.; Robinson, P.; Vasiliu, M. *Science* **2011**, 331, 1426.

(5) Wong-Foy, A. G.; Matzger, A. J.; Yaghi, O. M. *J. Am. Chem. Soc.* **2006**, 128, 3494.

(6) Farha, O. F.; Ozgur Yazaydin, A.; Eryazici, I.; Malliakas, C. D.; Hauser, B. G.; Katnatzidis, M. G.; Nguyen, S. T.; Snurr, R. Q.; Hupp, J. T. *Nature Chemistry* **2010**, 2, 944.

(7) Yan, Y., Lin, X., Yang, S., Blake, A. J., Dailly, A., Champness, N. R., Hubberstey, P., Schroeder, M. Exceptionally high H_2 storage by a metal–organic polyhedral framework. *Chem. Commun*. **2009**, 1025.

(8) Vitillo, J. G., Regli, L., Chavan, S., Ricchiardi, G., Spoto, G., Dietzel, P. D. C., Bordiga, S., Zecchina, A. *J. Am. Chem. Soc*. **2008**, 130, 8386.

(9) Zhao, Y.; Kim, Y.; Dillon, A. C.; Heben, M. J.; Zhang, S. B. *Phys. Rev. Lett*. **2005**, 94, 155504.

(10) Kubas, G. J.; Ryan, R. R.; Swanson, B. I.; Vergamini, P. J.; Wasserman, H. J. *J. Am. Chem. Soc*. **1984**, 106, 451.

(11) a) G. J. Kubas, *Chem. Rev*. **2007**, 107, 4152; b) Heinekey, D. M.; Lledós, A.; Lluch, J. M. *Chem. Soc. Rev*. **2004**, 33, 175; c) Morris, R. H. *Coord. Chem. Rev*. **2008**, 252, 2381.

(12) Yildirim, T.; Ciraci, S. *Phys. Rev. Lett*. **2005**, 94, 175501.

(13) a) Lee, H.; Choi, W. I.; Ihm, J. *Phys. Rev. Lett.* **2006**, 97, 056104; b) Lee, H.; Choi, W. I.; Nguyen, M. C.; Cha, M. H.; Moon, E.; Ihm, J. *Phys. Rev B* **2007**, 76, 195110.

(14) Phillips, A. B.; Shivaram, B. S. *Phys. Rev. Lett*. **2008**, 100, 105505.

(15) Durgun, E.; Ciraci, W.; Zhou, W.; Yildirim, T. *Phys. Rev. Lett*. **2006**, 97, 226102.

(16) a) Hamaed, A.; Trudeau, M.; Antonelli, D. M. *J. Am. Chem. Soc*. **2008**, 130, 6992; b) Hamaed, A.; Hoang, T. K. A.; Trudeau, M.; Antonelli, D. M. *J. Organomet. Chem*. **2009**, 694, 2793; c) Hamaed, A.; Mai, H, V.; Hoang, T. K. A.; Trudeau, M.; Antonelli, D. M. *J. Phys. Chem. C* **2010**, 114, 8651; d) Hoang, T. K. A.; Hamaed, A.; Trudeau, M.;

Antonelli, D. M. *J. Phys. Chem. C* **2009**, 113, 17240; e) Hu, X.; Skadtchenko, B. O.; Trudeau, M.; Antonelli, D. M. *J. Am. Chem. Soc*. **2006**, 128, 11740.

(17) Dincă, M.; Yu, A. F.; Long, J. R. *J. Am. Chem. Soc*. **2006**, 128, 8904.

(18) Sun, Y. Y.; Kim, Y.-H.; Zhang, S. B. *J. Am. Chem. Soc*. **2007**, 129, 12606.

(19) a) Skipper, C. V. J; Hamaed, A.; Antonelli, D.; Kaltsoyannis, N. *J. Am. Chem. Soc*. **2010**, 132, 17296; b) Skipper, C. V. J.; Hoang, T. K. A.; Antonelli, D. M.; Kaltsoyannis, N. *Chem. Eur. J*. **2012**, accepted.

Appendix

Appendix 1: Copyright of Wiley to reproduce article Hoang, T. K. A., Antonelli, D. M. Adv. Mater. 2009, 21, 1787 in the introduction chapter.

License number: 2810540078294.

Appendix 2: Permission from ACS to reproduce article in chapter 2.

Tuan K. A. Hoang, Ahmad Hamaed, Michel Trudeau, David M. Antonelli* "Bis(benzene) and Bis(cyclopentadienyl) V and Cr Doped Mesoporous Silica with High Enthalpies of Hydrogen Adsorption". *J. Phys. Chem. C* **2009**, 113 (39), 17240–17246.

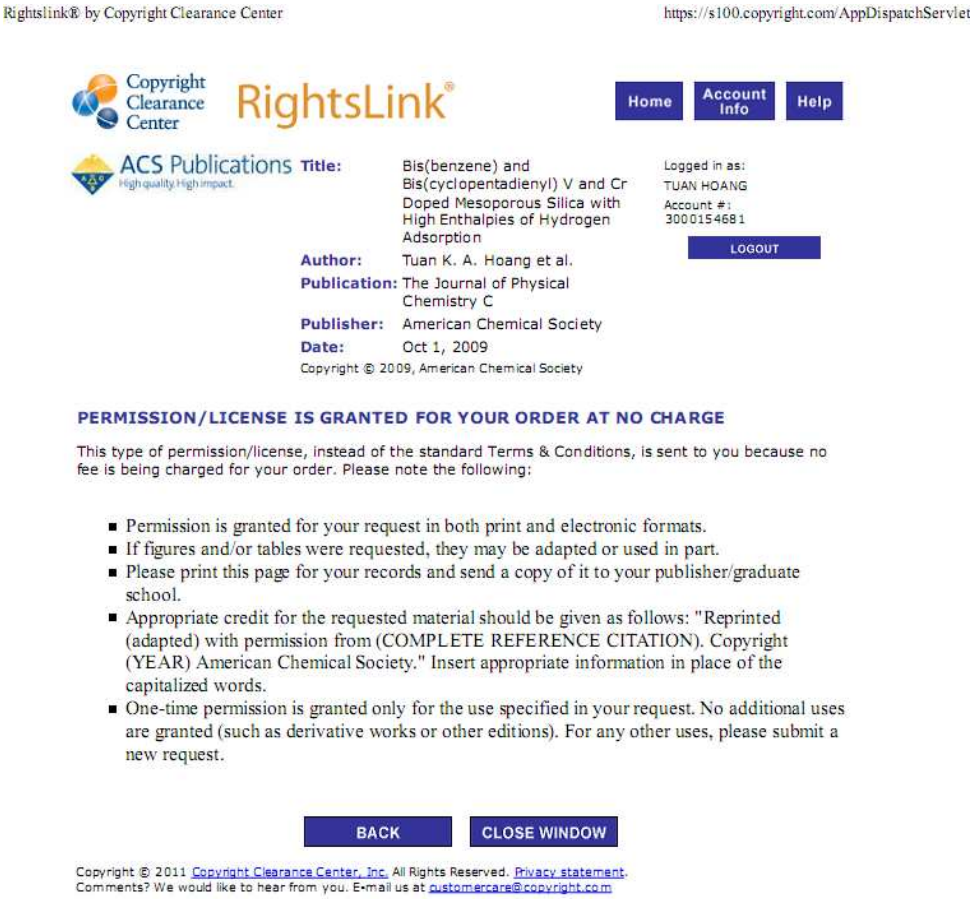

Rightslink® by Copyright Clearance Center https://s100.copyright.com/AppDispatchServlet

Copyright Clearance Center RightsLink® Home Account Info Help

ACS Publications High quality. High impact.

Title: Bis(benzene) and Bis(cyclopentadienyl) V and Cr Doped Mesoporous Silica with High Enthalpies of Hydrogen Adsorption

Author: Tuan K. A. Hoang et al.

Publication: The Journal of Physical Chemistry C

Publisher: American Chemical Society

Date: Oct 1, 2009

Copyright © 2009, American Chemical Society

Logged in as: TUAN HOANG Account #: 3000154681 LOGOUT

PERMISSION/LICENSE IS GRANTED FOR YOUR ORDER AT NO CHARGE

This type of permission/license, instead of the standard Terms & Conditions, is sent to you because no fee is being charged for your order. Please note the following:

- Permission is granted for your request in both print and electronic formats.
- If figures and/or tables were requested, they may be adapted or used in part.
- Please print this page for your records and send a copy of it to your publisher/graduate school.
- Appropriate credit for the requested material should be given as follows: "Reprinted (adapted) with permission from (COMPLETE REFERENCE CITATION). Copyright (YEAR) American Chemical Society." Insert appropriate information in place of the capitalized words.
- One-time permission is granted only for the use specified in your request. No additional uses are granted (such as derivative works or other editions). For any other uses, please submit a new request.

BACK CLOSE WINDOW

Copyright © 2011 Copyright Clearance Center, Inc. All Rights Reserved. Privacy statement.
Comments? We would like to hear from you. E-mail us at customercare@copyright.com

1 of 1 15/12/2011 12:56 AM

Appendix 3: Permission from ACS to reproduce article in chapter 3.

Tuan K. A. Hoang, Michael I. Webbs, Hung V. Mai, Ahmad Hamaed, Charles J. Walsby, Michel Trudeau, David M. Antonelli* "Design and synthesis of vanadium hydrazide gels for Kubas-type hydrogen adsorption: a new class of hydrogen storage materials". *J. Am. Chem. Soc*. **2010**, 132, 11792 – 11798.

Appendix 4: Permission from ACS to reproduce article in chapter 6.

Tuan K. A. Hoang, Ahmad Hamaed, Golam Moula, Ricardo Aroca, Michel Trudeau, David M. Antonelli* "Kubas-type Hydrogen Storage in V(III) Polymers Using Tri- and Tetradentate Bridging Ligands". *J. Am. Chem. Soc*. **2011**, 133, 4955 – 4964.

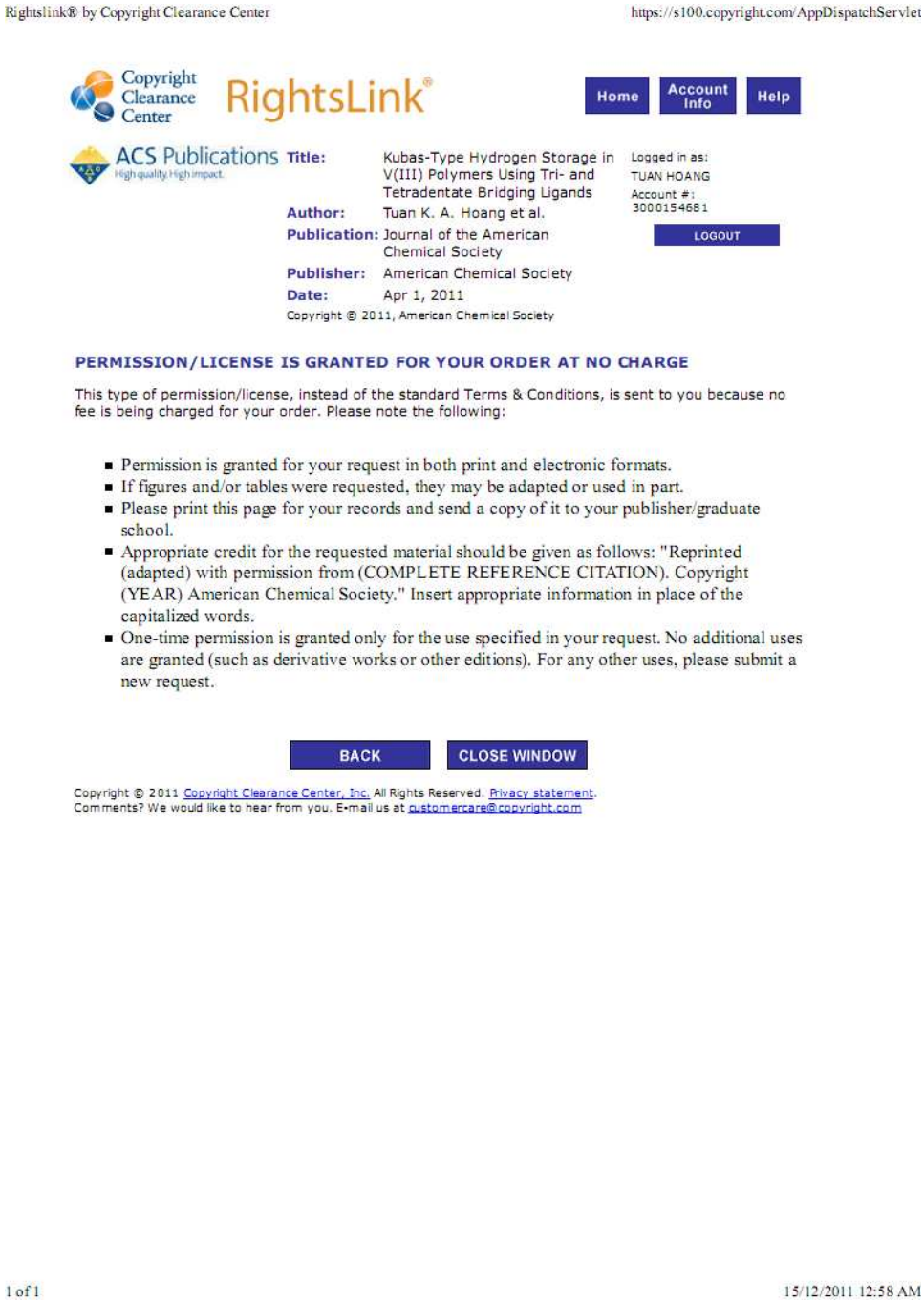

Rightslink® by Copyright Clearance Center https://s100.copyright.com/AppDispatchServlet

Copyright Clearance Center RightsLink® Home Account Info Help

ACS Publications High quality. High impact.

Title: Kubas-Type Hydrogen Storage in V(III) Polymers Using Tri- and Tetradentate Bridging Ligands

Author: Tuan K. A. Hoang et al.

Publication: Journal of the American Chemical Society

Publisher: American Chemical Society

Date: Apr 1, 2011

Copyright © 2011, American Chemical Society

Logged in as: TUAN HOANG
Account #: 3000154681
LOGOUT

PERMISSION/LICENSE IS GRANTED FOR YOUR ORDER AT NO CHARGE

This type of permission/license, instead of the standard Terms & Conditions, is sent to you because no fee is being charged for your order. Please note the following:

- Permission is granted for your request in both print and electronic formats.
- If figures and/or tables were requested, they may be adapted or used in part.
- Please print this page for your records and send a copy of it to your publisher/graduate school.
- Appropriate credit for the requested material should be given as follows: "Reprinted (adapted) with permission from (COMPLETE REFERENCE CITATION). Copyright (YEAR) American Chemical Society." Insert appropriate information in place of the capitalized words.
- One-time permission is granted only for the use specified in your request. No additional uses are granted (such as derivative works or other editions). For any other uses, please submit a new request.

BACK CLOSE WINDOW

Copyright © 2011 Copyright Clearance Center, Inc. All Rights Reserved. Privacy statement.
Comments? We would like to hear from you. E-mail us at customercare@copyright.com

1 of 1 15/12/2011 12:58 AM

VITA AUCTORIS

Name: Tuan Khoa Anh Hoang

Place of Birth: Hue City, Thua Thien Hue Province, Vietnam

Year of Birth: 1979

Education: Ho Chi Minh City University of Technology, Vietnam

1997 – 2002 B. Sc.

Ho Chi Minh City University of Technology, Vietnam

2002 – 2005 M. Sc.

University of Windsor, Canada

2007 – 2011 Ph. D.

List of Publications:

[1] Clair Skipper, Tuan K. A. Hoang, David M. Antonelli*, Nik Kaltsoyannis* "The First Atoms in Molecules Analysis of the Kubas Interaction: A study of Transition Metal Hydrazide Based Hydrogen Storage Materials", manuscript accepted at *Chem. Eur. J.* **2012**. Accepted.

[2] Ahmad Hamaed, Tuan K. A. Hoang, Golam Moula, Michel Trudeau, David M. Antonelli "Hydride-induced Amplification of Performance and Binding Enthalpies in Alkylchromium (II) Hydrazide Gels for Kubas-type Hydrogen Storage". *J. Am. Chem. Soc*. **2011**, 133, 15434 – 15443.

[3] Tuan K. A. Hoang, Ahmad Hamaed, Golam Moula, Ricardo Aroca, Michel Trudeau, David M. Antonelli* "Kubas-type Hydrogen Storage in V(III) Polymers Using Tri- and Tetradentate Bridging Ligands". *J. Am. Chem. Soc*. **2011**, 133, 4955 – 4964.

[4] Tuan K. A. Hoang, Michael I. Webbs, Hung V. Mai, Ahmad Hamaed, Charles J. Walsby, Michel Trudeau, David M. Antonelli* "Design and synthesis of vanadium hydrazide gels for Kubas-type hydrogen adsorption: a new class of hydrogen storage materials". *J. Am. Chem. Soc*. **2010**, 132, 11792 – 11798.

[5] Hung V. Mai, Tuan K. A. Hoang, Ahmad Hamaed, Michel Trudeau, David M. Antonelli* "Cyclopentadienyl Chromium Hydrazide Gel for Kubas-Type Hydrogen Storage". *Chem. Comm*. **2010**, 46, 3206 – 3208.

[6] Ahmad Hamaed, Hung V. Mai, Tuan K. A. Hoang, Michel Trudeau, David M. Antonelli* "Functionalized porous silicas with unsaturated early transition metal moieties as hydrogen storage materials: Comparison of metal and oxidation state". *J. Phys. Chem. C* **2010**, 114 (18), 8651 – 8660.

[7] Tuan K. A. Hoang, Ahmad Hamaed, Michel Trudeau, David M. Antonelli* "Bis(benzene) and Bis(cyclopentadienyl) V and Cr Doped Mesoporous Silica with High Enthalpies of Hydrogen Adsorption". *J. Phys. Chem. C* **2009**, 113 (39), 17240–17246.

[8] Tuan K. A. Hoang, David M. Antonelli* "Exploiting the Kubas Interaction in the Design of Hydrogen Storage Materials". *Adv. Mater*. **2009**, 21, 1787 – 1800.

[9] Ahmad Hamaed, Tuan K. A. Hoang, Michel Trudeau, David M. Antonelli* "Optimization of hydrogen storage capacity in silica-supported low valent Ti systems exploiting Kubas binding of hydrogen" *J. Organomet. Chem*. **2009**, 694, 2793 – 2800.

Presentation:

[1] Tuan K. A. Hoang, Michel Trudeau, David M. Antonelli* "Kubas-Type Hydrogen Storage in Metallo-Polymer Materials". Oral Presentation at the 94th Canadian Chemistry Conference and Exhibition, Montreal, QC, CA. June 5^{th} – 9^{th}, 2011.